COMET

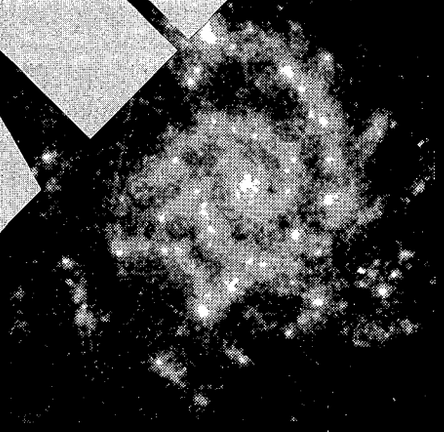

The NASA STI Program ... in Profile

Since its founding, NASA has been dedicated to ensuring U.S. leadership in aeronautics and space science. The NASA Scientific and Technical Information (STI) Program plays an important part in helping NASA maintain its leadership role.

The NASA STI Program provides access to the NASA STI Database, the largest collection of aeronautical and space science STI in the world. The Program is also NASA's institutional mechanism for disseminating the results of its research and development activities.

A number of specialized services help round out the Program's diverse offerings, including creating custom thesauri, translating material to or from 34 foreign languages, building customized databases, organizing and publishing research results.

For more information about the NASA STI Program, you can:

- **Phone** the NASA Access Help Desk at (301) 621-0390
- **Fax** your question to NASA Access Help Desk at (301) 621-0134
- Send us your question via the **Internet** to help@sti.nasa.gov
- **Write to:**

  NASA Access Help Desk
  NASA Center for AeroSpace Information
  800 Elkridge Landing Road
  Linthicum Heights, MD 21090-2934

COLLEGE OF ENGINEERING

VIRGINIA POLYTECHNIC INSTITUTE AND STATE UNIVERSITY

BLACKSBURG VIRGINIA

N81-33237 #

College of Engineering
Virginia Polytechnic Institute and State University
Blacksburg, Virginia 24061-4899

VPI-E-81-27 October 1981

An Endochronic Theory for Transversely Isotropic Fibrous Composites

Marek-Jerzy Pindera[1]

Carl T. Herakovich[2]

Department of Engineering Science and Mechanics

Interim Report 25
The NASA-Virginia Tech Composites Program

NASA Cooperative Agreement NCCI-15

Prepared for: Materials Application Branch
National Aeronautics & Space Administration
Langley Research Center
Hampton, VA 23665

[1]Graduate Student now with Materials Sciences Corporation

[2]Professor of Engineering Science and Mechanics

BIBLIOGRAPHIC DATA SHEET	1. Report No. VPI-E-81-27	2.	3. Recipient's Accession N

4. Title and Subtitle
AN ENDOCHRONIC THEORY FOR TRANSVERSELY ISOTROPIC FIBROUS COMPOSITES

5. Report Date
October 1981

6.

7. Author(s)
Marek-Jerzy Pindera and Carl T. Herakovich

8. Performing Organization No. VPI-E-81-27

9. Performing Organization Name and Address
Virginia Polytechnic Institute and State University
Engineering Science and Mechanics
Blacksburg, VA 24061-4899

10. Project/Task/Work Unit

11. Contract/Grant No.
NASA NCCI-15

12. Sponsoring Organization Name and Address
National Aeronautics & Space Administration
Langley Research Center
Hampton, Virginia 23665

13. Type of Report & Period Covered

14.

15. Supplementary Notes

16. Abstracts A rational methodology of modelling both nonlinear and elastic dissipative response of transversely isotropic fibrous composites is developed and illustrated with the aid of the observed response of graphite-polyimide off-axis coupons. The methodology is based on the internal variable formalism employed within the text of classical irreversible thermodynamics and entails extension of Valanis' endochronic theory to transversely isotropic media. Applicability of the theory t prediction of various response characteristics of fibrous composites illustrated by accurately modelling such often observed phenomena as: stiffening reversible behavior along fiber direction; dissipative resp in shear and transverse tension characterized by power-laws with diffe hardening exponents; permanent strain accumulation; nonlinear unloadin and reloading; and stress-interaction effects.

17. Key Words and Document Analysis. 17a. Descriptors
composites, nonlinear, endochronic, stress interaction, shear modulus, transversely isotropic, failure, experiment, graphite-polyimide

17b. Identifiers/Open-Ended Terms

17c. COSATI Field/Group

18. Availability Statement	19. Security Class (This Report)	21. No. of Pag
Distribution unlimited	UNCLASSIFIED	
	20. Security Class (This Page) UNCLASSIFIED	22. Price

ACKNOWLEDGEMENT

This work was supported by NASA Cooperative Agreement NCCI-15. Dr. John G. Davis, Jr. was the NASA Technical monitor and his assistance during the first author's residency at the NASA-Langley Research Center is gratefully acknowledged. The fabrication and preparation of the necessary specimens could not have been easily accomplished without the expertise and timely help of Mr. A. Shearin and Mr. T. Moore of NASA-Langley for which the authors are grateful.

This work constituted the first author's Ph.D. dissertation. He would like to extend special thanks to Professor E. Johnson for the many discussions that have contributed to the general content of this study. The authors also wish to thank the various members of the first author's Ph.D. committee for their timely suggestions regarding the relevant aspects of this work. Mr. D. Danello's technical assistance during the experimental stages is also much appreciated as is Ms. C. Barnett's typing of the manuscript.

TABLE OF CONTENTS

LIST OF FIGURES

Figure No. Page

LIST OF TABLES

1. DISCUSSION OF SIGNIFICANCE AND SCOPE OF THE UNDERTAKEN STUDY

1.1 Introduction

The analysis of nonlinear behavior and failure characteristics of unidirectional composites has received considerable attention in the past ten years due to recent advances in the analytical and technological areas of these high-strength, low-weight materials. As manufacturing capabilities improve resulting in more consistent mechanical properties of the cured composite, an obvious need arises to be able to accurately characterize their response in both the linear and nonlinear range. Such characterization is essential in predicting overall properties of given laminates which are composed of a number of individual laminae stacked at various fiber orientations with respect to the laminate geometrical boundaries as illustrated in Fig. 1.1.

The linear elastic behavior is well documented at both the micro- and macro-levels and thus will not be discussed further. The nonlinear behavior however, is or can be caused by a number of different independent or interdependent mechanisms acting on the micro-scale and can be therefore very complex. The need to recognize these mechanisms is desirable in formulating constitutive equations for the nonlinear range of composites. This in turn leads to the need of characterization of the mechanical response of individual constituents. On the other hand, the desirabil-

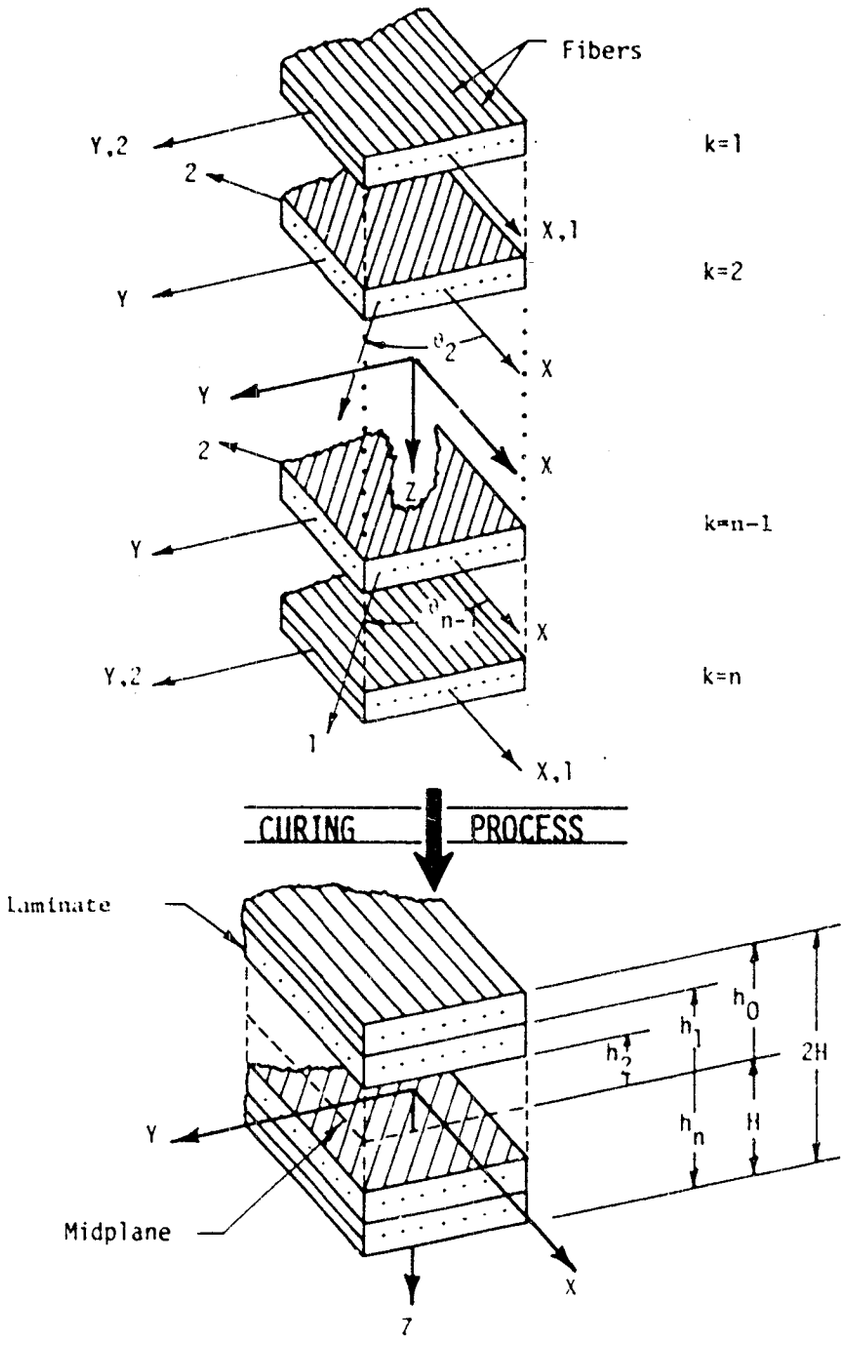

Fig. 1.1 Laminate geometry

ity of considering fibrous composites as homogeneous, orthotropic or transversely isotropic materials is obvious from analytical and design points of view. Ideally, therefore the constitutive equations ought to reflect the microstructure of the lamina as well as the properties of its constituents in a rational manner within the general framework of homogeneous anisotropic nonlinear analysis. The problem is essentially that of the transition from micro-to macroscales and the degree and extent to which the smearing idealization is valid and applicable.

The nonlinear behavior of a lamina can be caused by inherent material nonlinearities of the individual constituents, damage accumulation due to fiber or matrix cracking as well as crazing, interfacial debonding, geometric arrangement of the phases or any combination of the above. It is evident that residual stresses and any viscoelastic response of the constituents will play an important role in interacting with the above phenomena. Kinematic effects at finite strains will also contribute to the nonlinear response as will high stress gradients due to the heterogeneous nature of the medium. Material instabilities of the phases such as necking and microbuckling often cannot also be disregarded along with the degree of constraint afforded by the directional nature of the fibers and the resulting channeling effects.

It is doubtful that all of the above mentioned phe-

nomena taking place at the micro-level will manifest themselves in the same manner and on the same footing on the macro-scale. Accurate characterization of the macromechanical response necessitates therefore, at least conceptually, a certain degree of characterization of the constituent behavior of each phase and weighing of importance of each possible phenomena contributing to the nonlinear response at the macro-level.

On the other hand characterization of the nonlinear behavior of composites ought to be carried out in accordance with the known thermodynamic principles and general theorems governing behavior of various classes of materials. Concepts such as stable material or structural response for example are often useful ideas which can act as a guide in analyzing how the mechanical response on the micro-scale translates into global behavior [1].

A discussion and review of various approaches in dealing with nonlinear response and failure of unidirectional composites and their impact on laminate analysis at both the micro- and macro-levels cited by researchers in the field is presented in the following sections.

1.2 The Macro- vs Microscopic Approach

In the macroscopic approach the heterogeneous nature of the lamina is replaced by homogeneous medium with anisotropic properties whose symmetry is reflected in the microstructure of the material. It is presumed that the scale at

which the heterogeneous nature can be smeared out is definable although in practice this is done implicity rather than explicitly.

Recently, Spencer [2] outlined the method of formulation of constitutive equations for transversely isotropic and orthotropic materials with the aid of invariants reflecting the extent of symmetry of given medium in question. Linear elastic, finite elastic and plastic materials were considered with direct applicability to fiber-reinforced composites. The effect of kinematic constraints on incompressibility and inextensibility in certain directions was discussed as useful idealizations for the strongly directional nature of these materials.

The macroscopic formulation must necessarily be based on a set of comprehensive experiments if the ensuing equations are to be applicable to more than just a very limited type of loading paths. Nonlinear elastic (hyperelastic), elastic-plastic or more general models with dissipation mechanisms must reflect the actual experimental behavior for a wider class of loading than monotonic since these concepts are defined to a large extent by the unloading response. On the other hand, combined response is restricted by thermodynamic constraints which must be used to eliminate ambiguity or impose bounds on the material parameters which are, as well as those which are not, directly measurable by experiment. Furthermore, combined loading may serve to

establish the extent of certain coupling phenomena in the nonlinear range dictated perhaps by micromechanical considerations or it may be used to test the validity of certain hypotheses about the material behavior.

In the microscopic approach, the effect of the material properties of each constituent, their arrangement and shape on the overall properties of ensuing structure are analyzed. This invariably requires idealizations in order to keep the problem tractable since the approach involves determination of internal stress fields in the individual constituents and subsequent averaging throughout a representative volume element to obtain the overall properties of an equivalent anisotropic medium. Such procedure can be carried out in a deterministic, approximate, or stochastic manner by a number of different self-consistent, numerical or material modelling schemes which will be mentioned in the course of this review. It must be said that in situations where the composite nonlinearity is caused by the constituents nonlinearities and perfect bond is preserved during various loading stages between the phases, general theorems can be used in shedding light on the overall structural response. This apparently holds even for stable crack growth as long as the interfacial bond is preserved. Other damage accumulation mechanisms however require a totally different treatment partially based on thermodynamic constraints. The problem is further complicated by random nature of damage accumu-

lation present in many systems due to stochastic strength distributions of the individual constituents. The above difficulties resulted in an apparent separation in the methods of approach to nonlinear behavior and failure prevalent in the current literature.

1.3 Literature Review

1.3.1 Macroscopic Studies

One of the earliest attempts at analyzing nonlinear behavior of composites at the macro-level was carried out by Petit and Waddoups [3]. The authors considered unidirectional laminae under plane loading and assumed that material nonlinearities in the longitudinal, transverse and shear directions acted independently of each other during combined loading. This facilitated analysis of the nonlinear laminate response to a great extent and permitted the linearization of the stress-strain curves in a straightforward fashion. Furthermore the authors recognized that failure of a given ply in the laminate configuration did not necessarily imply total failure if the unfailed plies were still capable of supporting incremental loads. Failure of individual plies was determined on the basis of maximum strain criterion and it was assumed that failed plies unloaded along steep negative tangent modulus. Further assumptions were made about load bearing capabilities of failed plies. Transverse failure implied that load could still be carried

parallel to the fibers and in shear while shear failure allowed the ply to support load in parallel and transverse directions. Failure in the fiber direction on the other hand was taken to mean total degradation. Agreement with experimental data was fair to good for the various laminates tested as far as the stress-strain response was concerned. Failure predictions were generally less than good. The authors gave no consideration to unloading and thus no conclusion can be drawn regarding the nature of lamina nonlinearity.

Hahn and Tsai [4] on the other hand employed a complementary elastic energy density approach to formulate constitutive equations to model lamina nonlinearities in arbitrary material directions and subsequently specialized the formulation to handle shear nonlinearity only. Thus interaction between shear and normal stresses was absent and furthermore a unique relationship between stress and strain was a direct consequence of the elasticity formulation assumed to be valid for the considered systems. The theory was subsequently applied to unidirectional [4] and multidirectional composite systems [5]. The agreement appeared fair to poor and in the case of unidirectional laminae the elasticity assumption was never verified by cyclic tests. A claim was made that introduction of coupling between various stresses in the nonlinear range was unnecessary for the boron-epoxy system studied. This appeared somewhat arbitrary in view of

other reseachers' studies on this effect. In general, it would appear difficult to make reasonable predictions about the coupling problem in the nonlinear range without resorting to micromechanical considerations and/or sufficiently extensive testing program on specimens with consistent properties. This was absent in the early studies on the mechanical response of composites.

The Hahn-Tsai model was subsequently employed in the study of the dynamic response of a thin composite plate carried out by Benveniste and Aboudi [6]. The above analysis revealed the possibility of shock formation due to a smooth time-dependent input applied at the boundary of the plate. Careful and accurate characterization of the nonlinearities present in the response of composites thus cannot be overemphasized.

The approach taken by Sandhu [7] was to formulate incremental constitutive equations in terms of tangential properties of the lamina wherein the strain increment was expressed as a function of the stress increments through strain-dependent tangential properties. Since the tangential properties were assumed to be functions of all the strain components, biaxial loading was required to determine normal and transverse tangent moduli for the plane stress situation. No mention was made of the stress interaction in shear and unloading and thus it is difficult to envision the kind of nonlinearities that this formulation is intended to

model. A heuristic definition for equivalent strain was also proposed in view of unavailability of biaxial data. Furthermore, a failure criterion based on the total work to failure was proposed with independent longitudinal, transverse and shear contributions. This is interesting since it implies that failure is path-dependent in view of the incremental nature of the constitutive equations. It must also be mentioned that this was one of the few attempts cited in the literature to associate nonlinear behavior and failure. The theory was correlated with experiments on off-axis uni- and multidirectional laminate configurations under monotonically increasing loading.

Jones [8] proposed to model nonlinear behavior of transversely isotropic graphite by expressing secant material properties as functions of the strain energy to explain effects such as biaxial softening (decreasing Poisson's ratio) due to internal cracking. The material properties were allowed to vary independently and were expressed in the following manner:

$$\{\text{Material property}\}_i = A_i\left[1 - B_i\left(\frac{u}{u_{si}}\right)^{c_i}\right]$$

where $u = \frac{1}{2}\sigma_{ij}\varepsilon_{ij}$ is the equivalent elastic strain energy. Subsequent comparisons with biaxial experiments yielded deviations not exceeding three percent. Extensions to off-axis tests on 0°, 45°, 70° and 90° off-axis angles resulted in good agreement in certain strain ranges but poor in

others.

An attempt was subsequently made to extend the approach to unidirectional laminae [9] with the necessary modification that for high combined strain energies {material property}$_i$ could not decrease beyond a certain positive number in order to prevent the stress-strain curve from falling. Comparison was carried out with data on off-axis boron-epoxy laminae reported by Cole and Pipes [10]. Agreement was fair.

The above model has been exposed to a fair amount of criticism since its arbitrary formulation, which is totally removed from thermodynamic considerations, requires ad hoc arguments and modifications for application to different material systems.

Hashin, Rosen and Bagchi [11] proposed a deformation type theory to model lamina nonlinear behavior in shear and transverse directions. A loading function was assumed, based on invariants for the transversely isotropic system considered, which was employed to determine the functional form of the stress-dependent compliances. Stress interaction in the nonlinear range was assumed between transverse and shear stresses only for systems with stiff fibers in comparison with the matrix. Longitudinal stress was assumed not to influence shear and transverse strains and material was taken to be linearly elastic in the fiber direction. It was further presumed that the material unloaded along the

initial elastic modulus and thus the approach is reminiscent of the total deformation plasticity theory formulation. However, it is not clear if the loading function is associated with yielding or onset of nonlinearity of the composite and clearly the loading function and the nonlinear strains are not related to any potential. Thus the question of normality is not considered.

The concept of stress interaction introduced by Hashin on the other hand raises several questions one of which is the validity of various methods of determining the instantaneous shear modulus of unidirectional composites [12, 13].

The various phenomenological attempts to model nonlinear behavior and failure of composite materials have been influenced to a great extent by the early works of Hill [14] and others [15,16] on the orthotropic and slip theories of plasticity. This is understandable in view of the fact that a good number of advanced composites that exhibit nonlinear behavior are composed of stiff elastic fibers embedded in ductile nonlinear matrices which appear to possess plastic-like characteristics. It must be mentioned however that Hill's outline of anisotropic plasticity theory was based on the implicit assumption of weakly orthotropic behavior with intended applications to materials such as cold-rolled steel. Furthermore, the yield criterion was not based on invariance principles and thus was only defined with respect to the principal material coordinate system. Plastic flow

was characterized by incompressibility, isotropic hardening was inherent in the formulation, and normality and convexity conditions were preserved.

A number of authors attempted to generalize Hill's formulation. Dubey and Hillier [17] proposed a general yield criterion, coincident with the plastic potential, and an associated flow rule for arbitrary elastic-plastic anisotropic solids on the basis of invariance principles. Incompressibility, isotropic hardening were retained and the Bauschinger effect accommodated through retention of cubic terms in their tensor polynomial yield criterion. The authors presumed that the anisotropic coefficients remained constant during plastic flow.

Shih and Lee's formulation [18] followed essentially the same outline with two exceptions. Bauchinger effect was modelled via linear terms in the yield criterion which characterized kinematic hardening and allowance was made for variation of anisotropic parameters during the continuing deformation.

In extending Hill's ideas to composite materials it must be kept in mind that significant differences in mechanical behavior can be exhibited by materials that can be approximated as homogeneous at a certain level and those that possess significant heterogeneity and strong anisotropy at the same level. Whereas the idealization of incompressibility and failure by perfect plastic flow in weakly aniso-

tropic and stain-hardening metals is certainly justifiable, such assumptions are clearly not for strongly anisotropic composites with high volume fraction of oriented, elastic fibers. The formulation of failure in terms of definite surface or combination of surfaces in stress or strain spaces has inherent disadvantages such as path independency. The compressibility of certain composites and the question of path dependency of failure were recently studied and it was illustrated that both effects exist and can be significant [19,20].

Mulhern, Rogers and Spencer [21] developed a continuum model for fiber-reinforced plastic materials assumed to be inextensible in the fiber direction with the fibers being infinitely thin and characterizing the preferred orientation and constraint. The model was developed within the transversely isotropic framework and the matrix taken to be incompressible and rigid-perfectly plastic. The yield surface of the overall medium was formulated in terms of invariants characterizing transversely isotropic response with respect to the preferred orientation which was maintained during continuing deformation and plastic flow was associated with the yield surface. Since the matrix was assumed perfectly plastic, yielding in the matrix followed by unconstrained flow in the preferred directions was associated with failure. The analysis was applied to off-axis tests on unidirectional laminae and predictions compared with the experi-

mental data of Cooper [22] and Jackson and Cratchley [23]. Good agreement for angles greater than 5° for Cooper's data and 15° for Cratchley's data was found.

The theory was subsequently extended to include elastic fiber and elastic-plastic matrix response [24]. In constructing the theory the authors assumed that yielding was not affected by the normal stress in fiber direction and thus hysteresis loops could not be predicted in cyclic loading. This problem was treated by the authors in an earlier paper which dealt with axisymmetric deformation of a single elastic fiber with a plastic coating [25]. Thus the basis for bounds on error for the proposed theory has been laid out for this class of loadings.

Dvorak et al. [26] on the other hand employed the results of finite-element, microscopic studies on systems such as boron-aluminum to develop a continuum theory for the elastic-plastic response of fibrous composites. The theory is applicable to axisymmetric loading situtations: the yield surface was expressed in terms of macroscopic stresses and corresponding stress concentration factors presumed to be determined from microscopic analysis; the plastic strain increment remained normal to the yield surface and kinematic hardening was employed. Agreement with numerical analyses was shown to be very good for various loading programs.

The majority of macroscopic failure criteria cited in the literature have been formulated in terms of strains or

stresses and typically represent closed surfaces in their respective spaces. Failure is thus assumed to be path independent and no explicit mention is made of the mechanism leading to it. Generally speaking, two broad categories of failure criteria can be outlined: those with independent failure modes and those with interacting ones. The former is characterized by piecewise linear surfaces in the strain or stress space whereas the latter by piecewise smooth surfaces.

In the first category failure is predicted when any one of longitudinal, transverse and shear stresses or strains exceeds the limits determined by simple tests. These values are determined with respect to the material system of symmetry and thus cannot be transformed freely from one coordinate system to another. On the other hand they do emphasize the directional nature of the composite and it may even be argued that they predict the failure mode if not the mechanism. Maximum stress and strain theories have been extensively utilized by numerous authors mainly because of their simplicity. However, experiments performed on unidirectional off-axis composites with stiff fibers subjected to combined stresses along the axes of material symmetry have generally revealed the presence of normal stress interaction. Also, such tests strongly suggested the existence of smooth transition from normal to shear transverse failure mode [27]. Furthermore, certain conceptual inconsistencies

inherent in the above type of formulation have been pointed out in the literature [28].

Lance and Robinson [29] on the other hand proposed a maximum shear stress theory of plastic failure of fiber reinforced composites. The theory allowed for three independent shear failure modes of the matrix material and fibers and was expressed in terms of the maximum shear stress reaching critical values on three different planes. Yield criteria were developed for determining when the material may flow plastically in terms of the applied macrostresses and also the particular mode under which unrestricted flow occurs. The theory is reminiscent of the maximum resolved shear stress criterion proposed and verified by Schmid for single crystals of metals [30].

In order to take into account various interaction mechanisms revealed by early studies on unidirectional composites, different quadratic failure criteria have been proposed. These have been reviewed extensively in the literature [31,32,33] and thus only general concepts and methodologies will be discussed herein.

A popular approach is to express the failure condition in terms of a single closed surface generated by expanding the stress components in a power series in accordance with the principles of tensor algebra. This leads to the definition of a strength tensor which was perhaps introduced for the first time by Ashkenazi [34]. The resulting formulation,

which includes as many terms of different orders as deemed necessary for accurate failure characterization was introduced by Goldenblat and Kopnov [35] and subsequently adapted by Tsai and Wu [36] who considered only the quadratic expansion.

The invariant character of the tensor polynomial criterion made it very attractive for applications to multidirectional laminate configurations. However, it has been pointed out that the determination of certain interaction factors which can be obtained only under combined loading requires careful optimization [37]. While the exclusion of these interaction terms in not significant for off-axis unidirectional laminae as shown by Narayanaswami [38], the failure surface in the principal material stress space is very sensitive to small perturbations in these factors as demonstrated by Collins and Crane [39]. While the accuracy and convenience, as well as mathematical consistency of the quadratic tensor polynomial criterion has been illustrated by the studies of Wu [40], Cole and Pipes [10], Huang and Kirmser [41] and others, Tennyson, MacDonald and Nanyaro's experiments [42] indicated that for the glass-epoxy and graphite-epoxy systems that were studied a cubic representation was required since the quadratic formulation was too conservative.

One of the shortcomings of the tensor polynomial criterion is that it predicts the tensile failure stress in

terms of the compressive one and vice versa. This apparent physical inconsistency was pointed out by Hashin [43] who proposed to model the various complex failure mechanisms taking place at the micro-level by expressing failure condition in terms of four distinct quadratic polynomials. The polynomials were expressed in terms of invariants reflecting the transverse isotropy of the considered medium and were intended to model tensile and compressive fiber and matrix failures. The resulting failure envelope is thus piecewise smooth and twice differentiable. It must be pointed out that the above formulation is reminiscent of the early interaction formulas proposed by authors such as Norris [44].

1.3.2 Microscopic Studies

General groundwork for evaluation of overall macro-mechanical properties of fiber reinforced materials from their constituents has been laid out by Hill [45]. The class of materials was limited to transversely isotropic with elastic fibers and elastic-plastic matrices. For simplicity, Hill employed linearized yield surface appropriate for his transversely isotropic medium and an associated flow rule. Bounds were stated for the main overall moduli and flow stress at any stage of deformation. Uniaxial extension was discussed in detail and the entire analysis formulated in terms of incremental stresses and strains. The mechanical properties were thus expressed in

terms of instantaneous moduli.

Further discussion of the approach was continued by Dvorak and Bahei-el-din [46] who employed the self-consistent model together with a modified scheme in calculating internal stress fields, overall and local yield surfaces, instanteneous moduli, thermal coefficients, plastic strains and thermal microstresses. These were obtained for axisymmetric mechanical loads and uniform temperature changes while extensions to shear loads were briefly discussed.

Along the same lines, Sawicki [47] discussed elastic-plastic theory of composites with regular internal structure when both constituents obeyed the von Mises yield condition and an associated flow rule. Several examples were treated using Voight and Reuss idealizations in order to obtain easily Hill's stress and strain concentration factors for illustrative purposes.

Huang [48] attempted to predict overall plastic behavior of composites under polyaxial stresses that were composed of deformation theory type matrices and rigid inclusions. It was hoped that this model would be a useful idealization for real composites subjected to large strains. The above assumptions simplified the analysis considerably due to proportional loading in the matrix under proportionally varying surface tractions. The self-consistent scheme was employed in determining the stress concentration factors and only low fiber volume fractions were considered in

accordance with the assumption of noninteracting stress fields. The analysis was subsequently applied to unidirectional composites under transverse tension and an attempt was made to include elastic-plastic matrix response on a semi-empirical basis.

Tanaka, Wakashima and Mori [49] employed an energy balance method to determine plastic anisotropy and work hardening rate of a composite material with unidirectional and randomly oriented inclusions. They found that aligned fibers introduced strongly anisotropic mode of plastic deformation while isotropic deformation governed the response of randomly oriented inclusions. The micromechanics approach was based on Eshelby's model for stresses in homogeneously deformed inclusion with the matrix undergoing uniform plastic deformation [50,51]. The subsequent results indicated that the flow stress increase was linearly dependent on plastic tensile strain and the hardening coefficient varied strongly with off-axis fiber orientation and inclusion-to-matrix ratio. The mode of plastic deformation followed similar trends for the various plastic strain ratios.

Cho, McNamee and Chou [52] determined initial yielding of a laminated composite consisting of isotropic elastic-plastic layers obeying von Mises yield criterion and the associated flow rule. The approach was based on a three-dimensional theory for laminated media based on a combina-

tion of Voight and Reuss hypotheses and was initially developed to evaluate elastic compliances and stiffnesses of these materials. The analysis resulted in a yield condition of the same form as the tensor polynomial failure criterion without the linear terms for each individual layer. Thus the initial yield condition of an n-ply laminate was represented by n equations in terms of laminate macrostresses. This resulted in a set of intersecting and/or nonintersecting surfaces with the smallest inscribed envelope as the initial surface. An interesting consequence of the analysis was the implication that corners on the surface were possible. Convexity, of course, was preserved.

It was subsequently shown by Wakashima, Suzuki and Umekawa [53] that consideration of residual stresses in the micromechanical formulation will result in linear terms in the yield surface.

The methodology developed by Chou et al. was subsequently extended by Chou and Chou [54] to the discussion of plastic flow rules for the considered media. The analysis was restricted to materials obeying Hencky-type plastic flow rule and the stress and strain fields were assumed uniform for each layer within the representative volume element. Explicit anisotropic flow rules were subsequently derived for proportionally loaded layers that followed piece-wise linear stress-strain relations. The authors concluded that the symmetry of flow could be different from yielding and

plastic flow could occur under hydrostatic loading. Normality was not discussed and elastic unloading assumed to take place without any plastic loading.

A number of authors have employed numerical procedures such as the finite-element analysis to determine initial yield surfaces and subsequent stress-strain curves of unidirectional laminae under various combinations of surface displacements. Various regular arrays have been considered and analyses carried out on a representative repeating element of the regular array. Typically, elastic fibers with elastic-plastic von Mises, strain-hardening matrices have been considered to study the effect of various material parameters on the nonlinear response and yielding. The results of such analyses were subsequently employed by some authors to develop approximate continuum theories of elastic-plastic behavior of fibrous composites as mentioned in the preceding section [26].

Adams [55] studied the nonlinear response of unidirectional boron-aluminum and boron-epoxy systems under transverse loading with two different fiber volume fractions and rectangular and hexagonal geometries. The nonlinear stress-strain response was traced to the initiation of first failure in either of the constituents. Significant differences were noted for the two geometries. Agreement with experimental data was found to be reasonable for the rectangular array but poor for the square one. The effect of increasing

fiber volume fraction was to dramatically decrease the strain-hardening behavior. Residual stresses were not considered but it was suggested that they may have significant influence on the subsequent mechanical response.

Foye [56,57] considered the effect of matrix nonlinearities on post-yielding behavior of uni- and multidirectional laminate configurations under axial and combined loading. Effects such as the number of post-yielding load increments and number of plies in the unidirectional laminate on the stress-strain response in the nonlinear range were analyzed. It was demonstrated that the coupling effect between normal and shear stresses is significantly more noticeable for the shear than transverse stress-strain curve for a von Mises strain-hardening matrix. This is supported by experimental data reported by Cole and Pipes [10]. The author also concluded that the composites studied had the capacity for smoothing out any abrupt features of the matrix response. The predictions for multi-axial laminate behavior which was subsequently considered agreed well with experimental data for the fiber dominated configurations. Agreement with angle-ply laminates was fair to poor. Failure analysis was not considered.

Studies on initial yield surfaces using the finite-element analysis were also carried out by Lin, Salinas and Ito [58] for the boron-aluminum system subjected to plane combined loading. Yield surfaces were generated in the

principal normal stress plane that appeared to be convex and symmetric through the origin. Application of increasing shear stress caused the surface to shrink continuously. The above analysis was subsequently extended by the authors [59] to the problem of longitudinal loading of unidirectional laminae to determine the stress-strain response and progression of the elastic-plastic boundary. The results indicated that initiation of yielding took place at opposite corners of the fiber/matrix interface and proceeded inward the representative volume element with increasing deformation. The elastic limit macro-stresses appeared to vary inversely with the matrix stiffness. It was noted that once the matrix started yielding, the plastic zone expanded very fast with the increasing applied tractions.

Similar but more extensive study was carried out by Dvorak et al. [60,61]. Significant conclusions of the studies were that, generally speaking, yielding starts at the fiber/matrix interface for high fiber volume fractions, plastic zone expands very fast with increasing macrostress, yield surfaces are convex, temperature changes cause significant yielding and translation of the yield surface, composites yield under hydrostatic stress and exhibit volume changes and yielding in the fiber direction is controlled by the E_f/E_m ratio and fiber volume fraction. High ratios inhibit yielding in the longitudinal direction. Yielding in the transverse plane on the other hand is matrix yield

stress controlled. Also, high longitudinal and transverse shear stresses facilitate yielding under combined loading. On the basis of the above results an approximate continuum theory for elastic-plastic behavior of fibrous composites was developed as mentioned previously.

The analyses outlined above dealt primarily with nonlinearities caused by plastic flow of the matrix and in most cases no explicit mention was made of failure. Stowell and Liu [62] were perhaps the first to define independent failure modes for unidirectional metal matrix composites in a paper dealing with strengthening effects of stiff inclusions. They postulated three failure modes governed by the strength of the fibers and transverse and shear strengths of the matrix. Further work along the same lines was carried out the Kelly and Davies [63] who took into account the effect of fiber constraint on the matrix by multiplying the matrix strengths by an appropriate factor. Prager [64] on the other hand pointed out that matrix failure by plastic flow will be influenced by all the stress components and subsequently carried out failure analysis of unidirectional and angle-plies reinforced by infinitely thin, inextensible fibers and perfectly plastic matrix obeying the von Mises yield condition and associated flow rule. The analysis predicted trends postulated by Liu and Stowell. An interesting point brought forth was the prediction of compressive fiber stresses for the tensile off-axis loading of

unidirectional laminae in certain angle ranges.

McLaughlin and Batterman [65] on the other hand employed limit analysis to study plastic failure of composites composed of long, elastic perfectly-plastic fibers embedded in a strengthless matrix. Limit surfaces in laminate stress plane were determined and the effect of unequal compressive and tensile strength demonstrated. The analysis was subsequently extended by McLaughlin [66] to load-supporting matrices with both constituents being elastic-plastic with acceptable limit behavior. Numerical examples were worked out for off-axis unidirectional and angle-ply laminates and results compared with experiments carried out by Jackson and Cratchley [23] on reinforced aluminum with steel wire specimens. It was concluded that the theory predicted qualitative trends.

Experimental studies were carried out by Cooper [22] and Jackson and Cratchley [23] to verify Stowell's and Davies' hypotheses of independent failure modes on unidirectional and angle-ply configurations. Cooper's experiments generally revealed good agreement with theoretical predictions; however, modifications were necessary for thin sheets with few fibers across the thickness or weak fiber-matrix interfaces. Cratchley on the other hand concluded that the mode of composite fractures could be correlated quantitatively with fiber orientation for the metal matrix unidirectional composites studied. Poorer agreement however was

obtained for angle-plies.

The various analyses discussed in this section up to this point have been based on certain idealizations such as regular micro-structure or statistically homogeneous material behavior on the macroscale, perfect bond between fiber and matrix, flawless state of constituents at the beginning of loading and uniform properties of the phases with respect to geometry and stress levels. Thus the analysis of non-linear behavior has been carried out up to the initiation of first failure in either of the constituents whereas total failure was handled differently since it was not clear how failure at a point in a representative volume element translated into global response. The problem is further complicated by stochastic strength distributions introduced by size and manufacturing techniques in brittle fibers, absence of perfect interfacial bond which contributes to the introduction of cracks at various stages of deformation as well as residual stresses which can be sometimes sufficiently high to initiate yielding or cracking before actual application of mechanical loading. Visco-elastic response, if present, will also influence the above phenomena. These various effects have been studied by Stowell and Liu [62] and others and comprehensively outlined in a review paper of Kelly and Davies [63] on strengthening effects in composites where the limited usefulness of the strength predictions based on the rule of mixtures was demonstrated and the

concepts of ineffective length and associated transfer mechanisms summarized. These concepts were introduced by Dow [67], Cox [68] and Rosen [69] in their studies of the effect of broken or discontinuous fibers on the mechanical properties of composites.

Zweben and Rosen subsequently employed the idea of ineffective length in a more comprehensive statistical theory of strength of unidirectional composites subjected to longitudinal loads with elastic fibers obeying Weibull strength distribution [70]. Various modes of damage accumulation such as adjacent fiber break propagation due to localized stress concentrations caused by fiber breaks, bundle type failure and crack propagation in the matrix were discussed and critical stresses for each mode derived. In his subsequent attempts at analyzing the effect of constituent properties on failure modes of unidirectional composites Zweben [71] employed his so-called "materials modeling approach" to study the effect of matrix inelasticity and matrix splitting on the resulting failure surface of a composite subjected to combined axial and shear loads. It was demonstrated that the effect of fiber/matrix interface splitting manifested itself in lack of convexity which was retained only if plastic yielding of the matrix was considered alone.

In subsequent studies dealing with damage accumulation Kousiounolus and Williams [72], Goree [73] and Zweben [74]

examined the effect of oriented finite length cracks on the strength and mode of failure of unidirectioanl composites. On the basis of tests on off-axis laminae with edge cracks perpendicular to the load axis Williams concluded that the primary mode of failure in high fiber volume fraction composites is crack propagation by fiber/matrix interface debonding or matrix splitting. Zweben on the other hand employed the materials model approach to study notched unidirectional composites with central crack extending over multiple broken fibers perpendicular to fiber and load axis. The effect of matrix plasticity and interfacial failure was considered and the laminate was idealized to consist of two distict regions: the central core with the broken fibers and the outside undamaged region. Fiber stress concentration factors were determined and compared with Hedgepeth and van Dyke's analysis [75] which was based on the use of influence functions and superposition for infinite array of fibers embedded in elastic matrix. The results suggested significant reduction in stress concentration factors due to inelastic effect for a notch of arbitratary size. Goree's general approach followed Zweben's concepts but in the actual stress determination methodology individual broken fibers were considered resulting in a system of n+1 equations for the n broken fibers and the outside core. These were reduced to a pair of integral equations which were subsequently solved numerically. Good agreement with exper-

imental data for load vs. COD for the boron-epoxy system without matrix splitting was obtained. The author concluded that for yielding without splitting, fracture strength was crack length dependent whereas for large splitting no such dependency was found since failure occurred immediately in these cases regardless of the size of crack length.

Some theoretical articles have appeared recently that have attempted to deal with general concepts of damage accumulation on the microscale within the framework of the continuum model. Drucker [1] for instance discussed stable micro-crack propagation in a composite consisting of linear elastic fibers and elastic or elastic-plastic matrix. Convexity and normality were suggested to hold for situations where the interfacial bond remained intact. In systems where frictional effects are in evidence, such as those due to fiber pull-out or slippage, however, Drucker [76] illustrated that normality was not necessarily present. In still another paper it was demonstrated by Palmer, Maier and Drucker [77] that concave yield surfaces were possible for systems where the elastic response was affected by prior plastic deformation. An example of such a system is a stiffening spring placed in parallel with a plastic matrix cyclically loaded at various stress levels. It is clear therefore that various internal damage or dissipative mechanisms operative in composites may influence the global response in ways completely different from the generally

accepted ones and consequently their presence ought to be considered either implicitly or, wherever possible, explicitly in the formulation of constitutive equations.

Rice [73] on the other hand analyzed the structure of inelastic constitutive relations for solids on the basis of internal variable theory and discussed its application to metal plasticity. The class of solids for which the theory is applicable was presumed to be that whose inelastic behaviour at finite strain was due to specific structural rearrangement on the microscale of constituent elements. Normality of constitutive equations on the macroscale was shown to arise when each of the local microstructural rearrangements proceeded at a rate governed by its associated thermodynamic force. Although the possibility of extending Rice's methodology to model fiber breaks and other damage accumulation mechanisms as "specific structural rearrangements" in unidirectional composites exists this has not been carried out.

To avoid problems dealing with normality and convexity and to consider the influence of history of damage accumulation and deformation on the current stress and strain levels, Valanis [79,80] proposed a theory of visco-plasticity without a yield surface. The underlying principle was that the history of deformation was defined in terms of a time scale which in itself was a property of the material at hand. The theory was developed on the basis of the internal

variable formalism in conjunction with certain concepts of classical irreversible thermodynamics and was shown to resemble and reduce to theories of plasticity and viscoelasticity, respectively, upon imposition of suitable constraints on the material parameters involved. Although the theory was formulated for an arbitrary anisotropic medium, only the isotropic case was discussed in detail. Various loading programs were considered for several metals and surprisingly good correlation with experimental data was obtained for such phenomena as hysteresis loops and cross-hardening as well as nonlinear Poisson's strains.

Damage accumulation in composites has been studied by Hahn and Tsai [81] in 0°/90° laminates. The damage under consideration was the successive breakage of the 90° plies which resulted in the decrease of Young's modulus. Analytical model based on a bundle of elastic springs with variable strengths was postulated and compared with experimental data. More extensive studies along similar lines were carried out by Reifsnider et al. [82] who employed a shear-lag-like analysis at the laminate level and subsequently postulated and experimentally verified the existence of the so-called "characteristic damage state." Although the above analyses have dealt with laminate response, individual lamina behavior "in situ" was considered and thus these can be considered as micro-mechanical approaches.

Acoustic emission techniques have been employed by var-

ious authors to study damage accumulation such as fiber or matrix cracking or crazing and fiber/matrix debonding or slipping, all of which lead to generation and propagation of energy wave forms that can be picked by acoustic transducers located on the surface of the specimen [83]. Current attempts are aimed at correlating the emission frequencies, amplitudes and distribution with the various damage mechanisms.

Adams and Flitcroft [84] carried out experiments to determine the effect of shear damage on torsional behaviour of carbon-reinforced plastics. Torsional modulus and damping capacity of uniaxial specimens were measured as a function of strain amplitude, proportion and type of fiber and fiber surface treatment. It was found that after initiation of cracking, damping was a more sensitive indication of the presence of damage than the modulus.

Saint-John and Street [20] on the other hand demonstrated that loading paths can have a significant effect on failure stress levels of unidirectional composites. Such path dependency is not predicted by a number of failure conditions. An analytical study carried out by Akbarzadeh [85] with the help of finite-element analysis demonstrated that a single broken fiber has negligible effect on the longitudinal strength but the void caused at the breaking point can significantly affect the transverse strength.

Nonlinear stress-strain response may not be caused

solely by the constituent nonlinearities and damage accumulation mechanisms. Effects such as fiber waviness, uneven fiber distribution and kinematic effects at finite strains or large stress gradients can also be significant.

Mansfield and Purslow [86] studied analytically the influence of fiber waviness on shear and Young's moduli of unidirectional lamina using the material modelling approach. The study was undertaken to explain higher experimental values for the shear modulus than those predicted theoretically on the basis of various models. Analytical results indicated neglible effect on both moduli if constraints were imposed on allowable fiber and matrix deformation modes such that failure strains in either phase were not exceeded. This effectively imposed upper limits on the fiber wave amplitude to wavelength ratio which controlled the nonlinear behavior. The study revealed the possibility of significant influence of the fiber waviness for those systems with ductile matrices and flexible fibers.

Van Dreumel and Kamp [87] carried out an experimental study aimed at separating the influence of fiber waviness and fiber nonlinear response on the stiffening behavior of 0° graphite-epoxy laminae. Laminates with fibers having amplitude to wavelength ratios between 0.05/55 and 0.75/55 were tested and linear relationship was found between the longitudinal modulus and stress of the following form: $E = E_o + 2l\sigma$. The authors concluded that no significant influ-

ence of fiber waviness was found for the ratios tested as far as the longitudinal modulus was concerned. On the other hand, Purslow's analysis indicated that the ratios considered in Kamp's study would not result in significantly different responses. However, the strengths for the various waviness ratios varied between 1,440 and 2,000 n/mm2. Also, Poisson's ratio increased from 0.29 to 0.59 with increased waviness ratios in the range considered by the authors.

Craddock and Zak [88] developed a model intended to take into account the effect of uneven fiber distribution on premature yielding of the matrix. This was thought to be responsible for significantly nonlinear response of laminated tubes under combined loading very early during the deformation process. The approach followed Hill's formulation, but the strain concentration factors were expressed in terms of a distribution function describing the amount of matrix material of a given strain concentration level. Thus no explicit consideration of the actual goemetry was undertaken and volume integrations were replaced by integration over all possible strain concentrations defined by the author on the basis of certain heuristic arguments. Certain distribution functions were considered and it was shown that these modelled the nonlinear response of the tubes with sufficient accuracy.

Soldatov [89] discussed nonlinear response of a composite consisting of linearly elastic constituents on the

basis of geometrically nonlinear theory for small displacements and very non-uniform internal stress fields. The longitudinal extension of a meridionally axisymmetric cylinder with clamped ends was treated and the resulting Young's modulus of the structure turned out to be a function of the deformation level.

1.4 Literature Summary, Objectives and Outline of the Present Study

The above discussion brings forth the complexity of nonlinear response and failure exhibited by composite materials and rooted in the many different mechanisms operating at the micro-level. This helps to explain the apparent separation of approaches used to study the nonlinear response of composite materials. The various approaches at the micro-level cited in the literature have generally dealt with only certain of the mechanisms contributing to overall nonlinearities whereas the phenomenological or macro-level studies have often been based on heuristic developments that have either lacked thermodynamic foundations or theoretical-experimental correlation justifying the employed assumptions. On the other hand, the outlined discussion of the surveyed literature indicates that an attempt to consider all or most of the mechanisms at the micro-level in a rigorous fashion in the process of arriving at an averaged, macromechanical response would appear to pose an intractable problem. References [76] and [77] evince the dilemma very

clearly by illustrating how an isolated dissipation mechanism or even specific structural arrangement of material phases with known responses can destroy the otherwise well-established theoretical structure of a nonlinear constitutive model. However, the various micromechanical studies do establish the importance of each operative mechanism and its impact on the ensuing structural or macro response as well as the constitutive variables affecting it.

In summary, it is seen that a need exists for a unified, nonlinear continuum constitutive theory for fibrous composites that would be consistent with the current, generally accepted thermodynamic concepts and still be capable of reflecting the significant micromechanisms resulting in the observed nonlinear response. In subsequent chapters Valanis' endochronic theory which is based on the internal variable formalism employed within the context of classical irreversible thermodynamics is extended to transversely isotropic media and shown how it can fulfill the above requirement. The structural content of the present study aimed at accomplishing the above objective is given in what follows.

A brief outline of the internal variable formalism and the associated thermodynamic framework employed in the process of arriving at Valanis' endochronic constitutive theory is given in Chapter 2. General time-independent equations for transversely isotropic media are subsequently

developed to illustrate the extent of coupling present in the nonlinear (dissipative) domain. These are then shown to reduce to the isotropic formulation discussed by Valanis [79]. Certain other features of the endochronic theory that underline fundamental thermodynamic differences between this and plasticity or viscoelasticity theory are also briefly mentioned. These differences have not been in the author's opinion sufficiently emphasized in the published literature.

Applicability of the endochronic theory with regard to the prediction of nonlinear response of fibrous composites is illustrated with the aid of the observed response of off-axis, unidirectional Gr/Pi coupons. Chapter 3 outlines the experimental technique and associated testing program aimed at fulfilling the above objective. Generated experimental results are presented and discussed in Chapter 4. The actual experimental-theoretical correlation is carried out in Chapter 5 where the methodology employed in the course of specializing the general endochronic equations to model the response of this particular composite system is explicitly delineated. It is subsequently shown how certain micro-mechanics considerations can be incorporated into the structure of endochronic equations. The chapter closes with the introduction of a micromechanics-based failure condition, subsequent correlation with the observed ultimate stresses and comparison with other selected criteria. Conclusions and recommendations for further study follow in Chapter 6.

2. ENDROCHRONIC THEORY FOR TRANSVERSELY ISOTROPIC MEDIA

2.1 Introduction

The endochronic constitutive theory was developed by Valanis [79,80] in 1971 to explain certain responses exhibited by ductile metals in the nonlinear range that could not be treated easily and accurately by the various classical plasticity theories. Effects such as formation of hysterisis loops in loading/unloading cycles, cross-hardening in tension due to a prestrain in torsion and vice versa as well as other effects were predicted by Valanis for certain metals with surprising accuracy.

The theory is based on the methodology of irreversible thermodynamics and employs the approach and concepts of the internal variable formalism. Thus the system of constitutive equations governing the response of a given medium is consistent with the thermodynamic constraints. Employment of the Onsager's relations results in the constitutive equations possessing fading memory characteristics with respect to a deformation scale which is assumed to be a property of the material at hand. Thus the name endochronic. The deformation scale can be either time dependent or independent or both so that the classical linear viscoelastic relations are recovered directly as a special case.

Valanis has extended the theory in a series of papers [90-93] where he discusses both the strain and stress formu-

lation, various functional forms of his deformation scale and application to prediction of fracture. However, the explicit derivation of the constitutive equations is limited to isotropic media. An interesting feature of the theory is that the dissipative response of an isotropic medium is governed by two generally independent sets of "hardening" or relaxation/retardation exponents. In particular if a single set of internal variables is chosen to specify the irreversible behavior of the material at hand two characteristic exponents are obtained. In general therefore, the dissipative response in shear will exhibit different "hardening" behavior than that in tension. Consequently, a loose analogy can be drawn with the linearly elastic isotropic material whose response is defined by the two well-known elastic constants. The above is in direct contrast with the classical isotropic plasticity theories in which the decomposition of total strain into elastic and plastic portions together with the definition of a yield surface results in a single hardening exponent.

In what follows the endochronic theory is extended to transversely isotropic media and the dissipative response is shown to be controlled by four independent hardening exponents for the choice of a single set of so-called hidden coordinates as well as for a large number of such variables. In the latter case, a power law representation is possible leading to the above result as will be shown in Chapter 5.

There are however, apparently five independent hardening compliances due to coupling of the four dissipation modes.

2.2 Analytical Development

From the point of view of applying the endochronic theory to the prediction of the response of unidirectional fiber-reinforced composites (modelled as transversely isotropic continuum) it is advantageous to formulate the theory in terms of stresses as one of the sets of independent variables. The evaluation of the various constants in the model ought to be simpler and interpretation easier for the case of off-axis testing since then the loading along the principal material directions remains proportional and only three stress components are present.

Any irreversible process characterized by dissipation of energy is subject to the following laws of thermodynamics: Conservation of Energy and the Dissipation (Clausius-Duhem) Inequality. The first law of thermodynamics in conjunction with the principle of conservation of momentum takes the following form locally:

$$\dot{e} = \frac{\rho_o}{\rho} \sigma_{ij} \dot{\varepsilon}_{ij} - h_{i,i} + Q \qquad (2.1)$$

where

e = internal energy per unit volume

σ_{ij} = stress tensor

ε_{ij} = strain tensor

h_i = heat flux vector entering the body

~~Q = rate of heat absorption~~

ρ_o, ρ = densities of the medium in the undeformed and deformed configurations, respectively.

The dot denotes time derivative, comma differentiation with respect to the spatial coordinates and the above quantities are referred to the undeformed configuration in a rectangular Cartesian coordinate system. The rate of irreversible entropy generation can be expressed as:

$$\theta\dot{\gamma} = \frac{\rho_o}{\rho}\,\sigma_{ij}\dot{\varepsilon}_{ij} + \theta\dot{\eta} - \dot{e} - \frac{1}{\theta}\,h_i\,\theta_{,i} \qquad (2.2)$$

upon employing the first law to eliminate the heat absorption term in the classical definition. In the above

γ = irreversible entropy per unit volume

η = entropy per unit volume

θ = absolute temperature

$\theta_{,i}$ = temperature gradient in the material system

The Clausius-Duhem inequality states that the rate of irreversible entropy generation must be either zero or positive (for reversible or irreversible process, respectively) and so we have the following constraint on all the possible processes that a system can undergo:

$$\dot{\gamma} \geq 0 \qquad (2.3)$$

In the internal variable formalism an assumption is made that the state of a body undergoing an irreversible

process can be specified by a set of independent quantities such as strain, stress or temperature which are presumed measurable as well as a number of internal variables, independent of the observed variables, that control the irreversibilities. For the stress formulation for processes that occur at constant temperature (which will be assumed in the course of this work) it is convenient to define Gibbs' potential in the following manner:

$$G = G\left(\sigma_{ij}, \theta, \sum_{\alpha=1}^{n} q_{ij}^{\alpha}\right) = e - \theta\eta - \sigma_{ij}\varepsilon_{ij} \tag{2.4}$$

where it is assumed that the state of a body undergoing an irreversible process, such as dissipation of energy during deformation caused by various inherent micro-mechanisms (plastic slip, friction, void formation, etc.), can be adequately described by a set of n independent hidden or internal variables q_{ij}^{α}. These variables are assigned tensorial character so that they can be treated along the same lines as stress or strain variables in a consistent manner as discussed by Valanis [79].

Expressing the rate of internal energy in terms of the corresponding elements of Gibbs' potential in Eqn. (2.2), the Clausius-Duhem inequality becomes:

$$\theta\dot{\gamma} = -\left(\varepsilon_{ij}\dot{\sigma}_{ij} + \dot{G} + \eta\dot{\theta} + \frac{1}{\theta} h_i \theta_{,i}\right) \geq 0 \tag{2.5}$$

or since $$\dot{G} = \frac{\partial G}{\partial \sigma_{ij}} \dot{\sigma}_{ij} + \frac{\partial G}{\partial \theta} \dot{\theta} + \sum_{\alpha=1}^{n} \frac{\partial G}{\partial q_{ij}^{\alpha}} \dot{q}_{ij}^{\alpha}$$

we have:

$$\theta\dot{\gamma} = - \left[\left(\varepsilon_{ij} + \frac{\partial G}{\partial \sigma_{ij}} \right) \dot{\sigma}_{ij} + \left(\eta + \frac{\partial G}{\partial \theta} \right) \dot{\theta} + \frac{1}{\theta} h_i \theta_{,i} + \sum_{\alpha=1}^{n} \frac{\partial G}{\partial q_{ij}^{\alpha}} \dot{q}_{ij}^{\alpha} \right] \geq 0 \tag{2.6}$$

Since σ_{ij}, q_{ij}^{α} and θ are independent of each other and since their rates can always be varied independently of the respective total quantities (at least in principle), the following must hold in order to preserve the inequality for an arbitrary process:

$$\varepsilon_{ij} = - \frac{\partial G}{\partial \sigma_{ij}} ,$$

$$\eta = - \frac{\partial G}{\partial \theta} , \tag{2.7}$$

$$- \left(\sum_{\alpha=1}^{n} \frac{\partial G}{\partial q_{ij}^{\alpha}} \dot{q}_{ij}^{\alpha} + \frac{1}{\theta} h_i \theta_{,i} \right) \geq 0$$

In particular, if homothermal fields are assumed as is done in the present study, the last expression reduces to:

$$\theta\dot{\gamma} = - \sum_{\alpha=1}^{n} \frac{\partial G}{\partial q_{ij}^{\alpha}} \dot{q}_{ij}^{\alpha} \geq 0 \tag{2.8}$$

The Clausius-Duhem inequality will certainly be sat-

isfied for all processes if we allow:

$$-\frac{\partial G}{\partial q^{\alpha}_{ij}} = \bar{b}^{\alpha}_{ijk\ell}\,\dot{q}^{\alpha}_{k\ell} \quad \text{(no sum on } \alpha\text{)} \tag{2.9}$$

for each one of the n internal variables where the quantity $\bar{b}^{\alpha}_{ijk\ell}$ is a constant, positive-definite fourth-order tensor in the classical treatment. These are the much-discussed (and controversial) Onsager's relations which relate thermodynamic forces and the subsequent fluxes that characterize the irreversibilities in a linear manner. The dissipation inequality thus becomes:

$$\theta\dot{\gamma} = \sum_{\alpha=1}^{n} \bar{b}^{\alpha}_{ijk\ell}\,\dot{q}^{\alpha}_{ij}\,\dot{q}^{\alpha}_{k\ell} \tag{2.10}$$

Now let us consider time-independent, dissipative deformation processes. In this case the dissipation function must be independent of any change in the time scale, that is, $\dot{\gamma}$ must be homogeneous (of order 1) in $\dot{q}^{\alpha}_{ij}$. This will be satisfied if we let:

$$\bar{b}^{\alpha}_{ijk\ell} = \frac{b^{\alpha}_{ijk\ell}}{\frac{dz}{dt}}$$

where z is some function related to the deformation process at hand. The restriction on z imposed by the dissipation inequality is that dz must be always greater than zero during continuing irreversible deformation.

The point of departure for Valanis' endochronic theory

from other internal variable developments (c.f. Schapery [94]) is the assumption that the function z, called an intrinsic time scale, is a function of material deformation measures ξ or ψ given by

$$\xi = \int \sqrt{p_{ijk\ell}\, d\varepsilon_{ij}\, d\varepsilon_{k\ell}} \ , \quad d\varepsilon \geq 0 \quad : \text{strain formulation}$$

or

$$\psi = \int \sqrt{s_{ijk\ell}\, d\sigma_{ij}\, d\sigma_{k\ell}} \ , \quad d\psi \geq 0 \quad : \text{stress formulation}$$

where the fourth order, positive-definite tensors $p_{ijk\ell}$, $s_{ijk\ell}$ are material parameters reflecting the symmetry of the medium at hand.

The system of equations given by the first two of Eqn. (2.7) and Eqn. (2.9), where the time derivative is now replaced by the intrinsic time scale derivative $\frac{d}{dz}$, characterizes the response of the system during an irreversible process. It remains to specify the form of Gibbs' function about a stable equilibrium state $G_o = G_o(\sigma_{ij},\theta)$ which is commonly done by using quadratic expansion in the hidden variables. This implies that an irreversible process is close to stable equilibrium states that are defined by the potential G_o given only in terms of the measurable or directly controllable quantities. Thus following Valanis we assume that

$$G(\sigma_{ij},\theta,q^{\alpha}_{ij}) = G_o(\sigma_{ij},\theta) + \sum_{\alpha=1}^{n} B^{\alpha}_{ij}\sigma_i q^{\alpha}_j + \frac{1}{2}\sum_{\alpha=1}^{n} C^{\alpha}_{ij} q^{\alpha}_i q^{\alpha}_j \qquad (2.11)$$

where contracted notation has been employed and the matrices B^{α}_{ij}, C^{α}_{ij} are transversely isotropic and assumed constant with the plane of isotropy being 2-3. The requirement of the positive-definite character of incremental work done locally on the material system by an external agency at constant temperature in a reversible manner, i.e., $\delta\sigma_i\delta\varepsilon_j$, q^{α}_i = constant, imposes the following constraint on G_o:

$$\frac{\partial^2 G_o}{\partial\sigma_i\partial\sigma_j}\,\delta\sigma_i\delta\sigma_j \leq 0$$

with the equality holding for $\delta\sigma_i = 0$. Thus the matrix $\frac{\partial^2 G_o}{\partial\sigma_i\partial\sigma_j}$ must be negative-definite. On the other hand, maximization of entropy at a stable equilibrium state requires that:

$$\frac{\partial^2 G}{\partial q^{\alpha}_i \partial q^{\alpha}_j} = C^{\alpha}_{ij} \geq 0$$

where stable equilibrium is defined by $\frac{\partial G}{\partial q^{\alpha}_i} = 0$. At this point, using the above definition as a starting point, the difference between time-dependent response of materials such as viscoelastic materials discussed by Schapery within the internal variable thermodynamic framework and Valanis' theory can be clearly outlined. In the viscoelastic theory, the imposition of the constraint σ_i = const. or ε_i = const. (depending on the material) following an arbitrary defor-

mation history will result in the state of the body approaching the surface $\frac{\partial G}{\partial q_i^\alpha} = 0$ as $t \to \infty$ together with $\dot{q}_i^\alpha \to 0$. Thus stable equilibrium is always associated with the above two conditions. In the endochronic theory the vanishing of the rate of change of internal variables with respect to real time does not imply $\frac{\partial G}{\partial q_i^\alpha} = 0$ since rates are defined with respect to the intrinsic time scale which is tied to a measure of material deformation specified by either ε_{ij} or σ_{ij}. The condition $dz = 0$ on the other hand implies that $q_i^\alpha = \text{const.}$ and thus the rate of entropy production can be zero at any point on the Gibbs' potential and not just on the surface $\frac{\partial G}{\partial q_i^\alpha} = 0$.

In what follows the discussion will be at first restricted to a single tensorial internal variable in the quadratic expansion of Gibbs' potential given by Eqn. (2.11). Subsequently, an extension to the n dimensional case in the internal variables will be briefly discussed in anticipation of the specialization of the developed general endochronic equations aimed at modelling observed response of the Gr/Pi system. This will be carried out explicitly in Chapter 5 where Hashin-type equations for transversely isotropic fibrous composites will be generated with certain unloading features that reduce to anelastic response as a special case. The above decision to begin with the specific

and then generalize the formulation is motivated by notational clarity only.

The above formulation, while still leaving the ensuing constitutive equations sufficiently general, automatically excludes the reduction of the constitutive model to the classical plasticity formulation in its entirety. However, it has already been shown by Valanis that plasticity-like equations can be obtained if a judicious choice of material parameters is made in the strain formulation with a single internal variable. A similar result will be shown to occur in the stress formulation. However the quadratic expansion precludes the existence of a yield surface as will be discussed later. Thus Valanis' statements about "...a viscoplasticity theory without a yield surface..." will become quite clear. This is in direct contrast with Schapery's specialization of the viscoelastic equations to the time-independent case where the existence of a yield point, and thus presumably yield surface for the multi-axial loading case, is assumed.

Substituting the assumed Gibbs' function into the equations of motion given by the first of Eqn. (2.7) and Eqn. (2.9) for the case ϑ = constant the following set of relationships is obtained:

$$\begin{Bmatrix} \varepsilon_1 \\ \varepsilon_2 \\ \varepsilon_3 \end{Bmatrix} = -\begin{Bmatrix} \frac{\partial G_o}{\partial \sigma_1} \\ \frac{\partial G_o}{\partial \sigma_2} \\ \frac{\partial G_o}{\partial \sigma_3} \end{Bmatrix} - \begin{bmatrix} B_{11} & B_{12} & B_{12} \\ B_{12} & B_{22} & B_{23} \\ B_{12} & B_{23} & B_{22} \end{bmatrix} \begin{Bmatrix} q_1 \\ q_2 \\ q_3 \end{Bmatrix} \qquad (2.12)$$

$$\begin{Bmatrix} \varepsilon_4 \\ \varepsilon_5 \\ \varepsilon_6 \end{Bmatrix} = -\begin{Bmatrix} \frac{\partial G_o}{\partial \sigma_4} \\ \frac{\partial G_o}{\partial \sigma_5} \\ \frac{\partial G_o}{\partial \sigma_6} \end{Bmatrix} - \begin{bmatrix} \frac{1}{2}(B_{22}-B_{23}) & 0 & 0 \\ 0 & B_{66} & 0 \\ 0 & 0 & B_{66} \end{bmatrix} \begin{Bmatrix} q_4 \\ q_5 \\ q_6 \end{Bmatrix} \qquad (2.13)$$

And:

$$\begin{bmatrix} b_{11} & b_{12} & b_{12} \\ b_{11} & b_{22} & b_{23} \\ b_{12} & b_{23} & b_{22} \end{bmatrix} \begin{Bmatrix} \frac{dq_1}{dz} \\ \frac{dq_2}{dz} \\ \frac{dq_3}{dz} \end{Bmatrix} + \begin{bmatrix} C_{11} & C_{12} & C_{12} \\ C_{12} & C_{22} & C_{23} \\ C_{12} & C_{23} & C_{22} \end{bmatrix} \begin{Bmatrix} q_1 \\ q_2 \\ q_3 \end{Bmatrix}$$

$$= -\begin{bmatrix} B_{11} & B_{12} & B_{12} \\ B_{12} & B_{22} & B_{23} \\ B_{12} & B_{23} & B_{22} \end{bmatrix} \begin{Bmatrix} \sigma_1 \\ \sigma_2 \\ \sigma_3 \end{Bmatrix} \qquad (2.14)$$

$$\begin{bmatrix} \frac{1}{2}(b_{22}-b_{23}) & 0 & 0 \\ 0 & b_{66} & 0 \\ 0 & 0 & b_{66} \end{bmatrix} \begin{Bmatrix} \frac{dq_4}{dz} \\ \frac{dq_5}{dz} \\ \frac{dq_6}{dz} \end{Bmatrix} + \begin{bmatrix} \frac{1}{2}(C_{22}-C_{23}) & 0 & 0 \\ 0 & C_{66} & 0 \\ 0 & 0 & C_{66} \end{bmatrix} \begin{Bmatrix} q_4 \\ q_5 \\ q_6 \end{Bmatrix}$$

$$= - \begin{bmatrix} \frac{1}{2}(B_{22}-B_{23}) & 0 & 0 \\ 0 & B_{66} & 0 \\ 0 & 0 & B_{66} \end{bmatrix} \begin{Bmatrix} \sigma_4 \\ \sigma_5 \\ \sigma_6 \end{Bmatrix} \tag{2.15}$$

Equations (2.15) are already decoupled and so we can solve directly for q_4, q_5 and q_6 in terms of σ_4, σ_5 and σ_6 and substitute into Equations (2.13) to obtain shear strains in terms of shear stresses. Carrying this out explicitly we obtain:

$$\begin{aligned} \varepsilon_4 &= - \frac{\partial G_0}{\partial \sigma_4} + \int_0^z E \cdot \sigma_4(z') e^{-\lambda_4(z-z')} \, dz' \\ \varepsilon_5 &= - \frac{\partial G_0}{\partial \sigma_5} + \int_0^z F \cdot \sigma_5(z') e^{-\lambda_5(z-z')} \, dz' \\ \varepsilon_6 &= - \frac{\partial G_0}{\partial \sigma_6} + \int_0^z F \cdot \sigma_6(z') e^{-\lambda_6(z-z')} \, dz' \end{aligned} \tag{2.16}$$

where

$$\lambda_4 = \frac{C_{22}-C_{23}}{b_{22}-b_{23}}$$

$$\lambda_5 = \lambda_6 = \frac{C_{66}}{b_{66}}$$

$$E = \frac{1}{2}\,\frac{(B_{22}-B_{23})^2}{b_{22}-b_{23}}$$

$$F = \frac{(B_{66})^2}{b_{66}}$$

From the above it is seen that the hardening characterisitcs of the material along the principal material directions in shear are generally governed by two different exponents λ_4 and λ_5 which reflect different dissipation modes. In order to obtain the strain response in longitudinal and transverse tension it is necessary to uncouple Equations (2.14), that is to find the normal modes. In the isotropic case this is easily accomplished, as illustrated by Valanis, by decomposing strains and stresses into deviatoric and dilatational portions. For the transversely isotropic situation we proceed by first defining the following quantities:

$$\begin{aligned}
\bar{q}_1 &= q_1 \qquad \Rightarrow \hat{\bar{q}}_1 = \hat{q}_1\,, \qquad \bar{\sigma}_1 = \sigma_1 \\
\bar{q}_2 &= q_2 + q_3 \Rightarrow \hat{\bar{q}}_2 = \hat{q}_2 + \hat{q}_3\,, \quad \bar{\sigma}_2 = \sigma_2 + \sigma_3 \\
\bar{q}_3 &= q_2 - q_3 \Rightarrow \hat{\bar{q}}_3 = \hat{q}_2 - \hat{q}_3\,, \quad \bar{\sigma}_3 = \sigma_2 - \sigma_3
\end{aligned} \tag{2.17}$$

where the symbol "^" signifies derivative with respect to z.

Now, adding the third of Equations (2.14) to the second and rewriting the result in terms of the newly defined quantities together with the first yields the following set:

$$\begin{bmatrix} b_{11} & b_{12} \\ 2b_{12} & (b_{22}+b_{23}) \end{bmatrix} \begin{Bmatrix} \hat{\bar{q}}_1 \\ \hat{\bar{q}}_2 \end{Bmatrix} + \begin{bmatrix} C_{11} & C_{12} \\ 2C_{12} & (C_{22}+C_{23}) \end{bmatrix} \begin{Bmatrix} \bar{q}_1 \\ \bar{q}_2 \end{Bmatrix} = - \begin{bmatrix} B_{11} & B_{12} \\ 2B_{12} & (B_{22}+B_{23}) \end{bmatrix} \begin{Bmatrix} \bar{\sigma}_1 \\ \bar{\sigma}_2 \end{Bmatrix} \tag{2.18}$$

On the other hand, subtracting the third of Equations (2.14) from the second yields directly in the new notation:

$$(b_{22}-b_{23})\hat{\bar{q}}_3 + (C_{22}-C_{23})\bar{q}_3 = -(B_{22}-B_{23})\bar{\sigma}_3 \tag{2.19}$$

which can be integrated readily to produce:

$$\bar{q}_3 = - \int_0^z \frac{(B_{23}-B_{23})}{(b_{22}-b_{23})} \bar{\sigma}_3(z') e^{-\lambda_3(z-z')} \, dz' \tag{2.20}$$

where

$$\lambda_3 = \frac{(C_{22}-C_{23})}{(b_{22}-b_{23})} = \lambda_4$$

In this way the problem has been reduced to uncoupling a system of two instead of three equations. Now, the dissipation matrix in Equations (2.18) can be inverted to yield:

$$\begin{Bmatrix} \hat{\bar{q}}_1 \\ \hat{\bar{q}}_2 \end{Bmatrix} + \begin{bmatrix} C^*_{11} & C^*_{12} \\ C^*_{21} & C^*_{22} \end{bmatrix} \begin{Bmatrix} \bar{q}_1 \\ \bar{q}_2 \end{Bmatrix} = - \begin{bmatrix} B^*_{11} & B^*_{12} \\ B^*_{21} & B^*_{22} \end{bmatrix} \begin{Bmatrix} \bar{\sigma}_1 \\ \bar{\sigma}_2 \end{Bmatrix} \tag{2.21}$$

where

$$C_{11}^* = \left(\frac{1}{b_{11}(b_{22}+b_{23})-2b_{12}^2}\right)\cdot[C_{11}(b_{22}+b_{23})-2C_{12}b_{12}]$$

$$C_{12}^* = \left(\frac{1}{b_{11}(b_{22}+b_{23})-2b_{12}^2}\right)\cdot[C_{12}(b_{22}+b_{23})-(C_{22}+C_{23})b_{12}]$$

$$C_{21}^* = \left(\frac{1}{b_{11}(b_{22}+b_{23})-2b_{12}^2}\right)\cdot[2C_{12}b_{11}-2C_{11}b_{12}] \qquad (2.22)$$

$$C_{22}^* = \left(\frac{1}{b_{11}(b_{22}+b_{23})-2b_{12}^2}\right)\cdot[(C_{22}+C_{23})b_{11}-2C_{12}b_{12}]$$

with similar expressions for the matrix $[B^*]$.

The solution of the above system of equations can be obtained in a straight forward fashion in terms of the normal modes $\bar{y}_1$, $\bar{y}_2$ of $\{q\}$ as follows: define $\{\bar{q}\} = [P]\{\bar{y}\}$

$$[P]\{\hat{\bar{y}}\} + [C^*][P]\{\bar{y}\} = -[B^*]\{\bar{\sigma}\}$$

or $$\{\hat{\bar{y}}\} + [P]^{-1}[C^*][P]\{\bar{y}\} = -[P]^{-1}[B^*]\{\bar{\sigma}\} \qquad (2.23)$$

where $[P]^{-1}[C^*][P] = [\Lambda]$ = diagonal matrix.

The elements of the matrix $[\Lambda]$ are the eigenvalues of $[C^*]$ and are obtained from the determinantal equation:

$$\begin{vmatrix} C_{11}^*-\lambda & C_{12}^* \\ C_{21}^* & C_{22}^*-\lambda \end{vmatrix} = 0$$

Solving for the roots we obtain:

$$\lambda_1 = \frac{1}{2}\left|(C_{11}^*+C_{22}^*) - \sqrt{(C_{11}^*-C_{22}^*)^2+4C_{12}^*C_{21}^*}\right|$$

$$\lambda_2 = \frac{1}{2}\left|(C_{11}^*+C_{22}^*) + \sqrt{(C_{11}^*-C_{22}^*)^2+4C_{12}^*C_{21}^*}\right| \qquad (2.24)$$

The normalized eigenvector matrix [P] is taken in the following form:

$$[P] = \begin{vmatrix} 1 & \alpha_2 \\ \alpha_1 & 1 \end{vmatrix} \tag{2.25}$$

where

$$\alpha_1 = - \frac{(C^*_{11}-\lambda_1)}{C^*_{12}}$$

$$\alpha_2 = - \frac{(C^*_{22}-\lambda_2)}{C^*_{21}} = - \frac{C^*_{12}}{C^*_{21}} \alpha_1 \tag{2.26}$$

We note here that the above choice of the eigenvalues and eigenvectors will reduce the resulting endochronic equations to the isotropic form with $\alpha_1 = 2$, $\alpha_2 = -1$ as will be illustrated. Any other combination will yield results which do not appear to be reducible to the above special case.

Solving explicitly for the normal modes we obtain:

$$\bar{y}_1 = - \frac{1}{1-\alpha_1\alpha_2} \cdot \int_0^z [(B^*_{11}-\alpha_2 B^*_{21})\bar{\sigma}_1(z')+(B^*_{12}-\alpha_2 B^*_{22})\bar{\sigma}_2(z')]e^{-\lambda_1(z-z')}dz'$$

$$\bar{y}_2 = - \frac{1}{1-\alpha_1\alpha_2} \cdot \int_0^z [(B^*_{21}-\alpha_1 B^*_{11})\bar{\sigma}_1(z')+(B^*_{22}-\alpha_1 B^*_{12})\bar{\sigma}_2(z')]e^{-\lambda_2(z-z')}dz' \tag{2.27}$$

The superposition of the normal modes using the eigenvector matrix given by Equation (2.25) results in:

$$\bar{q}_1 = \bar{y}_1 + \alpha_2 \bar{y}_2$$

$$\bar{q}_2 = \alpha_1 \bar{y}_1 + \bar{y}_2$$

or, upon inverting the definitions given by Equations (2.17) we obtain:

$$\begin{aligned} q_1 &= \bar{y}_1 + \alpha_2 \bar{y}_2 \\ q_2 &= \tfrac{1}{2}[\alpha_1 \bar{y}_1 + \bar{y}_2 + \bar{q}_3] \\ q_3 &= \tfrac{1}{2}[\alpha_1 \bar{y}_1 + \bar{y}_2 - \bar{q}_3] \end{aligned} \tag{2.28}$$

where $\bar{q}_3$ is given by Equation (2.20).

Substituting the above relations into the expressions for strains given by Equations (2.12) we obtain the following set of equations:

$$\begin{aligned} \varepsilon_1 &= -\frac{\partial G_0}{\partial \sigma_1} - (B_{11}+B_{12}\alpha_1)\bar{y}_1 - (B_{12}+B_{11}\alpha_2)\bar{y}_2 \\ \varepsilon_2 &= -\frac{\partial G_0}{\partial \sigma_2} - [B_{12} + \tfrac{1}{2}(B_{22}+B_{23})\alpha_1]\bar{y}_1 \\ &\quad - [B_{12}\alpha_2 + \tfrac{1}{2}(B_{22}+B_{23})]\bar{y}_2 - \tfrac{1}{2}(B_{22}-B_{23})\bar{q}_3 \\ \varepsilon_3 &= -\frac{\partial G_0}{\partial \sigma_3} - [B_{12} + \tfrac{1}{2}(B_{22} + B_{23})\alpha_1]\bar{y}_1 \\ &\quad - [B_{12}\alpha_2 + \tfrac{1}{2}(B_{22} + B_{23}]\bar{y}_2 + \tfrac{1}{2}(B_{22} - B_{23})\bar{q}_3 \end{aligned} \tag{2.29}$$

The above formulation helps to bring forth the extent of coupling of the normal modes and their effect on the ensuing expressions for the normal strains. Combining Equ-

ations (2.27) with the above and rearranging yields the following results:

$$\varepsilon_1 = -\frac{\partial G_0}{\partial \sigma_1} + \int_0^z \bar{B}_{11}(z-z')\sigma_1(z')\,dz' + \int_0^z \bar{B}_{12}(z-z')[\sigma_2(z')+\sigma_3(z')]\,dz'$$

$$\varepsilon_2 = -\frac{\partial G_0}{\partial \sigma_2} + \int_0^z \bar{B}_{21}(z-z')\sigma_1(z')\,dz' + \int_0^z \bar{B}_{22}(z-z')\sigma_2(z')\,dz' + \int_0^z \bar{B}_{23}(z-z')\sigma_3(z')\,dz'$$

$$\varepsilon_3 = -\frac{\partial G_0}{\partial \sigma_3} + \int_0^z \bar{B}_{21}(z-z')\sigma_1(z')\,dz' + \int_0^z \bar{B}_{23}(z-z')\sigma_2(z')\,dz' + \int_0^z \bar{B}_{22}(z-z')\sigma_3(z')\,dz' \qquad (2.30)$$

where:

$$\bar{B}_{11}(z-z') = \left(\frac{1}{1-\alpha_1\alpha_2}\right)\cdot\left\{(B^*_{11}-B^*_{21}\alpha_2)\cdot(B_{11}+B_{12}\alpha_1)e^{-\lambda_1(z-z')} + (B^*_{21}-B^*_{11}\alpha_1)\cdot(B_{11}\alpha_2+B_{12})e^{-\lambda_2(z-z')}\right\}$$

$$\bar{B}_{12}(z-z') = \left(\frac{1}{1-\alpha_1\alpha_2}\right)\cdot\left\{(B^*_{12}-B^*_{22}\alpha_2)\cdot(B_{11}+B_{12}\alpha_1)e^{-\lambda_2(z-z')} + (B^*_{22}-B^*_{12}\alpha_1)\cdot(B_{11}\alpha_2+B_{12})e^{-\lambda_2(z-z')}\right\}$$

$$\bar{B}_{21}(z-z') = \left\{(B^*_{11}-B^*_{21}\alpha_2)\cdot[B_{12} + \tfrac{1}{2}(B_{22}+B_{23})\alpha_1]e^{-\lambda_1(z-z')}\right\}$$

$$+ (B^*_{21}-B_{11}\alpha_1)\cdot[B_{12}\alpha_2 + \tfrac{1}{2}(B_{22}+B_{23})]e^{-\lambda_2(z-z')}\Big\}$$

$$\cdot\left(\frac{1}{1-\alpha_1\alpha_2}\right)$$

$$\bar{B}_{22}(z-z') = \left\{B^*_{12}-B^*_{22}\alpha_2)\cdot[B_{12} + \tfrac{1}{2}(B_{22}+B_{23})\alpha_1]e^{-\lambda_1(z-z')}\right.$$

$$+ (B^*_{22}-B^*_{12}\alpha_1)\cdot[B_{12}\alpha_2 + \tfrac{1}{2}(B_{22}+B_{23}]e^{-\lambda_2(z-z')}\Big\}$$

$$\cdot\left(\frac{1}{1-\alpha_1\alpha_2}\right) + \frac{\frac{1}{2}(B_{22}-B_{23})^2}{(b_{22}-b_{23})}\, e^{-\lambda_3(z-z')}$$

$$\bar{B}_{23}(z-z') = \left\{(B^*_{12}-B^*_{22}\alpha_2)\cdot[B_{12} + \tfrac{1}{2}(B_{22}+B_{23})\alpha_1]e^{-\lambda_1(z-z')}\right.$$

$$+ (B^*_{22}-B^*_{12}\alpha_1)\cdot[B_{12}\alpha_2 + \tfrac{1}{2}(B_{22}+B_{23})]e^{-\lambda_2(z-z')}\Big\}$$

$$\cdot\left(\frac{1}{1-\alpha_1\alpha_2}\right) + \frac{\frac{1}{2}(B_{22}-B_{23})^2}{(b_{22}-b_{23})}\, e^{-\lambda_3(z-z')} = \bar{B}_{32}(z-z') \tag{2.31}$$

and where the elements B^*_{ij}'s have the same form as C^*_{ij}'s given by Eqations (2.22).

An interesting consequence of the above formulation is an apparent loss of transverse isotropy manifested by the expressions for $\bar{B}_{12}(z-z')$ and $\bar{B}_{21}(z-z')$ which are not immediately identical. In order to preserve transverse isotropy a constraint must be imposed by equating the corresponding coefficients of the eigenfunctions $e^{-\lambda_1(z-z')}$

and $e^{-\lambda_2(z-z')}$ in the expressions for $\bar{B}_{12}(z-z')$ and $\bar{B}_{21}(z-z')$. The transverse isotropy conditions thus become:

$$(B^*_{12}-B^*_{22}\alpha_2)\cdot(B_{11}+B_{12}\alpha_1) = (B^*_{11}-B^*_{21}\alpha_2)\cdot[B_{12} + \tfrac{1}{2}(B_{22}+B_{23})\alpha_1]$$

and (2.32)

$$(B^*_{22}-B^*_{12}\alpha_1)\cdot(B_{11}\alpha_2+B_{12}) = (B^*_{21}-B^*_{11}\alpha_1)\cdot[B_{12}\alpha_2 + \tfrac{1}{2}(B_{22}+B_{23})]$$

Substitution of the expressions for the elements B^*_{ij} given in terms of B_{ij} and b_{ij} in the above yields two identical sets of requirements for the preservation of transverse isotropy of the type:

$$\left[2B_{12}^2-B_{11}(B_{22}+B_{23})\right]\cdot\left[b_{12}+\left(\frac{b_{22}+b_{23}}{2}\right)\alpha_1+b_{11}\alpha_2+b_{12}\alpha_1\alpha_2\right] = 0$$

from which two conditions are obtained:

$$2B_{12}^2 - B_{11}(B_{22}+B_{23}) = 0 \qquad (2.33)$$

or

$$b_{12} + \frac{(b_{22}+b_{23})}{2}\alpha_1 + b_{11}\alpha_2 + b_{12}\alpha_1\alpha_2 = 0 \qquad (2.34)$$

The first condition apparently corresponds to the vanishing of the determinant

$$\begin{vmatrix} B_{11} & B_{12} \\ 2B_{12} & (B_{22}+B_{23}) \end{vmatrix}$$

which implies that the imposition of the stress state $\begin{Bmatrix}\sigma_1\\ \sigma_2\end{Bmatrix}$ effectively uncouples dissipation and mechanical stresses as seen in Equations (2.18). This is somewhat similar to the assumption of plastic incompressibility and consequently absence of plastic work in the presence of hydro-

static stresses that is used in the classical plasticity theories for isotropic media. In this formulation however, the above condition is not a necessary one, being merely a possibility.

On the other hand, substitution of the expression for α_1 and α_2 given by Equations (2.26) in the second condition together with the use of Equations (2.22) can be shown to satisfy it identically. The formulation thus appears to be internally consistent in that the transverse isotropy of the ensuing stress-strain response is preserved under all loading conditions.

Employing the equivalent transverse isotropy relations given by Equations (2.23) in Equations (2.31) we can express the kernels of the memory integrals as follows:

$$\begin{aligned}
\bar{B}_{11}(z-z') &= Ae^{-\lambda_1(z-z')} + Be^{-\lambda_2(z-z')} \\
\bar{B}_{12}(z-z') &= Ce^{-\lambda_1(z-z')} + De^{-\lambda_2(z-z')} \\
\bar{B}_{22}(z-z') &= \frac{C^2}{A} e^{-\lambda_1(z-z')} + \frac{D^2}{B} e^{-\lambda_2(z-z')} + Ee^{-\lambda_3(z-z')} \\
\bar{B}_{23}(z-z') &= \frac{C^2}{A} e^{-\lambda_1(z-z')} + \frac{D^2}{B} e^{\lambda_2(z-z')} - Ee^{-\lambda_3(z-z')}
\end{aligned} \tag{2.35}$$

where:

$$A = \frac{1}{\gamma}\cdot\left\{[B_{11}(b_{22}+b_{23}) - 2B_{12}b_{12}] - [2B_{12}b_{11} - 2B_{11}b_{12}]\alpha_2\right\}$$
$$\cdot(B_{11} + B_{12}\alpha_1)$$

$$B = \frac{1}{\gamma}\cdot\left\{[2B_{12}b_{11} - 2B_{11}b_{12}] - [B_{11}(b_{22}+b_{23}) - 2B_{12}b_{12}]\alpha_1\right\}$$
$$\cdot(B_{12} + B_{11}\alpha_2)$$

$$C = \frac{1}{\gamma}\cdot\left\{[B_{11}(b_{22} + b_{23}) - 2B_{12}b_{12}] - [2B_{12}b_{11} - 2B_{11}b_{12}]\alpha_2\right\}$$
$$\cdot[B_{12} + \tfrac{1}{2}(B_{22} + B_{12})\alpha_1] \qquad (2.36)$$

$$D = \frac{1}{\gamma}\cdot\left\{[2B_{12}b_{11} - 2B_{11}b_{12}] - [B_{11}(b_{22}+b_{23}) - 2B_{12}b_{12}]\alpha_1\right\}$$
$$\cdot[B_{12}\alpha_2 + \tfrac{1}{2}(B_{22} + B_{23})]$$

$$E = \tfrac{1}{2}(B_{22} - B_{23})^2/(b_{22} - b_{23})$$

and $$\gamma = \frac{1}{(1-\alpha_1\alpha_2)[b_{11}(b_{22}+b_{23}) - 2b_{12}^2]}$$

The set of equations given by Equations (2.16), (2.30), and (2.35) completely specifies the response of a transversely isotropic medium undergoing an irreversible deformation process. As is evident, the dissipative response is characterized by four independent retardation or "hardening" exponents and considerable coupling is present in the general transversely isotropic model. The contribution of each element of the matrix [B] and [b] to the coupling is clearly delineated in the above expressions. The coefficients A, B, C, D, E, and F of the eigenfunctions

that characterize the four independent dissipation modes comprise a total of six apparently independent constants. The three normal modes represented by λ_1, λ_2 and λ_3 are coupled by five of these constants in the expressions for $B_{11}(z)$, $B_{12}(z)$, $B_{22}(z)$ and $B_{23}(z)$ in such a way that these compliances are apparently independent. No apparent relationship between the coefficients A, B, C, D and E appears to be available.

2.3 Specialization to Isotropic Media

The developed set of constitutive equations can be readily reduced to the fully isotropic case by making use of the following identities:

$$B_{11} = B_{22}\,, \qquad B_{12} = B_{23}\,, \qquad B_{44} = \tfrac{1}{2}(B_{11} - B_{12})$$

with similar relationships for the elements C_{ij} and b_{ij}. Making use of the above we obtain the following relationships between C^*_{11}, C^*_{22}, C^*_{12} and C^*_{21} from Equations (2.22):

$$C^*_{11} - C^*_{22} = -C^*_{12}, \quad C^*_{21} = 2C^*_{12} \tag{2.37}$$

The expressions for the eigenvalues thus reduce to:

$$\lambda_{1,2} = \tfrac{1}{2}!(C^*_{11} + C^*_{22}1 \mp 3(C^*_{11} - C^*_{22})1 \tag{2.38}$$

so that the eigenvectors α_1 and α_2 given by the Equations (2.26) are now

$$\alpha_1 = -\frac{(C^*_{11} - \lambda_1)}{C^*_{12}} = -\frac{(C^*_{11} - 2C^*_{22} + C^*_{11})}{C^*_{12}} = 2$$

and (2.39)

$$\alpha_2 = -\frac{(C^*_{22} - \lambda_2)}{C^*_{21}} = -\frac{(C^*_{22} - 2C^*_{11} + C^*_{22})}{C^*_{21}} = -1$$

It can be easily verified that the transverse isotropy condition given by Equation (2.34) is identically satisfied by the above eigenvectors. The eigenvalues take on the following form upon substituting the simplified expressions for C^*_{11} and C^*_{22} in terms of C_{ij} and b_{ij}.

$$\lambda_1 = \left(\frac{C_{11} + 2C_{12}}{b_{11} + 2b_{12}}\right)$$

$$\lambda_2 = \left(\frac{C_{11} - C_{12}}{b_{11} - b_{12}}\right) = \lambda_3 \qquad (2.40)$$

These are the same as those obtained by Valanis [79] in his isotropic treatment and can be readily obtained through decomposition of stresses and strains as well as the internal variables into deviatoric and dilatational components. The kernels of the memory on the other hand become:

$$\bar{B}_{11}(z-z') = \frac{(B_{11}+2B_{12})^2}{3(b_{11}+2b_{12})} e^{-\lambda_1(z-z')} + \frac{2(B_{11}-B_{12})^2}{3(b_{11}-b_{12})} e^{-\lambda_2(z-z')}$$

$$\bar{B}_{12}(z-z') = \frac{(B_{11}+2B_{12})^2}{3(b_{11}+2b_{12})} e^{\lambda_1(z-z')} - \frac{(B_{11}-B_{12})^2}{3(b_{11}-b_{12})} e^{-\lambda_2(z-z')}$$

which again corresponds with Valanis' results.

2.4 Endochronic Theory and Plasticity

It has already been mentioned that a quadratic expansion of Gibbs' potential in terms of the internal variables about the equilibrium potential $G_0(\sigma_i,\theta)$ precludes rigorous reduction of the ensuing equations to the plasticity formulation. This can be easily shown as follows. In the classical plasticity formulation the total strain increment is assumed separable into two well-defined portions, fully recoverable (elastic) and permanent (plastic) increment. The plastic portion is usually associated with a yield surface through a normality condition. In terms of the thermodynamic internal variable formulation therefore there ought to be portions of Gibbs' potential on which the measurable quantities, in this case the stresses, could be varied in a reversible manner. That is, paths for which $\partial G/\partial q_i^\alpha = 0$ should be possible at any point of loading within and past the initial yield surface. The yield surface(s) are then represented by the conditions $\partial^2 G/\partial q_i^\alpha \partial q_j^\alpha = 0$ which denote neutral equilibrium states. The plastic deformation process would thus entail a sequence of alternating stable-unstable states described by local fluctuations in the Gibbs' potential about some mean or "hardening" state. Similar point of view has been taken by Ponter, Bataille and Kestin [95] in their description of the Frank-Read dis-

location generation mechanism using the internal variable approach.

It is clearly evident that a quadratic expansion cannot satisfy the above conditions in a nontrivial manner and so the total strain cannot be decomposed into elastic and plastic portions. Thus a well defined yield surface associated with certain regions of Gibbs' potential does not exist in this formulation if the outlined conditions are accepted as necessary for a reversible process.

On the other hand, plasticity-like equations, not associated with a yield condition, can be obtained in the stress formulation by setting the matrix [C] to zero. In such a case, the increments in the internal variables are proportional to the total stresses and so we have

$$d\varepsilon = d\left(\frac{\partial G_0}{\partial \sigma}\right) + \frac{B^2}{b}\,\sigma\,dz$$

for the one dimensional treatment. If G_0 is quadratic in stresses the above becomes

$$d\varepsilon = Ad\sigma + \frac{B^2}{b}\,\sigma\,dz$$

The above equation will be identical to Valanis' reduction of his strain formulation [79] to illustrate the relationship of the endochronic theory with classical plasticity formulation if the intrinsic time scale is expressed in terms of the strain measure given by

$$\xi = \int \sqrt{P_{ijk\ell} d\varepsilon_{ij} d\varepsilon_{k\ell}} \ .$$

On the other hand if the stress measure

$$\eta = \int \sqrt{S_{ijk\ell} d\sigma_{ij} d\sigma_{k}}$$

is employed in the intrinsic time scale then the fading memory character of the ensuing equations is lost. This will then preclude the generation of hysteresis loops during cyclic loading for the case $[C] \equiv [0]$ if the same time scale is employed throughout the entire deformation path.

2.5 Extension to Multi-Internal Variable Formulation

Extension of the endochronic formulation to multi-internal variable treatment is now quite straightforward since Equations (2.14) and (2.15) are solved independently for each set of internal variables specified by α. On the other hand, the second part of Equations (2.12) and (2.13) involves summation of each q_{ij}^{α} so that Equation (2.35) remains valid for every α as well. Generalizing Equation (2.35) we thus have

$$\bar{B}_{11}(z-z') = \sum_{\alpha=1}^{n} \left[A^{\alpha} e^{-\lambda_1^{\alpha}(z-z')} + B^{\alpha} e^{-\lambda_2^{\alpha}(z-z')} \right]$$

with similar expressions for the remaining kernels.

3. Experimental Technique

3.1 Introduction

Verification of the applicability of any constitutive theory to a particular material system is based on a set of experiments in which both the state of stress and strain are known with sufficient accuracy at the point of measurement. The most widely used testing technique is the tension test which allows the determination of Young's modulus, E_{xx}, and Poisson's ratio, ν_{xy}, with respect to the longitudinal axis of a coupon from a single experiment. For linearly elastic isotropic materials this is sufficient to determine the remaining constants. In the case of transversely isotropic, linearly elastic materials such as linearly elastic fibrous composites however, additional tests are required since the material response is described in terms of five independent parameters. Four of these parameters, a sufficient number for plane stress applications, can still be obtained from the tension test; however three different specimen orientations are required to accomplish this. The two Young's moduli E_{11}, E_{22} associated with the principal material directions (refer to Fig. 3.1) along with either ν_{12} or ν_{21} are obtained from tensile coupons with fibers aligned parallel and perpendicular to the load axis, respectively. The fourth independent material constant, the shear modulus G_{12} can be obtained from the so-called "off-axis tension

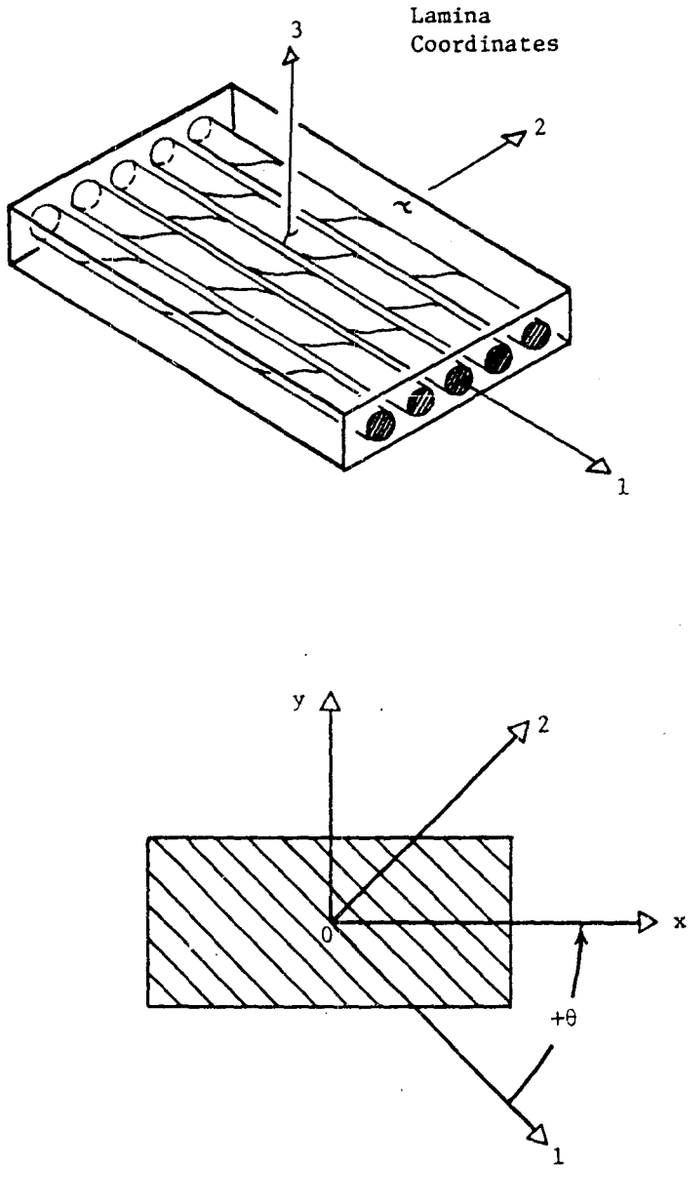

1, 2, 3 lamina coordinates

x, y, z laminate coordinates

Fig. 3.1 Lamina geometry and the associated coordinate systems

test" (see Fig. 3.2) as proposed by Chamis [96]. The alternative method of determining G_{12} is from a pure torsion test of thin-walled tubes with fibers wound either parallel or perpendicular to the torsion axis. Such a direct procedure, while being very desirable, can be prohibitive due to either excessive cost or technological difficulties associated with fabrication of such tubes.

The off-axis tension test can also be used to study the material response of a composite system in the nonlinear range. However, a single off-axis configuration such as the 10° off-axis coupon is often not sufficient to determine the pure nonlinear shear response. This is due to the possibility of various stress interactions taking place in the nonlinear range at the micro-level caused by the presence of three stress components along the principle material directions. Foye [56] for example demonstrated the influence of the transverse normal stress component on the shear strain response (and vice versa) along the material axes for composites with stiff, linearly elastic fibers and ductile matrices using a finite-element, micromechanical analysis. He showed that for combined normal-shear loading in a fixed ratio yielding initiated sooner and the extent of inelastic behavior was more pronounced than for either normal or shear stress acting alone (Fig. 3.3). Even in the case of less ductile matrices, the possibility of damage accumulation in the form of stable micro-crack evolution, crazing, etc.

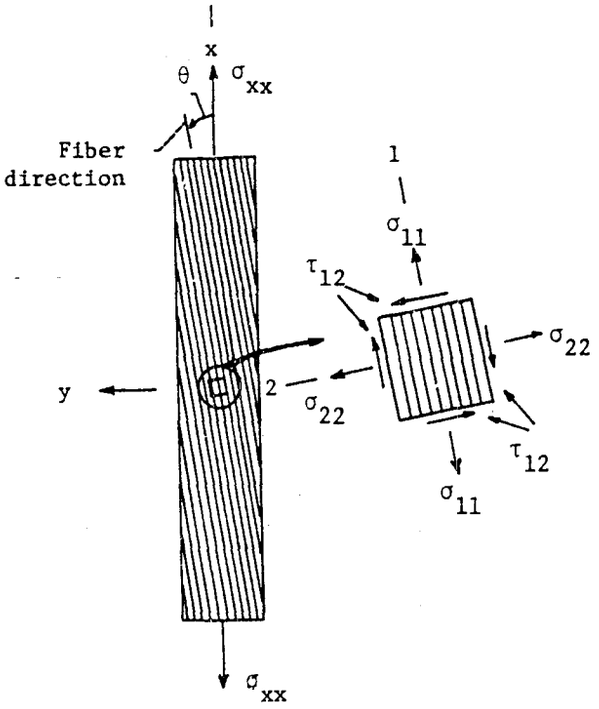

A) An off-axis tension test configuration

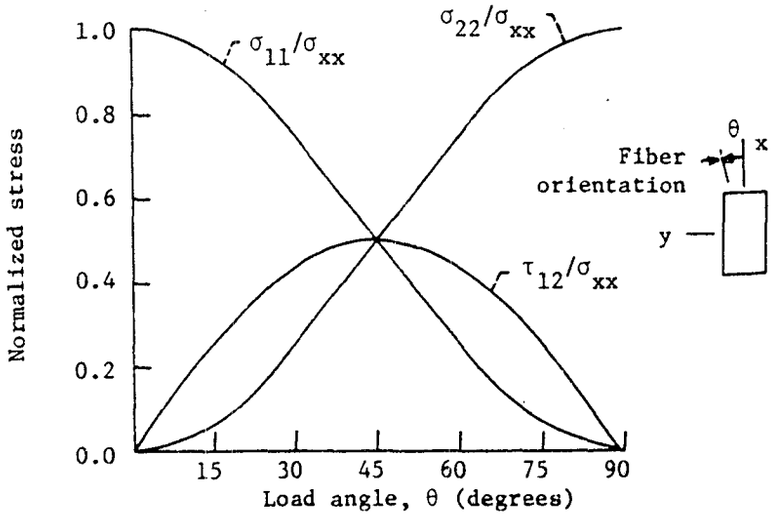

B) Resolved stress components in the lamina coordinate system

Fig. 3.2 An off-axis tension test configuration and the corresponding resolved stress components

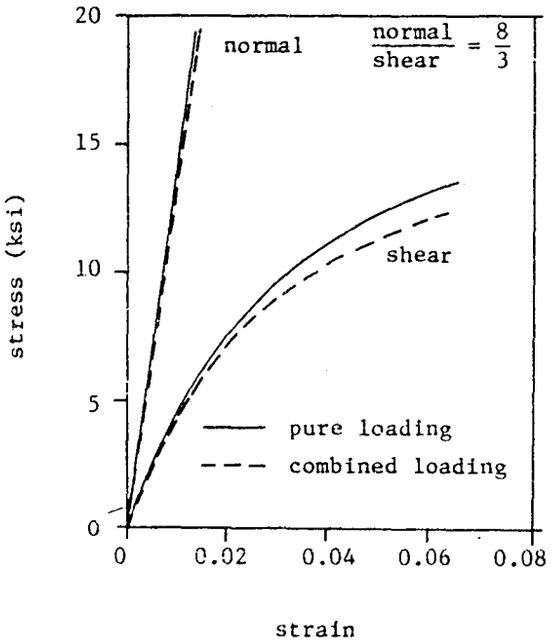

Fig. 3.3 Stress-strain curves for unidirectional Boron/Epoxy (50% fiber volume fraction) under combined loads, Ref. [56]

resulting in stress interaction cannot be overlooked.

In view of the above observations, a set of experiments on nine off-axis Gr/Pi coupon configurations including the 0° and 90° orientations was designed. The main objectives were extensive characterization of the room-temperature response of the Gr/Pi system for laminate type analysis including the extent of stress interaction in the nonlinear range, and subsequent correlation of the experimental results with the developed set of endochronic equations for transversely isotropic media as well as the possibility of deducing pure nonlinear shear response from the off-axis tests.

The test matrix is given in Table 3.1. In order to determine the type of nonlinearity exhibited by the system and thus the applicability of the endochronic theory, loading/unloading/reloading cycles at various stress levels were also included. All tests were carried out at a strain rate of 0.01 in/in/min and the possibility of time dependent response was not considered.

3.2 Test Method

In the tension test the strain is determined with the help of an electronic transducer such as a strain gage bonded to the coupon, whereas the stress response is obtained from a load cell which is an integral part of the testing machine. The load cell yields the force at any given stage of deformation which must be subsequently con-

Table 3.1 Test matrix for the Gr/Pi off-axis coupons

Fiber orientation with respect to the load axis	Type of loading (# coupons)	
	Monotonic	Cyclic
0°	3	3
5°	3	3
10°	4	3
15°	3	3
30°	3	2
45°	3	2
60°	3	2
75°	3	—
90°	3	—

verted to stress acting at the point where the strain gage is located. If the strain and thus stress field is homogeneous across the coupon at the location of the strain gage, then stress at that point is equivalent to average stress which is simply force divided by cross-sectional area of the specimen. The design of the tensile coupon as well as the gripping arrangement must therefore be such as to induce a homogeneous state of strain in the plane across the location of the strain gage.

In the case of isotropic materials the above is easily accomplished by using tapered geometries of tensile coupons to minimize perturbations in homogeneous strain field caused by the grips. The success of the method can be traced to the symmetry as well as fast rate of decay of these perturbations about loading axis of the specimen which in turn is a consequence of the specimen's isotropy.

In the case of off-axis, transversely isotropic tensile coupons on the other hand, the off-axis orientation effectively transforms the coupon into a completely anisotropic specimen in the coordinate system coincident with the load axis. If the ends of the coupon are rigidly gripped and prevented from rotation dictated by material's natural response during applied displacement at the grips, a highly inhomogeneous state of deformation will be induced. This is known as "the shear-coupling" effect and results in bending of the coupon in its own plane as illustrated in Fig. 3.4.

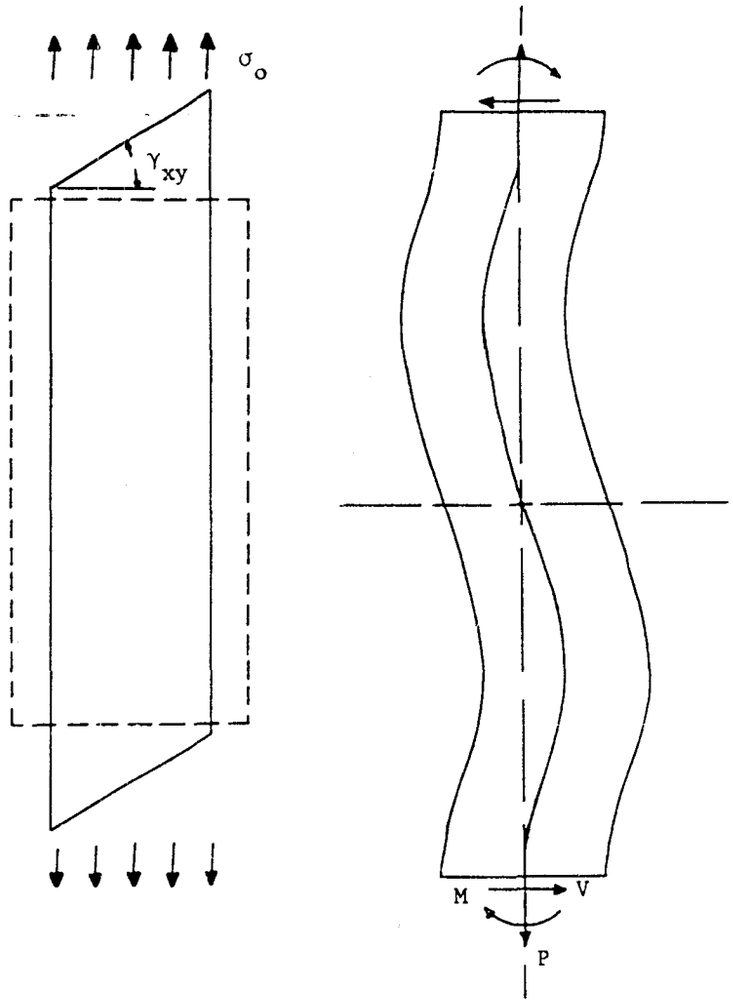

A) Uniform state of stress

B) Effect of clamped ends

Fig. 3.4 Influence of end constraints in the testing of anisotropic bodies, Ref. [97]

The extent of such "bending" and thus induced inhomogeneity in the stress field is a function of the specimen's geometry, that is aspect ratio, material parameters and off-axis orientation.

The first attempt to analyze the effect of shear-coupling, together with the parameters enumerated above, on the deformation field in an off-axis tensile specimen was carried out by Pagano and Halpin [97]. The approach employed was that of a plane stress elasticity formulation with idealized displacement boundary conditions at the grips which facilitated an analytical, closed form solution. Guided by experimental observation that the ends tend to pull out from under the grips in off-axis tension tests on soft composite systems, the authors constrained only the center-line of the specimen from rotation in their analytical model and thus were able to obtain their closed form results. This would thus appear to be the most favorable fixed, rigid grip formulation from the point of view of minimizing strain gradients induced by the gripping arrangement.

The thrust of the paper dealt with the effect of the already mentioned parameters on determination of Young's modulus E_{xx} in the coordinate system coincident with the load axis. It was shown that due to shear-coupling the effective Young's modulus is given by the following expression:

$$E^{**}_{xx} = E_{xx}\left(\frac{1}{1-\eta}\right) \tag{3.1}$$

where η, the shear-coupling coefficient, is:

$$\eta = \frac{6\bar{S}^2_{16}}{\bar{S}_{11}\left(6\bar{S}_{66} + \bar{S}_{11}\frac{\ell^2}{h^2}\right)} \tag{3.2}$$

Here:

E^{**}_{xx} = effective Young's modulus in the coordinate system coincident with the load axis

E_{xx} = true Young's modulus in the same coordinate system

$\bar{S}_{11}$, $\bar{S}_{16}$, $\bar{S}_{66}$ = elements of the transformed compliance matrix in the above coordinate system

ℓ,h = length and half the width of the tension specimen, respectively.

The above is based on the values of stress and strain at the center of the specimen (at the location of the strain gage). If the calculation is based on the average stress value and the center-point strain as is done in practice however, the following expression for the effective Young's modulus E^{*}_{xx} can be derived. The details are given in Appendix A.

$$E^{*}_{xx} = E_{xx}\left\{\frac{1 + 6\left(\frac{h}{\ell}\right)^2\left[\frac{\bar{S}_{66}}{\bar{S}_{11}} - \frac{2}{3}\left(\frac{\bar{S}_{16}}{\bar{S}_{11}}\right)^2\right]}{1 + 6\left(\frac{h}{\ell}\right)^2\left[\frac{\bar{S}_{66}}{\bar{S}_{11}} - \left(\frac{\bar{S}_{16}}{\bar{S}_{11}}\right)^2\right]}\right\} \tag{3.3}$$

The above expression will be closer to the true value E_{xx} than Eqn. (3.1) since the average stress is closer to

the actual value than the center-line stress in the absence of shear-coupling.

The ratio of true Young's modulus and the corresponding effective value based on average stress calculation is plotted in Fig. 3.5 for five values of G_{12} between 0.5 x 10^6 psi and 0.9 x 10^6 psi, three aspect ratios of 5, 10 and 20, E_{11} = 19.81 x 10^6 psi, E_{22} = 1.42 x 10^6 psi and ν_{12} = 0.35. The range of the above values is representative of the Gr/Pi system employed in this work as will be shown later. It is seen that the effect of shear-coupling on determination of true E_{xx} becomes quite small with aspect ratios above ten for most off-axis configurations of this particular composite system.

A rather interesting result, apparently not mentioned in the literature in this particular form, ensues if Pagano's model is used to determine variation in the elastic shear modulus G_{12} determined from various off-axis orientations in the presence of shear-coupling. The relationship between the true elastic shear modulus G_{12} and the corresponding effective value G^*_{12} can be shown to be given by the following expression:

$$G^*_{12} = \frac{-A \sin\theta\cos\theta}{2\sin\theta\cos\theta[(\bar{S}_{12}-\bar{S}_{11})(1+C)-(\bar{S}_{26}-\bar{S}_{16})B] + (\cos^2\theta-\sin^2\theta)[\bar{S}_{16}(1+C)-\bar{S}_{66}B]} \qquad (3.4)$$

where:

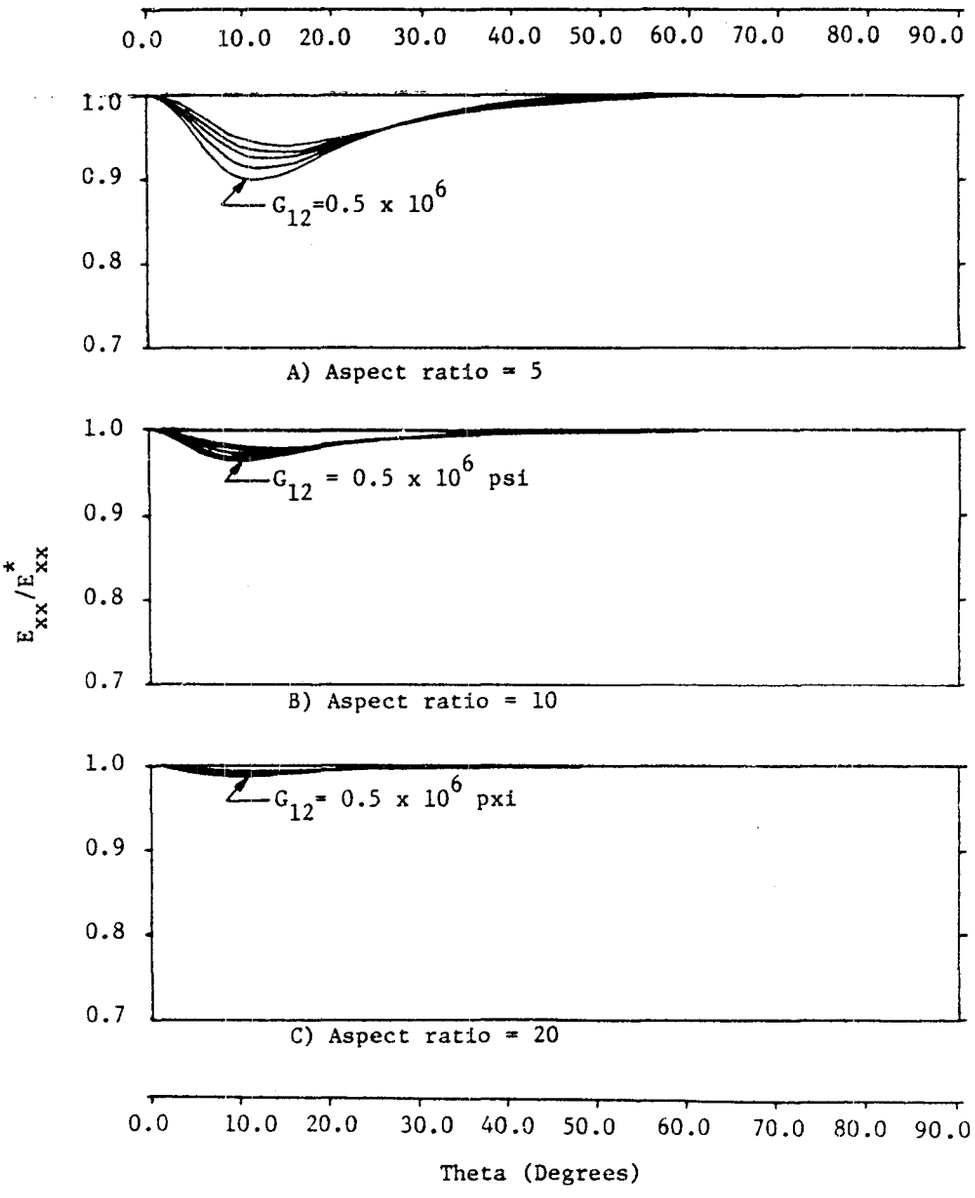

Fig. 3.5 Ratio of true Young's Modulus E_{xx} and the corresponding effective value E^*_{xx} as a function of the off-axis angle. Based on the Halpin-Pagano model and average stress calculation

$$A = 1 + 6\left(\frac{h}{\ell}\right)^2 \left[\left(\frac{\bar{S}_{66}}{\bar{S}_{11}}\right) - \frac{2}{3}\left(\frac{\bar{S}_{16}}{\bar{S}_{11}}\right)^2\right]$$

$$B = 6\left(\frac{h}{\ell}\right)^2 \left(\frac{\bar{S}_{16}}{\bar{S}_{11}}\right) \qquad (3.5)$$

$$C = 6\left(\frac{h}{\ell}\right)^2 \left(\frac{\bar{S}_{66}}{\bar{S}_{11}}\right)$$

The detailed derivation is given in Appendix A.

It is important to note that this expression is different from the expression for the effective shear modulus G_{12}^{**} say, using the familiar point transformation law with the apparent Young's modulus E_{xx}^{*} instead of E_{xx} as employed by Rizzo [98]. In effect, Rizzo's method neglects certain stress components and results in slightly different variations of G_{12}^{**} with the off-axis angle than those for G_{12}^{*} given by Eqn. (3.4) for this particular composite.

The expression for the effective shear modulus G_{12}^{*} is plotted in Fig. 3.6 for the same set of parameters as those employed in calculating effective Young's moduli E_{xx}^{*}'s of Fig. 3.5. From these graphical results it is evident that the error in the elastic shear modulus G_{12} obtained from an off-axis tension test in the presence of shear-coupling is significantly greater than the corresponding error in the value of E_{xx}. Even for high aspect ratios such as 20 the deviation is noticeable in low off-axis fiber orientation range for this particular composite

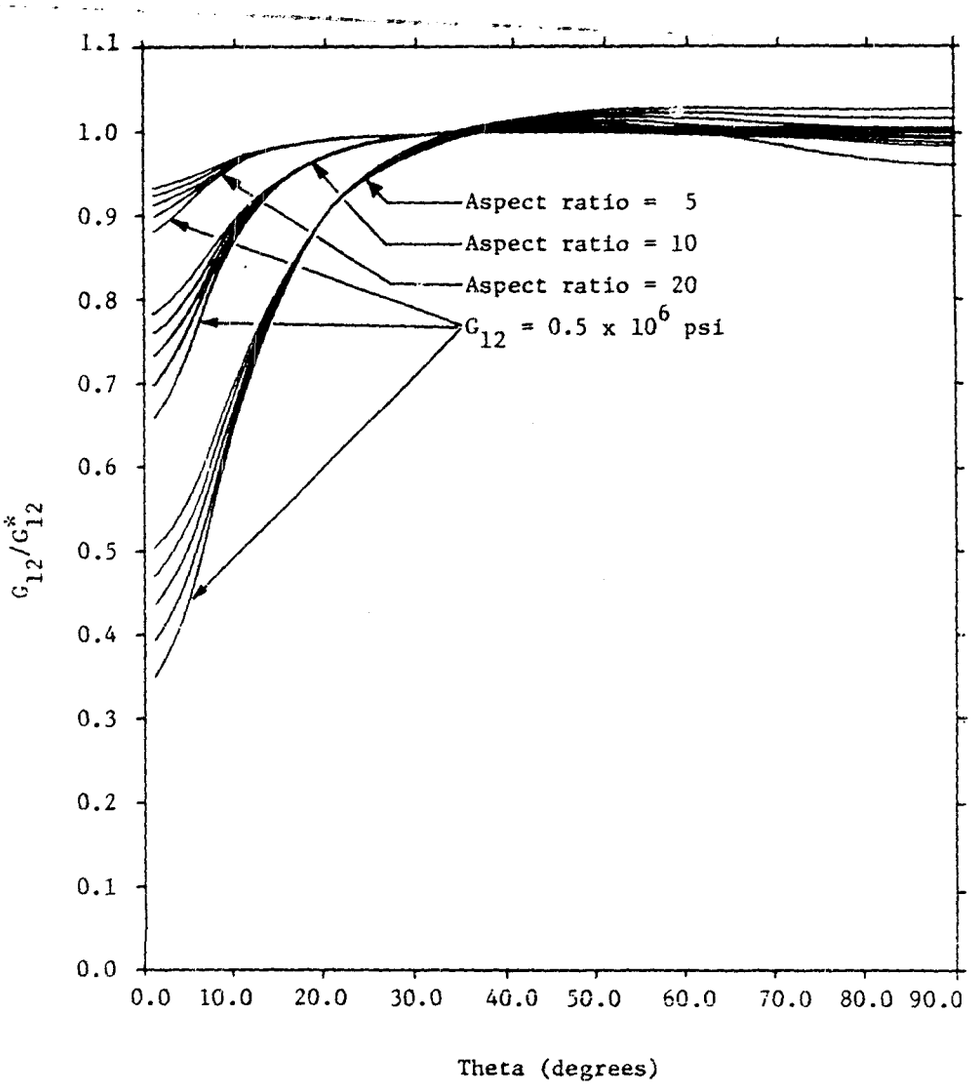

Fig. 3.6 Ratio of true shear modulus G_{12} and the corresponding effective value G^*_{12} as a function of the off-axis angle. Based on the Halpin-Pagano model and average stress calculation

system. The error can be directly traced to the presence of the shear stress component in the coordinate system parallel to the load axis induced by the grips which is neglected in the calculation of G_{12} as shown in Appendix A.

The extent of shear-coupling depends on two different and perhaps interrelated phenomena: the rigid clamping of specimen's ends and prevention of rotation of the grips. Pagano and Halpin state parenthetically in their study that the effect of clamping is the more dominant factor. Wu and Thomas [99], on the other hand, demonstrated experimentally that a rotating-type grip arrangement can noticeably reduce perturbations in the strain field caused by preventing a rigidly clamped specimen from rotating at the grips for 15° off-axis coupons with aspect ratios of 5, 4 and 2.5. A finite-element comparison study between fixed-grip, rotating and non-rotating boundary conditions was subsequently carried out by Rizzo [98] for several composite systems, aspect ratios and the 30° off-axis orientation. Results obtained by Rizzo numerically tend to support Wu and Thomas' contention about desirability of using a rotating, fixed-grip arrangement for off-axis tests.

In view of the above observations a rotating grip arrangement was designed. The grip assembly is shown in Fig. 3.7. The objectives of using such a design were several-fold. The first pertains to introduction of sufficiently homogeneous strain field at the location of strain

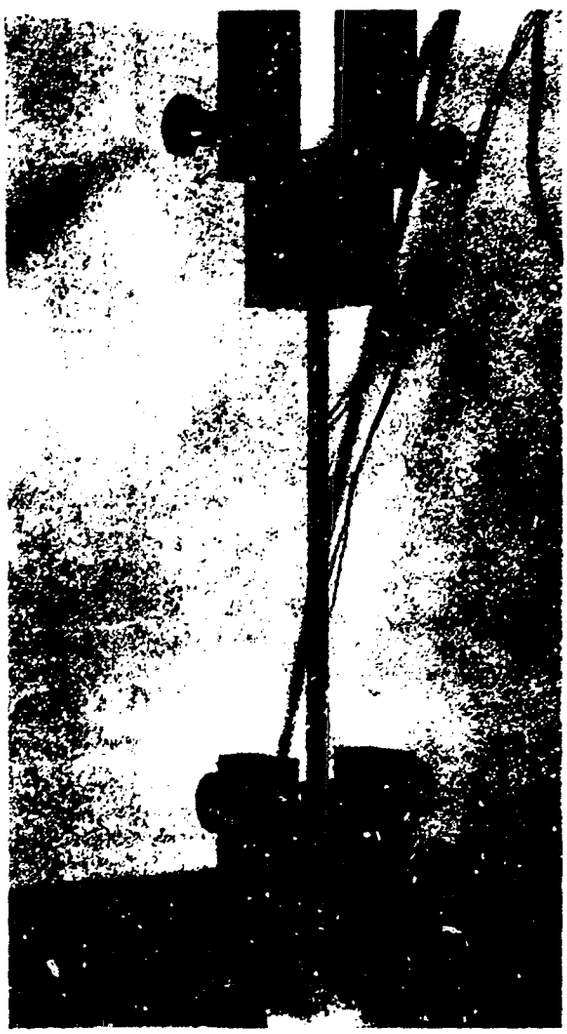

Fig. 3.7 Rotating end-grip test fixture assembly

gage (plane cutting through the mid-point of specimen) as mentioned previously. The second objective was to eliminate or reduce as much as possible stress concentrations in the grip region and thus obtain higher ultimate failure loads more representative of "true" material strength properties. The third objective was to study the experimental feasibility of such a test method and its advantages in determining material characteristics over the non-rotating grip arrangement. This category includes such aspects as reproducibility of test data, elimination of alignment problems, as well as a basis for future comparison studies between this method and the standard grip set-up.

3.3 Specimen Fabrication and Geometry

Three Gr/Pi unidirectional panels were fabricated from prepreg at the NASA-Langley facilities using in-house developed fabrication methods. The prepreg that was employed was composed of Celion 6000 graphite fibers developed by Celanese Corporation and a high-temperature polyimide system PMR-15 developed at NASA-Lewis. Fabrication technique utilized a drum winding apparatus designed for this purpose at NASA-Langley. Reference [100] compiled by Dr. J. G. Davis, Jr. discusses the above aspects in great detail.

The panels were rectangular plates, 26 in. by 50 in., the nominal thickness corresponding to a 12-ply lay-up, with the fiber direction parallel to the longer side. The ply

C2

thickness was a nominal 0.007 in. which resulted in laminate thicknesses in the vicinity of 0.075 in. after cure, varying nominally by $\pm$ 0.005 in. This particular fabrication process employed in conjunction with above type of prepreg yields a nominal fiber volume fraction of sixty percent. This was verified by cutting out several pieces of material from various locations in the panels and leeching away the matrix material. The numbers recorded ranged from 59.77% to 62.51% by volume. The matrix digestion process was carried out with a hot H_2SO_4 solution. Furthermore, each panel was C-scanned after its fabrication to determine presence of voids. The panels were found defect-free upon visual examination of the C-scan photographs.

Each panel was laid out into several areas from which specimens of different fiber orientations were cut out using a diamond-blade saw. Each specimen was assigned a triple number of the form X-YY-ZZ for easy identification. The first number refers to the panel from which the coupon was machined, the second to the coupon number and the third to off-axis fiber orientation. Table 3.2 gives the specimens used in the test program; their identification numbers, type of loading and physical dimensions used to reduce the experimental data. As can be seen the specimen dimensions are quite consistent.

The initial coupon geometry called for tabbed coupons of 0.5 in. x 14.0 in. with 2.5 in. at either end reserved

Table 3.2 Gr/Pi off-axis coupon specifications

Specimen Designation #	Loading Type	No. of unloading stress levels	Mid cross-sectional area	Average cross-sectional area
1-15-0°	Monotonic	—	0.0389	0.0387
1-16-0°	Monotonic	—	0.0387	0.0384
1-17-0°	Monotonic	—	0.0379	0.0378
1-18-0°	Cyclic	2	0.0379	0.0379
1-19-0°	Cyclic	3	0.0376	0.0376
1-21-0°	Cyclic	1	0.0379	0.0379
1-5-5°	Monotonic	—	0.0409	0.0412
1-6-5°	Monotonic	—	0.0407	0.0406
1-7-5°	Monotonic	—	0.0405	0.0404
1-16-5°	Cyclic	3	0.0397	0.0399
1-17-5°	Cyclic	4	0.0380	0.0386
1-18-5°	Cyclic	1	0.0366	0.0377
1-20-10°	Monotonic	—	0.0381	0.0383
1-15-10°	Monotonic	—	0.0371	0.0376
1-17-10°	Monotonic	—	0.0371	0.0376
1-18-10°	Monotonic	—	0.0358	0.0364
1-5-10°	Cyclic	3	0.0404	0.0399
1-7-10°	Cyclic	3	0.0393	0.0395
1-13-10°	Cyclic	2	0.0381	0.0382
2-4-15°	Monotonic	—	0.0396	0.0398
2-5-15°	Monotonic	—	0.0394	0.0396
2-6-15°	Monotonic	—	0.0393	0.0395
2-2-15°	Cyclic	3	0.0401	0.0402
2-3-15°	Cyclic	3	0.0397	0.0396
2-8-15°	Cyclic	5	0.0388	0.0389
2-8-30°	Monotonic	—	0.0405	0.0401
2-9-30°	Monotonic	—	0.0409	0.0404
2-15-30°	Monotonic	—	0.0409	0.0409
2-19-30°	Cyclic	4	0.0400	0.0406
2-22-30°	Cyclic	6	0.0393	0.0398
3-13-45°	Monotonic	—	0.0412	0.0410
3-15-45°	Monotonic	—	0.0413	0.0412
3-18-45°	Monotonic	—	0.0395	0.0397
3-21-45°	Cyclic	4	0.0411	0.0406
3-22-45°	Cyclic	3	0.0395	0.0399
2-10-60°	Monotonic	—	0.0404	0.0400
2-13-60°	Monotonic	—	0.0418	0.0417
2-15-60°	Monotonic	—	0.0419	0.0417

Table 3.2 cont'd.

Specimen Designation #	Loading Type	No. of unloading stress levels	Mid cross-sectional area	Average cross-sectional area
2-19-60°	Cyclic	4	0.0407	0.0410
2-20-60°	Cyclic	2	0.0410	0.0415
2-11-75°	Monotonic	——	0.0406	0.0404
2-14-75°	Monotonic	——	0.0406	0.0404
2-16-75°	Monotonic	——	0.0408	0.0407
1-13-90°	Monotonic	——	0.0398	0.0399
1-15-90°	Monotonic	——	0.0396	0.0396
1-16-90°	Monotonic	——	0.0395	0.0397

for tabs having the same fiber orientation and material composition as the specimen. This would have resulted in the specimens having aspect ratios of 18. The decision to bond tabs to the coupons was based on a limited, preliminary study carried out on a somewhat aged Gr/Pi system which indicated generally slightly higher strengths for tabbed coupons than untabbed ones. Unfortunately, after the tabs were bonded and several tests carried out it was discovered that an improper bonding technique used resulted in premature failures of the low off-axis configurations. A decision to cut the tabs off of all specimens for consistency was made which resulted in coupons having an aspect ratio of 10.

The question of tabbed versus untabbed unidirectional tensile coupons is still far from settled and some researchers prefer to use the untabbed geometry [101]. As will be shown in the Experimental Results section, this particular geometry yielded very consistent strength data.

In order to have as homogeneous a set of specimens as possible, the glass transition temperature of each panel based on several pieces of material taken from each panel was determined. Some variation (100°F or so) was found in some samples and therefore each specimen was subjected to a post-cure cycle shown in Fig. 3.8 to achieve a glass-transition temperature of approximately 620°F for all coupons.

The specimens were strain gaged with a single Micro-

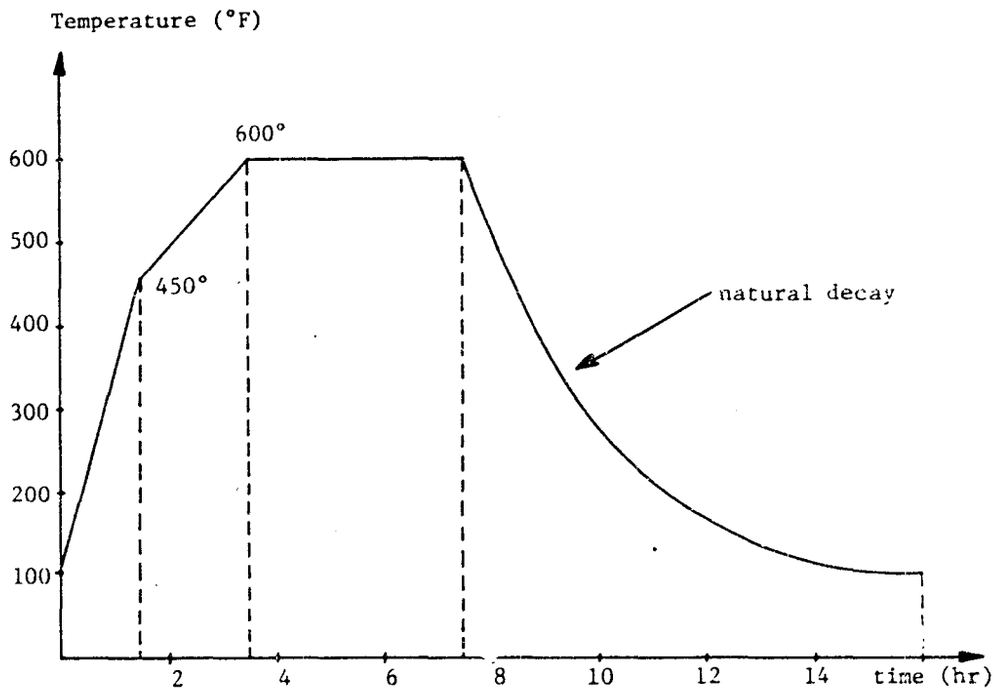

Fig. 3.8 Post-cure cycle employed for the Gr/Pi off-axis, unidirectional coupons

Measurements 45° rosette WK-06-060WR-350 bonded at the mid-point of the coupon and a uniaxial gage WK-06-062AP-350 mounted back-to-back with the rosette. The rosette enables one to determine the complete strain field at a point necessary for strain tensor transformation from one coordinate system to another while the uniaxial gage is used to determine presence of bending in the specimen. The alignment of each strain gage was checked under a microscope and misalignment angles with respect to the coupon's longitudinal axis were recorded for data reduction purposes. Generally, the misalignment angle was found to be small; very often less than 1.0°. A photograph showing dimensions of the 45° rosette and uniaxial gage with respect to the coupon's width is given in Fig. 3.9, while the specimen's geometry is shown in Fig. 3.10.

3.4 Experimental Set-Up: Testing Machine, Data Acquisition and Procedure

All tests were carried out in the Engineering Science and Mechanics Department at Virginia Tech using displacement rate controlled Instron Tensile Machine. The displacement rate was set at 0.05 in/min which yielded an average strain rate of 0.01 in/in/min. ASTM Standards recommend a strain rate between 0.01 and 0.02 in/in/min for this type of test. The lower bound was chosen in order to facilitate the acquisition of data controlled by a fixed scanning rate of 20 channels per second inherent in the data acquisition system

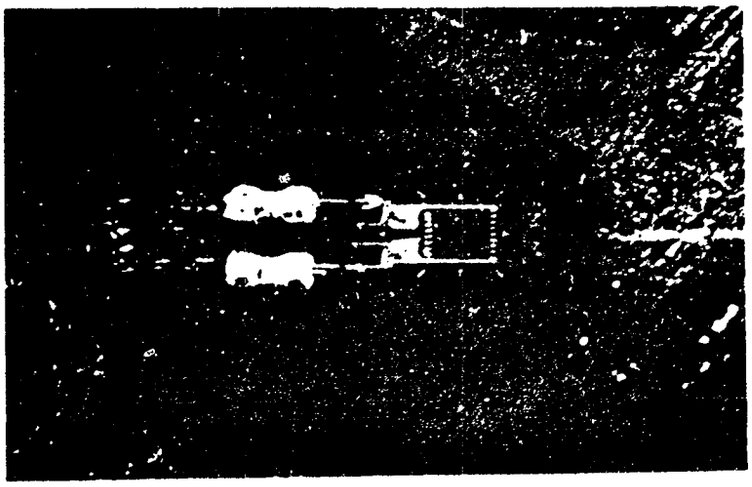

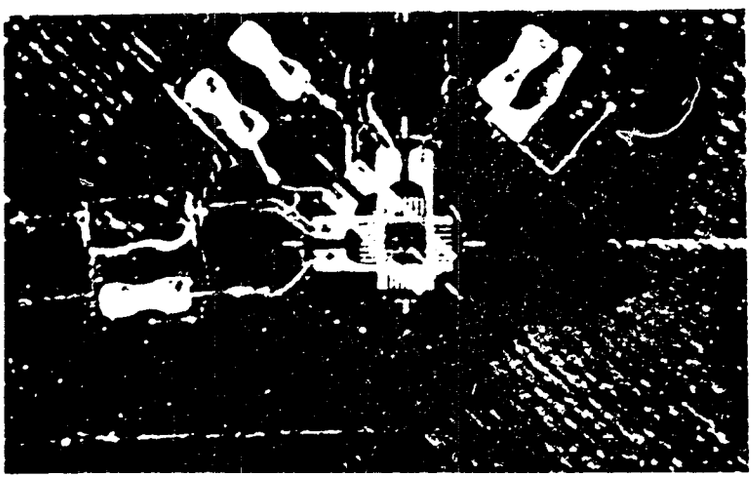

Fig. 3.9 Specimen strain gages

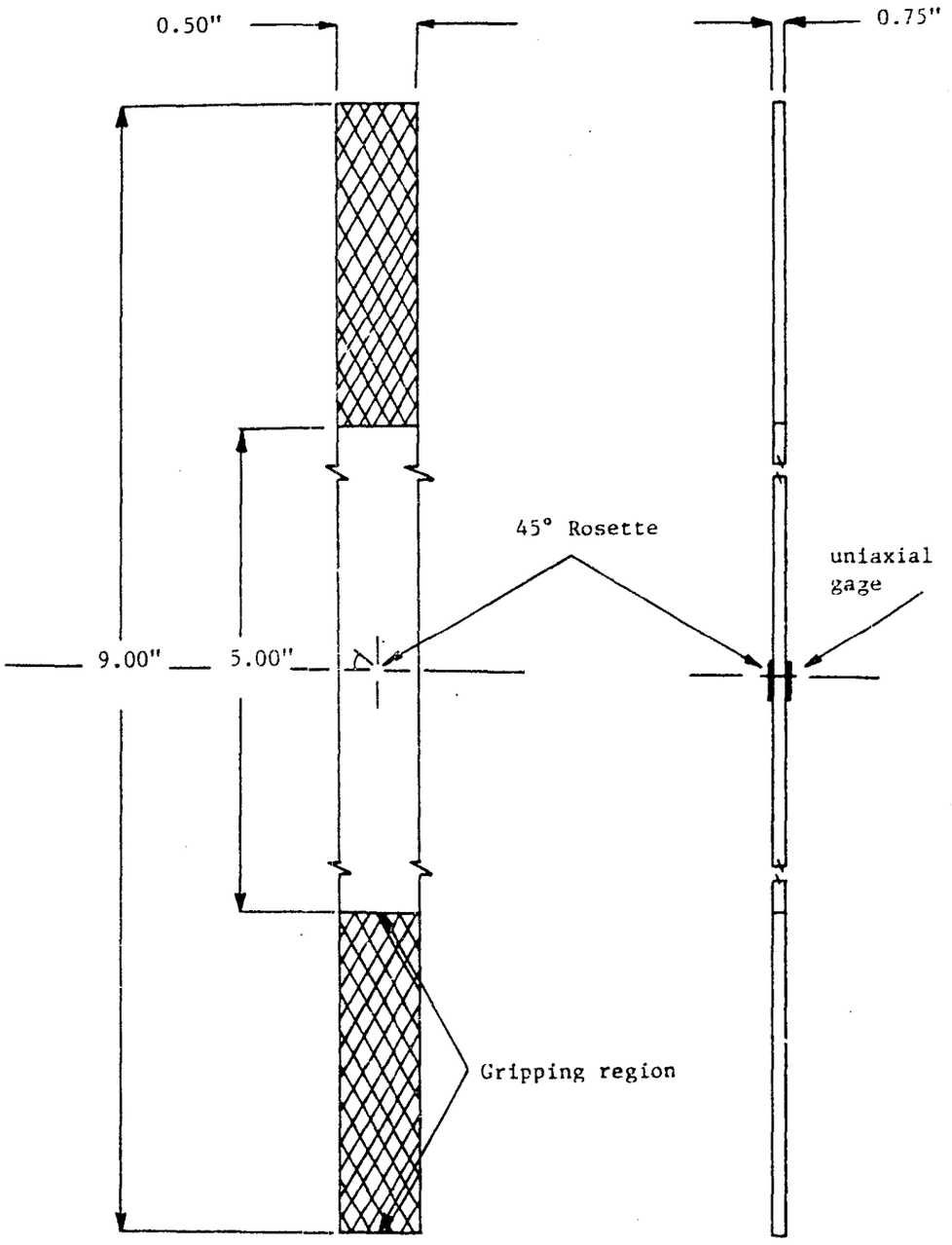

Fig. 3.10 Specimen dimensions

used for that purpose. The system consisted of Vishay 2120 Wheatstone Bridges, HP3495A scanner with an A/D converter and a Tektronix 4051 Minicomputer which recorded the output data on tape with the help of a data acquisition program developed for this purpose by Mr. David Danello of the ESM Department. Five recording channels were used; one for the load output and the remaining four for the strain gages. The above testing arrangement is shown in Fig. 3.11.

Monotonic loading tests were carried out first on all off-axis configurations in order to establish the ultimate stress levels on the basis of which cyclic tests could be performed. The stress levels at which unloading took place during cyclic tests were generally obtained by dividing the ultimate stress by the number of intended cycles so that they would be approximately evenly spaced. The various off-axis configurations were cycled to different stress levels ranging from one to six to establish a wide data base for the correlation of nonlinear response with permanent strain accumulation, unloading and reloading response.

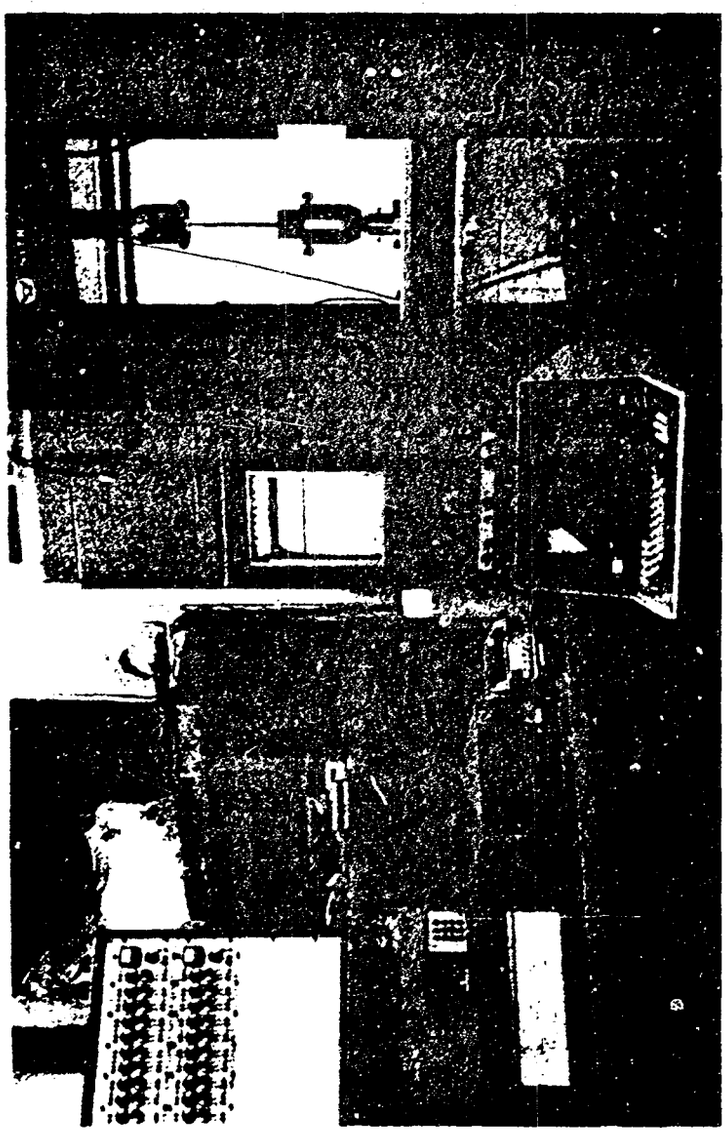

Fig. 3.11 Testing arrangement

4. EXPERIMENTAL RESULTS

4.1 Introduction

The reduction of experimental data was carried out with the help of a computer program that included the following features: correction for the small strain-gage misalignment, bending and transverse sensitivity effects and calculation of stresses based on cross-sectional area at midpoint of the coupon. The above were accomplished in the following fashion. First, the strain components in the coordinate system of the rosette were transformed (after evaluating the shear component through the appropriate transformation equations) to the coordinate system of the uniaxial gage located on the reverse side of the specimen. Subsequently, the transverse sensitivity effects were eliminated using the well-known relations [102]. These relations are given in Appendix B along with transverse sensitivity factors for the rosette and uniaxial gages. The amount of bending was determined by comparing the strain outputs of the longitudinal gages and subsequently used to eliminate bending effects in all the arms of the rosette. The resulting strains were then transformed to the lamina coordinate system through the misalignment angle of the uniaxial gage from which various responses along the material principal directions could be determined.

The reduced experimental data will be presented in

three parts. The initial (linearized) response will be discussed in the first section in the lamina as well as material principal coordinate system in terms of Young's modulus E_{xx}, Poisson's ratio ν_{xy}, shear modulus G_{12} and minor Young's modulus E_{22} under combined loading as functions of the off-axis fiber orientation. The second part will deal with the nonlinear response along the material principal directions under combined and, where applicable, pure loading conditions. Aspects such as the nonlinear elastic and initial hardening response, permanent strain accumulation as well as reloading response will be discussed in this section. Finally, strength data for monotonic and cyclic loading programs will be presented in the third part.

4.2 Initial (linearized) response

The correlation of initial elastic response in the lamina coordinate system with the transversely isotropic linear transformation equations for plane stress requires the knowledge of E_{11}, E_{22}, ν_{12} and G_{12}. The first three constants can be obtained with good accuracy from tension tests on the zero and ninety degree configurations. The shear modulus G_{12}, however, can exhibit some variations caused by the shear-coupling effect if the off-axis tension test method is employed for its determination as discussed previously. Since these lamina-configuration-dependent variations are not known for the particular test fixture

employed in the present study, it is not possible to determine G_{12} from a single off-axis orientation with great certainty. Rather it is more productive to examine trends exhibited by the various lamina stiffness components for various off-axis configurations with G_{12} as a parameter and correlate those with the trends exhibited by the observed effective shear modulus. In view of this, the comparison of experimentally obtained initial material response in the laminate and natural coordinate systems with the lamina stiffness transformation equations has been carried out for a relatively wide range of values of G_{12}. The particular value of G_{12} that yielded best agreement with the transformation equations was then selected for the discussion of the nonlinear response. The above procedure assumes a priori of course that the initial response can be approximated by a transversely isotropic model which can be defended only on the basis of consideration of the very fine and orderly oriented microstructure of the Gr/Pi lamina as well as the resulting experimental-theoretical correlation.

The Young's modulus E_{xx} in the laminate coordinate system as a function of the off-axis angle is presented in Fig. 4.1 for the range of G_{12} values: 0.5×10^6 psi $\leq G_{12} \leq 0.9 \times 10^6$ psi. The experimental results in the range $30° \leq \theta \leq 90°$ where shear-coupling effects are smallest suggest a value of G_{12} between 0.7×10^6 psi and 0.8×10^6 psi. The small deviation from the response bounded by these

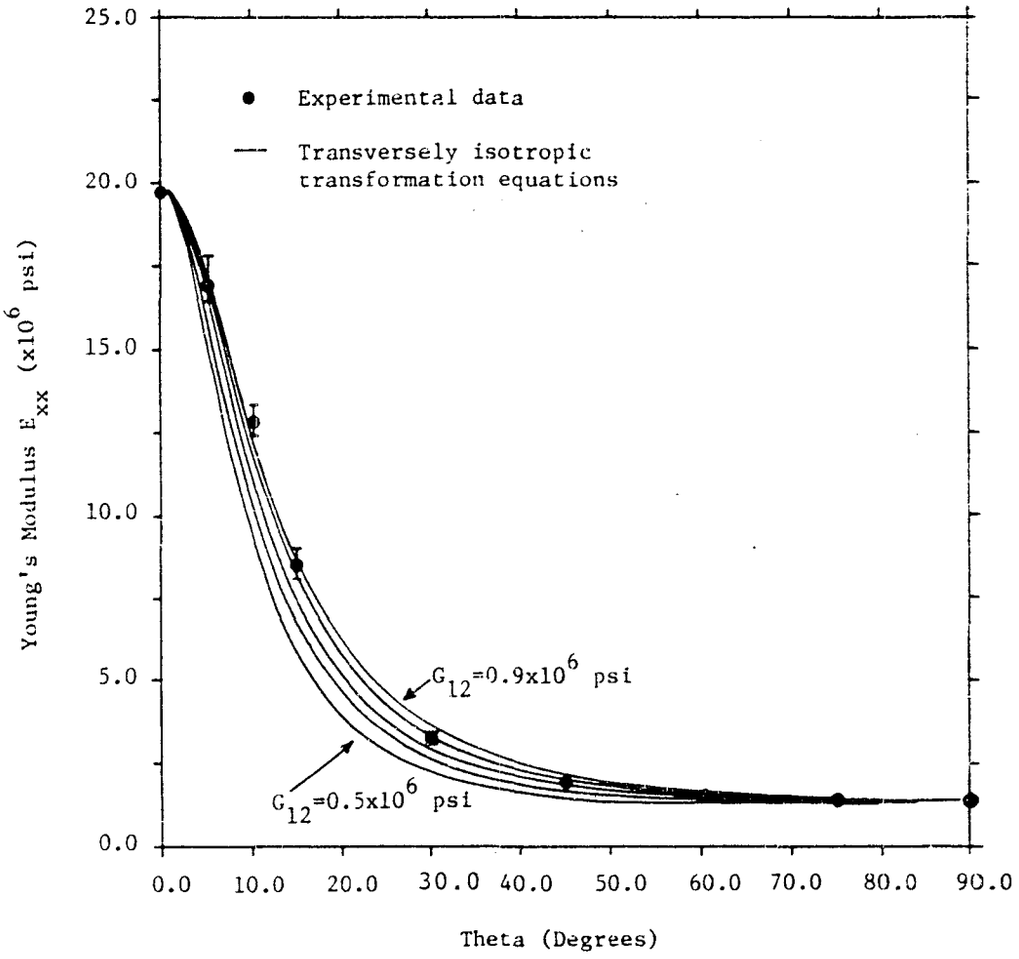

Fig. 4.1 Young's Modulus E_{xx} as a function of the off-axis angle for the range 0.5 x 10^6 psi $\leq G_{12} \leq$ 0.9 x 10^6 psi

two curves in the region $10° \leq \theta \leq 15°$ could be ascribed to the shear-coupling phenomena which can be noticeable for these configurations as illustrated in the previous chapter.

Fig. 4.2 illustrates the behavior of Poisson's ratio ν_{xy} in the lamina coordinate system as a function of the off-axis angle for the same range of G_{12} as above. Again, if the transversely isotropic model is chosen for the initial response of this particular system, then the value of G_{12} in the vicinity of 0.7×10^6 psi will yield reasonably good experimental-theoretical correlation. The small discrepancy in the low off-axis angle range will be subsequently explained by the shear-coupling effect using the Halpin-Pagano model. The deviation in the high off-axis angle range on the other hand could be attributed to strain-gage sensitivity or resolution problems since the transverse strains for these configurations are very small. Alternatively, it is possible that the initial response of this material system deviates slightly from the assumed transversely isotropic model.

Finally, the initial shear modulus G_{12} along the material principal coordinate system as determined from the various off-axis configurations is plotted in Fig. 4.3. Also plotted are the predictions of the effective shear modulus (with shear-coupling included) on the basis of Halpin-Pagano model for the range 0.5×10^6 psi $\leq G_{12} \leq 0.9 \times 10^6$ psi, c.f. Eqn. 3.4. In the off-axis range

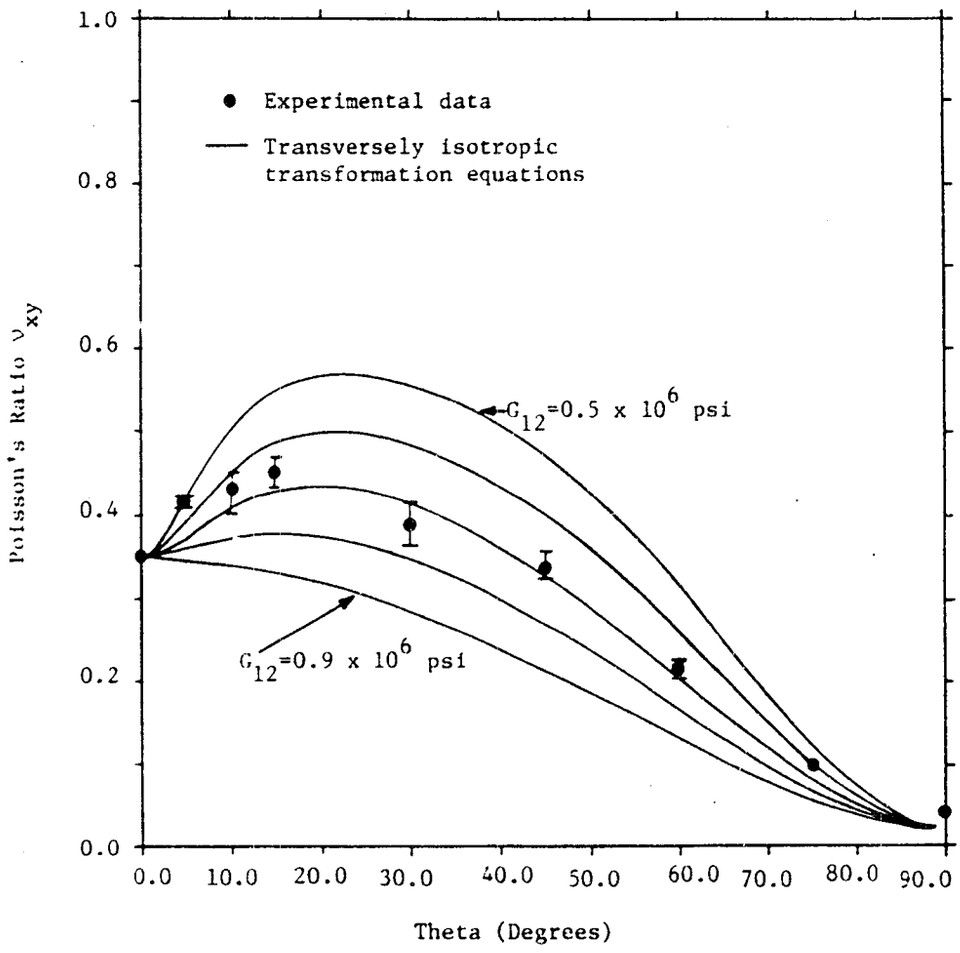

Fig. 4.2 Poisson's ratio ν_{xy} as a function of the off-axis angle for the range 0.5 x 10^6 psi $\leq G_{12} \leq$ 0.9 x 10^6 psi

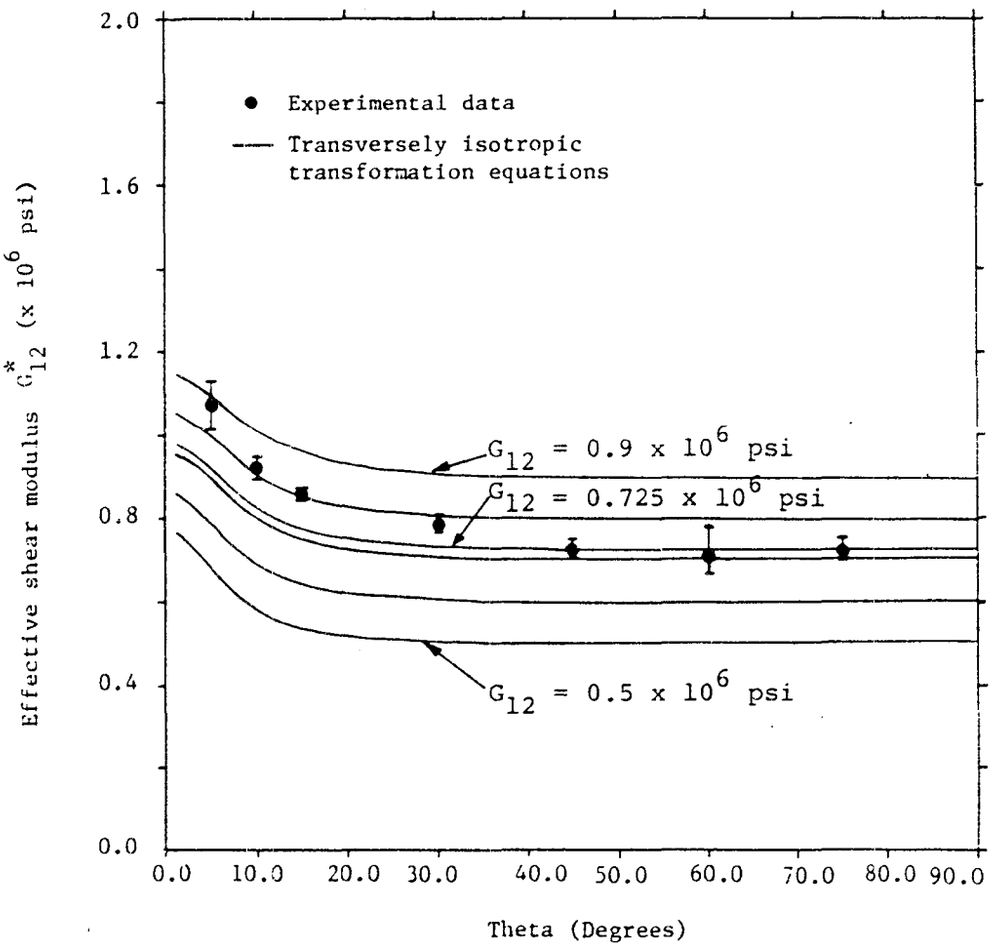

Fig. 4.3 Effective shear modulus G^*_{12} as a function of the off-axis angle for the range 0.5 x 10^6 psi $\leq G_{12} \leq$ 0.9 x 10^6 psi

$0 < \theta \leq 30°$, where the shear-coupling effect appears to be most significant, the deviations between experimentally obtained values of G_{12} and the corresponding effective values obtained from the above mentioned model do not exceed 13% if the true value of G_{12} is taken to be approximately 0.725×10^6 psi as suggested by the results from the 45° off-axis specimen. There appears to be little variation in G_{12} in the range $45° \leq \theta < 90°$ where shear-coupling is negligible.

In view of the above observations, a comparison between experimental results of initial lamina response and theoretical predictions of linear transformation equations has been reiterated on the basis of $G_{12} = 0.725 \times 10^6$ psi. The predictions of the Halpin-Pagano model have also been included in the subsequent figures to illustrate the effect of shear-coupling on the initial response for this particular value of G_{12}. Since it appears that the test fixture used in the present study produces somewhat greater shear-coupling effects than the Halpin-Pagano idealized "test fixture," the above will be a lower bound for the coupling effect. An upper bound would then be total constraint of the ends.

Fig. 4.4 shows the comparison between experimentally obtained values of E_{xx} and the predicted response. The experimental-theoretical correlation is seen to be excellent for the range $45° \leq \theta \leq 90°$. In the range $0° < \theta \leq 30°$ the deviations do not exceed 10% with the exception of the 10°

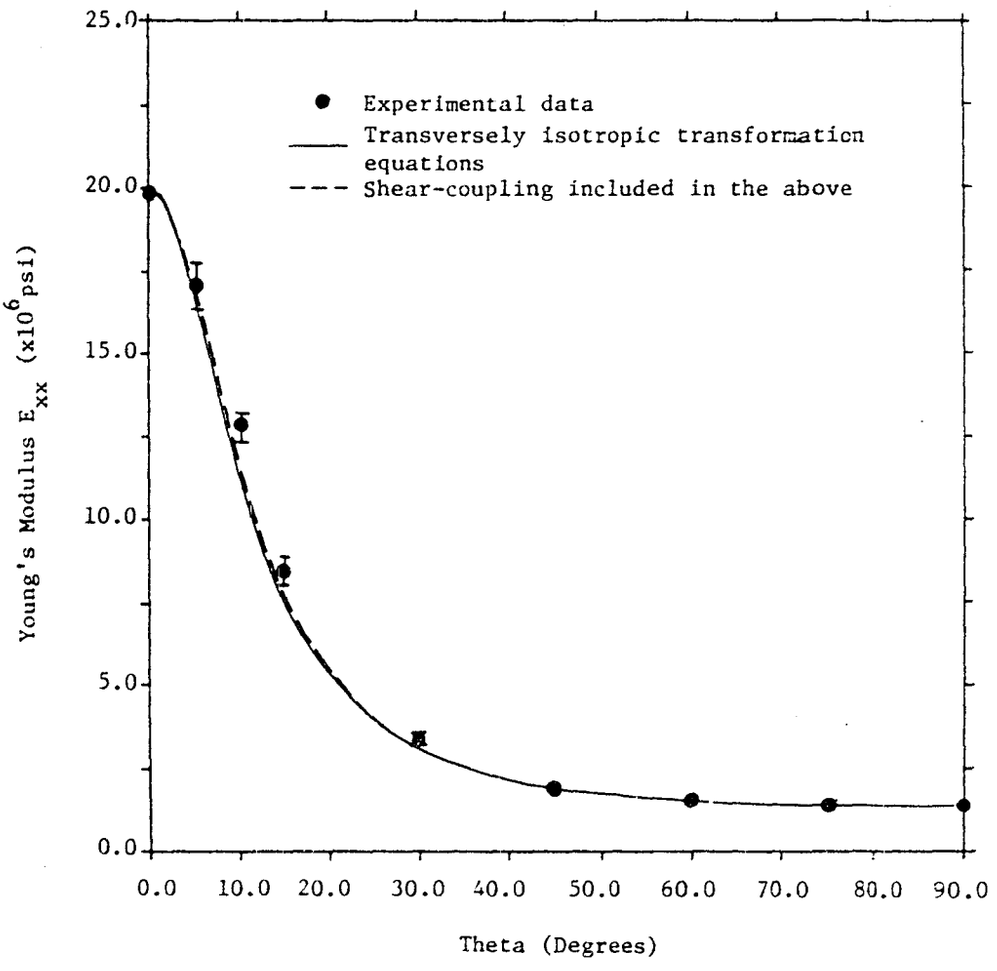

Fig. 4.4 Effective and true Young's Moduli E^*_{xx} and E_{xx} respectively, as functions of the off-axis angle for $G_{12} = 0.725 \times 10^6$ psi

off-axis specimen which yielded approximately a 14% discrepancy. The Halpin-Pagano model, represeted by the dashed curve, helps to reduce the above variations somewhat, however the results indicate again that the shear-coupling effect is apparently somewhat more pronounced, as far as E_{xx} is concerned, in this particular test fixture than in the Halpin-Pagano model.

The variation of Poisson's ratio ν_{xy} with the off-axis angle is shown in Fig. 4.5 for the above value of G_{12}. The dashed curve is the effective ratio based on the already mentioned model and it is seen that a significant portion of the observed discrepancy in experimental-theoretical correlation can be well explained on the basis of shear-coupling effect.

Finally, the experimentally determined initial minor Young's modulus $E_{22}(\theta)$ under combined loading in the material principal coordinate system for the various off-axis configurations is presented in Fig. 4.6 along with the theoretical predictions with and without shear-coupling. Since the loading is proportional, we can express $E_{22}(\theta)$ for combined loading as follows:

$$E_{22}(\theta) = \frac{1.0}{(S_{22} + S_{12}\ \text{cotan}^2\theta)} = \frac{E_{22}}{[1 - \nu_{12}(\frac{E_{22}}{E_{11}})\text{cotan}^2\theta]} \qquad (4.1)$$

The effective value of $E^{*}_{22}(\theta)$ based on the Halpin-Pagano model can then be derived, using the same procedure as out-

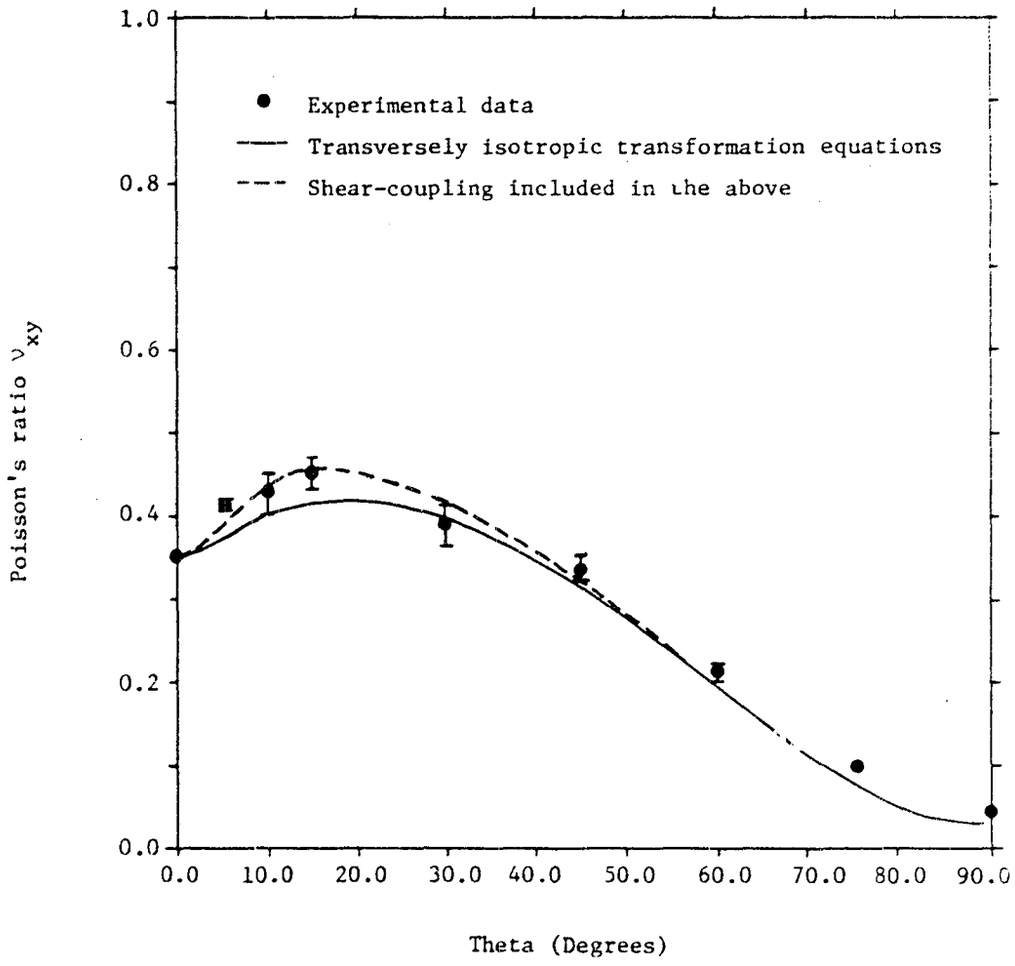

Fig. 4.5 Effective and true Poisson's ratios ν^{*}_{xy} and ν_{xy} respectively, as functions of the off-axis angle for $G_{12} = 0.725 \times 10^{6}$ psi

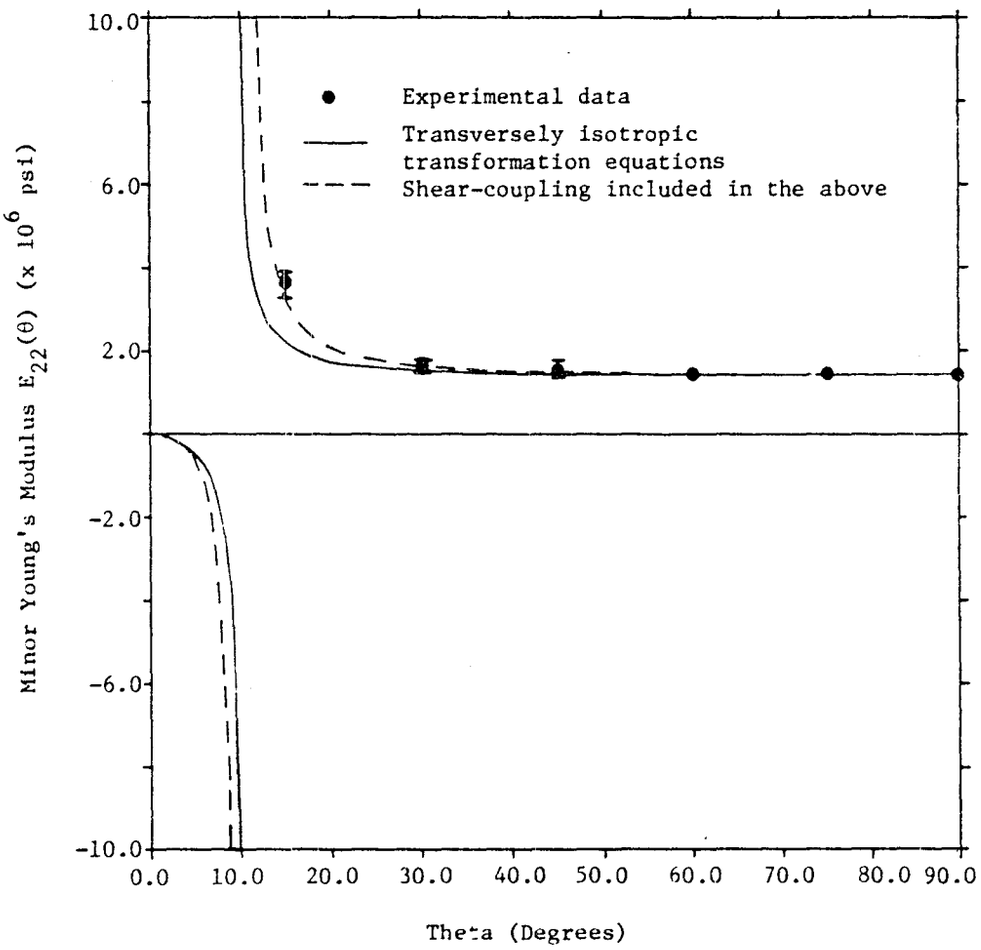

Fig. 4.6 Effective and true minor Young's Moduli $E^*_{22}(\theta)$ and $E_{22}(\theta)$ under combined loading, respectively as functions of the off-axis angle for $G_{12} = 0.725 \times 10^6$ psi

lined in Appendix A, yielding:

$$E^{*}_{22}(\theta) = A \sin^2\theta/\{\sin^2\theta[\bar{S}_{11}(1+C)-\bar{S}_{16}B] + \\ + \cos^2\theta[\bar{S}_{12}(1+C)-\bar{S}_{26}B] - \sin\theta\cos\theta[\bar{S}_{16}(1+C)-\bar{S}_{66}B]\} \quad (4.2)$$

where A, B and C have been defined in Chapter 3.

It is seen that good experimental-theoretical correlation is obtained using the Halpin-Pagano shear-coupling model (given by the dashed curve) for the range of off-axis configurations presented even in the region where $E_{22}(\theta)$ changes rapidly.

Table 4.1 summarizes the initial response results. The data presented in Figs. 4.1-4.6 represent averages of all specimens tested including those loaded cyclically, except where indicated by an asterisk in the table. These tests yielded drastically different results from the average trend and were thought to be caused by faulty strain gages.

4.3 Nonlinear Response

4.3.1 Longitudinal Response

The nonlinear response along and transverse to the fiber direction for a typical 0° coupon is illustrated in Figs. 4.7 and 4.8. The longitudinal stress-strain response exhibits a stiffening, esentially bi-modulus behavior with the average initial and final moduli of 19.81×10^6 psi and 23.28×10^6 psi, respectively. The response appears to be practically reversible for the testing parameters used as

Table 4.1 Initial response (moduli) data of the Gr/Pi coupons

* - excluded from averaging

Specimen designation #	Young's Modulus E_{xx} (msi)	Poisson's ratio ν_{xy}	Shear modulus G_{12} (x10^5)	Minor Young's Modulus $E_{22}(\theta)$ (msi-comb. load)
1-15-0°	19.68	0.298*	not applicable	not applicable
1-16-0°	19.84	0.342	"	"
1-17-0°	19.72	0.360	"	"
1-18-0°	18.40*	0.348	"	"
1-19-0°	19.72	0.348	"	"
1-21-0°	20.08	0.350	"	"
0° average	19.81	0.350		
1-5-5°	16.39	Not avail.	Not avail.	Not avail.
1-6-5°	16.50	"	"	"
1-7-5°	16.41	"	"	"
1-16-5°	17.79	0.420	10.12	"
1-17-5°	17.98	0.319*	9.19	"
1-18-5°	17.92	0.409	11.26	"
5° average	17.16	0.414	10.69	
1-12-10°	12.99	0.445	9.43	Not avail.
1-15-10°	12.40	0.400	8.96	"
1-17-10°	13.27	0.298*	9.40	"
1-18-10°	13.39	0.420	9.47	"
1-5-10°	12.66	0.432	9.19	"
1-7-10°	12.40	0.454	9.08	"
1-13-10°	13.16	0.532*	10.64*	"
10° average	12.89	0.430	9.25	
2-4-15°	9.05	0.329*	8.93*	2.04*
2-5-15°	8.51	0.435	8.72	3.28
2-6-15°	8.58	0.439	8.62	3.64
2-2-15°	8.51	0.379*	8.99*	2.60*
2-3-15°	8.10	0.471	8.50	3.77
2-8-15°	8.47	0.460	8.47	3.85
15° average	8.54	0.45	8.58	3.64

Table 4.1 cont'd.

Specimen designation #	Young's Modulus E_{xx} (msi)	Poisson's ratio ν_{xy}	Shear modulus G_{12} ($x10^5$)	Minor Young's Modulus $E_{22}(\theta)$ (msi-comb. load)
2-8-30°	3.23	0.397	7.76	1.64
2-9-30°	3.21	0.366	7.62	1.64
2-15-30°	3.53	0.413	8.09	1.83
2-19-30°	3.50	0.385	8.01	1.69
2-22-30°	3.33	0.395	7.81	1.76
30° average	3.36	0.391	7.86	1.71
3-13-45°	1.90	0.355	7.06	1.62
3-15-45°	1.98	0.337	7.37	1.56
3-18-45°	1.95	0.343	7.13	1.73
3-21-45°	1.91	0.329	7.04	1.56
3-22-45°	1.99	0.327	7.55	1.43
45° average	1.95	0.338	7.23	1.58
2-10-60°	1.59	0.216	7.81	1.48
2-13-60°	1.50	0.227	6.67	1.51
2-15-60°	1.51	0.224	6.67	1.42
2-19-60°	1.57	0.204	7.55	1.41
2-20-60°	1.47	0.218	6.79	1.43
60° average	1.53	0.218	7.10	1.45
2-11-75°	1.46	0.095	6.94	1.50
2-14-75°	1.44	0.096	7.53	1.42
2-16-75°	1.44	0.111	6.93	1.42
75° average	1.45	0.101	7.13	1.45
1-13-90°	1.40	0.048	not applicable	1.40
1-15-90°	1.43	0.047	"	1.43
1-16-90°	1.44	0.046	"	1.44
90° average	1.42	0.047	"	1.42

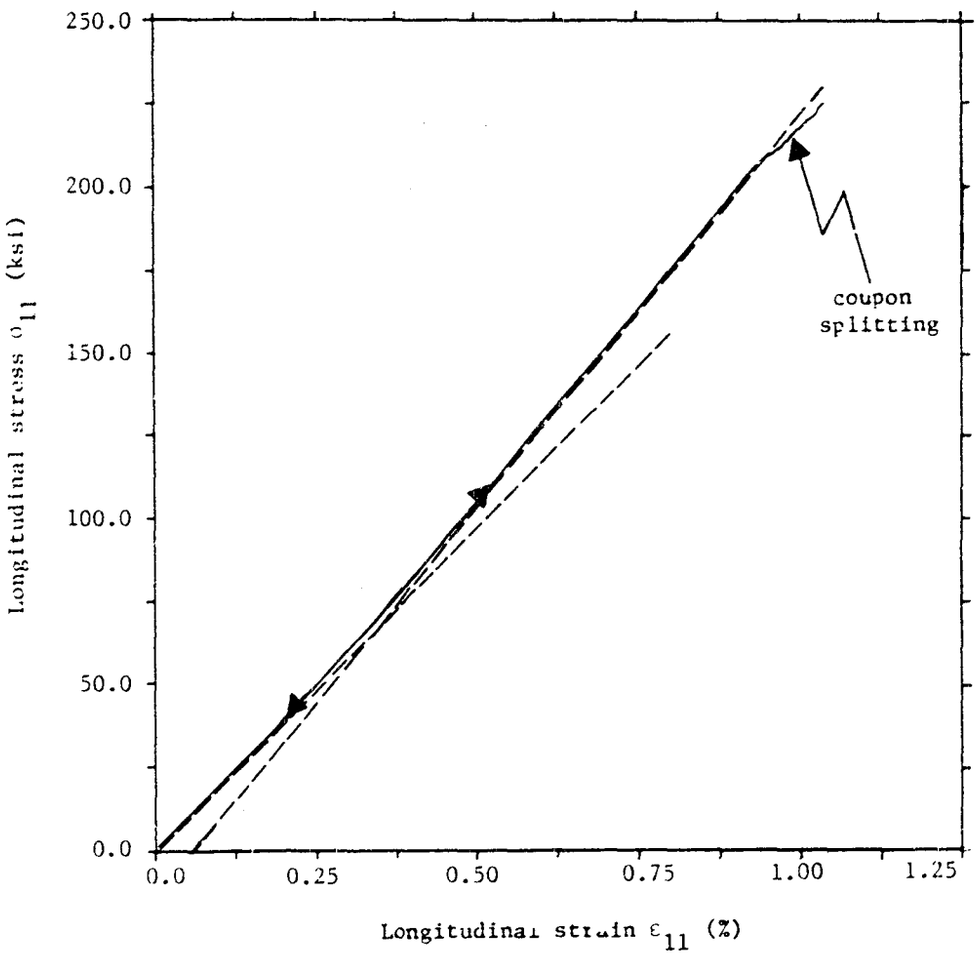

Fig. 4.7 Longitudinal stress-strain response of a 0° Gr/Pi coupon in pure tension

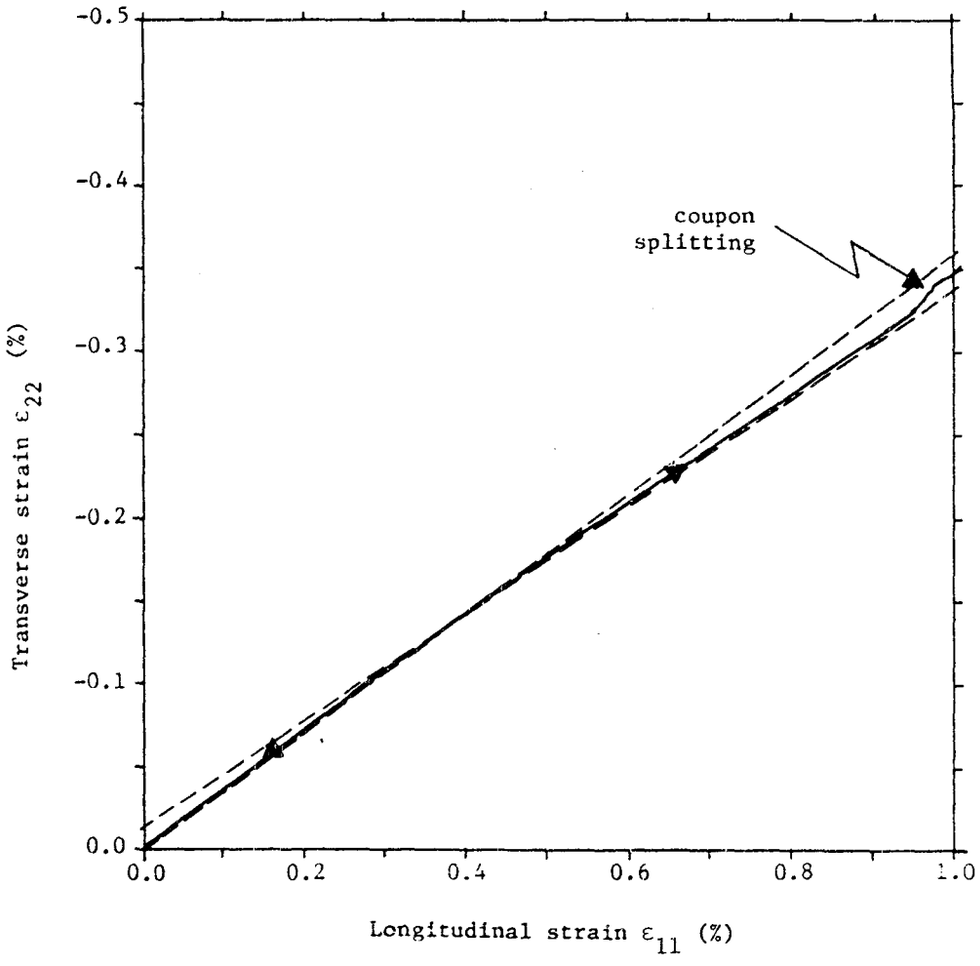

Fig. 4.8 Poisson's response of a 0° Gr/Pi coupon in pure tension

verified by cyclic tests at several unloading stress levels. The strain-strain (Poisson's) behavior also appears to be of a bi-modulus, virtually reversible character with the average initial and final ratios of 0.350 and 0.318, respectively.

4.3.2 Shear Response

The nonlinear shear response on the other hand exhibits a significant amount of nonlinearity and dissipation in the majority of the off-axis configurations tested. This is illustrated in Fig. 4.9 which shows the uncorrected resolved shear stress-strain behavior of a typical 15° off-axis coupon cycled at several stress levels (i.e. uncorrected for shear-coupling as discussed previously). Such pronounced nonlinearity and dissipation loops are more evident in the low than high off-axis orientations due to significantly higher ultimate strains present in the former cases.

In order to be able to compare the monotonic shear response of the various configurations on an equal footing it was necessary to devise a method to eliminate the shear-coupling both in the linear and nonlinear range in a consistent fashion. The presence or absence of the so-called stress-interaction phenomenon could then be ascertained from such comparison. To this end, the Halpin-Pagano model was utilized in which now the constant material parameters were replaced by the corresponding secant properties since the derived equations remain also valid in the case of total

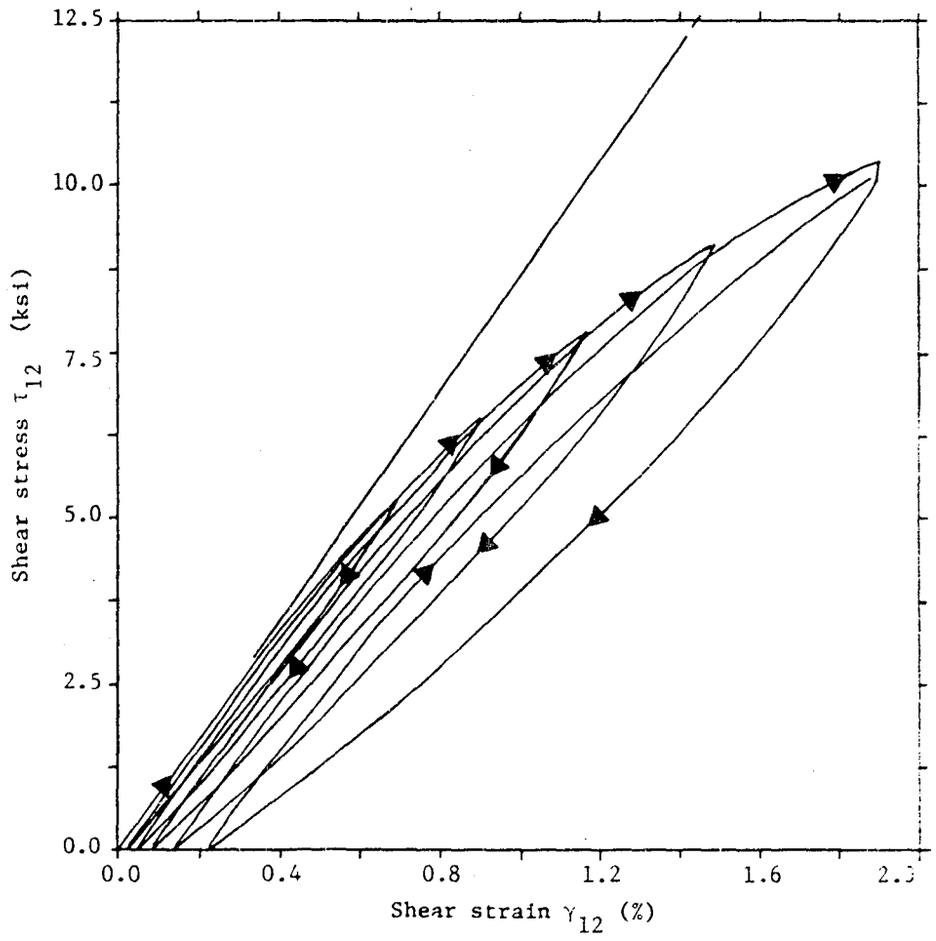

Fig. 4.9 Resolved shear stress-strain response of a typical Gr/Pi 15° coupon in cyclic loading. Shear-coupling not eliminated

deformation-type constitutive response. In order to bring the experimentally observed initial values of the shear modulus in correspondence with the initial Halpin-Pagano effective value predictions, a factor representing the ratio of the two was employed and assumed to hold true in the nonlinear range as well. This factor, although being dependent on the off-axis orientation, did not vary significantly in the average sense in the range $5° \leq \theta \leq 30°$, where shear-coupling is most significant, as can be verified from Fig. 4.3. Since the effective secant properties are known from experiment, the extended Halpin-Pagano model can now be employed to find the "true" secant properties in an iterative fashion. This in turn allows one to find the corrected value of stress at each strain level (since in the model, the center-line strain remains constant and equal to the applied average strain) and thus the corrected or "true" stress-strain response. The above scheme was thought not to depart significantly from the "exact" method (most likely based on a finite-element model) in view of the fairly good correlation between the experimental results and Halpin-Pagano predictions in the linear range.

Fig. 4.10 illustrates the corrected shear response in the material principal coordinate system for the off-axis angles in the range $10° \leq \theta \leq 75°$. The effect of the combined state of stress on the shear response manifesting itself in the so-called stress-interaction phenomenon is

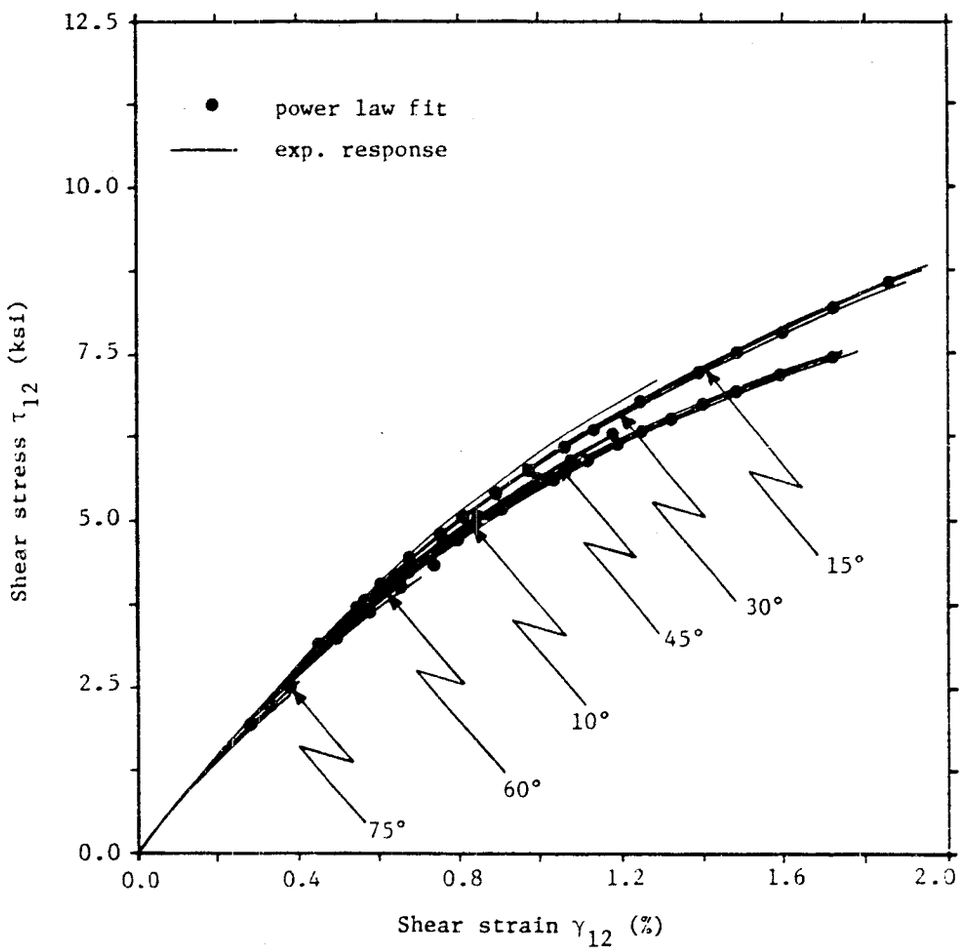

Fig. 4.10 Corrected resolved shear stress-strain response of the Gr/Pi coupons in the range $10° \leq \theta \leq 75°$. Corrected on the basis of the Halpin-Pagano model

clearly visible. Of particular technological interest is the relative response of the 10° off-axis coupon in relation to other off-axis orientations. It appears that the shear response is not a monotonically decreasing function of the increasing off-axis angle with respect to stiffness in the nonlinear range. The reversal of the stress-strain curves in the 15° - 30° off-axis range that is seen in Fig. 4.10 would point to the importance of the longitudinal stress σ_{11} on the nonlinear shear behavior.

In order to study the character of the nonlinear shear response, the nonlinear strain (that portion of strain that deviated from the linear behavior) together with the corresponding stress level was plotted on the log-log graph for each off-axis orientation before and after the corrections mentioned previously. The corrected results are illustrated in Fig. 4.11 where it is apparent that a power-law predicts the shear response with very good accuracy. Although the power exponent varies slightly with different off-axis angles and with specimens of the same orientation, the hardening exponent n_6 and shift parameters $A^*_{66}(\theta)$ obtained from Fig. 4.11 (i.e. dashed curves) results in very good prediction of the overall shear behavior for each configuration. This is shown in Fig. 4.10 where the predicted response is represented by the indicated symbols. The extent of variation in the shift parameters $A_{66}(\theta)$ is a clear indication of the amount of stress interaction present in the shear mode in

this Gr/Pi system. It ought to be mentioned that the hardening exponent n_6 was not affected significantly by the correction scheme outlined previously. The shift parameters $A_{66}(\theta)$ however, were affected and could be brought into coincidence with the uncorrected results by shifting log-log plots for each off-axis configuration horizontally. The above indicates, as was subsequently verified, that the ratio of corrected to uncorrected secant shear moduli remained nearly constant along the entire deformation path.

The cyclic shear response is illustrated in Figs. 4.12 and 4.13 where the permanent strain and the corresponding unloading stress level have been plotted on log-log scale. Taking the experimental scatter of each configuration into account as well as the inherent inaccuracy of strain determination at low deformation levels it is seen that the unloading behavior can be predicted with sufficient accuracy by a power-law with the same exponent as that for the initial hardening response. The shift parameters characterizing unloading (permanent strain vs unloading stress) have been subsequently determined on the basis of the above value of hardening exponent.

The cyclic response in shear has been corrected for shear-coupling in the same manner as the monotonic data by determining the hardening envelope for each cycled coupon. No significant differences were found between hardening envelopes of cyclic tests and monotonic hardening curves for

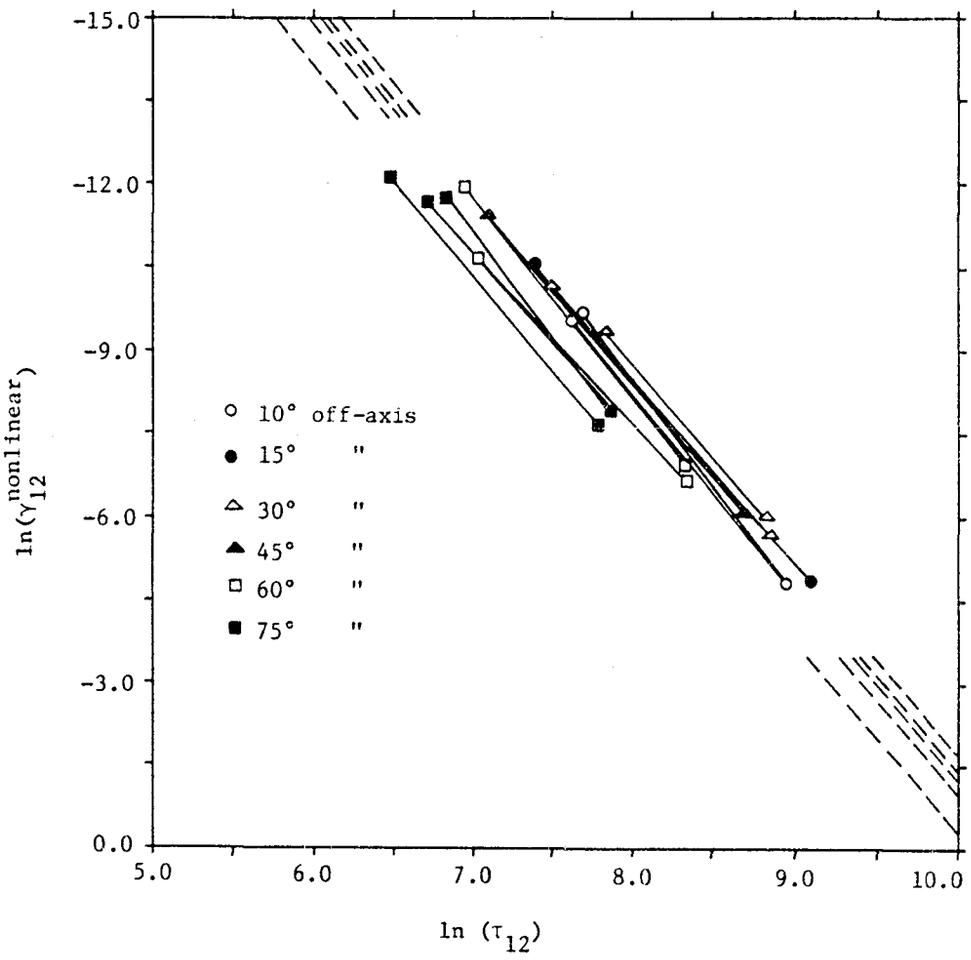

Fig. 4.11 Log-log graph of the resolved shear stress and nonlinear portion of the corresponding shear strain of the Gr/Pi coupons in the range $10° \leq \theta \leq 75°$

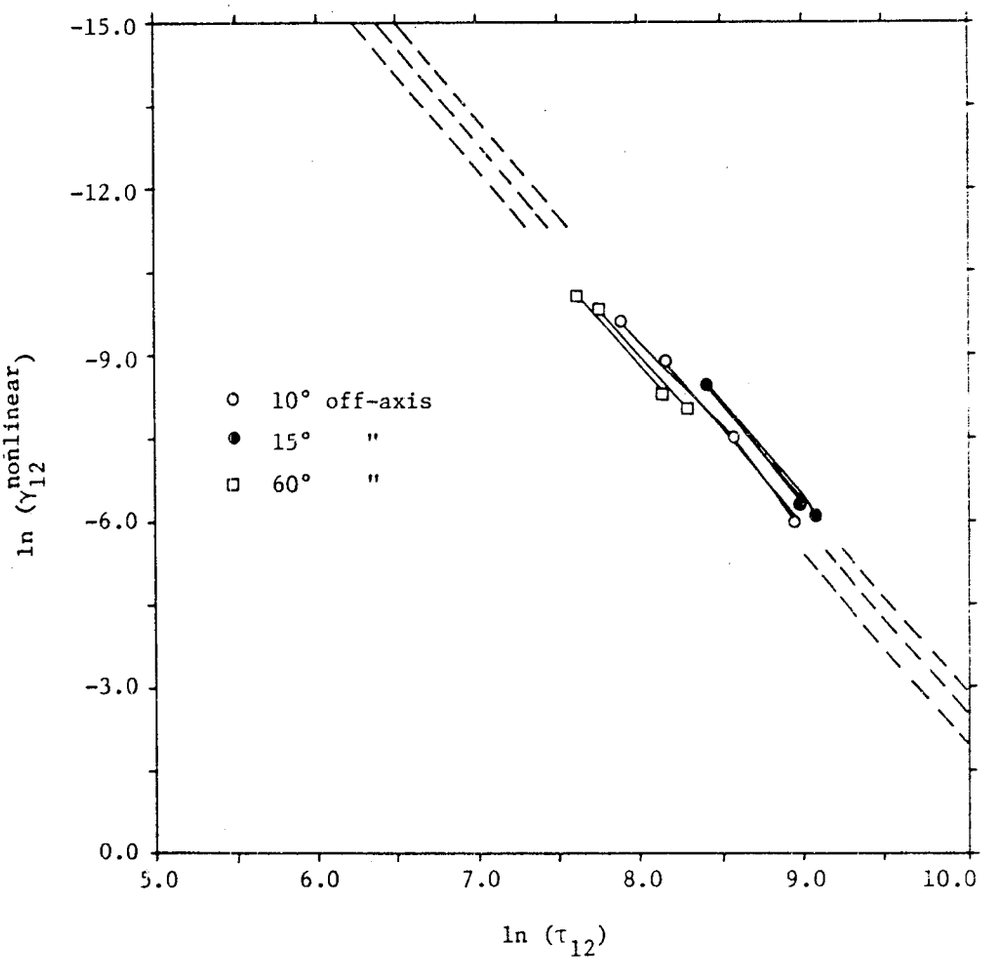

Fig. 4.12 Log-log graph of the resolved permanent shear strain and the corresponding unloading shear stress in the cyclically loaded Gr/Pi 10°, 15° and 60° coupons

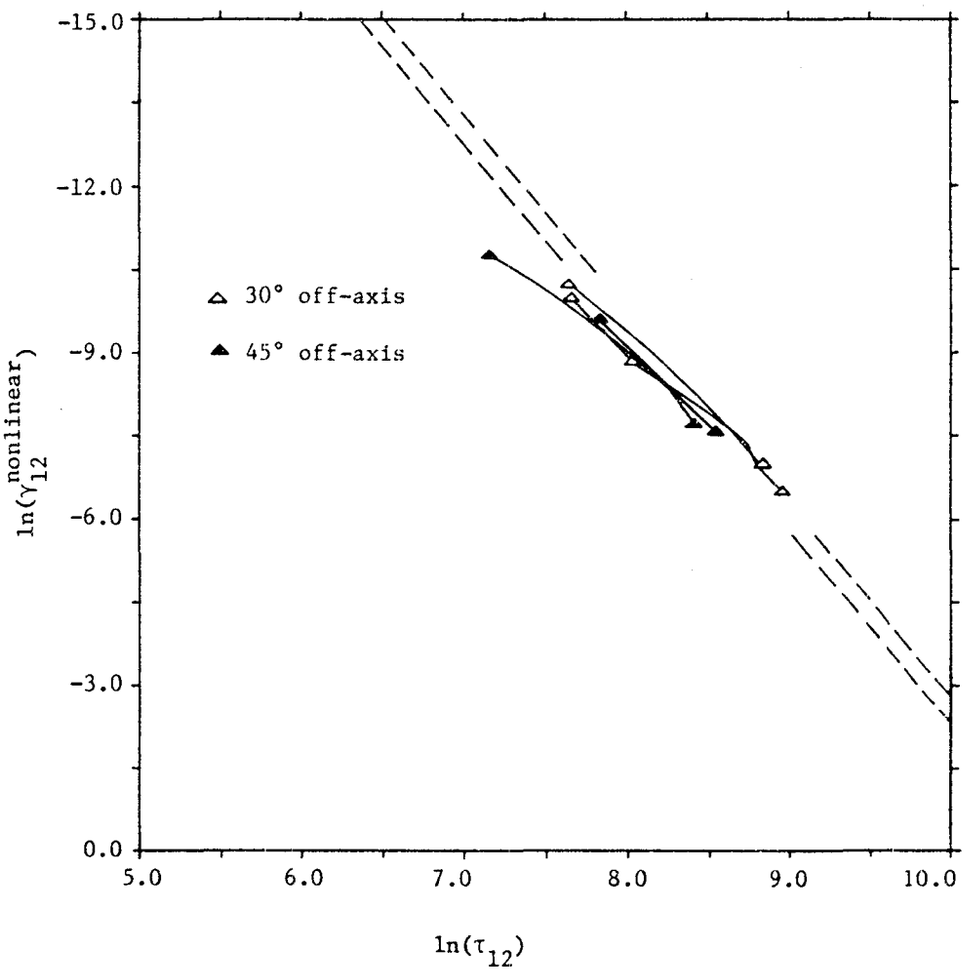

Fig. 4.13 Log-log graph of the resolved permanent shear strain and the corresponding unloading shear stress in the cyclically loaded Gr/Pi 30° and 45° coupons

given off-axis orientation. The uncorrected monotonic and cyclic stress-strain curves can be nearly brought into coincidence by merely rotating the graph of one by a small amount about the origin relative to the other, indicating that the small differences present in specimens of the same orientation are most likely caused by slight material or experimental variations.

The coincidence of the hardening envelope obtained from a cyclic test with the monotonic response suggests a change in the reloading characteristics within the region bounded by the envelope. Two points of interest have been observed. First, there appears to be a noticeable change in the initial shear moduli at the points of reloading i.e. $\sigma_6 = 0$, for low off-axis configurations. This is particularly noticeable in the 5° and 10° off-axis coupons where the influence of longitudinal stress σ_{11} is significant. The initial shear moduli at points of reloading decrease with the number of cycles for the above orientations suggesting material degradation due perhaps to micro-crack growth. The hardening exponent on the other hand exhibits a bi-modulus character, remaining constant and significantly smaller than the exponent characterizing monotonic loading within the envelope and increasing sharply in the vicinity of the last (maximum) unloading level. This is illustrated in Fig. 4.14 for a typical 10° off-axis specimen.

Table 4.2 summarizes the monotonic and cyclic response

Table 4.2 Summary of monotonic and cyclic response of the Gr/Pi coupons in terms of hardening exponents and parameters

off-axis fiber orientation	$A^{*}_{66}(\theta)$ based on $n_6 = 3.467$	$A^{*unl}_{66}(\theta)$ based on $n_6 = 3.467$	$A^{*unl}_{66}(\theta)/A^{*}_{66}(\theta)$ ratio	$A^{*}_{22}(\theta)$ based on $n_2 = 2.670$ linear analysis	$A^{*}_{22}(\theta)$ based on $n_2 = 2.303$ nonlinear analysis of Chap. 5
10°	2.57632×10^{-16}	7.56813×10^{-17}	0.305	—	—
15°	1.64273×10^{-16}	4.82565×10^{-17}	0.285	5.38494×10^{-13}	7.17800×10^{-12}
30°	1.64273×10^{-16}	3.82565×10^{-17}	0.285	—	—
45°	2.21746×10^{-16}	8.36408×10^{-17}	0.397	1.14294×10^{-13}	2.31873×10^{-12}
60°	3.47767×10^{-16}	1.21697×10^{-16}	0.365	2.23936×10^{-14}	8.19567×10^{-13}
75°	6.66161×10^{-16}	—	—	1.70948×10^{-14}	7.05408×10^{-12}
90°	—	—	—	1.39961×10^{-14}	6.38280×10^{-13}

for the various coupons tested. It must be noted that the unloading shift parameters follow the same trend as those for monotonic loading with the exception of 45° off-axis coupons. This is indicated by the ratio of unloading to loading shift parameters given in the table. This ratio does not vary significantly for the 10°, 15° and 30° off-axis configurations. The 60° orientation yielded a somewhat higher ratio, while still retaining the above trend, which could be attributable perhaps to the difficulty of measuring accurately small permanent strains inherent at high off-axis angles.

4.3.3 Transverse Response

The transverse response in the material principal coordinate system exhibits very little nonlinearity, dissipation or permanent strain accumulation as can be seen in Fig. 4.15 which shows the behavior of a typical 60° off-axis coupon. Similar response has been observed for other configurations. Cyclic experiments have not been performed for 75° and 90° off-axis orientations due to small strains at failure and the response of testing machine overshadowing the material response at points of stress reversals.

The corrected monotonic stress-strain curves for the off-axis orientations $15° \leq \theta \leq 90°$ are shown in Fig. 4.16. These have been plotted with the Poisson's strains eliminated in order to illustrate the extent of stress inter-

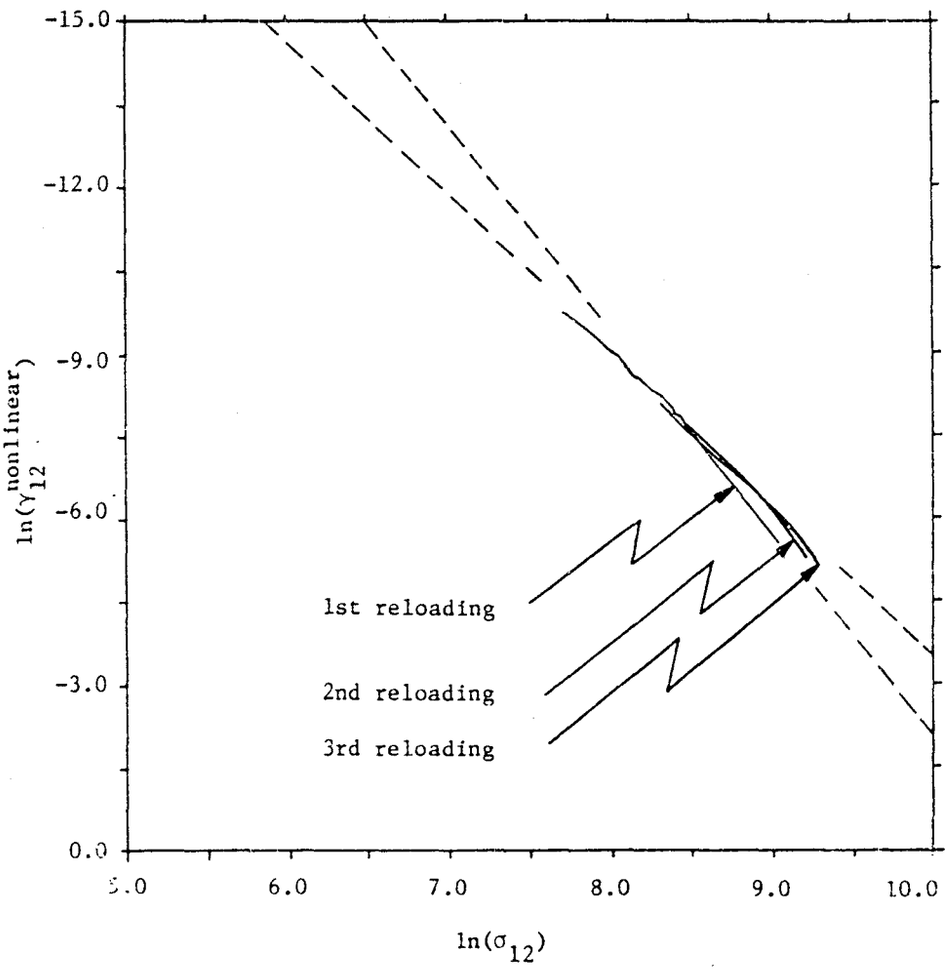

Fig. 4.14 Reloading shear stress-strain response of a typical Gr/Pi 10° coupon cyclically loaded to increasing stress level

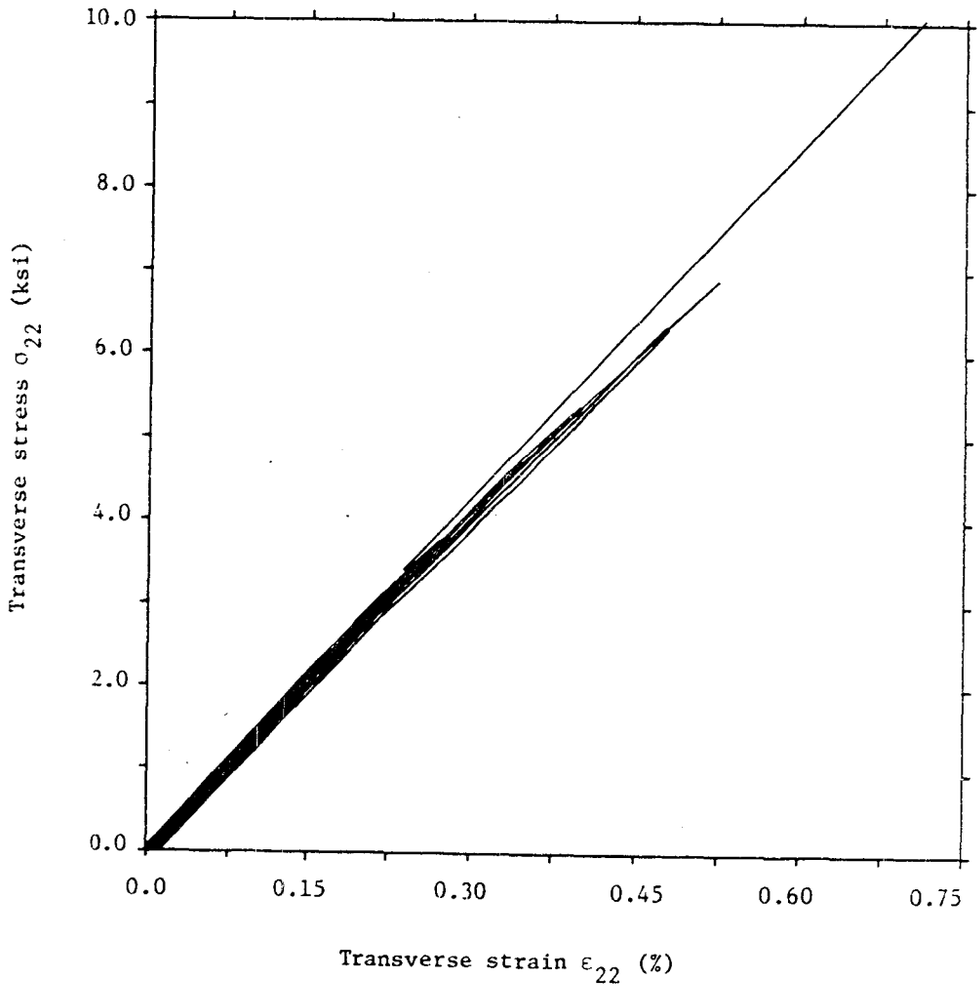

Fig. 4.15 Resolved transverse stress-strain response of a typical Gr/Pi 60° coupon in cyclic loading. Shear-coupling not eliminated

action present. Poisson's strains were assumed to be linearly dependent on the associated longitudinal stress. The nonlinear portion of transverse strain as a function of stress on the other hand has been plotted on log-log scale of Fig. 4.17 to determine the nature of nonlinearity. It can be observed that a power-law representation with the same hardening exponent for all the configurations (with the exception of the 30° orientation) will yield good characterization of the transverse response under combined as well as pure loading. Again, as in the case of the off-axis shear response, the variations in shift parameters $A_{22}(\theta)$ clearly indicate the degree of stress interaction present. The transverse stress-strain response predicted on the basis of the determined hardening exponent and shift parameters of Fig. 4.17 is given by the indicated symbols in Fig. 4.16.

The Poisson's response of the 90° configuration on the other hand remains virtually constant with very little variation from specimen to specimen despite noticeable deviation from transversely isotropic behavior. As mentioned previously, this could be caused by strain gage sensitivity problems associated with measuring such small strains.

The cyclic response in the transverse direction appears to follow similar trends as those of the shear response. However, because the associated strains are very small and the possibility of error relatively large, no detailed discussion beyond the above observation will be attempted.

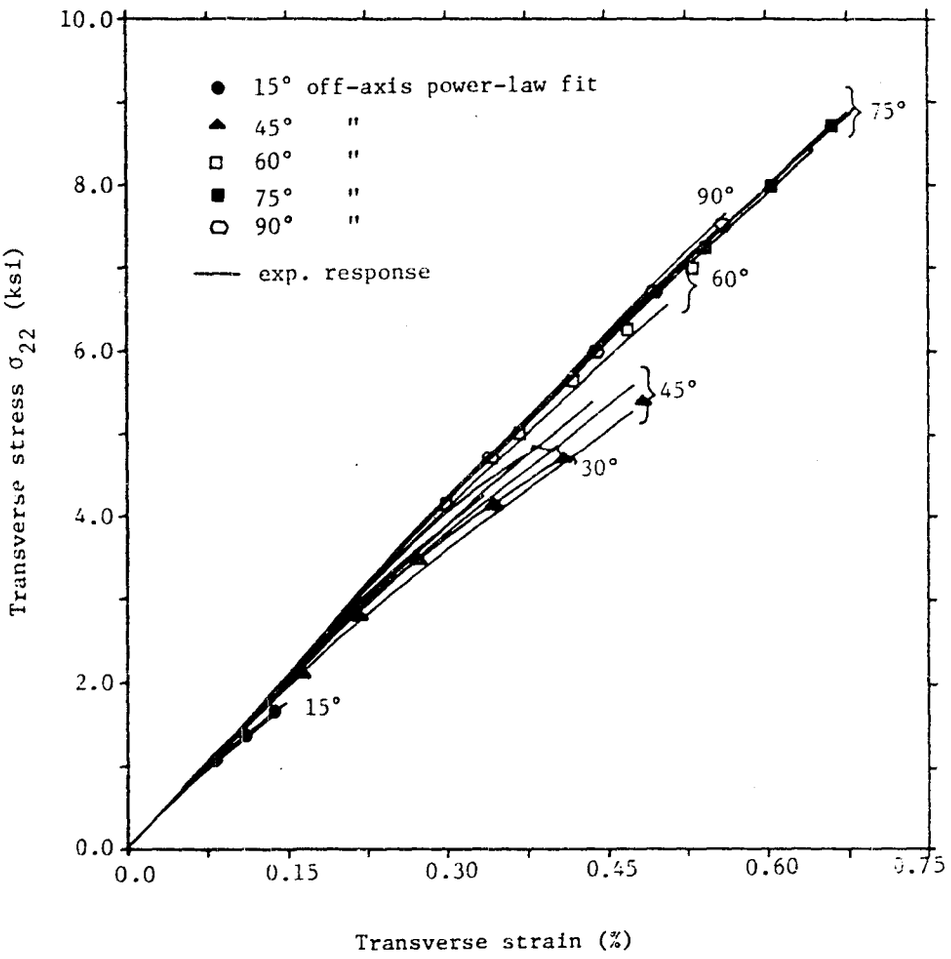

Fig. 4.16 Corrected resolved transverse stress-strain response of the Gr/Pi coupons in the range $15° \leq \theta \leq 90°$. Poisson's strain eliminated assuming linear response. Corrected on the basis of the Halpin-Pagano model

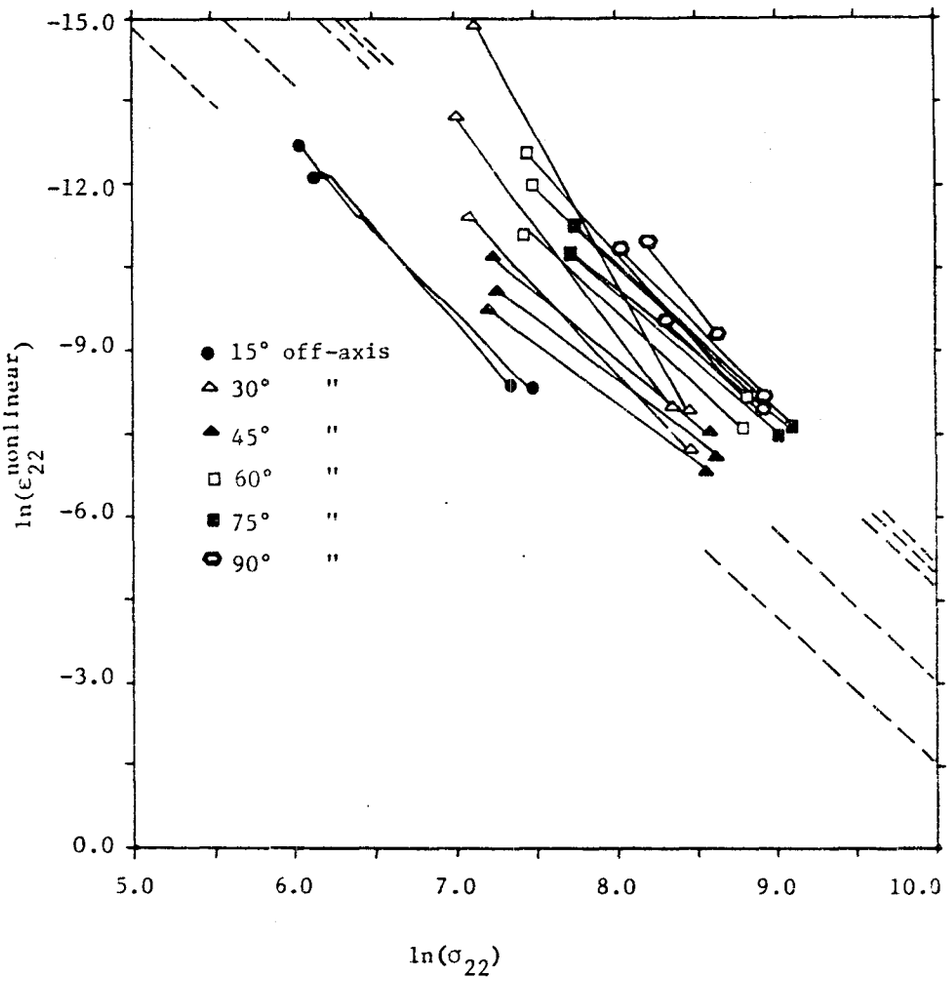

Fig. 4.17 Log-log graph of the resolved transverse stress and nonlinear portion of the corresponding strain of the Gr/Pi coupons in the range $15° \leq \theta \leq 90°$

4.4 Failure

The ultimate axial stress σ_{xx} as a function of the off-axis angle for the various configurations tested is illustrated in Fig. 4.18 for both monotonic and cyclic cases. Several noteworthy aspects regarding failure have been observed. First of all, all the specimens, with the exception of 0° configuration, failed or fractured along the fiber direction as revealed by visual examination of the fracture surfaces. These surfaces were quite smooth even at low off-axis angles. The coupons generally failed away from grip regions with the exception of the 5° off-axis orientations pointing to the new test fixture's capability of inducing test-section failures. Fracture location of the 5° off-axis coupons was indicative of the "scissoring effect" due to the fibers originating in the endgrips (see test specimen dimensions of Fig. 3.10). The 0° coupons on the other hand either failed explosively, first splitting along the fibers and subsequently shattering which gave them a broom-like appearance or fractured perpendicular to the fibers producing a jagged surface. The typical failed specimens of each orientation are shown in Fig. 4.19.

The ultimate lamina stresses, longitudinal and transverse strains as well as measured fracture angles are reported in Table 4.3. As can be observed the strength data is relatively consistent with deviations from the average behavior on the order of few percent for most off-axis

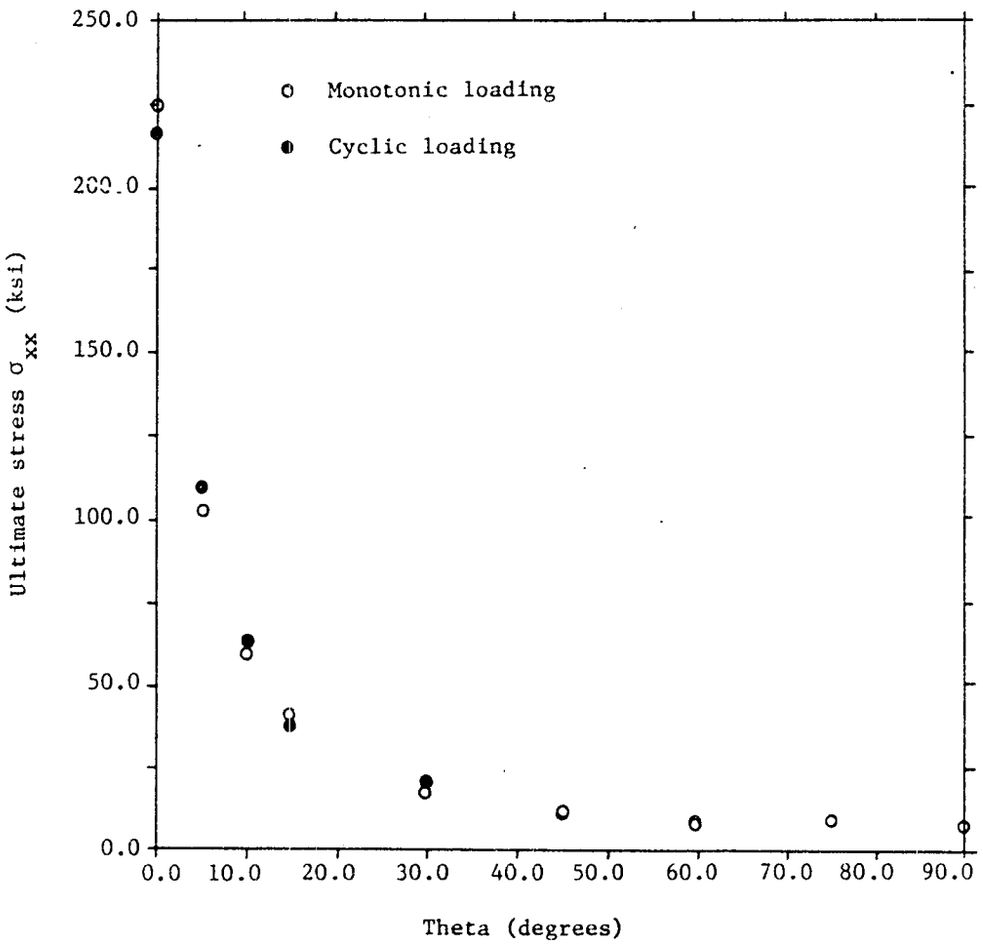

Fig. 4.18 Ultimate stress as a function of the fiber orientation

Fig. 4.19 Failed, unidirectional, off-axis Gr/Pi tension coupons

Table 4.3 Summary of ultimate stresses, strains and fracture angles of the Gr/Pi coupons

* - excluded from averaging
/ - separates monotonic and cyclic average strength data

Specimen designation #	Ultimate stress σ_{xx} (psi)	% difference σ_{xx} from average	Ultimate strain ϵ_{xx} (%)	Fracture angle
1-15-0°	224,679	-0.3	1.0491	90° - jagged
1-16-0°	227,132	+0.7	1.0548	90° - jagged
1-17-0°	224,274	-0.5	1.0379	split & shatter
1-18-0°	170,976*	—	0.8443	split & shatter
1-19-0°	211,436	-2.4	0.9803	split & shatter
1-21-0°	221,900	+2.4	1.0323	split & shatter
0° average	225,362/ 216,668			
1-5-5°	105,660	+2.9	0.6724	5°
1-6-5°	98,939	-3.6	0.6221	5°
1-7-5°	103,432	+0.7	0.6908	5.2°
1-16-5°	107,557	-1.2	0.6581	4.5°
1-17-5°	110,000	+1.0	0.6415	4.5°
1-18-5°	109,153	+0.2	0.6379	4.75°
5° average	102,677/ 108,903			
1-12-10°	58,924	+0.2	0.5792	9.5°
1-15-10°	55,859	-4.9	0.5488	9.5°
1-17-10°	59,973	+2.0	0.5844	9.75°
1-18-10°	60,335	+2.6	0.5976	10.4°
1-5-10°	63,490	+1.2	0.6421	9.5°
1-7-10°	62,086	-1.0	0.6450	9.75°
1-13-10°	62,598	-0.2	0.6259	9.75°
10° average	58,773/ 62,725			
2-4-15°	42,475	+2.8	0.6351	14.8°
2-5-15°	40,457	-2.1	0.6272	14.5°
2-6-15°	41,018	-0.7	0.6683	14.75°
2-2-15°	39,202	-3.5	0.6022	14.75°
2-3-15°	33,955	-10.4	0.5235	14.5°
2-8-15°	40,515	+6.9	0.6617	14.5°
15° average	41,317/ 37,891			

Table 4.3 (cont'd.) Summary of ultimate stresses, strains and fracture angles of the Gr/Pi coupons

/ - separates monotonic and cyclic average strenght data

Specimen designation #	Ultimate stress σ_{xx} (psi)	% difference σ_{xx} from average	Ultimate strain ε_{xx} (%)	Fracture angle
2-8-30°	18,617	+5.0	0.7807	30°
2-9-30°	17,433	-1.6	0.7027	30°
2-15-30°	17,115	-3.4	0.6223	30°
2-19-30°	17,200	-7.0	0.7176	29.75°
2-22-30°	19,796	+7.0	0.8216	30°
30° average	17,722/ 18,498			
3-13-45°	11,893	-1.9	0.7864	45.2°
3-15-45°	12,276	+1.2	0.7983	45.2°
3-18-45°	12,228	+0.8	0.8100	45°
3-21-45°	11,302	+2.6	0.7360	44.5°
3-22-45°	10,721	-2.6	0.6422	44.25°
45° average	12,132/ 11,011			
2-10-60°	9,304	+5.1	0.6341	60.4°
2-13-60°	9,210	+4.0	0.6817	61.2°
2-15-60°	8,043	-9.1	0.5845	59°
2-19-60°	9,226	+3.2	0.6592	60°
2-20-60°	8,658	-3.2	0.6400	60.5°
60° average	8,793/ 8,942			
2-11-75°	8,793	-2.3	0.6322	75.8°
2-14-75°	8,830	-1.9	0.6583	75.6°
2-16-75°	9,387	+4.3	0.7077	74.8°
75° average	9,003			
1-13-90°	7,600	+1.5	0.5674	90.25°
1-15-90°	5,723	—	0.4062	90°
1-16-90°	7,367	-1.5	0.5419	90°
90° average	7,484			

configurations. The observed differences in strength between monotonic and cyclic tests do not appear to be significant and their apparent randomness tends to be indicative of slight material variations rather than the particular testing program. However, one important pecularity has been brought forth by the cyclic tests. All of the configurations, with the exception of the 15° off-axis coupons, failed at stress levels above the maximum unloading stress irrespectively of the number of times they were cycled (3, 4, 5, or 6). All three 15° off-axis coupons on the other hand failed below the maximum unloading stress pointing to the possibility of path dependent failure for this orientation. It must be noted that in most cases the maximum unloading stress was chosen fairly close to the ultimate stress of the particular configuration cycled, as determined from monotonic tests. Such peculiar response is illustrated in Fig. 4.9.

4.5 Summary of Observed Response of the Gi/Pi System

i) Initial (linearized) response can be very well approximated for most off-axis configurations by a transversely isotropic model with $G_{12} = 0.725 \times 10^6$ psi yielding best fit with the experimental data.

ii) Longitudinal stress-strain response appears to be reversible with a stiffening, bi-modulus character. Major Poisson's ratio also exhibits a bi-modulus, reversible appearance. Experimental data reported in the literature as well as tests performed on the graphite fibers employed in this particular system (courtesy of Celenese Corporation) suggest that the stiffening

characteristics are due to straightening of the cellular structure of graphite fibers. Thus if dissipation due to fiber breakage, fiber/matrix interface debonding, matrix crazing, etc. is taking place it has negligible effect on the overall response in the fiber direction under the outlined testing conditions.

iii) Shear response in the material principal coordinate system exhibits considerable nonlinearity and dissipation as well as measurable permanent strain accumulation as verified by cyclic tests. Monotonic shear response for the various off-axis configurations tested can be described with good accuracy by a power-law relation with a constant hardening exponent and orientation-dependent shift parameters. This is indicative of the so-called stress interaction phenomenon in which the longitudinal stress σ_{11} also plays a role for this particular material system. Monotonic and cyclic responses are similar in the sense that the shift parameters for both types of loading follow the same trend for most off-axis configurations. Hardening envelopes of cyclic tests furthermore coincide to a large extent with monotonic curves and the material "remembers" the last unloading point while generating hysteresis loops during reloading within the hardening envelope.

iv) Monotonic transverse response follows the same trends as in shear except that the amount of nonlinearity and dissipation is significantly smaller in this case. Power-law behavior with a smaller hardening exponent is applicable, stress interaction is noticeable and the minor Poisson's ratio remains practically constant until failure.

v) Failure characteristics appear to exhibit two distinct modes: fracture along the fiber direction resulting in visually smooth surfaces for all the off-axis orientations with the exception of the 0° coupons which failed either perpendicular to the fibers or by splitting and then exploding which resulted in their final broom-like appearance.

5. APPLICATION OF ENDOCHRONIC THEORY TO THE OBSERVED RESPONSE OF THE GR/PI SYSTEM

5.1 Introduction

The observations on the experimentally determined response of the Gr/Pi system outlined in the previous chapter will form a basis for the development of a material model utilizing the previously developed general equations of endochronic theory. The discussions will be divided into three sections. The first part will deal with the apparent reversible behavior that has been observed in the fiber direction. To this end a potential is proposed which models the stiffening, bi-modulus reversible response parallel and perpendicular to the fibers. Certain properties as well as thermodynamic constraints on the newly introduced potential will be briefly outlined and the various constants evaluated from experimental data.

The combined response is discussed in the second section where the specialization of the general endochronic equations for transversely isotropic media is caried out explicitly to demonstrate their applicability to this particular material system. Theoretical-experimental correlation will be subsequently carried out for the various off-axis configurations in both monotonic and cyclic modes after evaluation of the necessary material parameters employing phenomenological as well as micromechanics-aided approach.

Finally, the failure characteristics will be examined

in the third part where the predictions of two representative and currently used criteria as well as a newly proposed micromechanics-based failure condition will be compared with the observed monotonic response.

5.2 Reversible Response

In order to model the reversible portion of the response a potential of the following form is proposed:

$$-G_o = \frac{1}{2} A_{ij}\sigma_i\sigma_j + \frac{1}{\alpha}\left(e^{-\alpha\sqrt{\ell_{ij}\sigma_i\sigma_j}} - 1\right) + \sqrt{\ell_{ij}\sigma_i\sigma_j} \tag{5.1}$$

so that the reversible strains are given by:

$$\varepsilon_i^R = -\frac{\partial G_o}{\partial \sigma_i} = A_{ij}\sigma_j + \frac{\ell_{ij}\sigma_j}{\sqrt{\ell_{mn}\sigma_m\sigma_n}}\left[1 - e^{-\alpha\sqrt{\ell_{mn}\sigma_m\sigma_n}}\right] \tag{5.2}$$

In the above the following are assumed at the outset: ℓ_{ij} is positive-definite and the parameter α whose significance will be shortly discussed is greater than zero. Applying the restriction $\delta^2(-G_o) \geq 0$ and examining the limiting behavior of the above, the following thermodynamic constraints are obtained as is illustrated in Appendix C:

$$\lim_{\sigma_i \to 0} \delta^2(-G_o) = (A_{ij} + \alpha\ell_{ij})\delta\sigma_i\delta\sigma_j \geq 0 \tag{5.3}$$

so that $(A_{ij} + \alpha\ell_{ij})$ must be positive-definite;

$$\lim_{\sigma_i \to \infty} \delta^2(-G_o) = A_{ij}\delta\sigma_i\delta\sigma_j \geq 0 \tag{5.4}$$

and therefore A_{ij} by itself must also be positive-definite.

Furthermore, it can also be shown (See Appendix C) that the above constraints in conjunction with the initial two assumptions are sufficient for the condition $\delta^2(-G_0) \geq 0$ to hold true for all plane stress loading situations.

At the outset we limit our discussion of the nonlinear elastic response to normal strains along and perpendicular to the fibers in view of lack of evidence of initial stiffening in shear. Thus we assume that $\ell_{44} = \ell_{55} = \ell_{56} = 0$ which is consistent with the constraint given above.

The physical significance of the various material parameters can best be illustrated through hypothetical loading experiments along the specified material principal directions. Let us consider the following loading situation to illustrate the general methodology.

Example: $\sigma_1 \neq 0$, all other zero

The following plane stress-strain equations are obtained from Eqns. 5.2

$$\varepsilon_1^R = A_{11}\sigma_1 + \sqrt{\ell_{11}}(1 - e^{-\alpha\sqrt{\ell_{11}}\sigma_1})$$

$$\varepsilon_2^R = A_{12}\sigma_1 + \frac{\ell_{12}}{\sqrt{\ell_{11}}}(1 - e^{-\alpha\sqrt{\ell_{11}}\sigma_1}) \qquad (5.5)$$

The significance of the various material parameters is brought forth by examining the limiting behavior of the above system of equations. Differentiating the first of

Eqns. 5.5 with respect to σ_1 we obtain:

$$\frac{\partial \varepsilon_1^R}{\partial \sigma_1} = A_{11} + \alpha \ell_{11} e^{-\alpha \sqrt{\ell_{11}} \sigma_1}$$

so that:

$$\left.\frac{\partial \varepsilon_1^R}{\partial \sigma_1}\right|_{\sigma_1=0} = A_{11} + \alpha \ell_{11} \, , \quad \left.\frac{\partial \varepsilon_1^R}{\partial \sigma_1}\right|_{\sigma_1=\infty} = A_{11} \tag{5.6}$$

and since $\alpha > 0$, A_{11}, $\ell_{11} \geq 0$; the initial compliance (stiffness) is greater (smaller) than the limiting compliance (stiffness) in case of strict inequality of the second relation so that stiffening response in the fiber direction has been generated. The initial and final responses along the fiber direction are thus, respectively:

$$\begin{aligned} \varepsilon_1^R(\sigma_1 \to 0) &= (A_{11} + \alpha \ell_{11}) \sigma_1 \\ \varepsilon_1^R(\sigma_1 \to \infty) &= A_{11} \sigma_1 + \sqrt{\ell_{11}} \end{aligned} \tag{5.7}$$

and thus $\sqrt{\ell_{11}}$ is the $\sigma_1 = 0$ intercept of the final limiting response. The geometric interpretation of α can now be obtained upon finding the intersection of the two limiting curves. Setting $\varepsilon_1^R(\sigma_1 \to 0) = \varepsilon_1^R(\sigma_1 \to \infty)$ we obtain:

$$\alpha = \frac{1}{\sqrt{\ell_{11}} \, \sigma_1^*} \tag{5.8}$$

where σ_1^* is the common stress at the intersection of these two curves. We can therefore adjust the initial stiffening response in conjunction with the "knee" of the stress-strain

curve by varying the parameter α for a given ℓ_{11}. The features of the model outlined above are illustrated in Fig. 5.1 for the longitudinal stress-strain response. In summary we note that the three material parameters A_{11}, ℓ_{11} and α can easily be obtained from a single longitudinal tension test, i.e. Eqns. 5.6 and 5.7.

Some of the interesting features of the Poisson's or strain-strain behavior in longitudinal tension inherent in the model are best examined by separating the response into constant and stress-dependent components. Equating the exponential parts of Eqns. 5.5 and then differentiating with respect to the ε_1-strain we obtain:

$$\frac{\partial \varepsilon_2}{\partial \varepsilon_1} = -\nu_{12} = \frac{\ell_{12}}{\ell_{11}} + \frac{(A_{12}\,\ell_{11} - A_{11}\ell_{12})}{\ell_{11}} \frac{\partial \sigma_1}{\partial \varepsilon_1} \tag{5.9}$$

Three types of longitudinal strain-strain response are now possible depending on the value of the term $(A_{12}\ell_{11} - A_{11}\ell_{12})$

$$\text{i)} \quad A_{12}\ell_{11} - A_{11}\ell_{12} = 0; \quad \frac{\partial \varepsilon_2}{\partial \varepsilon_1} = \text{constant}$$

$$\text{ii)} \quad A_{12}\ell_{11} - A_{11}\ell_{12} < 0; \quad \frac{\partial \varepsilon_2}{\partial \varepsilon_1} = \text{constant} - f(\sigma_1), \quad f'(\sigma_1) > 0 \tag{5.10}$$

$$\text{iii)} \quad A_{12}\ell_{11} - A_{11}\ell_{12} > 0; \quad \frac{\partial \varepsilon_2}{\partial \varepsilon_1} = \text{constant} + f(\sigma_1), \quad f'(\sigma_1) > 0$$

Thus either a constant, stiffening or softening

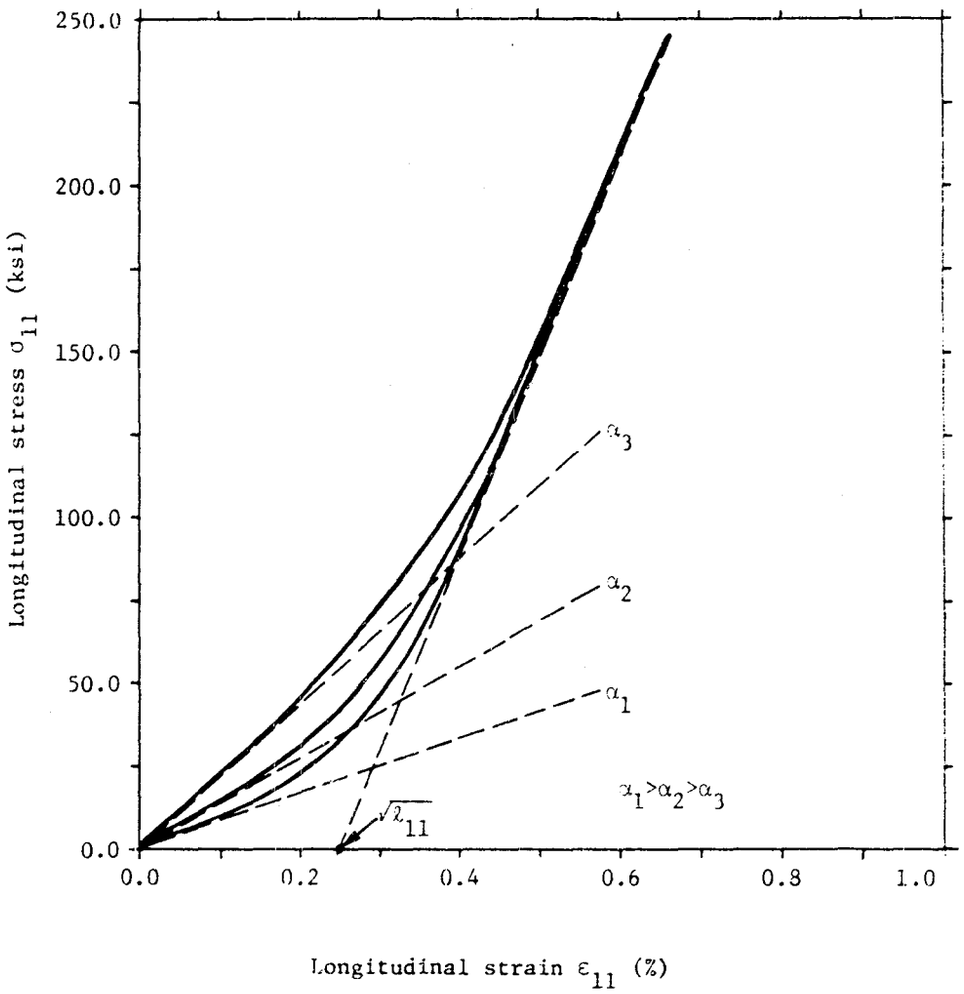

Fig. 5.1 Longitudinal stress-strain response of a hypothetical 0° Gr/Pi coupon illustrating certain features of stiffening behavior of the proposed model

Poisson's response can be generated according to the above scheme. The unknown constants A_{12} and ℓ_{12} are obtained by examining the limiting response as outlined previously. To this end it is more convenient to express the instantaneous Poisson's ratio in a more direct way by differentiating the second of Eqns. 5.5 with respect to the ε_1-strain to obtain:

$$\frac{\partial \varepsilon_2}{\partial \varepsilon_1} = (A_{12} + \alpha \ell_{12} e^{-\alpha \sqrt{\ell_{11}}\, \sigma_1}) \frac{\partial \sigma_1}{\partial \varepsilon_1} \tag{5.11}$$

so that

$$\left.\frac{\partial \varepsilon_2}{\partial \varepsilon_1}\right|_{\sigma_1=0} = (A_{12} + \alpha \ell_{12}) \left.\frac{\partial \sigma_1}{\partial \varepsilon_1}\right|_{\sigma_1=0}, \quad \left.\frac{\partial \varepsilon_2}{\partial \varepsilon_1}\right|_{\sigma_1=\infty} = A_{12} \left.\frac{\partial \sigma_1}{\partial \varepsilon_1}\right|_{\sigma_1=\infty} \tag{5.12}$$

and thus the entire treatment in analyzing major Poisson response follows along the same lines as that for the longitudinal behavior. The discussion regarding the transverse response is evidently completely analogous.

The various material parameters of the proposed elastic potential have been evaluated on the basis of average limiting responses of the tested coupons using the relations developed above. Since the transverse response appears to be coupled, consisting of reversible and dissipative portions conceptually speaking, a similar condition to the first of Eqns. 5.10 was employed to find a relationship between A_{22} and ℓ_{22} in view of the available observed response, i.e. $A_{12}\ell_{22} - A_{22}\ell_{12} = 0$. These parameters are

Table 5.1 Elastic material parameters of the "nonlinear" elastic potential G_0 for the Gr/Pi composite system

A_{11}	A_{12}	A_{22}	A_{66}
0.04296×10^{-6}	-0.01366×10^{-6}	0.54370×10^{-6}	1.37931×10^{-6}
ℓ_{11}	ℓ_{12}	ℓ_{22}	α
0.37800×10^{-6}	-0.20000×10^{-6}	7.95988×10^{-6}	1.991×10^{-2}

$$-G_0 = \frac{1}{2} A_{ij}\sigma_i\sigma_j + \frac{1}{\alpha}\left(e^{-\alpha\sqrt{\ell_{ij}\sigma_i\sigma_j}} - 1\right) + \sqrt{\ell_{ij}\sigma_i\sigma_j}$$

given in Table 5.1 and it can be easily verified by inspection that they obey the derived thermodynamic constraints. The predicted average response in longitudinal tension is shown in Figs. 5.2 and 5.3 with selected experimental data included for comparison. The agreement appears to be good. It must be mentioned that even better agreement can be obtained if specific coupons are used to evaluate the necessary parameters and then compared directly with the predicted response on a one-to-one, instead of average, basis.

The proposed elastic model predicts that the reversible portion of the total response in transverse tension yields stiffening response whereas the character of the transverse dissipative behavior has been determined in the preceeding chapter on the basis of deviation from linearized stress-strain relation. To correct this discrepancy the transverse hardening response has been re-evaluated using the newly proposed nonlinear equations to eliminate the reversible portion of the total response. The results are illustrated in Fig. 5.4. Two noteworthy aspects can be delineated; the decrease in the hardening exponent and the subsequent increase in the shift parameters, and considerable reduction in the fluctuations of the hardening exponent from orientation to orientation for most off-axis angles. Thus it appears that the newly introduced elastic potential brings more consistency to the observed dissipative portion of the total transverse response when analyzed in the outlined

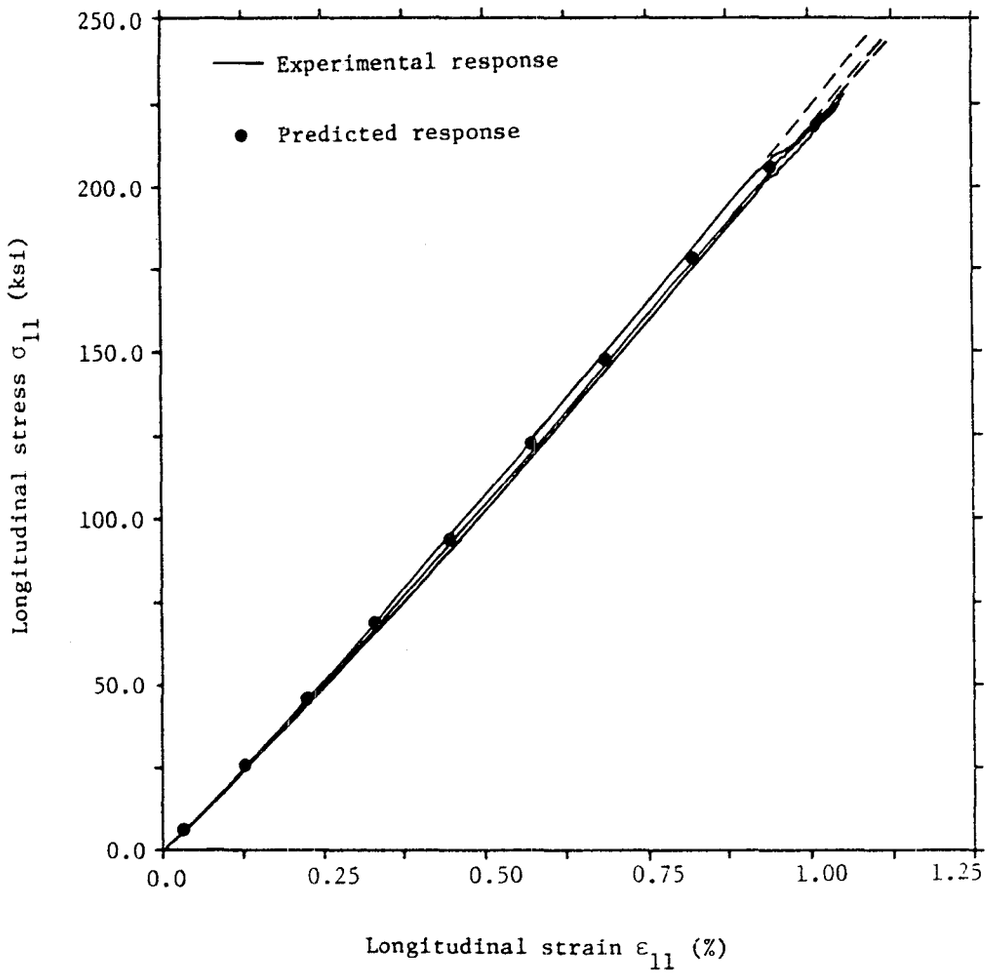

Fig. 5.2 Longitudinal tension of 0° Gr/Pi coupons - predicted and observed stress-strain response

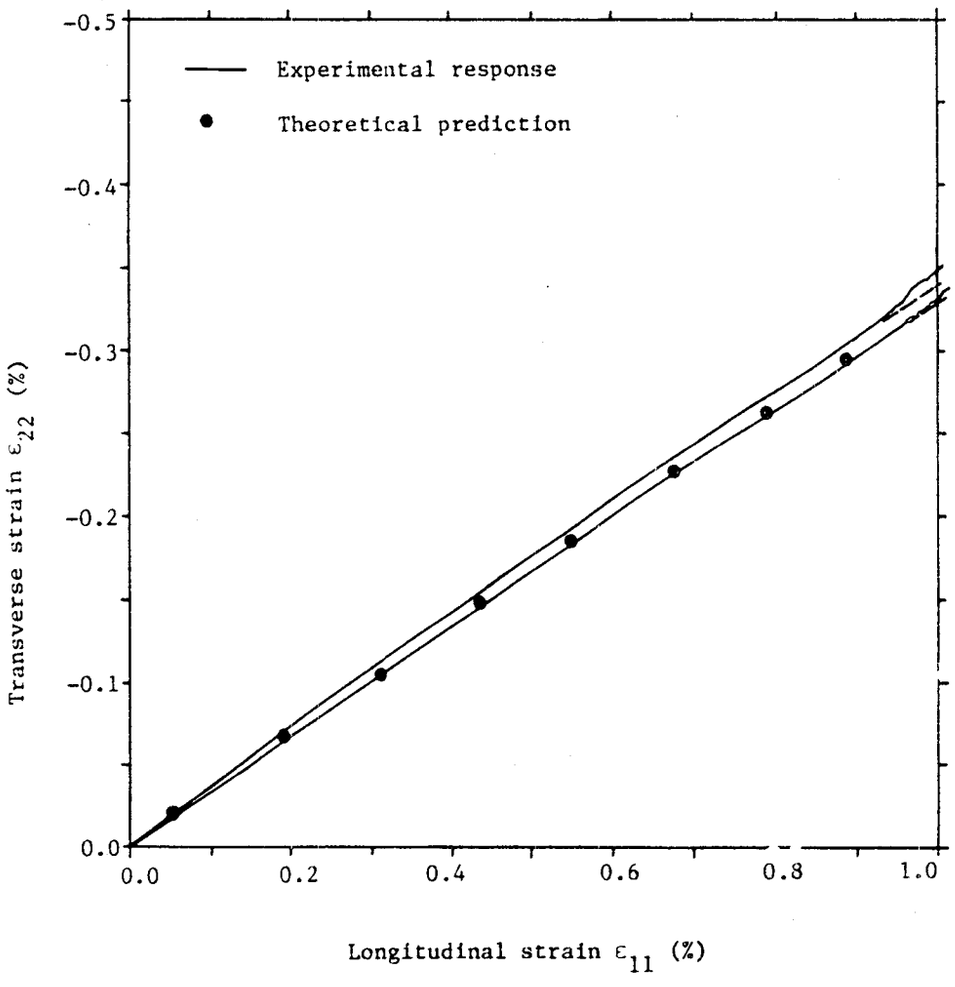

Fig. 5.3 Longitudinal tension of 0° Gr/Pi coupons - predicted and observed Poisson's response

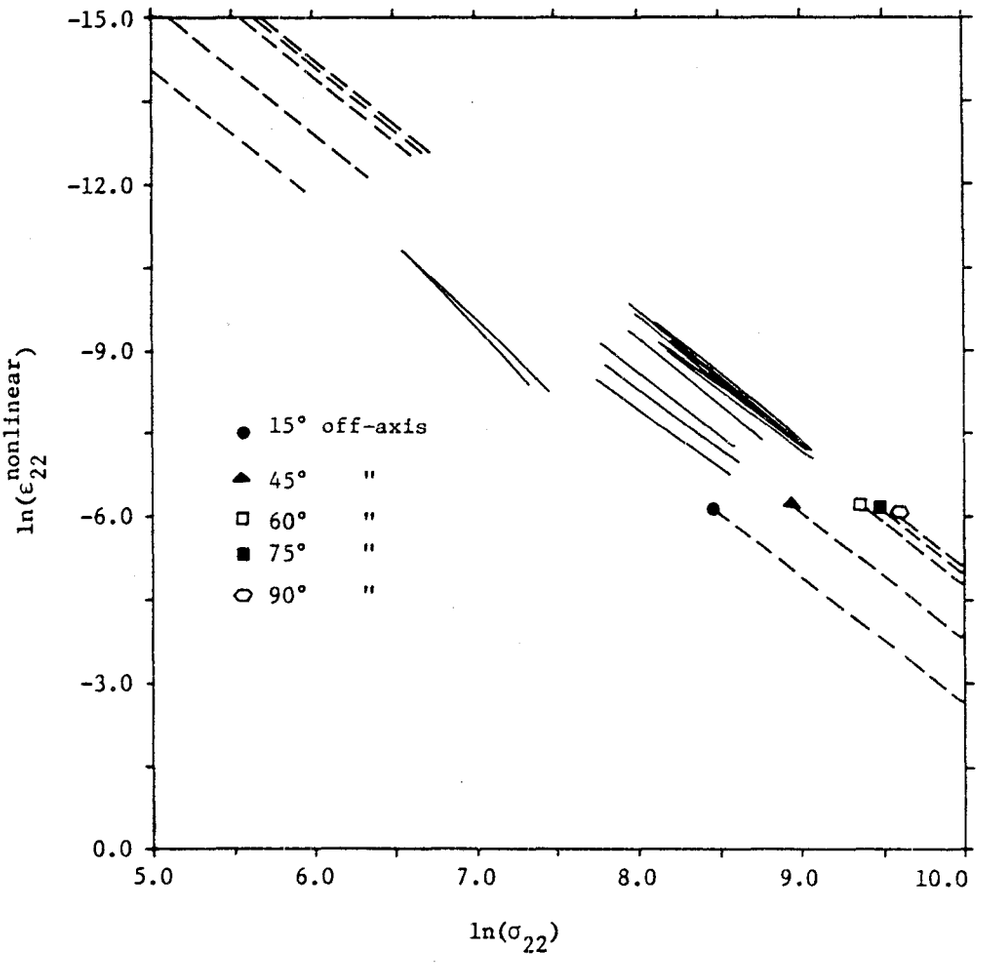

Fig. 5.4 Log-log graph of the resolved transverse stress and dissipative portion of the corresponding strain of the Gr/Pi coupons in the range $15° \leq \theta \leq 90°$ re-examined with the nonlinear elastic model

manner.

5.3 Combined Response

In specializing the general equations developed in Chapter II to model the dissipative portion of the experimentally determined response of the Gr/Pi system we are guided by the two observations of power-law relationship between stress and dissipative strain and apparent reversible behavior along fiber direction. The first observation implies "the presence" of large number of internal variables while the second restricts the influence of dissipation modes to the plane of transverse isotropy, that is;

$$b_{11}^{\alpha} = b_{12}^{\alpha} = 0, \quad B_{11}^{\alpha} = B_{12}^{\alpha} = 0, \quad C_{11}^{\alpha} = C_{12}^{\alpha} = 0 \qquad (5.13)$$

for each internal variable specified by α. On the basis of the above observations we assume that the response of this particular composite system can be approximated by the following set of equations, c.f. Eqns. 2.12-2.15:

$$\begin{Bmatrix}\varepsilon_1\\ \varepsilon_2\\ \varepsilon_3\end{Bmatrix} = -\begin{Bmatrix}\frac{\partial G_0}{\partial\sigma_1}\\ \frac{\partial G_0}{\partial\sigma_2}\\ \frac{\partial G_0}{\partial\sigma_3}\end{Bmatrix} - \sum_{\alpha=1}^{n}\begin{bmatrix}0 & 0 & 0\\ 0 & B_{22}^{\alpha} & B_{23}^{\alpha}\\ 0 & B_{23}^{\alpha} & B_{22}^{\alpha}\end{bmatrix}\begin{Bmatrix}q_1^{\alpha}\\ q_2^{\alpha}\\ q_3^{\alpha}\end{Bmatrix}$$

$$\begin{Bmatrix}\varepsilon_4\\ \varepsilon_5\\ \varepsilon_6\end{Bmatrix} = -\begin{Bmatrix}\frac{\partial G_0}{\partial\sigma_4}\\ \frac{\partial G_0}{\partial\sigma_5}\\ \frac{\partial G_0}{\partial\sigma_6}\end{Bmatrix} - \sum_{\alpha=1}^{n}\begin{bmatrix}\frac{1}{2}\left(B_{22}^{\alpha}-B_{23}^{\alpha}\right) & 0 & 0\\ 0 & B_{66}^{\alpha} & 0\\ 0 & 0 & B_{66}^{\alpha}\end{bmatrix}\begin{Bmatrix}q_4^{\alpha}\\ q_5^{\alpha}\\ q_6^{\alpha}\end{Bmatrix} \tag{5.14}$$

$$\begin{bmatrix}0 & 0 & 0\\ 0 & b_{22}^{\alpha} & b_{23}^{\alpha}\\ 0 & b_{23}^{\alpha} & b_{22}^{\alpha}\end{bmatrix}\begin{Bmatrix}\frac{dq_1^{\alpha}}{dz}\\ \frac{dq_2^{\alpha}}{dz}\\ \frac{dq_3^{\alpha}}{dz}\end{Bmatrix} + \begin{bmatrix}0 & 0 & 0\\ 0 & C_{22} & C_{23}\\ 0 & C_{23}^{\alpha} & C_{22}^{\alpha}\end{bmatrix}\begin{Bmatrix}q_1^{\alpha}\\ q_2^{\alpha}\\ q_3^{\alpha}\end{Bmatrix} = -\begin{bmatrix}0 & 0 & 0\\ 0 & B_{22}^{\alpha} & B_{23}^{\alpha}\\ 0 & B_{23}^{\alpha} & B_{22}^{\alpha}\end{bmatrix}\begin{Bmatrix}\sigma_1\\ \sigma_2\\ \sigma_3\end{Bmatrix}$$

$$\begin{bmatrix} \frac{1}{2}(b_{22}^{\alpha}-b_{23}^{\alpha}) & 0 & 0 \\ 0 & b_{66}^{\alpha} & 0 \\ 0 & 0 & b_{66}^{\alpha} \end{bmatrix} \begin{Bmatrix} \frac{dq_4^{\alpha}}{dz} \\ \frac{dq_5^{\alpha}}{dz} \\ \frac{dq_6^{\alpha}}{dz} \end{Bmatrix} + \begin{bmatrix} \frac{1}{2}(c_{22}^{\alpha}-c_{23}^{\alpha}) & 0 & 0 \\ 0 & c_{66}^{\alpha} & 0 \\ 0 & 0 & c_{66}^{\alpha} \end{bmatrix} \begin{Bmatrix} q_4^{\alpha} \\ q_5^{\alpha} \\ q_6^{\alpha} \end{Bmatrix}$$

$$= - \begin{bmatrix} \frac{1}{2}(B_{22}^{\alpha}-B_{23}^{\alpha}) & 0 & 0 \\ 0 & B_{66}^{\alpha} & 0 \\ 0 & 0 & B_{66}^{\alpha} \end{bmatrix} \begin{Bmatrix} \sigma_4 \\ \sigma_5 \\ \sigma_6 \end{Bmatrix}$$

so that the solution of the above can be readily obtained as a special case of the general equations developed in Chapter 2. The relevant system of equations for plane stress loading situations takes on the following form upon employing the constraints given by Eqns. 5.13 in Eqns. 2.35 for each value of α and then carrying out the required summation over all α's:

$$\varepsilon_1 = - \frac{\partial G_0}{\partial \sigma_1}$$

$$\varepsilon_2 = - \frac{\partial G_0}{\partial \sigma_2} + \int_0^z \bar{B}_{22}(z-z')\sigma_2(z')dz' \qquad (5.15)$$

$$\varepsilon_6 = - \frac{\partial G_0}{\partial \sigma_6} + \int_0^z \bar{B}_{66}(z-z')\sigma_6(z')dz'$$

where the functions $\bar{B}_{22}(z)$ and $\bar{B}_{66}(z)$ are given by:

$$\bar{B}_{22}(z) = \frac{1}{2}\sum_{\alpha=1}^{n} \frac{(B_{22}^{\alpha}+B_{23}^{\alpha})^2}{(b_{22}^{\alpha}+b_{23}^{\alpha})} e^{-\lambda_2^{\alpha} z} + \frac{(B_{22}^{\alpha}-B_{23}^{\alpha})^2}{(b_{22}^{\alpha}-b_{23}^{\alpha})} e^{-\lambda_3^{\alpha} z}$$

$$\bar{B}_{66}(z) = \sum_{\alpha=1}^{n} \frac{(B_{66}^{\alpha})^2}{b_{66}^{\alpha}} e^{-\lambda_6^{\alpha} z} \qquad (5.16)$$

$$\lambda_2^{\alpha} = \frac{(C_{22}^{\alpha}+C_{23}^{\alpha})}{(b_{22}^{\alpha}+b_{23}^{\alpha})}, \quad \lambda_3^{\alpha} = \frac{(C_{22}^{\alpha}-C_{23}^{\alpha})}{(b_{22}^{\alpha}-b_{23}^{\alpha})}, \quad \lambda_6^{\alpha} = \frac{C_{66}^{\alpha}}{b_{66}^{\alpha}}$$

Thus in general for this specialized case, the response in the transverse direction to the fibers will be governed by two independent sets of hardening exponents. This is due to coupling between transverse normal and shear response in the plane of isotropy as can be easily deduced by observing that $\lambda_3^{\alpha} = \lambda_4^{\alpha}$. In particular, if the hardening response is similar in shear and transverse tension in the 2-3 plane, which corresponds to the case

$$b_{23}^{\alpha} = B_{23}^{\alpha} = C_{23}^{\alpha} = 0,$$

then $\lambda_2^{\alpha} = \lambda_3^{\alpha}$, and so one set of hardening exponents ensues in the transverse mode. Thus,

$$\bar{B}_{22}(z) = \sum_{\alpha=1}^{n} \frac{(B_{22}^{\alpha})^2}{b_{22}^{\alpha}} e^{-\lambda_2^{\alpha} z} \quad \text{where now } \lambda_2^{\alpha} = \frac{C_{22}^{\alpha}}{b_{22}^{\alpha}}$$

as will be assumed henceforth.

In order to obtain the power-law approximation we proceed as follows. Integrating Eqns. 5.15 by parts we have for ε_6, say;

$$\varepsilon_6 = -\frac{\partial G_0}{\partial \sigma_6} + \sum_{\alpha=1}^{n}\left(\frac{1}{\lambda_6^\alpha}\right)\frac{\left(B_{66}^\alpha\right)^2}{b_{66}^\alpha} e^{-\lambda_6^\alpha(z-z')}\,\sigma_6(z')\Big|_0^z$$

$$- \int_0^z \sum_{\alpha=1}^{n}\left(\frac{1}{\lambda_6^\alpha}\right)\frac{\left(B_{66}^\alpha\right)^2}{b_{66}^\alpha} e^{-\lambda_6^\alpha(z-z')}\,\frac{\partial \sigma_6(z')}{\partial z'}\,dz' \qquad (5.17)$$

The above can be rewritten as:

$$\varepsilon_6 = -\frac{\partial G_0}{\partial \sigma_6} + \sigma_6(0)\sum_{\alpha=1}^{n}\left(\frac{1}{\lambda_6^\alpha}\right)\frac{\left(B_{66}^\alpha\right)^2}{b_{66}^\alpha}\left(1 - e^{-\lambda_6^\alpha z}\right)$$

$$+ \int_0^z \sum_{\alpha=1}^{n}\left(\frac{1}{\lambda_6^\alpha}\right)\frac{\left(B_{66}^\alpha\right)^2}{b_{66}^\alpha}\left(1 - e^{-\lambda_6^\alpha(z-z')}\right)\frac{\partial \sigma_6(z')}{\partial z'}\,dz'$$

as can be verified readily by integrating out the first part of the kernel. The power-law approximation ensues if a sufficiently large number of internal variables is assumed so that we can write:

$$\sum_{\alpha=1}^{n}\left(\frac{1}{\lambda_6^\alpha}\right)\frac{\left(B_{66}^\alpha\right)^2}{b_{66}}\left(1 - e^{-\lambda_6^\alpha z}\right) \approx B_{66}^\circ \cdot z^{n_6}\,, \quad n_6 > 1$$

and similarily (5.19)

$$\sum_{\alpha=1}^{n}\left(\frac{1}{\lambda_2^\alpha}\right)\frac{\left(B_{22}^\alpha\right)^2}{b_{22}^\alpha}\left(1 - e^{-\lambda_2^\alpha z}\right) \approx B_{22}^\circ \cdot z^{n_2}\,, \quad n_2 > 1$$

as the above are merely summations of monotonically increasing functions with different rates of asymptotic decay and different transition points. More precisely, power-law dependence results if a continuous distribution of retarda-

tion times λ_2^{α}'s and λ_6^{α}'s, is assumed by drawing a parallel analogy with standard viscoelastic treatment for such a case [94, 103].

As $\sigma_6(0) = \sigma_2(0) = 0$, which is a commonly assumed requirement of the intrinsic time scale, the relevant total plane stress constitutive equations thus become:

$$\varepsilon_1 = A_{11}\sigma_1 + A_{12}\sigma_2 + \frac{(\ell_{11}\sigma_1+\ell_{12}\sigma_2)}{\sqrt{\ell_{11}\sigma_1^2+2\ell_{12}\sigma_1\sigma_2+\ell_{22}\sigma_2^2}}\left[1-e^{-\alpha\sqrt{\ell_{11}\sigma_1^2+2\ell_{12}\sigma_1\sigma_2+\ell_{22}\sigma_2^2}}\right]$$

$$\varepsilon_2 = A_{12}\sigma_1 + A_{22}\sigma_2 + \frac{(\ell_{12}\sigma_1+\ell_{22}\sigma_2)}{\sqrt{\ell_{11}\sigma_1^2+2\ell_{12}\sigma_1\sigma_2+\ell_{22}\sigma_2^2}}\left[1-e^{-\alpha\sqrt{\ell_{11}\sigma_1^2+2\ell_{12}\sigma_1\sigma_2+\ell_{22}\sigma_2^2}}\right] + \int_0^z B_{22}^{\circ}\cdot(z-z')^{n_2}\frac{\partial\sigma_2(z')}{\partial z'}\,dz' \qquad (5.20)$$

$$\varepsilon_6 = A_{66}\sigma_6 + \int_0^z B_{66}^{\circ}\cdot(z-z')^{n_6}\frac{\partial\sigma_6(z')}{\partial z'}\,dz'$$

Thus for monotonically increasing and proportional loading for instance the choice of the intrinsic time scale of the form $dz = d\psi = \sqrt{s_{ij}d\sigma_i d\sigma_j}$ will result in the type of equations that Hashin proposed to model the response of transversely isotropic composites as can be readily verified

by direct integration of the above equations. The above scheme however is evidently more general since it allows for all the stress interaction components to be included in a rational and consistent manner. The presence or absence and degree of such stress interactions can be brought forth only through experiment or some micromechanics analytical or numerical scheme as that of Foye [56] mentioned previously. In what follows, the various parameters of the chosen intrinsic time scale will be at first determined directly on the basis of available experimental data without attaching any physical significance to them. Subsequently, one possible method of determining these parameters on the basis of both the available experimental data and micromechanical considerations will be illustrated in order to study the feasibility of incorporating micromechanics in a fairly elementary way into the constitutive framework to model some of the mechanisms contributing to the dissipative response of this particular fibrous composite.

5.3.1 Experimental-Theoretical Correlation

i) Phenomenological approach - Monotonic response

The material parameters governing the dissipative response of the proposed model can be obtained from the off-axis tension test once a choice of the intrinsic time scale is made. On the basis of the observed response of the Gr/Pi system it will be assumed that $dz = d\psi$ for the monotonic

loading so that the relevant Eqns. 5.20 can be directly integrated to yield:

$$\varepsilon_2 = \varepsilon_2^R + \frac{B_{22}^\circ}{n_2+1}\left(s_{11}\text{cotan}^4\theta+(2s_{12}+s_{66})\text{cotan}^2\theta+s_{22}\right)^{n_2/2}\cdot\sigma_2^{(n_2+1)}$$

$$\varepsilon_6 = \varepsilon_6^R + \frac{B_{66}^\circ}{n_6+1}\left(s_{11}\text{cotan}^2\theta+(2s_{12}+s_{66})+s_{22}\tan^2\theta\right)^{n_6/2}\cdot\sigma_6^{(n_6+1)} \qquad (5.21)$$

where R stands for reversible as before and use has been made of the fact that for proportional loading situations all the various stress components can be expressed in terms of the desired one and the related ratios of trigonometric functions relating the components to a single loading parameter. In the above formulation, one of the positive constants B_{22}°, B_{66}° is somewhat arbitrary since only the ratio $B_{22}^\circ/B_{66}^\circ$ can be determined in view of s_{ij} assumed to be completely unknown. For convenience therefore, B_{66}° is set equal to unity. In what follows, the components s_{ij} of the endochronic time measure will be determined on the basis of the resolved off-axis shear response along material principal directions. We note that as the combination $(2s_{12} + s_{66})$ always appears together, there are essentially three unknown parameters s_{11}, s_{22} and $(2s_{12} + s_{66})$ that have to be evaluated. Thus three off-axis tests are required in

this scheme. By the same token, it is not possible to determine s_{66}, i.e. pure shear component of the endochronic time measure, directly using this approach.

Defining the shear hardening parameter $A^*_{66}(\theta)$ as follows:

$$A^*_{66}(\theta) = \frac{B^\circ_{66}}{(n_6+1)}\left\{s_{11}\text{cotan}^2\theta+s_{22}\tan^2\theta+(2s_{12}+s_{56})\right\}^{n_6/2} \quad (5.22)$$

and utilizing the hardening parameters of three different off-axis tests to solve for s_{11}, s_{22} and $(2s_{12} + s_{66})$ we obtain:

$$s_{11}=(n_6+1)^{\frac{2}{n_6}}\left\{\frac{\left\{A^*_{66}(\theta_1)^{\frac{2}{n_6}}-A^*_{66}(\theta_2)^{\frac{2}{n_6}}\right\}\left\{t\theta_1-t\theta_3\right\}-\left\{A^*_{66}(\theta_1)^{\frac{2}{n_6}}-A^*_{66}(\theta_3)^{\frac{2}{n_6}}\right\}\left\{t\theta_1-t\theta_2\right\}}{\left\{c\theta_1-c\theta_2\right\}\left\{t\theta_1-t\theta_3\right\}-\left\{c\theta_1-c\theta_3\right\}\left\{t\theta_1-t\theta_2\right\}}\right\}$$

$$s_{22}=(n_6+1)^{\frac{2}{n_6}}\left\{\frac{\left\{A^*_{66}(\theta_1)^{\frac{2}{n_6}}-A^*_{66}(\theta_2)^{\frac{2}{n_6}}\right\}\left\{c\theta_1-c\theta_3\right\}-\left\{A^*_{66}(\theta_1)^{\frac{2}{n_6}}-A^*_{66}(\theta_3)^{\frac{2}{n_6}}\right\}\left\{c\theta_1-c\theta_2\right\}}{\left\{t\theta_1-t\theta_2\right\}\left\{c\theta_1-c\theta_3\right\}-\left\{t\theta_1-t\theta_3\right\}\left\{c\theta_1-c\theta_2\right\}}\right\}$$

$$(2s_{12}+s_{66})= \left\{(n_6+1)A^*_{66}(\theta_i)\right\}^{\frac{2}{n_6}} - \left\{s_{11}c\theta_i + s_{22}t\theta_i\right\} \quad (5.23)$$

where i can be either 1, 2 or 3, $t\theta_i \equiv \tan^2\theta$ and $c\theta_i \equiv \text{cotan}^2\theta_i$.

With s_{ij} parameters known, the scaling constant B°_{22} is easily determined from the transverse tension test. We thus obtain:

$$B^{\circ}_{22} = (n_2 + 1)A^{*}_{22}(90°)/S_{22}^{\frac{n_2}{2}} \qquad (5.24)$$

with $A^{*}_{22}(\theta)$ defined in a similar manner as $A^{*}_{66}(\theta)$.

As the shear and transverse hardening parameters are strongly nonlinear functions of a specific functional form of the off-axis angle, they are naturally sensitive to the choice of off-axis orientations used to determine their endochronic parameters. Thus in order to cover the major portion of the off-axis range with a good degree of accuracy it is necessary to choose the three off-axis orientations with the above in mind. The configurations that yielded best agreement with experimental data were found to be 10°, 30° and 60°. The experimental and predicted values of the shear and transverse hardening parameters are shown in Figs. 5.5 and 5.6, and it is seen that the agreement is quite good over the range of significant nonlinearities occurring in practice. The actual experimental and predicted stress-strain response in monotonic shear and transverse tension for the various off-axis configurations is shown in Fig. 5.7 and 5.8. The correlation is evidently good.

ii) Micromechanics approach

The micromechanics approach employed in the formulation of the intrinsic time measure is based on Hill's stress concentration factors relating the average stresses in either phase of the composite to the average applied

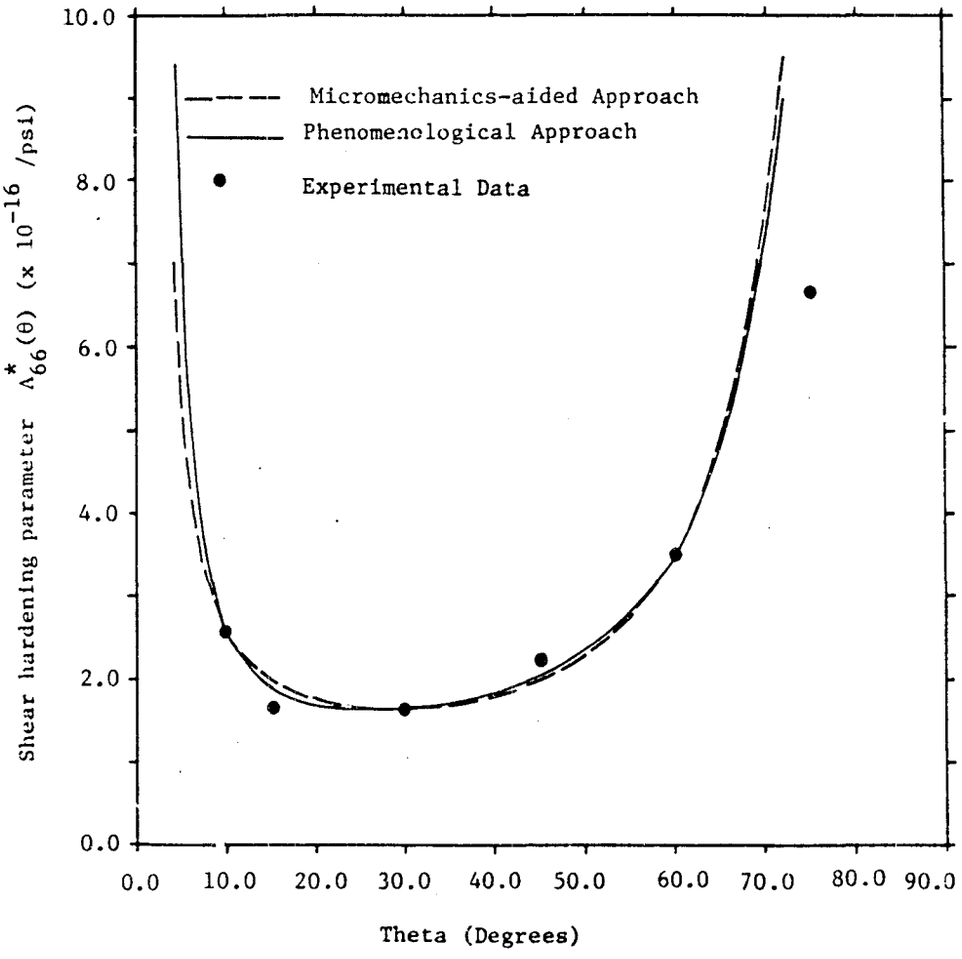

Fig. 5.5 Shear hardening parameters $A^*_{66}(\theta)$ as functions of the off-axis angle

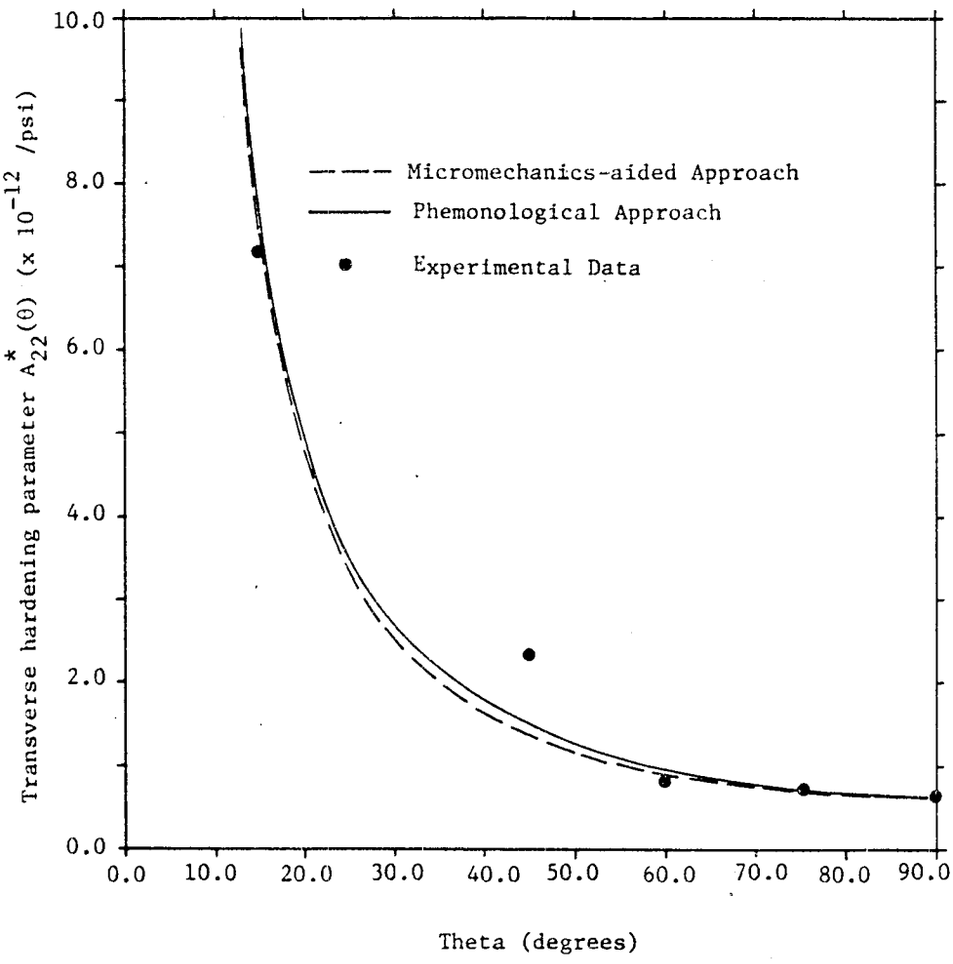

Fig. 5.6 Transverse hardening parameters $A_{22}^{*}(\theta)$ as functions of the off-axis angle

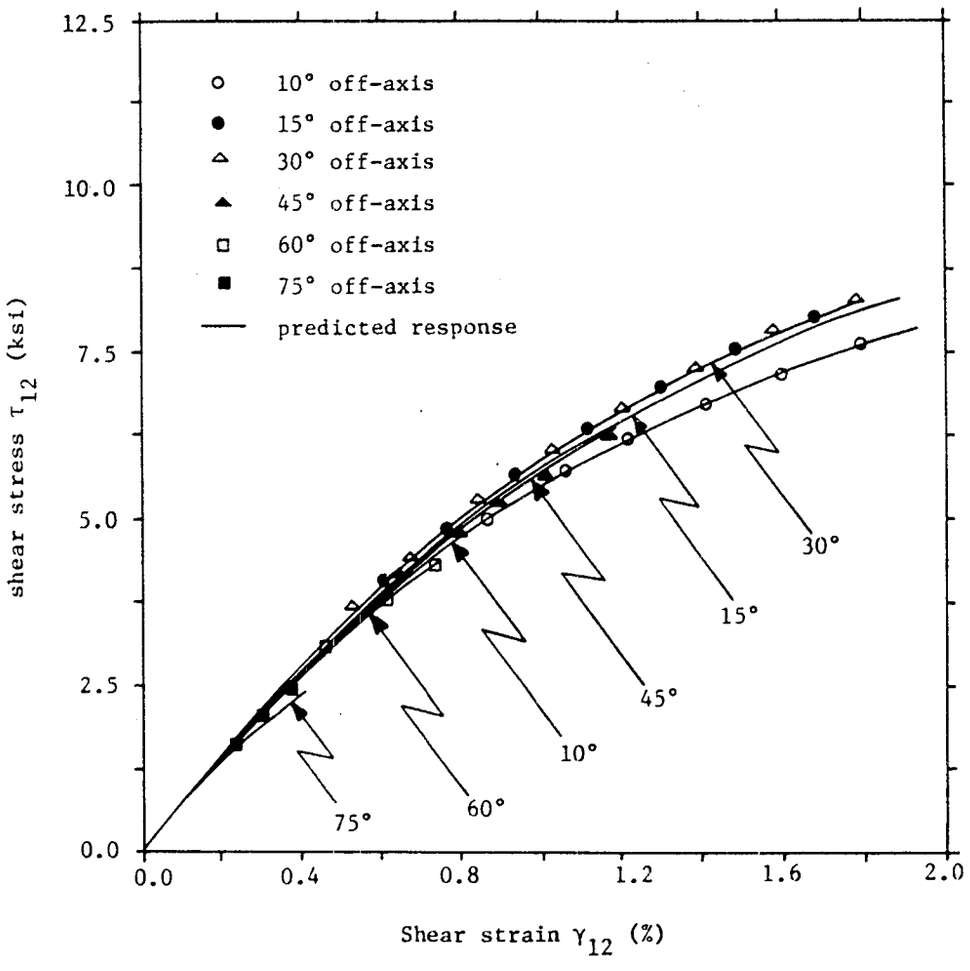

Fig. 5.7 Resolved shear stress-strain response of the Gr/Pi coupons in the range $10° \leq \theta \leq 75°$

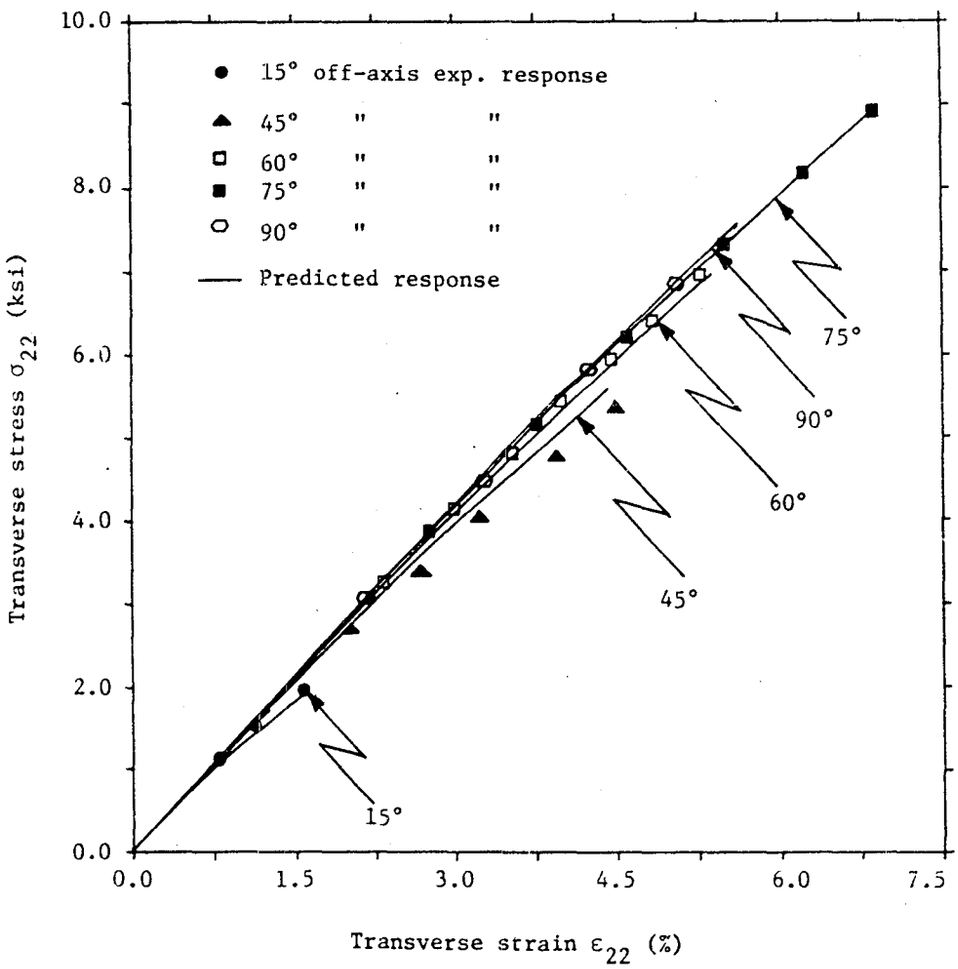

Fig. 5.8 Resolved transverse stress-strain response of the Gr/Pi coupons in the range $15° \leq \theta \leq 90°$

stresses in the elastic domain [104]. The elements of the so-called stress concentration matrix can be determined once the initial (linearized) compliance or stiffness elements of the constituents and overall composite are specified. The stress concentration factors for the matrix phase for example are given by the following equations:

$$[M] - [M^f] = c_m[M^m] - [M^f][B^m] \tag{5.25}$$

where $[M]$, $[M^f]$ and $[M^m]$ are the compliance matrices of the composite, fiber and matrix phase, respectively; c_m matrix volume fraction and $[B^m]$ the stress concentration matrix of the material matrix phase.

It is subsequently assumed that the dissipation taking place in the composite is caused by two coupled phenomena: shearing deformation of the matrix phase governed by the average deviatoric stress components in that phase not deviating significantly from the initial average stress ratios, and perhaps micro-void coalescence due to crazing caused primarily by the longitudinal elongation governed by the stress σ_1. The second mechanism is included to account for the significant σ_1 stress interaction present in the observed response which cannot be explained on the basis of matrix octahedral shear stress formulation alone. In fact, the evidence of some form of stable damage accumulation in this composite system is substantially supported by the tests carried out on pure polyimide specimens as well as by

the off-axis shear reloading response along the material principal directions as discussed in Chapter 4. Although ambient temperature tension and torsion tests on polyimide specimens at strain rates of 0.02 in/in/min indicated some nonlinearity and dissipation present in cyclic tests, the extent of the above was insufficient to explain the pronounced hysterisis loops observed in the tested composite coupons in the combined shear mode.

Tension tests were carried out under plane stress conditions according to the ASTM standard test method D638-77a and produced permanent strains in the neighborhood of 0.05% upon unloading linearly from 80% of ultimate load for example. The average strength of the tested polyimide specimens was 5313 psi at the corresponding strain of 1.21%. Torsion tests on the other hand were carried out on solid cylindrical specimens 2.0 in long and 0.5 in in diameter and yielded virtually no measurable permanent strain upon unloading from as high as 80% of ultimate torque. The shear strength was determined at approximately 6470 psi with strain of 4.66%. The shear stress-strain curves were practically linear to stress levels as high as 4250 psi with deviation of about 0.25% strain from linearity at failure. While this particular shear test method can significantly mask the extent of material nonlinearity, absence of hysterisis loop and permanent strain upon unloading would

appear to indicate the brittle and to a large extent reversible nature of this material's response at room temperature. Furthermore, the decrease in the composite shear modulus at points of reloading observed in cyclic tests does point to some material degradation caused by the deformation process. The above phenomenon is markedly noticeable at low off-axis configurations where the longitudinal stress σ_1 is significant.

With the above observations in mind the intrinsic time scale is formulated as follows:

$$dz = a d\sigma_1 + \sqrt{\frac{1}{2} d\sigma'_{im} \, d\sigma'_{im}} \quad , \text{ no sum on m} \tag{5.26}$$

where $a > 0$ is the only restriction needed for monotonic tensile loadings to ensure that $dz > 0$. Employing Hill's stress concentration factors, the second part of dz can be expressed in terms of the external stress increments so that we have:

$$dz = a d\sigma_1 + \sqrt{s_{ij} d\sigma_i d\sigma_j} \tag{5.27}$$

where now,

$$s_{11} = \frac{1}{3}\left(B^m_{11} - B^m_{21}\right)^2 \qquad s_{66} = \left(B^m_{66}\right)^2$$

$$s_{12} = \frac{1}{6}\left(B^m_{11} - B^m_{21}\right)\left(2B^m_{12} - B^m_{22} - B^m_{23}\right)$$

$$s_{22} = \frac{1}{6}\left[\left(B^m_{22} - B^m_{12}\right)^2 + \left(B^m_{22} - B^m_{23}\right)^2 + \left(B^m_{12} - B^m_{23}\right)\right]^2$$

and the elements of the matrix $[B^m]$ are given in terms of

the initial (linearized) moduli of the constituent phases and composite in Appendix D along with the methodology of their explicit determination on the basis of available experimental data and certain other assumptions.

The necessity of including the first term in the time scale can be readily demonstrated by finding the location of minimum value of $A^*_{66}(\theta)$ for the case a = 0. From Eqn. 5.22 we readily obtain the condition

$$\theta_{min} = \tan^{-1}\left(\frac{s_{11}}{s_{22}}\right)^{\frac{1}{4}} = 10.06°$$

for the set of stress concentration factors for this system as determined in Appendix D. The actual response on the other hand indicated that the minimum of $A^*_{66}(\theta)$ occurs between 15° and 30°.

Thus two resolved off-axis shear responses are needed now to determine the material parameters a and B°_{66}, whereas B°_{22} is obtained from the transverse tension test as before. The off-axis configurations used to that effect that yielded best agreement with the experimental data were 10° and 60° orientations. The results are included in Figs. 5.5 and 5.6 for comparison with the phenomenological approach. While the correlation is slightly less favorable than that of the previous method, the advantage of such micromechanics-aided approach is the possibility of deducing the pure shear response as well as the utilization of only two off-axis

tests.

iii) Cyclic response

It has been observed in Chapter 4 that the unloading and subsequent reloading response appears to be independent of initial loading path in the sense that the material remembers the previous unloading stress level while generating hysterisis loops within the envelope bounded by that level. This type of response is apparently difficult to predict with a single stress-based time scale. In view of the above as well as other experimental observations on cyclic response outlined in Chapter 4 it is proposed to introduce a second time scale operative within the region bounded by the maximum stress level. This inner scale would be reset at every point of stress reversal within the stated region so that fading memory effects would only be present on any one path segment that does not undergo reversal of stress direction.

The introduction of an inner time scale and thus a discontinuity in the overall intrinsic deformation scale requires re-examination of thermodynamic constraints since the Clausius-Duhem inequality considered in Chapter 2 along with Onsanger's relations ensure positive character of dissipation locally only. The resetting or sudden jump in the intrinsic time scale z imposes certain constraints on the choice of the inner scale that can be obtained by exam-

ination of the required positive character of dissipated work globally, that is in a given stress cycle. With the above in mind we propose that the inner deformation scale applicable on any given path within the region bounded by the maximum unloading stress level be of the form:

$$dz^i = \beta dz, \ \beta > 0, \ i \equiv \text{inner} \tag{5.28}$$

and examine the validity of the above as well as limitation imposed by global thermodynamic considerations on β. To this end we consider the total response in a pure shear loading-unloading-reloading cycle.

A) loading up to $\sigma_6 = \sigma_6^*$

The intrinsic time scale and the ensuing stress-strain response is given by:

$$z = \sqrt{s_{66}}\,\sigma_6, \qquad \frac{\partial \sigma_6}{\partial z} = \frac{1}{\sqrt{s_{66}}}$$

$$\varepsilon_6 = A_{66}\sigma_6 + \int_0^z \frac{B^\circ_{66}}{\sqrt{s_{66}}}\,(z - z')^{n_6}\,dz'$$

$$= A_{66}\sigma_6 + \frac{B^\circ_{66}}{(n_6+1)}(\sqrt{s_{66}})^{n_6}\,\sigma_6^{(n_6+1)} \tag{5.29}$$

B) unloading from $\sigma_6 = \sigma_6^*$ to $\sigma_6 = 0$

The intrinsic scale now becomes

$$z^i = \beta\sqrt{s_{66}}(\sigma_6^* - \sigma_6), \ \frac{\partial \sigma_6}{\partial z^i} = -\frac{1}{\beta\sqrt{s_{66}}}$$

which is valid within the envelope bounded by the maximum stress level so that the integration of constitutive equations is carried out as follows:

$$\varepsilon_6 = A_{66}\sigma_6 + \int_0^{z^*} \frac{B^\circ_{66}}{\sqrt{s_{66}}} (z^*-z')\, dz' - \int_0^{z^i} \frac{B^\circ_{66}}{\beta\sqrt{s_{66}}}(z^i-z^{i'})\, dz^{i'} \tag{5.30}$$

where $z^* = \sqrt{s_{66}}\ \sigma_6^*$ and thus the first integral represents the dissipative portion of strain at $\sigma_6 = \sigma_6^*$ and can just as well be obtained from Eqn. 5.29 by using the above equality. Performing the necessary integration and substitution, Eqn. 5.30 becomes:

$$\varepsilon_6 = A_{66}\sigma_6 + \frac{B^\circ_{66}}{(n_6+1)}(\sqrt{s_{66}})^{n_6}(\sigma_6^*)^{(n_6+1)} - \frac{B^*_{66}}{(n_6+1)}\left(\beta\sqrt{s_{66}}\right)^{n_6}(\sigma_6^*-\sigma_6)^{(n_6+1)} \tag{5.31}$$

Thus at $\sigma_6 = 0$, i.e. at the completion of the stress cycle, the permanent strain is given by:

$$\varepsilon_6^P = \frac{B^\circ_{66}}{(n_6+1)}(\sqrt{s_{66}})^{n_6}(\sigma_6^*)^{(n_6+1)}\left(1 - \beta^{n_6}\right) \tag{5.32}$$

Furthermore,

$$\frac{\partial^2\varepsilon_6}{\partial\sigma_6^2} = - n_6 B^\circ_{66}\left(\beta\sqrt{s_{66}}\right)^{n_6}(\sigma_6^*-\sigma_6)^{(n_6-1)} \tag{5.33}$$

Thus for $0 \leq \beta \leq 1$, the permanent strain after one cycle is positive and the unloading response is concave with respect to the stress axis ensuring that the work dissipated by the

material is positive.

C) Reloading up to $\sigma_6 = \sigma_6^*$

The reloading response is now given by the following equation

$$\varepsilon_6 = A_{66}\sigma_6 + \frac{B^\circ_{66}(\sqrt{s_{66}})^{n_6}}{(n_6+1)} (\sigma_6^*)^{(n_6+1)} (1-\beta^{n_6}) + \beta^{n_6}\sigma_6^{(n_6+1)} \tag{5.34}$$

so that at $\sigma_6 = \sigma_6^*$ we obtain:

$$\varepsilon_6\left[z_6^i=\beta\sqrt{s_{66}}\ \sigma_6^*\right] = A_{66}\sigma_6^* + \frac{B^\circ_{66}}{(n_6+1)}(\sqrt{s_{66}})^{n_6}\left[\sigma_6^*\right]^{(n_6+1)}$$

and we have arrived at the same point on the hardening envelope while generating a hysterisis loop since Eqn. 5.34 is convex with respect to the stress axis. The response in the region past the unloading stress σ_6^* is given now by Eqn. 5.38 and the associated time scale z indicating the dual character of the dissipative behavior. Several things will be noted from the above analysis. Permanent strain accumulation is governed by the parameter β. For $\beta = 1$, anelastic response is generated. Permanent strain accumulation as a function of the unloading stress level exhibits similar response as the corresponding quantitites in monotonic loading except for the scale factor β; precisely as has been observed to a large extent for the Gr/Pi system.

The application of the above model to prediction of off-axis shear response is now straightforward since the only parameter that remains to be determined is β - which is

readily obtained on the basis of experimental results of Chapter 4.

The cyclic response in shear is compared with the predictions of the model in Figs. 5.9, 5.10 and 5.11 for the 10°, 15° and 30° off-axis configurations to illustrate the degree of applicability of the proposed model. The correlation appears to be good if the unloading stresses based on the corresponding strains obtained from experimental data are employed in predicting cyclic response as has been done in the above comparison.

iv) Lamina response predictions

The developed set of constitutive equations is utilized in this section to predict the response of Gr/Pi unidirectonal off-axis coupons in the lamina coordinate system. This is the most general test of the model's applicability since it employs the response predictions of the proposed nonlinear elastic potential as well. Selected cases will only be presented for reasons of brevity and space limitation.

As the point of immediate interest was verification of the model's ability to predict nonlinear response, the experimental data were reduced with the aid of Halpin-Pagano's equations and a correction factor so that the initial moduli coincided with transversely isotropic transformation predictions. The reduction procedure was the same

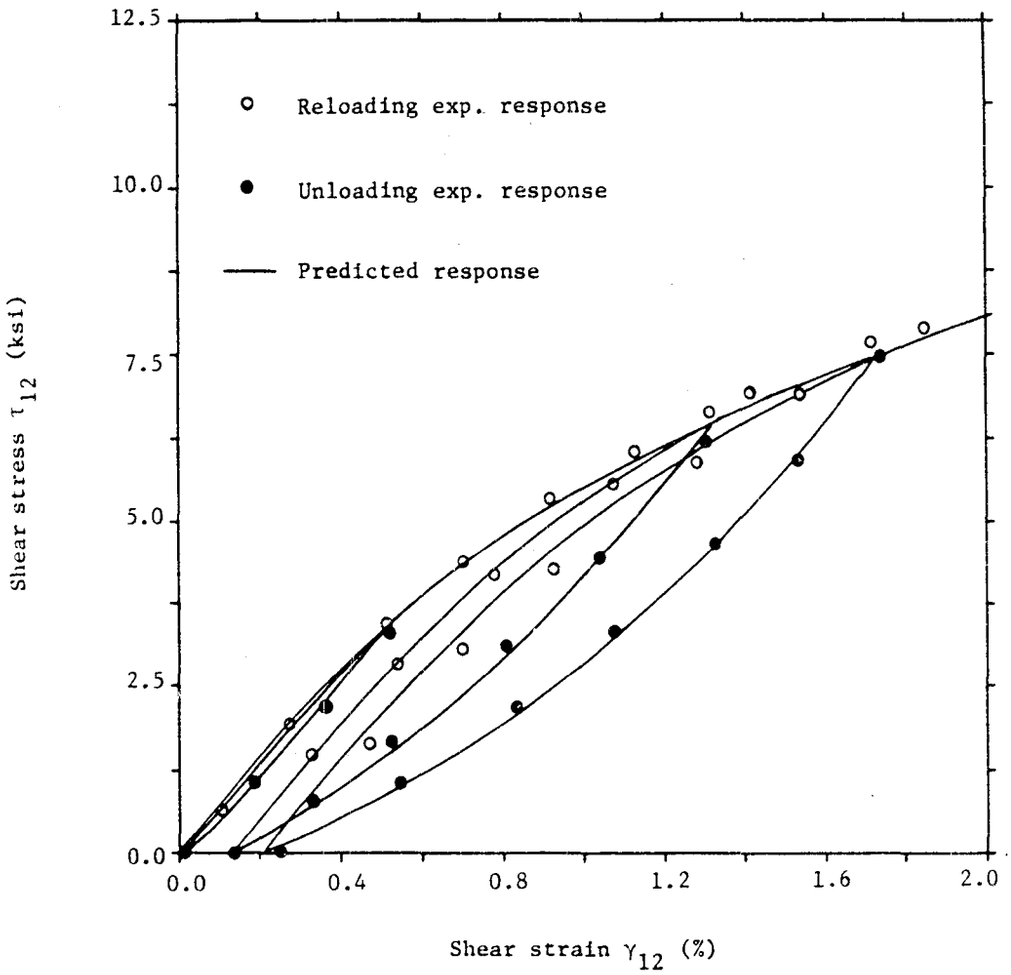

Fig. 5.9 Resolved shear stress-strain cyclic response of the Gr/Pi 10° coupon

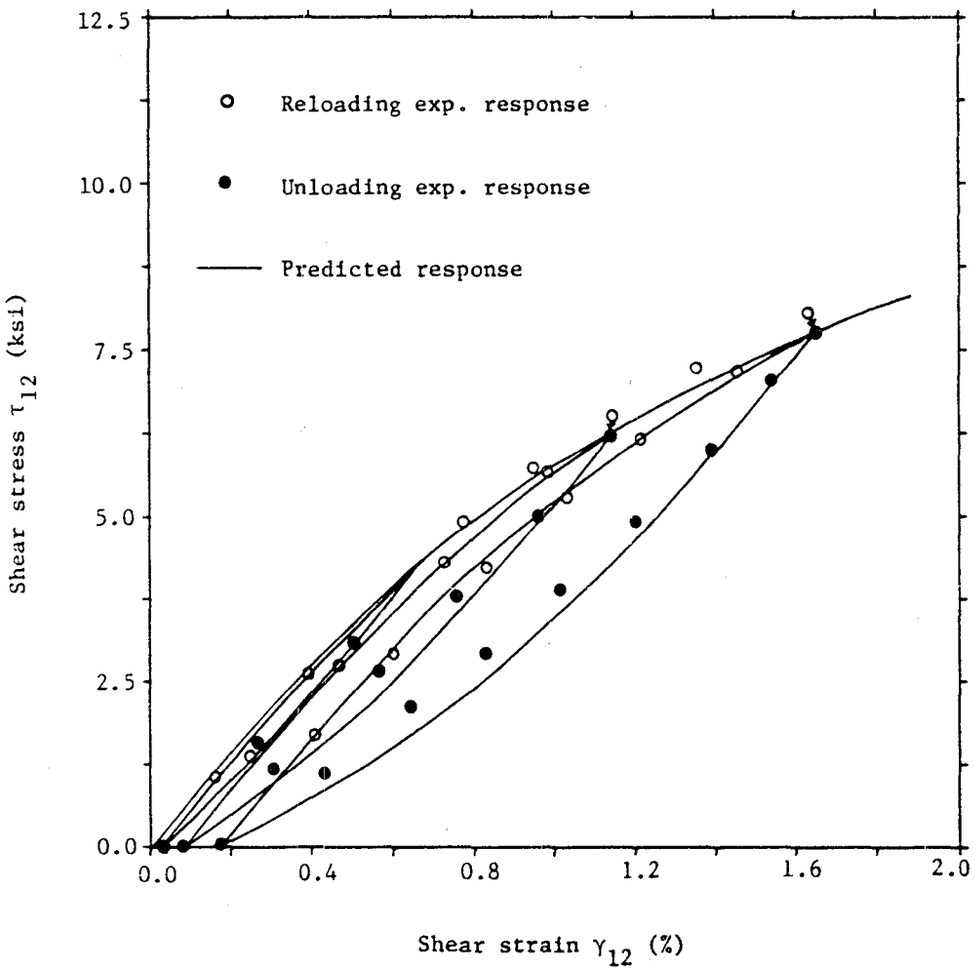

Fig. 5.10 Resolved shear stress-strain cyclic response of the Gr/Pi 15° coupon

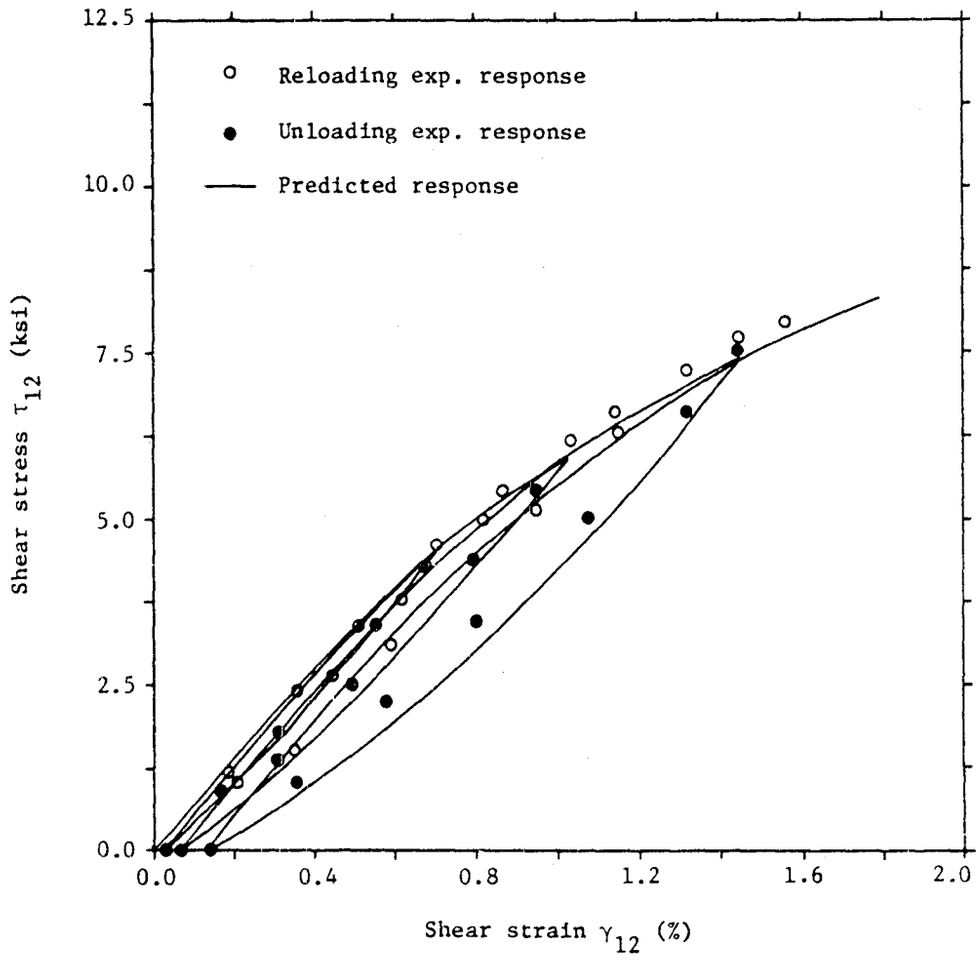

Fig. 5.11 Resolved shear stress-strain cyclic response of the Gr/Pi 30° coupon

as that employed in Chapter 4. Furthermore, in order to clearly demonstrate the extent of scatter present in coupons of the same orientation, actual experimental response of each coupon is presented in the following graphs along with theoretical predictions.

Figures 5.12 and 5.13 illustrate the stress-strain response σ_{xx} vs ε_{xx} in the lamina coordinate system for the six off-axis configurations tested. The correlation is excellent for the 30°, 45°, 60° and 75° orientations and good for 10° and 15° off-axis angles. The reason for the slightly poorer agreement for the high off-axis configurations could be two-fold: method of reducing the data in the high shear-coupling region and/or overestimation of the transverse normal strain ε_{22} due to highly nonlinear nature of $A^{*}_{22}(\theta)$ at low off-axis angles (see Fig. 5.6). The maximum difference between predicted and mean experimental response is approximately 10% (i.e. difference in strains at failure) for the 10° and 15° orientations, while for the remaining ones it is quite negligible. Figures 5.14 through 5.17 illustrate Poisson's response in the lamina coordinate system for the same configurations as cited above. The correlation is evidently very good for all the off-axis orientations.

5.4 Failure Analysis

The Tsai-Wu as well as the maximum stress failure criterion have been chosen for comparison with the observed

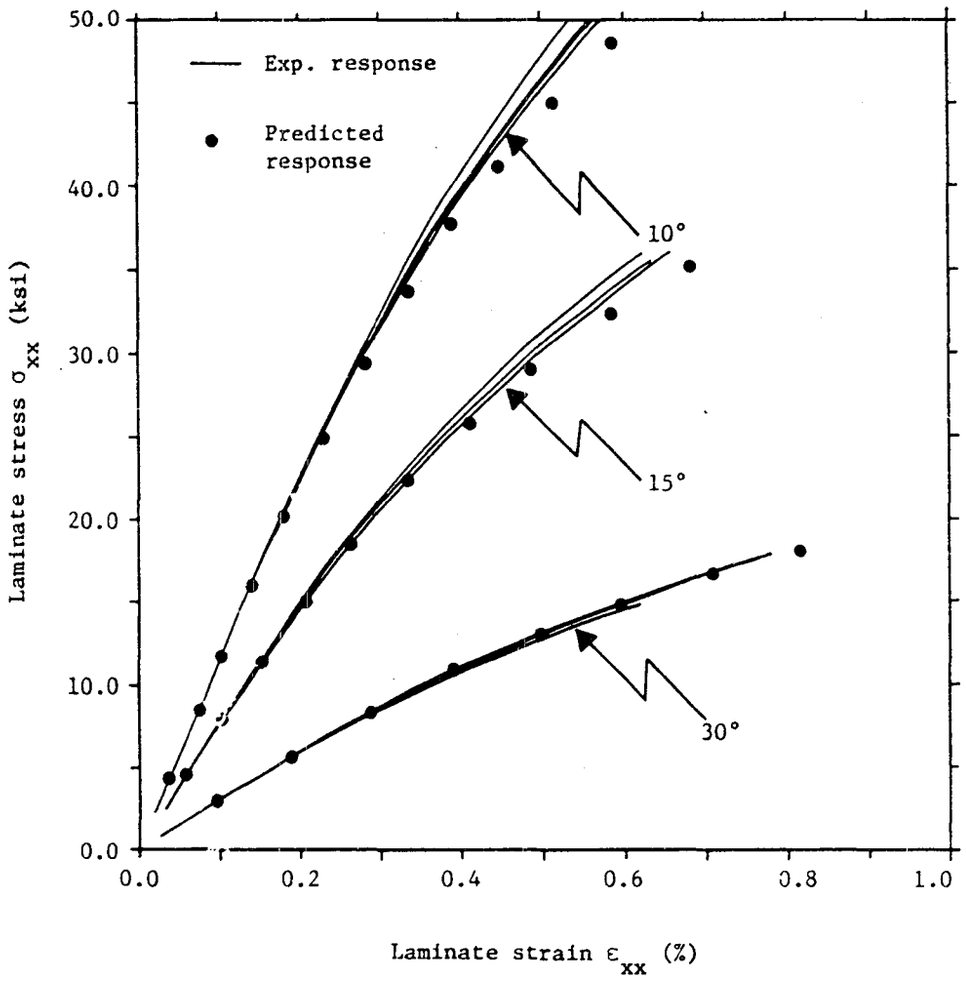

Fig. 5.12 Stress-strain response of the Gr/Pi 10°, 15° and 30° coupons

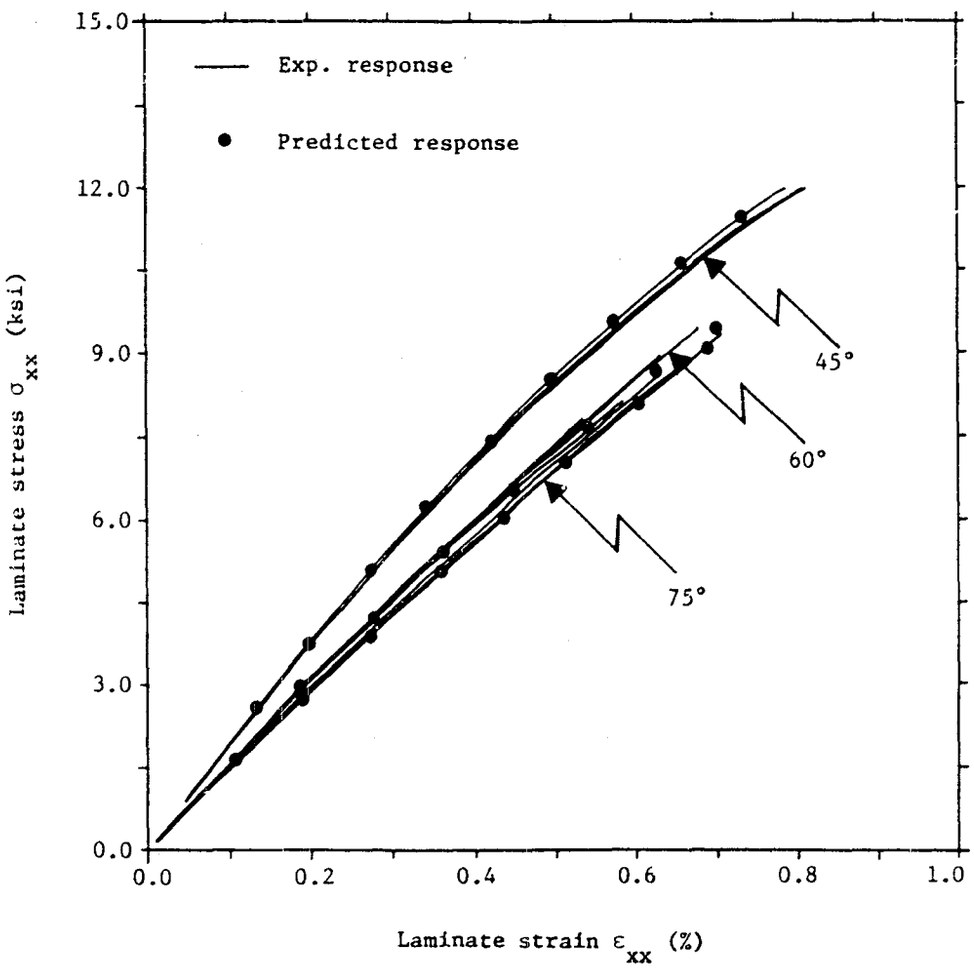

Fig. 5.13 Stress-strain response of the Gr/Pi 45°, 60° and 75° coupons

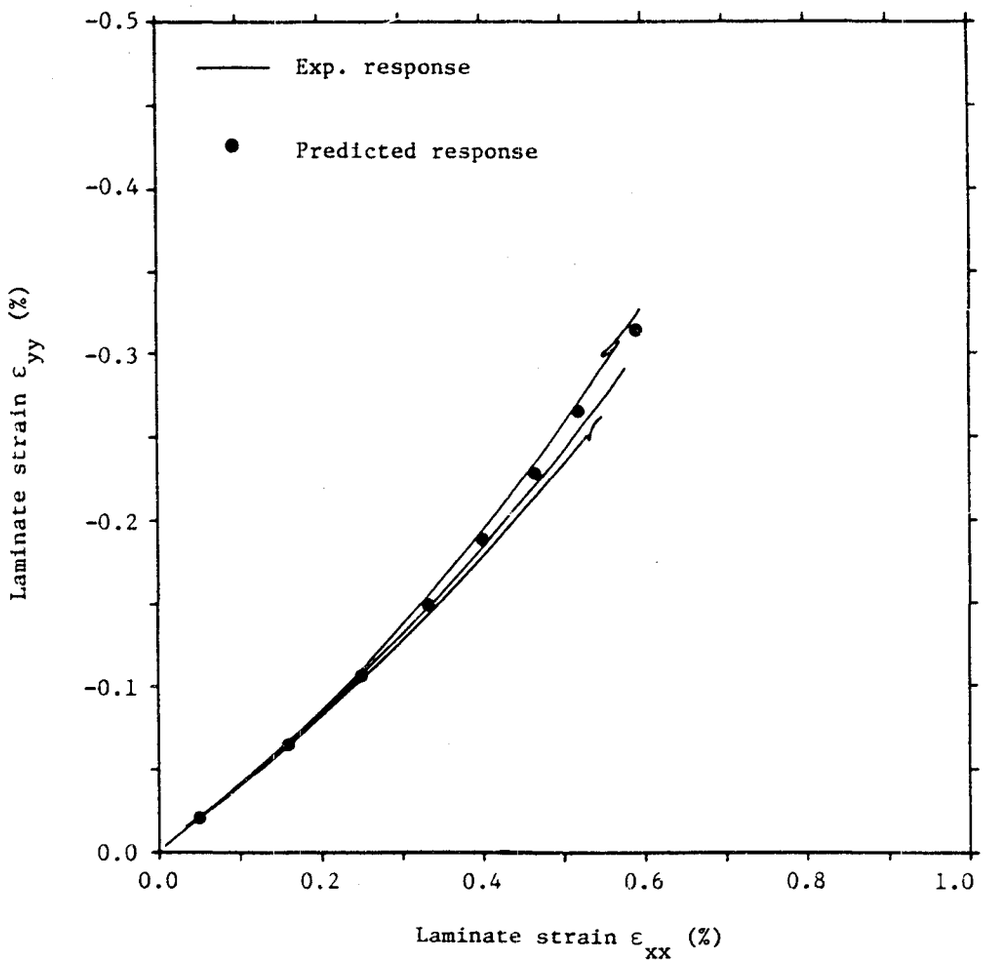

Fig. 5.14 Poisson's response of the Gr/Pi 10° coupon

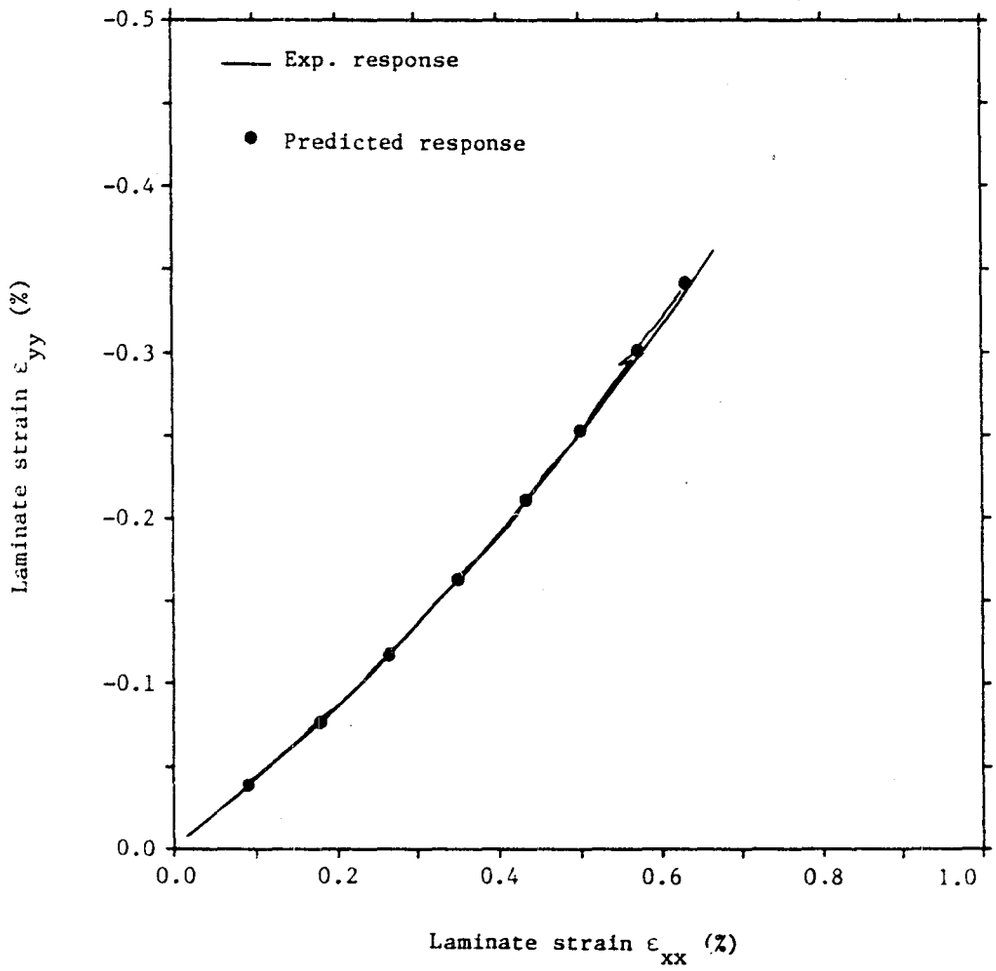

Fig. 5.15 Poisson's response of the Gr/Pi 15° coupon

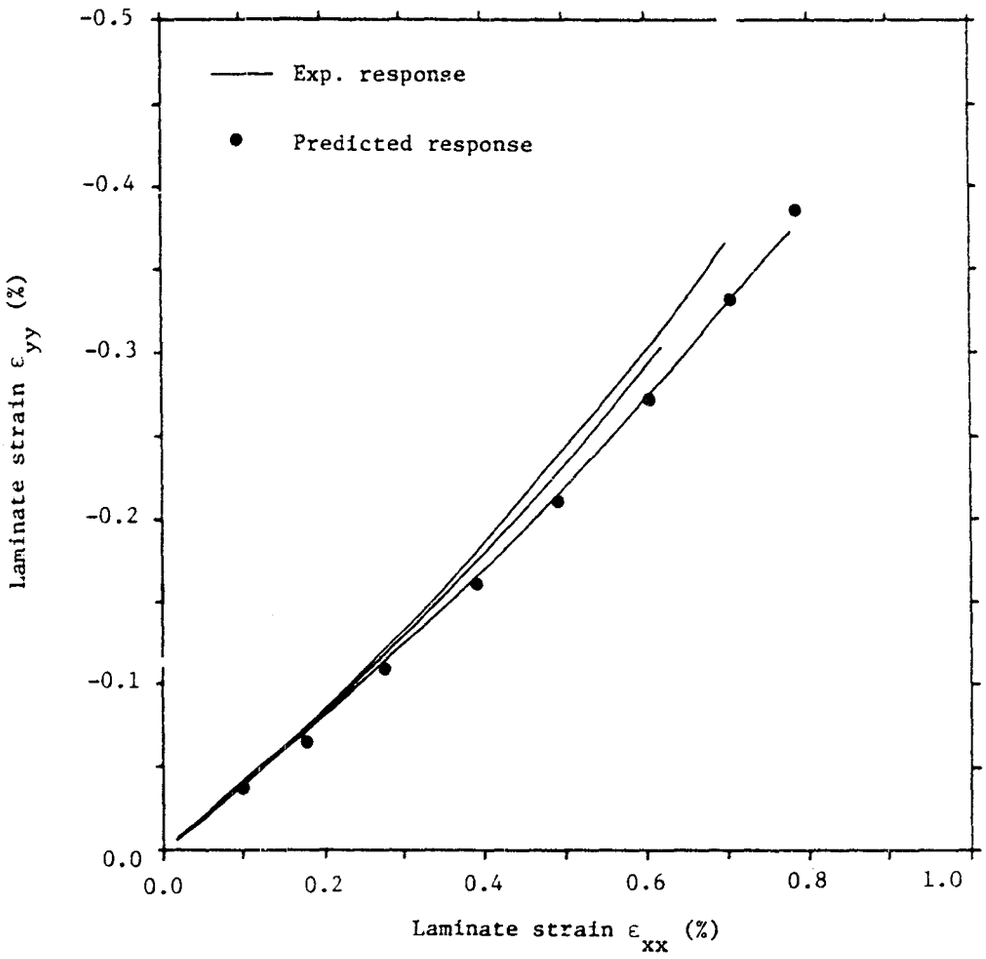

Fig. 5.16 Poisson's response of the Gr/Pi 30° coupon

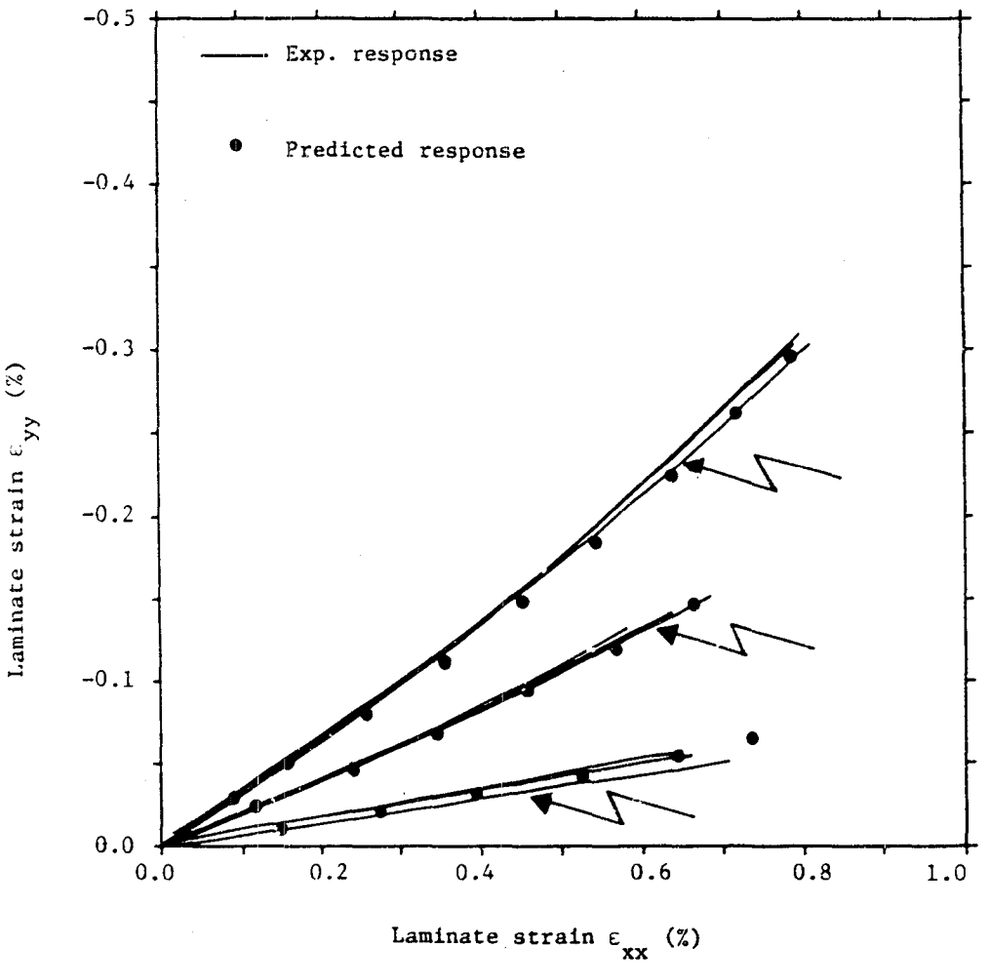

Fig. 5.17 Poisson's response of the Gr/Pi 45°, 60° and 75° coupons

strengths as they are representative of the two broad categories of phenomenological strength criteria outlined in Chapter 1. The shear-coupling phenomenon has been included in the calculation of strength predictions by taking into account the shear stress component induced by the grips on the basis of Halpin-Pagano model.

According to the maximum stress criterion failure occurs when any one of the stress components along principal material directions reaches a maximum value determined from simple uniaxial tests, i.e. when $\sigma_1 = \sigma_1^{max}$, $\sigma_2 = \sigma_2^{max}$ or $\sigma_6 = \sigma_6^{max}$. In what follows average stresses will be employed. Taking shear-coupling into account the above conditions can be expressed in the lamina coordinate system as follows:

$$\sigma_{xx}(\theta) = \frac{\sigma_1^{max}}{[\cos^2\theta + 2\sin\theta\cos\theta A(\theta)]}$$

$$\sigma_{xx}(\theta) = \frac{\sigma_2^{max}}{[\sin^2\theta - 2\sin\theta\cos\theta A(\theta)]} \qquad (5.35)$$

$$\sigma_{xx}(\theta) = \frac{\sigma_6^{max}}{[-\sin\sigma\cos\theta + (\cos^2\theta - \sin^2\theta)A(\theta)]}$$

where $$A(\theta) = -\left(\frac{2h}{\ell}\right)^2\left(\frac{\bar{S}_{16}}{\bar{S}_{11}}\right)\left\{\frac{1}{1 + 6\left(\frac{h}{\ell}\right)^2\left[\left(\frac{\bar{S}_{66}}{\bar{S}_{11}}\right) - \frac{2}{3}\left(\frac{\bar{S}_{16}}{\bar{S}_{11}}\right)^2\right]}\right\}$$

C3

As the pure shear strength data was not available, corrected ultimate stress of the 15° off-axis coupon was employed in place of σ_6^{max} as this configuration yielded the highest resolved shear strength, i.e. approximately 8600 psi.

On the other hand, the tensor polynomial criterion in its simplest form predicts failure to occur when the condition

$$F(\sigma_i) = F_{ij}\sigma_i\sigma_j = 1 \tag{5.36}$$

is satisfied for a given loading situation. Linear terms of the form $F_i\sigma_i$ that represent compressive/tensile differences will be neglected in the present comparison due to insufficient data. In the above, the so-called strength tensors F_{ii} (no sum) are given by the following

$$F_{11} = \frac{1}{\left(\sigma_1^{max}\right)^2}, \quad F_{22} = \frac{1}{\left(\sigma_2^{max}\right)^2}, \quad F_{66} = \frac{1}{\left(\sigma_6^{max}\right)^2}$$

whereas F_{12} must be determined from biaxial test results. Furthermore, the stability condition $F_{11}F_{22} \geq F_{12}^2$ must be satisfied in order that $F(\sigma_i)$ remain positive-definite.

As there are essentially two unknown parameters F_{12} and F_{66} that cannot be determined directly in the present analysis, they must be evaluated indirectly from strength data of two off-axis configurations. Various combinations of the required orientations were utilized and it was discovered that none of them yielded results compatible with the above stability condition. The results are given in Table 5.2. In view of this it was subsequently assumed that

Table 5.2 Determination of F_{12} and F_{66} on the basis of strength data obtained from one and two off-axis tension tests - sensitivity study vis-à-vis the stability condition $F_{11}F_{22} \stackrel{?}{\geq} F_{12}^2$

Off-axis orientations employed	F_{12}	F_{66}	$F_{11}F_{22} \stackrel{?}{\geq} F_{12}^2$
10°, 15°	-0.9199×10^{-7}	0.1920×10^{-6}	No
10°, 30°	0.1497×10^{-7}	-0.1811×10^{-7}	No
10°, 45°	-0.4454×10^{-7}	0.9881×10^{-7}	No
10°, 60°	0.9621×10^{-7}	-0.1777×10^{-6}	No
15°, 30°	0.1719×10^{-6}	-0.3316×10^{-6}	No
15°, 45°	0.1871×10^{-7}	-0.2768×10^{-7}	No
15°, 60°	0.3432×10^{-6}	-0.6716×10^{-6}	No
30°, 45°	-0.1510×10^{-5}	0.3029×10^{-3}	No
30°, 60°	0.1797×10^{-5}	-0.3570×10^{-5}	No
45°, 60°	0.2057×10^{-4}	-0.4113×10^{-4}	No
10°	-0.1132×10^{-8} *	0.1352×10^{-7}	No
15°	-0.2049×10^{-8} *	0.1352×10^{-7}	No
30°	-0.8614×10^{-9} *	0.1352×10^{-7}	No
45°	-0.1893×10^{-8} *	0.1352×10^{-7}	No
60°	0.5821×10^{-9} *	0.1352×10^{-7}	Yes

$F_{11} = 0.1969 \times 10^{-10}$

$F_{22} = 0.1785 \times 10^{-7}$

*F_{66} evaluated on the basis of $\sigma_6^{max} = 8{,}600$ psi

σ_6^{max} = 8600 psi and various off-axis orientations employed to determine F_{12}. The configuration that satisfied the stability condition turned out to be the 60° orientation.

A common practice is to set $F_{12} = 0$ which often does not significantly affect off-axis strength predictions as mentioned in Chapter 1 (c.f. Ref. [38]). This was done and subsequently F_{66} determined from the available strength data of various configurations. The 30° off-axis orientation yielded F_{66} that produced σ_6^{max} closest to 8600 psi and thus this was employed in subsequent experimental-theoretical correlation. The critical stress $\sigma_{xx}(\theta)$ predicted by the Tsai-Wu criterion is given by the following expression which includes the effect of shear-coupling:

$$\sigma_{xx}^{crit.}(\theta) = \frac{1}{\sqrt{F_{11}F_1(\theta)+2F_{12}F_2(\theta)+F_{22}F_3(\theta)+F_{66}F_4(\theta)}} \tag{5.37}$$

where; $F_1(\theta) = \left[\cos^2\theta + 2\sin\theta\cos\theta A(\theta)\right]^2$

$F_2(\theta) = \left[\cos^2\theta + 2\sin\theta\cos\theta A(\theta)\right]\left[\sin^2\theta - 2\sin\theta\cos\theta A(\theta)\right]$

$F_3(\theta) = \left[\sin^2\theta - 2\sin\theta\cos\theta A(\theta)\right]^2$

$F_4(\theta) = \left[-\sin\theta\cos\theta + (\cos^2\theta - \sin^2\theta)A(\theta)\right]^2$

Table 5.3 gives the predictions of the maximum stress and the tensor polynomial criteria based on the outlined methods of evaluating the necessary strength parameters along with the observed data for easy comparison. Figure 5.18 illustrates

Table 5.3 Ultimate stress predictions as functions of the off-axis angle of the tensor-plynomial, maximum stress and the proposed independent mode, micromechanics-aided strength criteria

Ultimate laminate stress according to:					
Off-axis orientation	Experimental observations (monotonic)	Tensor Polynom. $F_{12}=0.0$ $F_{66}=0.118\times10^{-7}$	Tensor Polynom. $F_{12}=0.582\times10^{-9}$ $F_{66}=0.135\times10^{-7}$	Maximum Stress	Independent mode, micromechanics-aided criterion
0°	225,362	225,362	225,362	225,362 L	225,362 L
5°	102,677	109,448	100,608	117,222 S	129,528 MSH
10°	58,773	57,627	52,174	56,569 S	63,452 MSH
15°	41,317	37,466	33,947	37,006 S	39,714 MSH
30°	17,722	17,722	16,418	20,147 S	17,847 MSH
45°	12,132	11,696	11,158	15,153 T	12,132 MSH
60°	8,853	9,048	8,853	10,005 T	10,034 MDN
75°	9.003	7,839	7,796	8,023 T	8,028 MDN
90°	7,484	7,484	7,484	7,484 T	7,484 MDN

L = Longitudinal stress failure
S = Shear stress failure
T = Transverse stress failure
MSH = Matrix shear and hydrostatic stress failure
MDN = Matrix deviatoric stress failure: normal components only

} all defined with respect to the lamina coor. system

the experimental-theoretical failure correlation of the two outlined criteria and it is seen that the effect of shear-transverse stress interaction is quite evidently pointing to the applicability of the tensor polynomial furmulation for this composite system.

In order to gain some insight into failure mechanisms of this composite system a limited micromechanics analysis was carried out and a simple strength criterion proposed to account for the observed apparent failure modes. Comparison of the strengths of 90° laminae in transverse tension and pure polyimide matrix revealed that the stresses in the matrix phase of the composite at failure were significantly higher than the ultimate stress of the polyimide specimen tested by itself. This is indicative of some form of the matrix material's insensitivity to certain stress combinations as far as failure is concerned. Subsequent comparison of the ultimate stresses in the matrix phase of the lamina and pure sample in terms of the second invariant of stress deriviators yielded surprisingly close correlation. While the pure matrix specimen failed at $I_2' = 3067$ psi in tension, the corresponding second invariant of the deviatoric average stresses in the matrix phase of the 90° lamina turned out to be $I_2' = 2986$ psi. On the other hand, the ultimate shear stress of the polyimide was 6470 psi while that of the composite at least 8600 psi. The above strengths (i.e. tension and torsion) of the polyimide matrix are therefore not

related to a single invariant pointing to at least two distinct failure mechanisms.

Two well known deformation mechanisms in glassy polymers are normal yielding (crazing) and shear yielding [105]. Crazing is inhibited by hydrostatic stress causing cavitation of the microscopic cracks which leads to reduction of stress concentrations around those locations. Shearing deformation on the other hand is in fact influenced by hydrostatic stress due to void formation and resulting decrease in load bearing capability of the material in shear. The observed ultimate stresses of Gr/Pi laminae in transverse tension could therefore be indicative of the presence of the first mechanism discussed above. Furthermore, the apparent shear-transverse stress interaction evident in Fig. 5.18 may be the result of the influence of hydrostatic state of stress in the matrix and therefore be indicative of the second mechanism.

In view of the above discussion and the related experimental observations three independent failure modes are assumed: one due to fiber fracture caused by the longitudinal stress σ_1 and the remaining two having roots in the matrix phase. The latter are taken to be caused either by the resolved matrix average shear stress parallel to the fiber direction and aided by hydrostatic stress or the part of the second deviatoric stress invariant that consists of normal matrix stresses only in the material principal

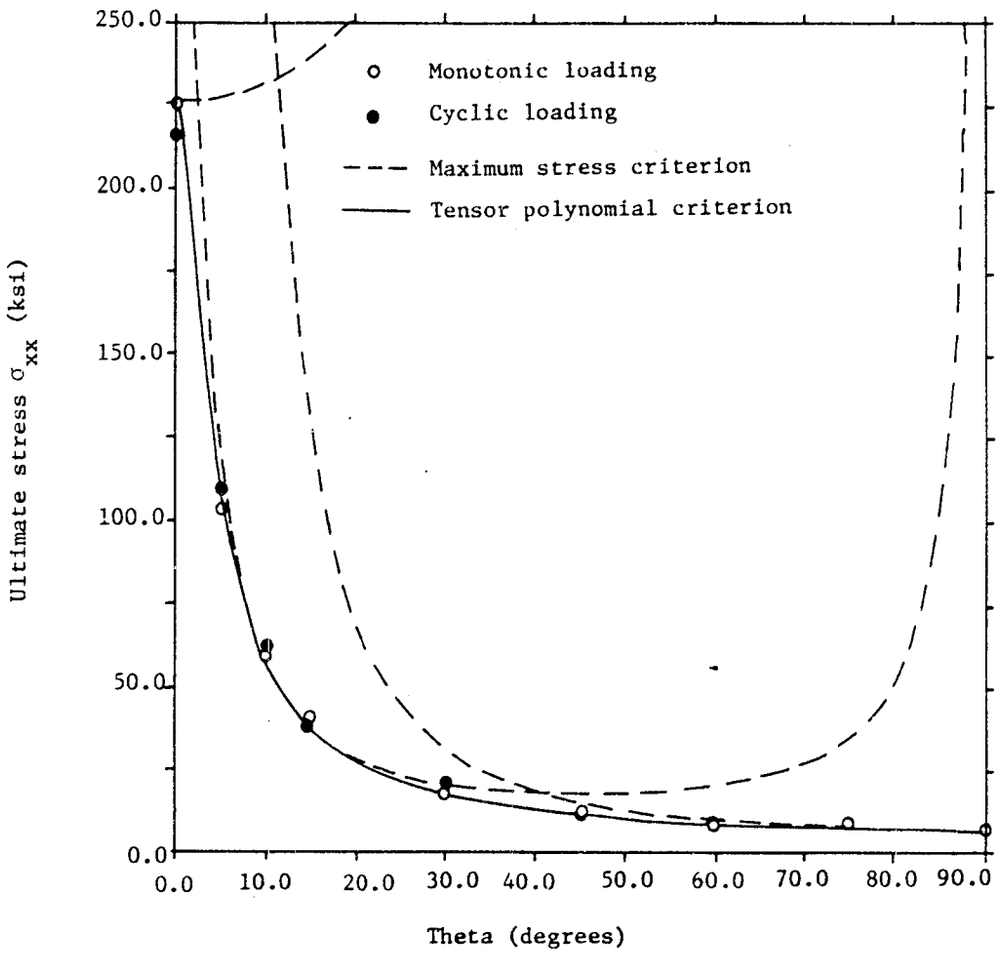

Fig. 5.18 Ultimate stress of the Gr/Pi off-axis coupons as a function of the off-axis angle according to tensor-polynomial and maximum stress failure criteria

coordinate system. Expressed analytically, failure occurs when any one of the above modes reaches a maximum value:

$$FM_{\ell} = \sigma_1 = \sigma_1^{max}$$

$$FM_{msh} = |\sigma_{6m}| + \frac{\mu}{3}(\sigma_{1m} + \sigma_{2m} + \sigma_{3m}) \tag{5.38}$$

$$FM_{mdn} = \frac{1}{\sqrt{6}}\left[(\sigma_{1m}-\sigma_{2m})^2 + (\sigma_{2m}-\sigma_{2m})^2 + (\sigma_{1m}-\sigma_{3m})^2\right]^{1/2}$$

where m stands for the matrix phase and Hill's stress concentration factors relate the matrix and externally applied stresses as before. The interaction constant μ has been determined on the basis of 15°, 30°, 45° and 60° off-axis tension tests and found to vary negligibly for the 30° and 45° orientations and by 18% and 26% for the 15° and 60° orientations, respectively, with the 45° one used as reference. On the other hand, pure polyimide strength data was utilized to determine FM_{msh} and FM_{mdn}.

The predictions of the outlined criteria are illustrated in Fig. 5.19 along with experimentally observed strength data whereas the actual numerical results are given in Table 5.3 for comparison with the other schemes. The proposed micromechanics-aided strength criterion compares favorably with both the experimental data and tensor polynomial formulation (with the exception of the 5° off-axis orientation) without possessing any apparent sensitivity problems. That is, sufficiently wide range of the off-axis orientations exists for this particular system to enable one

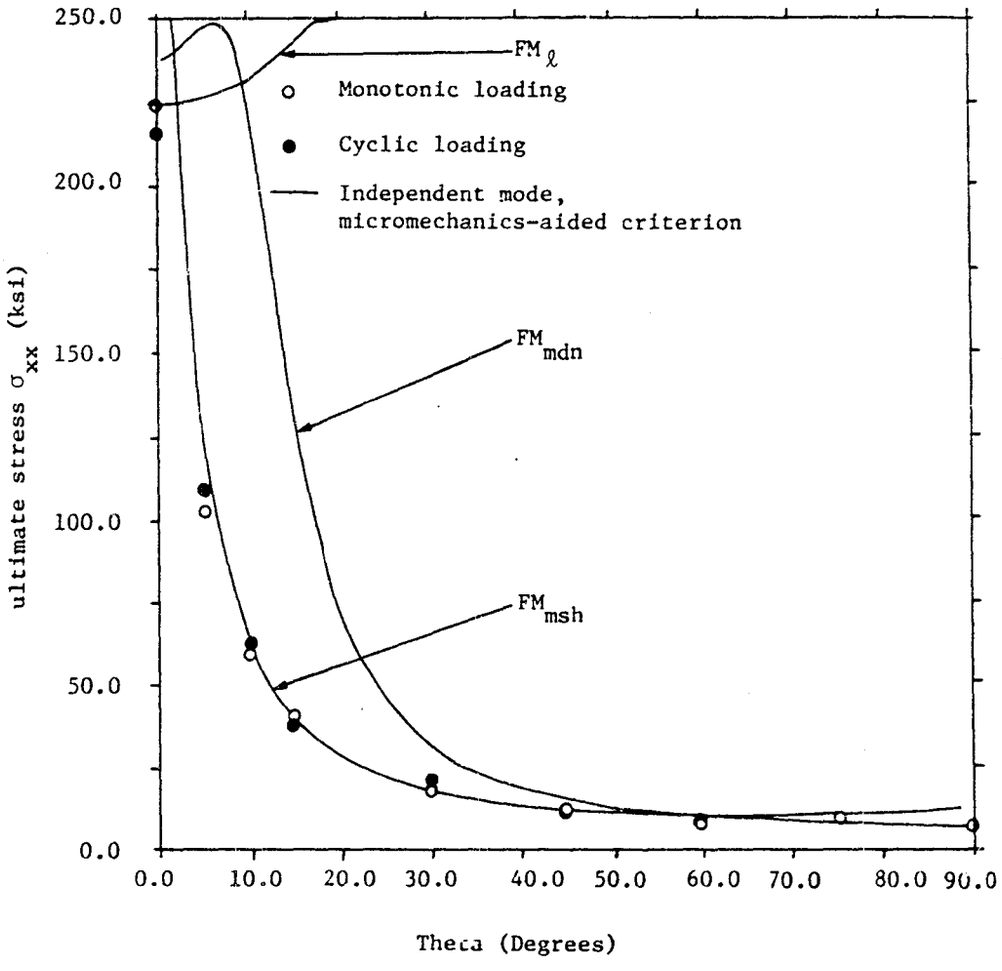

Fig. 5.19 Ultimate stress of the Gr/Pi off-axis coupons as a function of the off-axis angle according to the proposed independent-mode, micromechanics-aided failure criterion

to determine the interaction constant μ with little variation.

6. SUMMARY, CONCLUSIONS AND RECOMMENDATIONS FOR FURTHER STUDY

A constitutive formulation consistent with thermodynamic constraints that was developed by Valanis to model observed dissipative response of isotropic materials such as strain-hardening steels has been extended to transversely isotropic media. The objective of the above was to fulfill an existing need of modelling observed nonlinear response of fibrous composites in a rational manner that would be sufficiently general to predict the following types of material response often observed in these advanced, man-designed materials:

i) linear or nonlinear elastic response along fiber direction.

ii) dissipation in shear and transverse tension characterized by permanent strain-accumulation, nonlinear unloading and reloading resulting in generation of hysterisis loops and caused by various dissipative and/or damage nucleation mechanisms such as matrix plasticity, void or crack formation, crazing, fiber slippage or fiber/matrix debonding to name the better known phenomena.

iii) dissimilar strain-hardening in shear and transverse tension characterized by different hardening exponents in commonly employed power-law approximations.

iv) influence of transverse stress on the nonlinear shear strain and vice versa - an often observed phenomenon commonly referred to as stress-interaction.

v) often highly nonlinear response along certain material directions, e.g. shearing parallel to fibers, characterized by continuous rates of hardening and relatively small failure strains with no readily noticeable transition point between reversible and dissipative responses. This type of behavior is difficult to predict

with conventional plasticity theories as remarked by Valanis due to the sensitivity of the manner in which yield surface expands or translates to the definition of initial yield.

Extension of Valanis' "endochronic theory of plasticity" to transversely isotropic media entailed a solution of an auxiliary set of six, first order differential equations of motion defined with respect to a deformation measure or "intrinsic time scale" characteristic of the particular material at hand. These equations relate changes in the so-called internal variables which characterize various irreversiblities in the system to external variables such as stress or strain and form a basis of Valanis' treatment of the internal variable formalism and the associated thermodynamic framework vis-à-vis time-independent deformation of dissipative media. The above first order system is coupled through transversely isotropic matrices and thus consists of three coupled and three uncoupled equations of motion. Uncoupling of the required equations was accomplished through a simple transformation of the independent variables which effectively reduced the formulation from a 3 x 3 to a 2 x 2 eigenvalue-eigenvector problem for each set of coupled internal variables characterizing the dissipative response of considered media.

General solution of the above system resulted in a set of fading memory-type equations relating stresses to strains through path-dependent integrals functionally dependent on

the intrinsic time measure which is assumed to be a material property. The kernels of the integrals consist of sums of exponential eigenfunctions coupled via the eigenvectors mentioned above whose rate of decay is controlled by five independent retardation or "hardening" exponents. The developed general transversely isotropic equations have been shown to reduce to Valanis' isotropic formulation upon specialization of the various matrices that control motion of the system to the isotropic form. Furthermore, a power-law formulation or approximation with five independent hardening exponents ensues if a large number of internal variables is assumed in the expansion of Gibbs' potential about equilibrium or initial state of the system.

Applicability of the general endochronic equations for transverse isotropic media to prediction of nonlinear response of fibrous composites has been demonstrated through specialization of the developed constitutive equations in a fashion commensurate with the observed response of Gr/Pi composite system. This particular material system has been chosen due to its potential usefulness in advanced space vehicle applications currently under consideration at the NASA-Langley Research Center. In particular, items i) through v) regarding the often observed response of fibrous composites enumerated at the beginning of this section have also been observed in this material system under plane

stress, ambient temperature, proportional loading conditions. This has been accomplished via the commonly employed off-axis tension test method which entails loading of thin, unidirectional composite coupons with high aspect ratios and fibers oriented at an angle to the load axis. High aspect ratios are required in order to reduce the adverse effect of the well-known shear-coupling phenomenon on the experimentally determined stress-strain response caused by rigid gripping of the specimen's ends. A new test fixture which permitted the gripped ends of the specimen to rotate to some extent with the rotating and deforming material was designed to eliminate as much as possible the above phenomenon as well as reduce stress concentrations in the neighborhood of the grips. This would also then, at least it was assumed in priciple, result in ultimate strengths or failures more representative of the "true" material response.

The presence of shear-coupling has been demonstrated in this study to have a much more pronounced effect on determination of the shear modulus G_{12} in the material principal coordinate system than on the Young's Modulus E_{xx} in the lamina coordinate system in low off-axis orientations even with high aspect ratios. The above result followed from an auxiliary analytical study based on the Halpin-Pagano model and was motivated by the significant variations in the inital shear modulus along fiber direction for the various

off-axis orientations tested. Subsequent comparison between the experimental data and predictions of the above model yielded sufficiently good correlation trend-wise to attribute at least a significant portion of the observed variations to this phenomenon. The above comparison has revealed that the newly developed test fixture produced somewhat greater shear-coupling effects than the Halpin-Pagano model if it is assumed that this is the only cause of the observed variations as has been done here in the course of experimental-theoretical correlation on the basis of the developed transversely isotropic model. The Halpin-Pagano model is based on highly idealized boundary conditions that call for prevention of rotation of the specimen's centerline only which in turn facilitates a closed form analytical solution for the inhomogeneous strain field induced by the grips.

With the generated response of the Gr/Pi composite system in mind it has been demonstrated that the endochronic formulation is sufficiently general to allow uncoupling of dissipation along particular material directions from the corresponding reversible modes in a consistent fashion by setting certain coupling parameters to zero. This then enables one to obtain elastic response in the fiber direction with the introduction of a potential constructed in terms of external variables such as stress, only. In this particular case, a "nonlinear" potential has been proposed that accurately predicts the observed stiffening response of

the Gr/Pi composite in pure tension parallel to the fibers. An interesting consequence of the introduction of the above elastic potential turned out to be more consistent analysis of generated data in the dissipative region in transverse tension, namely, less scatter and fluctuation in the hardening exponents was observed when the potential was employed to separate elastic and irreversible strains of the various configurations.

Dissimilar hardening characteristics in shear and transverse tension that have been observed to obey power-laws with different hardening exponents and surprising accuracy in this particular system can also be accommodated by this theory. Hardening is associated with dissipation modes that are represented by second order tensors and their rates with respect to the intrinsic time scale and which are also coupled by matrices characterizing the degree of given material's symmetry. Since for transversely isotropic materials shearing parallel to the fibers is independent of transverse tension, the hardening exponents characterizing dissipation in these two directions will generally be different and indeed this is reflected by the recorded data. Single hardening exponent in transverse tension on the other hand theoretically implies similar recorded data. A single hardening exponent in transverse tension that has been observed in this Gr/Pi system on the other hand theoretically implies similar response in shear and tension, in the plane

of isotropy characterized by the same hardening exponent.

The observed dissipative response of the Gr/Pi system determined in a series of cyclic tests at various stress levels necessitated introduction of the concept of a second or inner time scale operative within the region bounded by the maximum unloading stress level on any given path not undergoing a reversal of loading direction. Introduction of the above concept required imposition of an additional thermodynamic constraint in order to ensure that the dissipated work was positive in the global sense, that is, in any given stress cycle. This was equivalent to the incorporation of Illyushin's Postulate into the endochronic theory framework which was originally developed with a single time scale z for all loading situtations whose only constraint, $dz > 0$, was sufficient to satisfy the Clausius-Duhem Inequality for every deformation process. It was subsequently shown that an inner time scale of the form $dz^i = \beta dz$, $0 < \beta \leq 1$, yielded predictions that correlated sufficiently well with the observed behavior both in terms of permanent strain accumulation and cyclic stress-strain response.

A fundamental aspect of the endochronic theory is the concept of intrinsic time measure and the associated material parameters or elements of the material metric that define it. This is one of the major differences that sets this theory apart from, say, incremental plasticity theories in which deformation measure is defined in terms of plastic

strain arc length which is common to all plastic media and is therefore not a material property. The stress interaction in shear and transverse tension apparently evident in the generated data lends force to the utility of the theory regarding application to fibrous composites as it is a significant confirmation of the manifestation of such a material "property" as the intrinsic time measure. To be sure, shear-coupling must be taken into account in the above observations as its effect has been eliminated with the aid of the Halpin-Pagano model in order to compare the nonlinear response of the various configurations on the same footing and thus establish the presence of stress-interaction. However, the reduced data showed very good consistency with distinct bounds for the significantly nonlinear shear responses along the fiber direction of the various configurations. Furthermore, experimental and analytical studies referenced in the outlined literature review do point to the presence of such stress-interaction. A consequence of technological importance of such phenomenon is the need for more than one off-axis tension test for the determination of the nonlinear shear response in the material principal coordinate system.

The elements of the intrinsic time measure and related constants in the integrals characterizing dissipation have been evaluated with good accuracy vis-à-vis predicted response on the basis of resolved shear response along fiber

direction obtained from 10°, 30° and 60° off-axis tension tests and transverse tension of 90° coupon. Other off-axis configurations yielded worse correlation with experimental data due to highly nonlinear behavior of the orientation-dependent shift parameters characterizing stress-interaction. However, pure shear response could not be determined using the above method as the intrinsic time parameters s_{66} and s_{12} characteristic of shear and coupled transverse-normal response respectively always appeared in combination for this type of tension test.

A micromechanics-aided approach based on Hill's stress concentration factors was subsequently employed to demonstrate the feasibility of incorporating certain micromechanical considerations into the endochronic framework via the intrinsic time measure. This was accomplished by assuming the observed dissipation to be a function of deviatoric stresses in the matrix whose trajectories do not deviate significantly from the initial directions under proportional loading of the coupon. The elements of the metric s_{ij} then become functions of the matrix stress concentration functions that are determined from the knowledge of the initial composite, fiber and matrix compliances. The above assumption,however, was insufficient to account for the significant σ_1 interaction observed in the Gr/Pi resolved shear stress response and thus an extra term reflecting possible crack evolution caused by the longi-

tudinal stress was incorporated into the intrinsic time measure. The presence of damage accumulation due to σ_1 in this material system is supported to an extent by noticeable degradation in the initial shear modulus at points of reloading for low off-axis configurations. The above micromechanics-aided scheme required only two off-axis tension tests for determination of the material parameters and yielded comparable results to those of the purely phenomenological approach when the 10° and 60° off-axis results were utilized for that purpose.

The limited failure analysis carried out in this study produced several notable results. First of all, the newly designed text fixture yielded very consistent strength data with average differences often less than 3% and test section failures for most off-axis configurations. No significant differences were found between ultimate loads of monotonic and cyclic tests with the exception of the 15° off-axis coupons. These failed consistently below the maximum unloading stress level and thus this could be indicative of path-dependent failure modes along certain stress trajectories for this particular composite system.

The observed ultimate load as a function of the off-axis angle correlated well with a quadratic tensor polynomial criterion with F_{12} set equal to zero. Relaxation of this constraint necessitated use of two off-axis test results for determination of F_{12} and F_{66} with the consequence that

none of the available pairs produced results that satisfied the stability condition $E_{11}F_{22} \geq F_{12}^2$. A distinct mode failure criteria based on three possible failure mechanisms was subsequently proposed and the necessary strength parameters evaluated from both the coupon and matrix ultimate load data with the aid of Hill's stress concentration factors. The assumed mechanisms are given by the following:

i) failure due to fiber breakage and governed by the longitudinal stress σ_1.

ii) failure governed by a critical value of the second invariant of the average matrix stress deviators excluding shear components, i.e., consisting of normal stresses only

iii) failure governed by a critical value of the average matrix shear stress parallel to the fiber direction and influenced by the mean matrix pressure.

Predictions of the proposed criterion correlated well with the recorded data and Tsai-Wu quadratic criterion for most off-axis configurations. Furthermore, the coupling parameter for the shear and mean stress failure interaction could be obtained from the generated data with little fluctuation in the off-axis range $30° \leq \theta \leq 45°$.

With the above discussion in mind, the following recommendations regarding future work in this area follow from the present study:

i) in view of the pronounced effect of shear-coupling on G_{12} in low off-axis configurations even with relatively large aspect ratios for material systems such as Gr/Pi, the 45° coupon is recommended for determination of the shear modulus G_{12}.

ii) the possibility of the presence of stress-interaction phenomenon even in relatively brittle systems such as Gr/Pi requires more than one off-axis test for determination of nonlinear shear response in the material principal system. Three off-axis tension tests are therefore recommended to establish the extent of stress-interaction: 10°, 30° and 60° configurations might be considered as they cover a significant portion of possible stress-interaction range without being adversely influenced to a large extent by strain-gage sensitivity problems.

iii) pure torsion tests on thin, unidirectional tubes are recommended to determine how well the micromechanics-aided prediction of pure shear response correlates with the actual one. This might help to establish a viable off-axis tension test method to determine the nonlinear shear response in the presence of stress-interaction.

iv) consideration of the effect of small perturbations in the intrinsic time scale about some mean path on predictions of the total constitutive response appears to be warrented. Recent series of publications [106, 107,108] are indicative of some controversy regarding the various aspects of the endochronic theory, including the one outlined above, which is still considered to be in its infancy.

v) further investigation into compliance degradation in cyclic tests at points of reloading in the considered system would appear to be desirable. The functional form of intrinsic time scale chosen for this particular constitutive model does not predict this phenomenon; however, this does not affect the experimental-theoretical correlation significantly.

vi) SEM investigation of fracture surfaces would be beneficial in estimating the extent of various failure modes at any particular off-axis angle. This would subsequently facilitate correlation between the observed failure modes and the proposed failure criterion reflecting the assumed mechanisms proposed in this study.

REFERENCES

1. Drucker, D. C., "Yielding, Flow and Failure," Inelastic Behavior of Composite Materials, (Herakovich - editor), AMD No. 13, Am. Soc. Mechanical Engineers, 1975, p.1.

2. Spencer, A. J. M., "The Formulation of Constitutive Equations for Anisotropic Solids," paper presented at Euromech Colloquium 115 entitled Mechanical Behaviour of Anisotropic Solids, Grenoble, France, June 19 - 22, 1979.

3. Petit, P. H. and Weaddoups, M. E., "A Method of Predicting the Nonlinear Behavior of Laminated Composites," J. Composite Materials, Vol. 3, January 1969, p. 2.

4. Hahn, H. T. and Tsai, S. W., "Nonlinear Elastic Behavior of Unidirectional Composite Laminae," J. Composite Materials, Vol. 7, January 1973, p. 102.

5. Hahn, H. T., "Nonlinear Behavior of Laminated Composites," J. Composite Materials, Vol. 7, April 1973, p. 257.

6. Benveniste, Y. and Aboudi, J., "The Non-linear response of a Fibre-Reinforced thin Plate under Dynamic Loading," Fibre Science and Technology, Vol. 7, 1974

7. Sandhu, R. S., "Nonlinear Behavior of Unidirectional and Angle Ply Laminates," J. Aircraft, Vol. 13, No. 2

8. Jones, R. M., and Nelson, D. A. R., Jr., "A New Material Model for the Nonlinear Biaxial Behavior of ATJ-S Graphite," J. Composite Materials, Vol. 9, January 1975, p. 10.

9. Jones, R. M. and Morgan, H. S., "Analysis of Nonlinear Stress-Strain Behavior of Fiber-Reinforced Composites," J. Composite Materials, Vol. 15, No. 12, December 1977.

10. Cole, B. and Pipes, R., "Filamentary Composite Laminates Subjected to Biaxial Stress Fields," AFFDL-TR-73-115, 1974.

11. Hashin, Z., Bagchi, D. and Rosen, B. W., "Non-linear Behavior of Fiber Composite Laminates," NASA CR-2313, April 1974.

12. Rosen, R. W., "A Simple Procedure for Experimental Determination of the Longitudinal Shear Modulus of Unidirectional Composites," J. Composite Materials, Vol. 6, October 1972, p. 552.

13. Chamis, C. C. and Sinclair, J. H., "Low Off-Axis Tensile Test for Intralaminar Shear Characterization of Fiber Composites," NASA TN D-8215, April 1976.

14. Hill, R., "A Theory of the Yielding and Plastic Flow of Anisotropic Metals," Proc. Royal Soc., (London), Series A, Vol. 193, No. 1033, 1948, p. 281.

15. Smith, G. F., "On the Yield Conditions for Anisotropic Materials," Quarterly of Applied Mathematics, Vol. 20, No. 3, October 1962, p. 241-247.

16. Batdorf, S. B. and Budiansky, B., "A Mathematical Theory of Plasticity Based on the Concept of Slip," NACA TN No. 1971, April 1949.

17. Dubey, R. N. and Hillier, M. J., "Yield Criteria and the Bauschinger Effect for a Plastic Solid," Journal of Basic Engineering, Paper No. 71-MET-P., March 1972, p. 238.

18. Shih, C. F. and Lee, D., "Further Developments in Anisotropic Plasticity," Journal of Engineering Materials and Technology, Vol. 100, July 1978, p. 294.

19. Smith, A., Reynolds, W. N. and Hancox, N. L., "Bulk Compressibility of Carbon Fibre Reinforced Plastics," J. Composite Materials, Vol. 7, January 1973, p. 138.

20. Saint-John, C. F. and Street, K. N., "B-Al Composite Failure under Combined Torsion and Tension Loading," J. Composite Materials, Vol. 8, July 1974, p. 266.

21. Mulhern, J. F., Rogers, T. G. and Spencer, A. J. M., "A Continuum Model for Fibre-Reinforced Plastic Materials," Proc. Roy. Soc., Series A. Vol. 301, 1967, p. 473-492.

22. Cooper, G. A., "Orientation Effects in Fibre-Reinforced Metals," J. Mech. Phys. Solids, Vol. 14, 1966, p. 103-111.

23. Jackson, P. W. and Cratchley, D., "The Effect of Fibre Orientation on the Tensile-Strength of Fibre-Reinforced Metals," J. Mech. Phys. Solids, Vol. 14, 1955, p. 49-64.

24. Mulhern, J. F., Rogers, T. G. and Spencer, A. J. M., "A Continuum Teory of a Plastic-Elastic Fibre-Reinforced Material," Int. J. Engr. Sci., Vol. 7, 1969, p. 129-152.

25. Mulhern, J. F., Rogers, T. G., and Spencer, A. J. M., "Cyclic Extension of an Elastic Fibre with an Elastic-Plastic Coating," J. Inst. Maths. Applics., Vol. 3, 1967, p. 21-40.

26. Dvorak, G. J. and Rao, M. S. M., "Axisymmetric Plasticity Theory of Fibrous Composites," Int. J. Engr. Sci., Vol. 14, 1976, p. 361-373.

27. Tsai, S. W., "Strength Characterisitcs of Composite Materials," NASA CR-224, April 1965.

28. Tsai, S. W. and Hahn, H. T., "Failure Analysis of Composite Materials," Inelastic Behavior of Composite Materials, (Herakovich - editor), AMD No. 13, Am. Soc. Mechanical Engineers, 1975, p. 73.

29. Lance, R. H. and Robinson, D. N., "A Maximum Shear Stress Theory of Plastic Failure of Fiber-Reinforced Materials," J. Mech. Phys. Solids, Vol. 19, 1971, p. 49-60.

30. Schmid, E. and Boas, W., Kriställplastizität, Julius Springer, Berlin, 1935.

31. Sandhu, R. S., "A Survey of Failure Theories of Isotropic and Anisotropic Materials," AFDL-TR-72-71.

32. Sendeckyj, G. P., "A Brief Survey of Empirical Multiaxial Strength Criteria for Composites," Testing and Design (Second Conference), ASTM STP 797, April 1971, p. 41-51.

33. Kaminski, B. E. and Lantz, R. B., "Strength Theories of Failure for Anisotropic Materials," Composite Materials: Testing and Design, ASTM STP 460, 1969, p. 160.

34. Ashkenazi, E. K., "Problems of the Anisotropy of Strength," Mekhanika Polimerov, Vol. 1, No. 2, 1965

35. Goldenblat, I. I. and Kopnov, V. A., "Strength of Glass-Reinforced Plastics in Complex Stress State," Mekhanika Polimerov, Vol. 1, 1965, p. 70; English Translation: Polymer Mechanics, Vol. 1, 1966, p. 54.

36. Tsai, S. W. and Wu, E. M., "A General Theory of Strength for Anisotropic Materials," J. Composite Materials, Vol. 5, January 1971, p. 58.

37. Wu, E. M., "Optimal Experimental Measurements of Anisotropic Failure Tensors," J. Composite Materials, Vol. 6, 1972, p. 472-489.

38. Narayanaswami, R., "Evaluation of the Tensor Polynomial and Hoffman Strength Theories for Composite Materials," J. Composite Materials, Vol. 11, October 1977, p. 366.

39. Collins, B. R. and Crane, R. L. "A Graphical Representation of the Failure Surface of a Composite," J. Composite Materials, Vol. 5, July 1971, p. 408.

40. Wu, E. M., "Phenomenological Anisotropic Failure Criterion," Composite Materials, Vol. 2, Mechanics of Composite Materials, ed. by G. P. Sendeckyj, 1974, p. 353, Academic Press, New York.

41. Huang, C. and Kirmser, P. G., "A Criterion of Strength for Orthotropic Materials," Fibre Science and Technology, Vol. 8, 1975.

42. Tennyson, R. C., MacDonald, D. and Nanyaro, A. P., "Evaluation of the Tensor Polynomial Failure Criterion for Composite Materials," J. Composite Materials, Vol. 12, January 1978, p. 63.

43. Hashin, Z., "Failure Criteria for Unidirectional Fiber Composites," J. Applied Mechanics, Vol. 47, No. 2, 1980

44. Norris, C. B., "Strength of Orthotropic Materials Subjected to Combined Stress," Forest Products Laboratory, Report 1816, 1962.

45. Hill, R., "Theory of Mechanical Properties of Fibre-Strengthened Materials: II. Inelastic Behaviour," J. Mech. Phys. Solids, Vol. 12, 1964, p. 213-218.

46. Dvorak, G. J. and Bahei-el-din, Y. A., "Elastic-Plastic Behavior of Fibrous Composites," J. Mech. Phys. Solids, Vol. 27, p. 51-72.

47. Sawicki, A., "Elasto-Plastic Theory of Composites with Regular Internal Structure," paper presented at Euromech Colloquium 115 entitled "Mechanical Behavior of Anisotropic Solids," Grenoble, France, June 19-22, 1979.

48. Huang, W., "Plastic Behavior of Some Composite Materials," J. Composite Materials, Vol. 5, July 1971, p. 320.

49. Tanaka, K., Wakashima, K. and Mori, T., "Plastic Deformation Anisotropy and Work-Hardening of Composite Materials," J. Mech. Phys. Solids, Vol. 21, 1973, p. 207-214.

50. Eshelby, D., "The Determination of the Elastic Field of an Ellipsoidal Inclusion, and Related Problems," Proc. Royal Soc., (London), Series A, Vol. 241A, 1957, p. 376.

51. Eshelby, D., "The Elastic Field Outside an Ellipsoidal Inclusion," Proc. Royal Soc., (London) Series A, Vol. 252A, 1959, p. 561.

52. Chou, P. C., McNamee, B. M. and Chou, D. K., "The Yield Criterion of Laminated Media," J. Composite Materials, Vol. 10, January 1976, p. 55.

53. Wakashima, K., Suzuki, Y. and Umekawa, S., "A Micromechanical Prediction of Initial Yield Surfaces of Unidirectional Composites," J. Composite Materials, Vol. 13, October 1979, p. 288.

54. Chou, P. C. and Chou, D. K., "Plastic Flow Rules of Laminated Composites," J. Composite Materials, Vol. 10, January 1976, p. 55.

55. Adams, D. F., "Inelastic Analysis of a Unidirectional Composite Subjected to Transverse Normal Loading," J. Composite Materials, Vol. 4, July 1970, p. 310.

56. Foye, R. L., "Theoretical Post-Yielding Behavior of Composite Laminates, Part I - Inelastic Micromechanics," J. Composite Materials, Vol. 7, April 1973, p. 178.

57. Foye, R. L., "Theoretical Post-Yielding Behavior of Composite Laminates, Part II - Inelastic Macromechanics," J. Composite Materials, Vol. 7, July 1973, p. 310.

58. Lin, T. H. Salinas, D. and Ito, Y. M., "Initial Yield Surface of a Unidirectionally Reinforced Composite," J. of Applied Mechanics, Vol. 39, No. 2, 1972, p. 321.

59. Lin, T. H., Salinas, D. and Ito, Y. M., "Elastic-Plastic Analysis of Unidirectional Composites," J. of Composite Materials, Vol. 6, 1972, p. 48.

60. Dvorak, G. J., Rao, M. S. M. and Tarn, J. Q., "Yielding in Unidirectional Composites under External Loads and Temperature Changes," J. Composite Materials, Vol. 7, April 1973, p. 194.

61. Dvorak, G. J., Rao, M. S. M. and Tarn, J. Q., "Generalized Initial Yield Surfaces for Unidirectional Composites," J. of Applied Mechanics, Vol. 41, No. 1, 1974, p. 249.

62. Stowell, E. A. and Liu, T. S., "On the Mechanical Behaviour of Fibre-Reinforced Crystalline Materials," J. Mech. Phys. Solids, Vol. 9, 1961, p. 242-260.

63. Kelly, A. and Davis, G. J., "The Principles of the Fibre Reinforcement of Metals," Metall. Rev., Vol. 10, No. 1, 1965, p. 212.

64. Prager, W., "Plastic Failure of Fiber-Reinforced Materials," J. of Applied Mechanics, Vol. 36, No. 3, 1969, p. 542.

65. McLaughlin, P. V., Jr., "Limit Behavior of Fibrous Materials," Int. J. Solids Structures, Vol. 16, 1970, p. 1357-1376.

66. McLaughlin, P. V., Jr., "Plastic Limit Behavior and Failure of Filament Reinforcement Materials," Int. J. Solids, Structures, Vol. 8, 1972, p. 1299-1318.

67. Dow, N. F., Gen. Elect. Rep. No. R63-SD61, 1963.

68. Cox, H. L., "Elasticity and Strength of Paper and Other Fibrous Materials," Br. J. Appl. Phys., Vol. 3, 1952, p. 72.

69. Rosen, B. W., "Tensile Failure of Fibrous Composites," AIAA Journal, Vol. 2, No. 11, November 1964.

70. Zweben, C. and Rosen, B. W., "A Statistical Theory of Material Strength with Application to Composite Materials," J. Mech. Phys. Solids, Vol. 18, 1970, p. 189-206.

71. Zweben, C., "Failure Analysis of Unidirectional Fiber Composites under Combined Axial Tension and Shear," J. Mech. Phys. Solids, Vol. 22, 1974, p. 193-215.

72. Kousiounolos, P. N. and Williams, J. H., Jr., "Heterogeneous Anisotropic Model for Notched Fibre Composites," Fibre Science and Technology, Vol. 10, 1977

73. Goree, J. G., "Analysis of a Unidirectional Composite Containing Broken Fibers and Matrix Damage," Annual Report, NASA Grant NSG-1297.

74. Zweben, C., "An Approximate Method of Analysis for Notched Unidirectional Composites," Engineering Fracture Mechanics, Vol. 6, 1974, p. 1-10.

75. Hedgepeth, J. M., "Stress Concentrations in Filamentary Structures," NASA TN D-882, Langley Research Center, 1961.

76. Drucker, D. C., "Coulomb Friction, Plasticity, and Limit Loads," J. of Applied Mechanics, Vol. 21, Trans. of the ASME, Vol. 76, 1954, p. 71.

77. Palmer, A. C., Maier, G. and Drucker, D. C., "Normality Relations and Convexity of Yield Surfaces for Unstable Materials or Structural Elements," J. of Applied Mechanics, Vol. 34, Trans. of the ASME, Vol. 89, June 1967, p. 464.

78. Rice, R. R., "Inelastic Constitutive Relations for Solids: An Internal-Variable Theory and its Applications to Metal Plasticity," J. Mech. Phys. Solids, Vol. 19, 1971, p. 433-454.

79. Valanis, K. C., "A Theory of Viscoplasticity without a Yield Surface, Part I. General Theory," Archives of Mechanics, Vol. 23, No. 4, 1971, p. 517-533.

80. Valanis, K. C., "A Theory of Viscoplasticity without a Yield Surface, Part II. Applications to Mechanical Behavior of Metals," Archives of Mechanics, Vol. 23, No. 4, 1971, p. 535-551.

81. Hahn, H. T. and Tsai, S. W., "On the Behavior of Composite Laminates after Initial Failures," J. Composite Materials, Vol. 8, July 1974, p. 288.

82. Reifsnider, K. L. and Talug, A., "Analysis of Fatigue Damage in Composite Laminates," Int. J. Fatigue, January 1980, p. 3-11.

83. Williams, J. H. and Lee, S. S., "Acoustical Emission Monitoring of Fiber Composite Materials and Structures," J. Composite Materials, Vol. 12, October 1978, p. 348.

84. Adams, R. D. and Flitcroft, J. E., "Effects of Shear Damage on the Torsional Behaviour of Carbon Fiber Reinforced Plastics," J. Composite Materials, Vol. 7, January 1973, p. 68.

85. Akbarzadeh, A., "Effect of Broken Fibres on the Strength of Unidirectional Composite Materials," Fiber Science and Technology, Vol. 11, 1978 , p. 217.

86. Mansfield, E. H. and Purslow, D., "The Influence of Fiber Waviness on the Moduli of Unidirectional Fiber Reinforced Composites," CP No. 1339, December 1974.

87. van Dreumel, W. H. M. and Kamp, J. L. M., "Non-Hookean Behaviour in the Fibre Direction of Carbon-Fibre Composites and the Influence of Fibre Waviness on the Tensile Properties," J. Composite Materials, Vol. 11, October 1977, p. 461.

88. Craddock, J. N., Zak, A. R. and Majerus, J. N., "Nonlinear Response of Composite Material Structures," J. Composite Materials, Vol. 11, April 1977, p. 204.

89. Soldatov, M. M., "Investigation of Nonlinear Properties of Composites Consisting of Linear-Elastic Components," translated from Mekhanika Polimerov, No. 5, p. 898-905, September-October 1973.

90. Valanis, K. C., "On the Foundations of the Endochronic Theory of Viscoplasticity," Archives of Mechanics, Vol. 27, No. 5-6, 1975, p. 857-868.

91. Valanis, K. C., "An Energy-Probability Theory of Fracture, (An Endochronic Theory)," Journal de Mécanique, Vol. 14, No. 5, 1975, p. 843-862.

92. Valanis, K. C. "Some Recent Developments in the Endochronic Theory of Plasticity - te Concept of Internal Barriers," Constitutive Equations in Viscoplasticity: Phenomenological and Physical Aspects, AMD - Vol. 21, 1976, p. 15-32.

93. Valanis, K. C., "Fundamental Consequences of a New Intrinsic Time Measure - Plasticity as a Limit of the Endochronic Theory," Archives of Mechanics, Vol. 32, No. 2, 1980, p. 171-191.

94. Schapery, R. A., "On a Thermodynamic Constitutive Theory and Its Applications to Various Nonlinear Materials," Proceedings, IUTAM Symposium, East Kilride, 1968, p. 259.

95. Ponter, A. R. S., Boitaille, J., Kestin, J., "A Thermodynamic Model for Time Independent Plastic Deformation of Solids," National Science Foundation Report No. ENG 74-13217, 1978.

96. Chamis, C. C. and Sinclair, J. H., "10° Off-Axis Tensile Test for Intralaminar Shear Characterization of Fiber Composites," NASA TN D-8215, 1976.

97. Pagano, N. J., and Halpin, J. C., "Influence of End Constraint in the Testing of Anisotropic Bodies," J. Composite Materials, Vol. 2, No. 1, 1968, p. 18.

98. Rizzo, R. R., "More on the Influence of End Constraints on Off-Axis Tensile Tests," J. Composite Materials, Vol. 3, 1969, p. 202.

99. Wu, E. M. and Thomas, R. L., "Off-Axis Test of a Composite," J. Composite Materials, Vol. 2, No. 4, 1968, p. 523.

100. Davis, J. G., Jr., editor, "Composites for Advanced Space Transportation Systems - (CASTS)," NASA TM 80038, 1979.

101. Private communication with Prof. K. L. Reifsnider.

102. "Errors Due to Transverse Sensitivity," M-M Tech Note TN - 137: Transverse Sensitivity Errors.

103. Williams, M. L., "Structural Analysis of Viscoelastic Materials," AIAA Journal, Vol. 2, No. 5, 1964, p. 785.

104. Hill, R., "Elastic Properties of Reinforced Solids: some Theoretical Principals," J. Mech. Phys. Solids, Vol. 11, 1963, p. 357-372.

105. Hertzberg, R. W., Deformation and Fracture Mechanics of Engineering Materials, John Wiley and Sons, 1976, p. 214.

106. Rivlin, R. S., "Some Comments on the Endochronic Theory of Plasticity," Int. J. Solids Structures, Vol. 17, 1981, p. 231-248.

107. Valanis, K. C., "On the Substance of Rivlin's Remarks on the Endochronic Theory," Int. J. Solids Structures, Vol. 17, 1981, p. 249-265.

108. Rivlin, R. S., "Comments on 'On the Substance of Rivlin's Remarks on the Endochronic Theory' by K. C. Valanis," Int. J. Solids Structures, Vol. 17, 1981, p. 267-268.

Appendix A

EFFECTIVE ELASTIC MODULI IN THE PRESENCE OF SHEAR-COUPLING

The relationship between stress and strain at the mid-point of an off-axis tension coupon whose center-line is prevented from rotation has been shown by Pagano and Halpin [97] to be of the following form:

$$\begin{Bmatrix} \varepsilon_{xx} \\ \varepsilon_{yy} \\ \gamma_{xy} \end{Bmatrix} = \begin{bmatrix} \bar{S}_{11} & \bar{S}_{12} & \bar{S}_{16} \\ \bar{S}_{12} & \bar{S}_{22} & \bar{S}_{26} \\ \bar{S}_{16} & \bar{S}_{26} & \bar{S}_{66} \end{bmatrix} \begin{Bmatrix} \sigma_{xx} \\ 0 \\ \tau_{xy} \end{Bmatrix} \tag{A.1}$$

with σ_{xx} and τ_{xy} given by:

$$\sigma_{xx} = C_2$$
$$\tau_{xy} = -C_o h^2 \tag{A.2}$$

where:

$$C_o = \frac{6\bar{S}_{16}\varepsilon_o}{6h^2(\bar{S}_{11}\bar{S}_{66} - \bar{S}_{16}^2) + \bar{S}_{11}^2 \ell^2}$$

$$C_2 = \frac{C_o}{\bar{S}_{16}} \cdot (6\bar{S}_{66}h^2 + \bar{S}_{11}\ell^2) \tag{A.3}$$

ε_o = applied center-line displacement, constant along center-line

and the remaining terms are the same as defined previously.

The above expressions are referred to the coordinate system aligned with longitudinal (load) axis of the coupon.

Using Eqns. (A.2) and (A.3) we can express τ_{xy} in terms of σ_{xx} as follows:

$$\tau_{xy} = \frac{-\sigma_{xx}}{\left(\frac{\bar{S}_{66}}{\bar{S}_{16}}\right) + \frac{1}{6}\left(\frac{\ell}{h}\right)^2 \left(\frac{\bar{S}_{11}}{\bar{S}_{16}}\right)} \qquad \text{(A.4)}$$

so that the first of Eqns. (A.1) becomes:

$$\varepsilon_{xx} = \bar{S}_{11} \left\{ \frac{1 + 6\left(\frac{h}{\ell}\right)^2 \left[\left(\frac{\bar{S}_{66}}{\bar{S}_{11}}\right) - \left(\frac{\bar{S}_{16}}{\bar{S}_{11}}\right)^2\right]}{1 + 6\left(\frac{h}{\ell}\right)^2 \left(\frac{\bar{S}_{66}}{\bar{S}_{11}}\right)} \right\} \sigma_{xx} \qquad \text{(A.5)}$$

Defining $E^{**}_{xx} = \frac{\sigma_{xx}}{\varepsilon_{xx}}$, we obtain Pagano's and Halpin's expression given by Eqn. (3.1). However, in practice we use the actual strain as obtained from strain gage located at the center of specimen, i.e. ε_{xx}, and average stress based on the load and specimen's cross-sectional area. The expression for total load necessary to deform the specimen derived by Pagano is given by:

$$P = t\int_{-h}^{h} \sigma_{xx}\left(\frac{\ell}{2}, y\right) dy = 2th\left(C_2 - \frac{2\bar{S}_{16}h^2}{3\bar{S}_{11}} C_o\right)$$

Thus the relation between average stress $\bar{\sigma}_{xx} = \frac{P}{2th}$ and σ_{xx} is obtained as:

$$\sigma_{xx} = \left\{ \frac{1 + 6\left(\frac{h}{\ell}\right)^2 \left(\frac{\bar{S}_{66}}{\bar{S}_{11}}\right)}{1 + 6\left(\frac{h}{\ell}\right)^2 \left[\left(\frac{\bar{S}_{66}}{\bar{S}_{11}}\right) - \frac{2}{3}\left(\frac{\bar{S}_{16}}{\bar{S}_{11}}\right)^2\right]} \right\} \bar{\sigma}_{xx} \qquad \text{(A.6)}$$

so that upon substituting the above expression into Eqn.

(A.5) we obtain E^*_{xx} given by Eqn. (3.3).

Now, the shear strain along principal material axes 1-2 given in terms of the measured quantities in the x-y coordinate system is obtained from the standard tensor transformation relations. These yield:

$$\gamma_{12} = 2\sin\theta\cos\theta(\varepsilon_{yy} - \varepsilon_{xx}) + (\cos^2\theta - \sin^2\theta)\gamma_{xy} \quad (A.7)$$

or, in terms of σ_{xx} and τ_{xy} given by Eqns. (A.1), the above becomes:

$$\gamma_{12} = [2\sin\theta\cos\theta(\bar{S}_{12} - \bar{S}_{11}) + (\cos^2\theta - \sin^2\theta)\bar{S}_{16}]\sigma_{xx} + [2\sin\theta\cos\theta(\bar{S}_{26} - \bar{S}_{16}) + (\cos^2\theta - \sin^2\theta)\bar{S}_{66}]\tau_{xy} \quad (A.8)$$

Using Eqns. (A.4) and (A.6) we can express the above relationship in terms of the applied average stress $\bar{\sigma}_{xx}$ in the x-y coordinate system as follows:

$$\gamma_{12} = \bar{\sigma}_{xx}\{2\sin\theta\cos\theta[(\bar{S}_{12}-\bar{S}_{11})(1+C)-(\bar{S}_{26}-\bar{S}_{16})B]+ (\cos^2\theta-\sin^2\theta)[\bar{S}_{16}(1+C)-\bar{S}_{66}B]\}/A \quad (A.9)$$

This unusual arrangement does serve a purpose as will be seen subsequently.

Now, using the point transformation relations, the shear stress in the 1-2 coordinate system can be expressed in the following fashion:

$$\tau_{12} = -\sigma_{xx}\sin\theta\cos\theta + (\cos^2\theta - \sin^2\theta)\tau_{xy} \quad (A.10)$$

However, in practice we use the following relation to obtain τ_{12}:

$$\tau_{12} = -\bar{\sigma}_{xx}\sin\theta\cos\theta \tag{A.11}$$

which amounts to disregarding shear-coupling stresses. Substituting the expression for σ_{xx} in terms of τ_{12} obtained from the above relation into Eqn. (A.9) we arrive at the effective shear modulus G^*_{12} of Eqn. (3.4). If Eqn. (A.10) is employed on the other hand, the exact result

$$\frac{\tau_{12}}{\gamma_{12}} = S_{66}$$

is obtained since then all the stress components have been taken into account in the standard point transformation relations.

In a similar manner as that used to derive E^*_{xx}, the effective Poisson's ratio ν^*_{xy} can be obtained from the first two of Eqns. (A.1). Employing Eqn. (A.4) to express τ_{xy} in terms of σ_{xx} the following result is obtained:

$$\nu^*_{xy} = -\frac{\varepsilon_{yy}}{\varepsilon_{xx}} = -\left[\frac{\bar{S}_{12} - \dfrac{\bar{S}_{26}}{\dfrac{\bar{S}_{66}}{\bar{S}_{16}} + \frac{1}{6}\left(\frac{\ell}{h}\right)^2\left(\dfrac{\bar{S}_{11}}{\bar{S}_{16}}\right)}}{\bar{S}_{11} - \dfrac{\bar{S}_{16}}{\dfrac{\bar{S}_{66}}{\bar{S}_{16}} + \frac{1}{6}\left(\frac{\ell}{h}\right)^2\left(\dfrac{\bar{S}_{11}}{\bar{S}_{16}}\right)}}\right] \tag{A.12}$$

APPENDIX B

TRANSVERSE SENSITIVITY CORRECTION

The following corrections for the true strain outputs ε_{xx}, $\varepsilon_{45°}$, ε_{yy} in the coupon coordinate system have been employed in the process of data reduction as cited in Reference [102]:

$$\varepsilon_{xx} = \frac{(1 - \nu_o K_t)}{(1 - K_t^2)} (\hat{\varepsilon}_{xx} - K_t \hat{\varepsilon}_{yy})$$

$$\varepsilon_{45°} = \frac{(1 - \nu_o K_t)}{(1 - K_t^2)} [\hat{\varepsilon}_{45°} - K_t(\hat{\varepsilon}_{xx} + \hat{\varepsilon}_{yy} - \hat{\varepsilon}_{45°})]$$

$$\varepsilon_{yy} = \frac{(1 - \nu_o K_t)}{(1 - K_t^2)} (\hat{\varepsilon}_{yy} - K_t \hat{\varepsilon}_{xx})$$

where $\hat{\varepsilon}_{xx}$, $\hat{\varepsilon}_{45°}$ and $\hat{\varepsilon}_{yy}$ are the apparent strains recorded by the tree arms of the 45° rosette. K_t is the transverse sensitivity factor characteristic of each strain gage and ν_o Poisson's ratio of the material used for calibrating the gages, typically 0.285. The transverse sensitivity factors of the 45° rosette and uniaxial gages employed in the present study were:

K_t(uniaxial) = - 0.8%

K_t(rosette) = - 0.3%

APPENDIX C

NONLINEAR ELASTIC POTENTIAL G_o AND ASSOCIATED THERMODYNAMIC CONSTRAINTS

The proposed nonlinear elastic potential is reproduced below for convenience.

$$-G_o = \frac{1}{2} A_{ij}\sigma_i\sigma_j + \frac{1}{\alpha}(e^{-\alpha\sqrt{\ell_{ij}\sigma_i\sigma_j}} - 1) + \sqrt{\ell_{ij}\sigma_i\sigma_j} \qquad (C.1)$$

Applying the stability condition $-\delta^2 G_o \geq 0$ we obtain:

$$-\delta^2 G_o = A_{ij}\delta\sigma_i\delta\sigma_j + \frac{\ell_{ij}\delta\sigma_i\delta\sigma_j}{\sqrt{\ell_{mn}\sigma_m\sigma_n}}(1 - e^{-\alpha\sqrt{\ell_{mn}\sigma_m\sigma_n}})$$

$$- \frac{(\ell_{ij}\sigma_j\delta\sigma_i)^2}{(\ell_{mn}\sigma_m\sigma_n)^{3/2}}(1 - e^{-\alpha\sqrt{\ell_{mn}\sigma_m\sigma_n}})$$

$$+ \frac{(\ell_{ij}\sigma_j\delta\sigma_i)^2}{(\ell_{mn}\sigma_m\sigma_n)} e^{-\alpha\sqrt{\ell_{mn}\sigma_m\sigma_n}} \geq 0 \qquad (C.2)$$

Series expansion of the exponential terms and subsequent simplification of the resulting expression yields:

$$-\delta^2 G_o = A_{ij}\delta\sigma_i\delta\sigma_j + \alpha\ell_{ij}\delta\sigma_i\delta\sigma_j(1 - \frac{\alpha\sqrt{}}{2!} + \frac{\alpha^2\sqrt{}^2}{3!} - \ldots)$$

$$+ \frac{\alpha(\ell_{ij}\sigma_j\delta\sigma_j)^2}{(\ell_{mn}\sigma_m\sigma_n)}[\alpha\sqrt{}(\frac{1}{2!} - 1) + \alpha^2\sqrt{}^2(\frac{1}{2!} - \frac{1}{3!})$$

$$+ \alpha^3\sqrt{}^3(\frac{1}{4!} - \frac{1}{3!}) + \ldots] \geq 0 \qquad (C.3)$$

where $\sqrt{} = \sqrt{\ell_{mn}\sigma_m\sigma_n}$. Thus from Eqn. (C.3) it is clear that:

$$\lim_{\sigma_i \to 0}(-\delta^2 G_o) = (A_{ij} + \alpha\ell_{ij})\delta\sigma_i\delta\sigma_j \geq 0 \qquad (C.4)$$

whereas from Eqn. (C.2) we readily obtain:

$$\lim_{\sigma_i \to \infty} (-\delta^2 G_o) = A_{ij}\delta\sigma_i\delta\sigma_j \geq 0 \qquad (C.5)$$

In order to show that the above constraints are sufficient for the stability condition to be satisfied for all plane stress loading situations, Eqn. (C.2) is rearranged as follows:

$$-\delta^2 G_o = A_{ij}\delta\sigma_i\delta\sigma_j + \frac{(1-e^{-\alpha\sqrt{\ell_{mn}\sigma_m\sigma_n}})}{\sqrt{\ell_{mn}\sigma_m\sigma_n}}\left[\ell_{ij}\delta\sigma_i\delta\sigma_j - \frac{(\ell_{ij}\sigma_i\delta\sigma_j)^2}{(\ell_{mn}\sigma_m\sigma_n)}\right]$$

$$+ \alpha\,\frac{(\ell_{ij}\sigma_i\delta\sigma_j)^2}{(\ell_{mn}\sigma_m\sigma_n)}\,e^{-\alpha\sqrt{\ell_{mn}\sigma_m\sigma_n}} \geq 0 \qquad (C.6)$$

The above will be certainly satisfied if

$$\ell_{ij}\delta\sigma_i\delta\sigma_j - \frac{(\ell_{ij}\sigma_i\delta\sigma_j)^2}{(\ell_{mn}\sigma_m\sigma_n)} \geq 0$$

For plane stress applications, expansion of the above yields:

$$[\ell_{11}\sigma_1^2+2\ell_{12}\sigma_1\sigma_2+\ell_{22}\sigma_2^2+\ell_{66}\sigma_6^2]\cdot[\ell_{11}\delta\sigma_1^2+2\ell_{12}\delta\sigma_1\delta\sigma_2+\ell_{22}\delta\sigma_2^2+\ell_{66}\delta\sigma_6^2]$$

$$- [\ell_{11}\sigma_1\delta\sigma_1+\ell_{12}(\sigma_1\delta\sigma_2+\sigma_2\delta\sigma_1)+\ell_{22}\sigma_2\delta\sigma_2+\ell_{66}\sigma_6\delta\sigma_6] \geq 0$$

Omitting superfluous algebra, the above can be shown to reduce to the following form:

$$(\sigma_1\delta\sigma_2-\sigma_2\delta\sigma_1)^2(\ell_{11}\ell_{22}-\ell_{12}^2)$$

$$+ \ell_{66}\{\ell_{11}(\sigma_6\delta\sigma_1-\sigma_1\delta\sigma_6)^2 + \ell_{22}(\sigma_6\delta\sigma_2-\sigma_2\delta\sigma_6)^2$$

$$+ 2\ell_{12}(\sigma_6\delta\sigma_1-\sigma_1\delta\sigma_6)(\sigma_6\delta\sigma_2-\sigma_2\delta\sigma_6)\} \geq 0$$

The first part is always positive or zero since ℓ_{ij} is positive-definite, whereas the second part is a quadratic form with coefficients ℓ_{ij} and thus must also be positive or zero for the same reason.

APPENDIX D

HILL'S STRESS CONCENTRATION FACTORS

Hill's stress concentration factors can be obtained explicitly in terms of the composite, fiber and matrix compliances, respectively, upon inverting Eqn. (5.25). Assuming that the individual phases are isotropic and employing the following definition:

$$[M] - [M^f] = [\Delta M]$$

$$[M^m] - [M^f] = [\Delta m]$$

the elements of the stress concentration matrix for the matrix phase become $[B^m] = \frac{1}{c_m}[\Delta m]^{-1}[\Delta M]$, or:

$$B^m_{11} = \frac{1}{c_m}[\Delta m^{-1}_{11}\ \Delta M_{11} + 2\Delta m^{-1}_{12}\Delta M_{12}]$$

$$B^m_{12} = \frac{1}{c_m}[\Delta m^{-1}_{11}\ \Delta M_{12} + \Delta m^{-1}_{12}(\Delta M_{22} + \Delta M_{23})]$$

$$B^m_{13} = B^m_{12}$$

$$B^m_{21} = \frac{1}{c_m}[\Delta m^{-1}_{11}\ \Delta M_{12} + \Delta m^{-1}_{12}(\Delta M_{11} + \Delta M_{12})]$$

$$B^m_{22} = \frac{1}{c_m}[\Delta m^{-1}_{11}\ \Delta M_{22} + \Delta m^{-1}_{12}(\Delta M_{12} + \Delta M_{22})]$$

$$B^m_{23} = \frac{1}{c_m}[\Delta m^{-1}_{11}\ \Delta M_{23} + \Delta m^{-1}_{12}(\Delta M_{12} + \Delta M_{22})]$$

$$B^m_{66} = \frac{1}{c_m}\ \Delta m^{-1}_{66}\ \Delta M_{66}$$

where $[\Delta m]^{-1}$ is the inverse of $[\Delta m]$ defined by $[\Delta m]^{-1}[\Delta m] = [I]$, $[I]$ being unit (diagonal) matrix. The elements of

$[\Delta m]^{-1}$ are given by:

$$\Delta m_{11}^{-1} = \frac{\Delta m_{11}^2 - \Delta m_{12}^2}{(\Delta m_{11}^3 - 3\Delta m_{11}\Delta m_{12}^2 + 2\Delta m_{12}^2)}$$

$$\Delta m_{12}^{-1} = \frac{\Delta m_{12}^2 - \Delta m_{11}\Delta m_{12}}{(\Delta m_{11}^3 - 3\Delta m_{11}\Delta m_{12}^2 + 2\Delta m_{12}^2)}$$

where:

$$\Delta m_{11} = \frac{(E^f - E^m)}{E^f E^m}$$

$$\Delta m_{12} = \frac{(E^m \nu^f - E^f \nu^m)}{E^f E^m}$$

$$\Delta m_{66} = \frac{(G^f - G^m)}{G^f G^m}$$

and also:

$$\Delta M_{11} = \frac{(E^f - E_{11})}{E^f E_{11}}$$

$$\Delta M_{12} = \frac{(E_{11} \nu^f - E^f \nu_{12})}{E^f E_{11}}$$

$$\Delta M_{22} = \frac{(E^f - E_{22})}{E^f E_{22}}$$

$$\Delta M_{23} = \frac{(E_{22} \nu^f - E^f \nu_{23})}{E^f E_{22}}$$

$$\Delta M_{66} = \frac{(G^f - G_{12})}{G^f G_{12}}$$

The material parameters needed for determination of the stress concentration factors are given below.

$E^m = 0.4535 \times 10^6$ psi $\qquad E^f = 31.90 \times 10^6$ psi

$G^m = 0.1609 \times 10^6$ psi $\qquad G^f = 11.77 \times 10^6$ psi *

$\nu^m = 0.391 \qquad \nu^f = 0.355$ *

$$E_{11} = 19.81 \times 10^6 \text{ psi}$$

$$E_{22} = 1.42 \times 10^6 \text{ psi}$$

$$G_{12} = 0.725 \times 10^6 \text{ psi}$$

$$\nu_{23} = \nu_{12} = 0.350 \text{ *}$$

It is of interest to note that the isotropic relationship $G^m = \frac{E^m}{2(1+\nu^m)}$ is satisfied within 2% for the matrix employed in this work. The starred quantitites have been determined indirectly (these are usually unavailable due to difficulties associated with their measurement) in the following fashion:

i) ν^f has been determined from the relation $\varepsilon_{11}^m = \varepsilon_{11}^f$ which can be shown to be given by:

$$\left[M_{11}^m + M_{11}^f\left(\frac{c_m}{c_f}\right)\right] B_{11}^m + \left[2M_{12}^m + 2M_{12}^f\left(\frac{c_m}{c_f}\right)\right] B_{21}^m = \frac{1}{c_f} M_{11}^f$$

It was possible to satisfy the above relation to within less than 3% (i.e. % difference between left and right side of the equation) with the above value of ν^f.

ii) G^f has been determined from the isotropic relation

$$G^f = \frac{E^f}{2(1+\nu^f)}$$

iii) ν_{23} has been assumed to be equal to ν_{12}. This is a common assumption employed by various researchers, c.f. Ref. [100].

In order to determine the effect of variation in ν^f on the stress concentration factors, B^m_{11}, B^m_{21}, B^m_{12}, B^m_{22} and B^m_{23} have been plotted as functions of ν^f in the range $0.0 \leq \nu^f \leq 0.5$ in the following figures. It is seen that B^m_{12}, B^m_{22} and B^m_{23} vary negligibly whereas the functions B^m_{11} and B^m_{21} are nearly linearly dependent on ν^f. Also plotted is the variation in B^m_{66} due to G^f and it follows that B^m_{66} does not change significantly over a wide range of the fiber shear modulus. In particular, the range of G^f of immediate interest is bounded by $0.0 \leq \nu_f \leq 0.5$. This yields 10.63×10^6 psi $\leq G_f \leq 15.95 \times 10^6$ psi which evidently does not influence B^m_{66} significantly.

The stress concentration factors determined on the basis of the material parameters given above are the following:

$B^m_{11} = 0.0255$ $B^m_{12} = 0.6522$

$B^m_{21} = 0.0038$ $B^m_{22} = 1.2265$

$B^m_{23} = 0.4591$ $B^m_{66} = 0.5416$

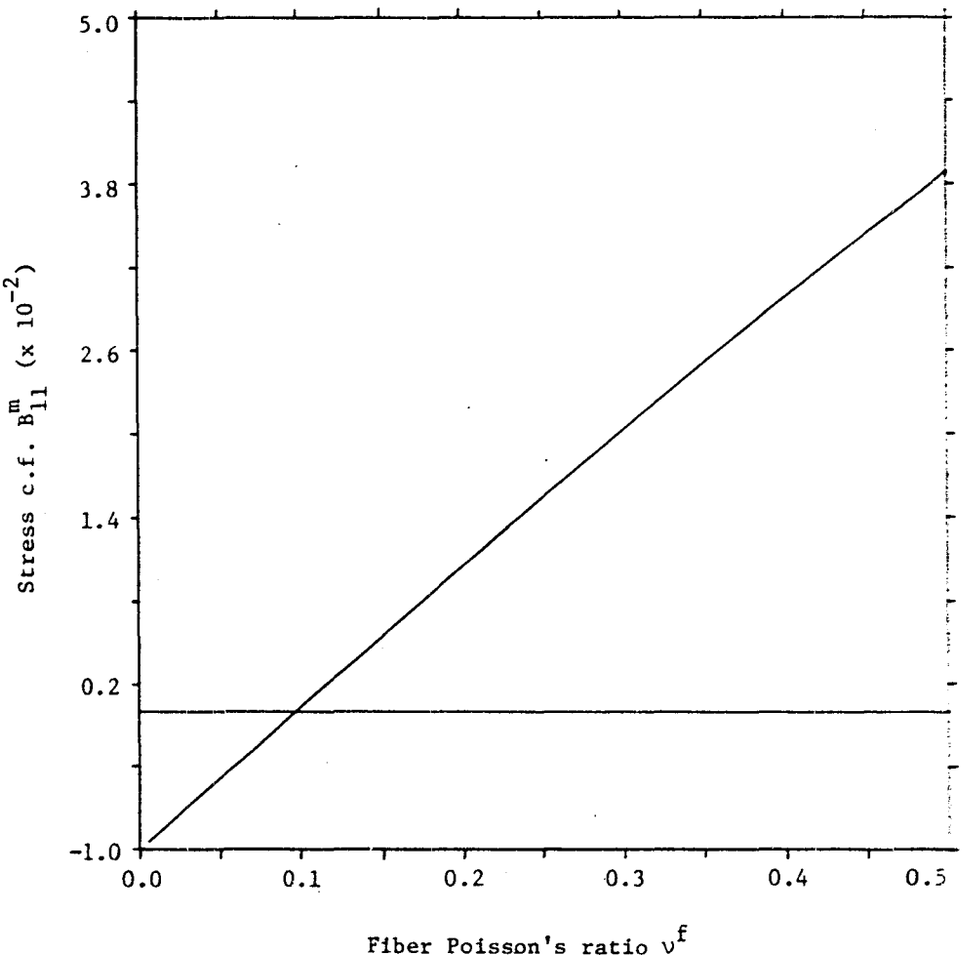

Fig. D.1 Matrix stress concentration factor B_{11}^m as a function of the fiber Poisson's ratio ν^f

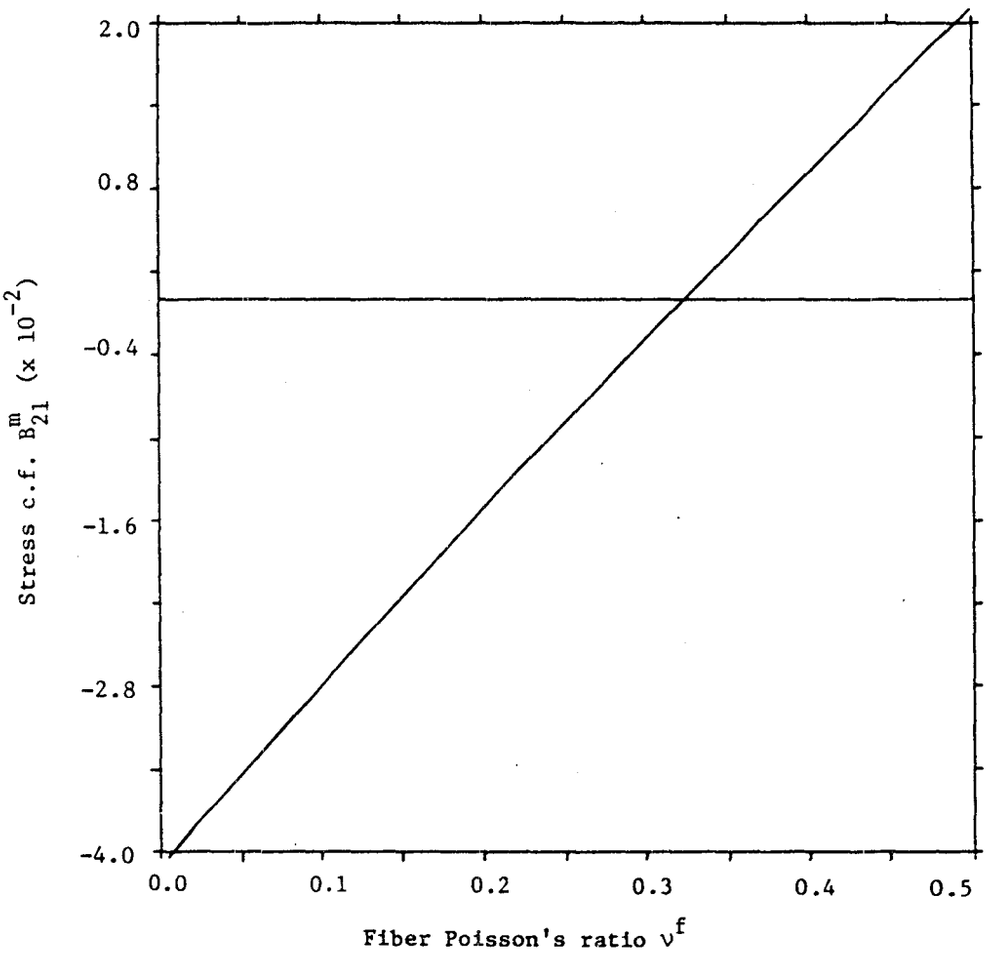

Fig. D.2 Matrix stress concentration factor B_{21}^m as a function of the fiber Poisson's ratio ν^f

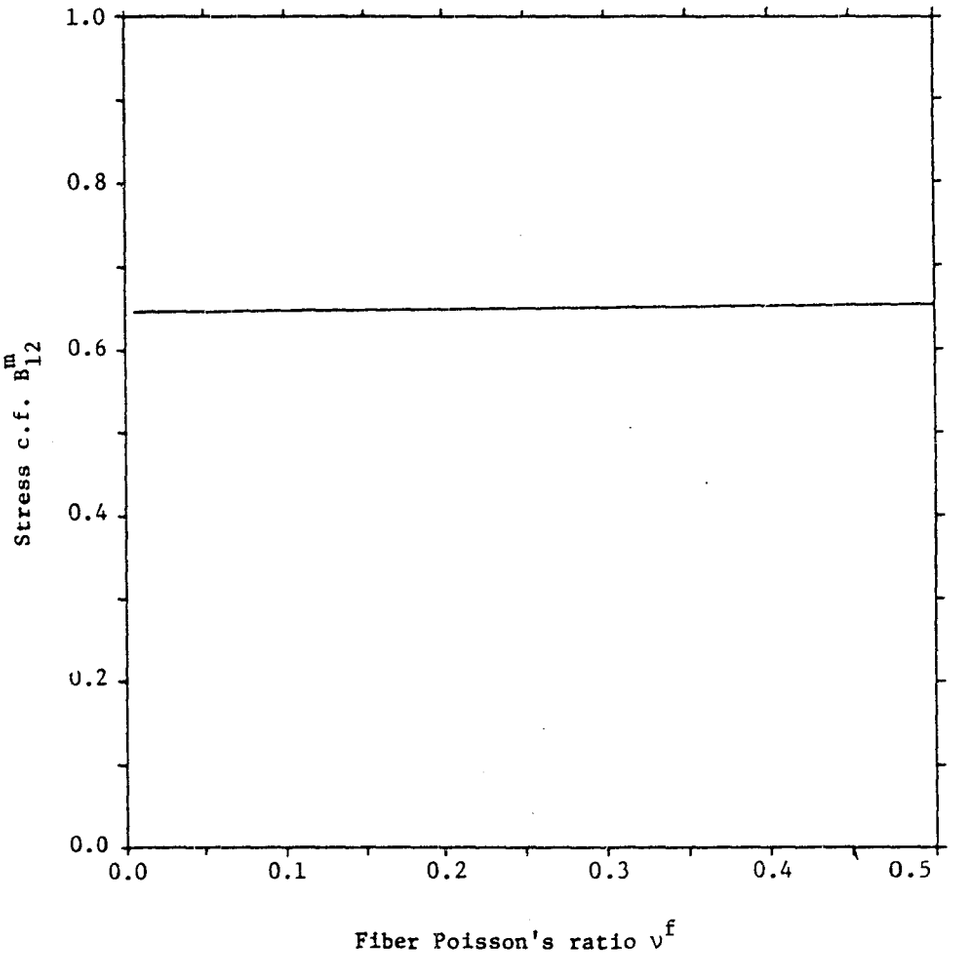

Fig. D.3 Matrix stress concentration factor B_{12}^m as a function of the fiber Poisson's ratio ν^f

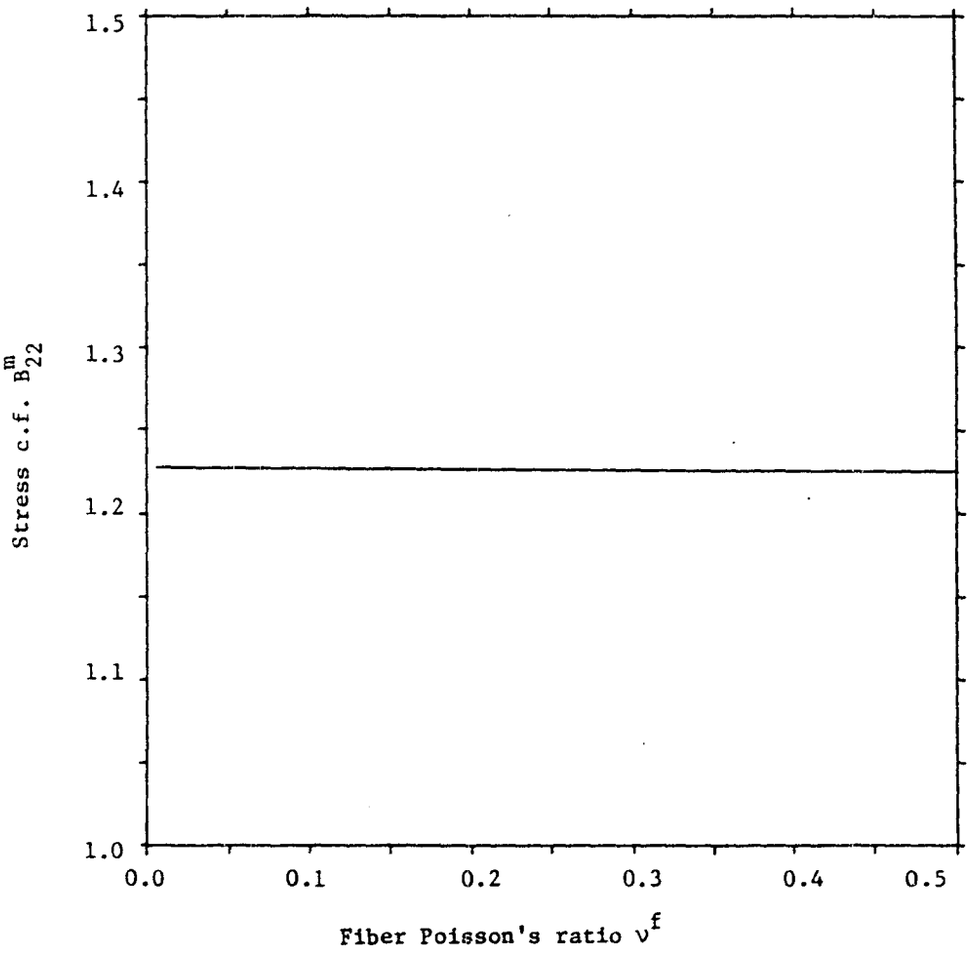

Fig. D.4 Matrix stress concentration factor B_{22}^m as a function of the fiber Poisson's ratio ν^f

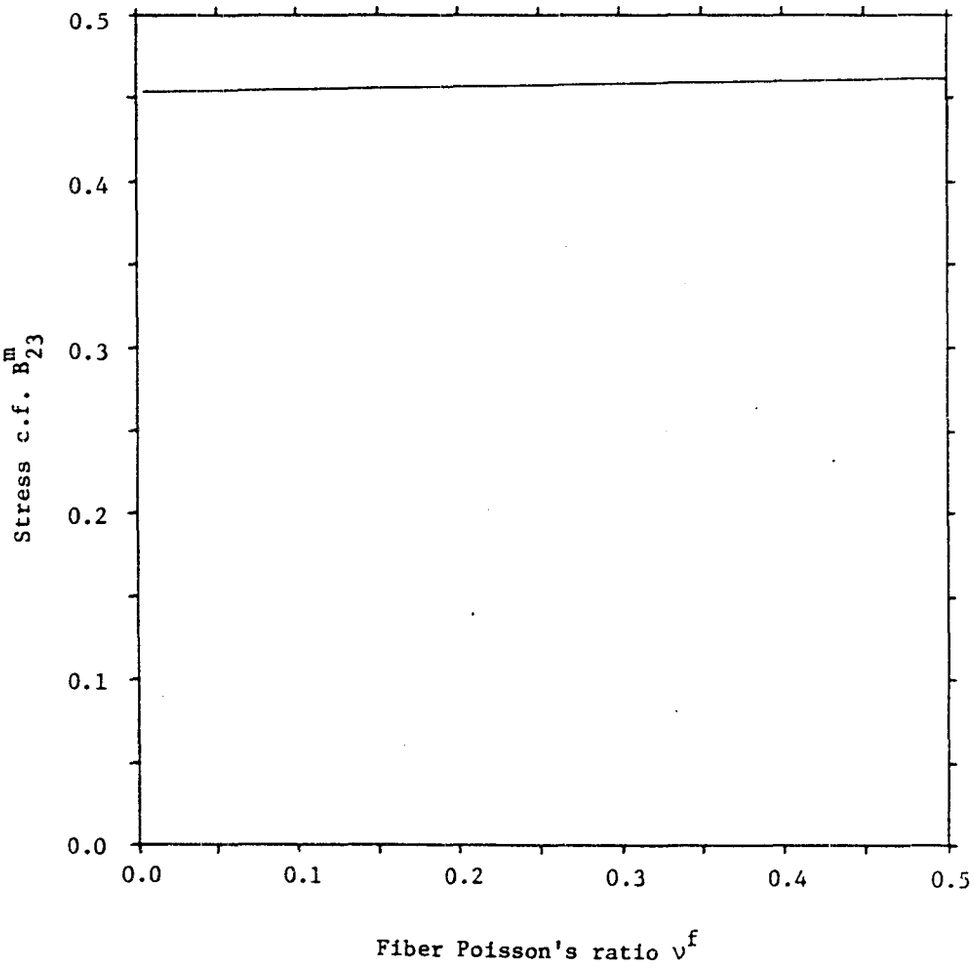

Fig. D.5 Matrix stress concentration factor B_{23}^m as a function of the fiber Poisson's ratio ν^f

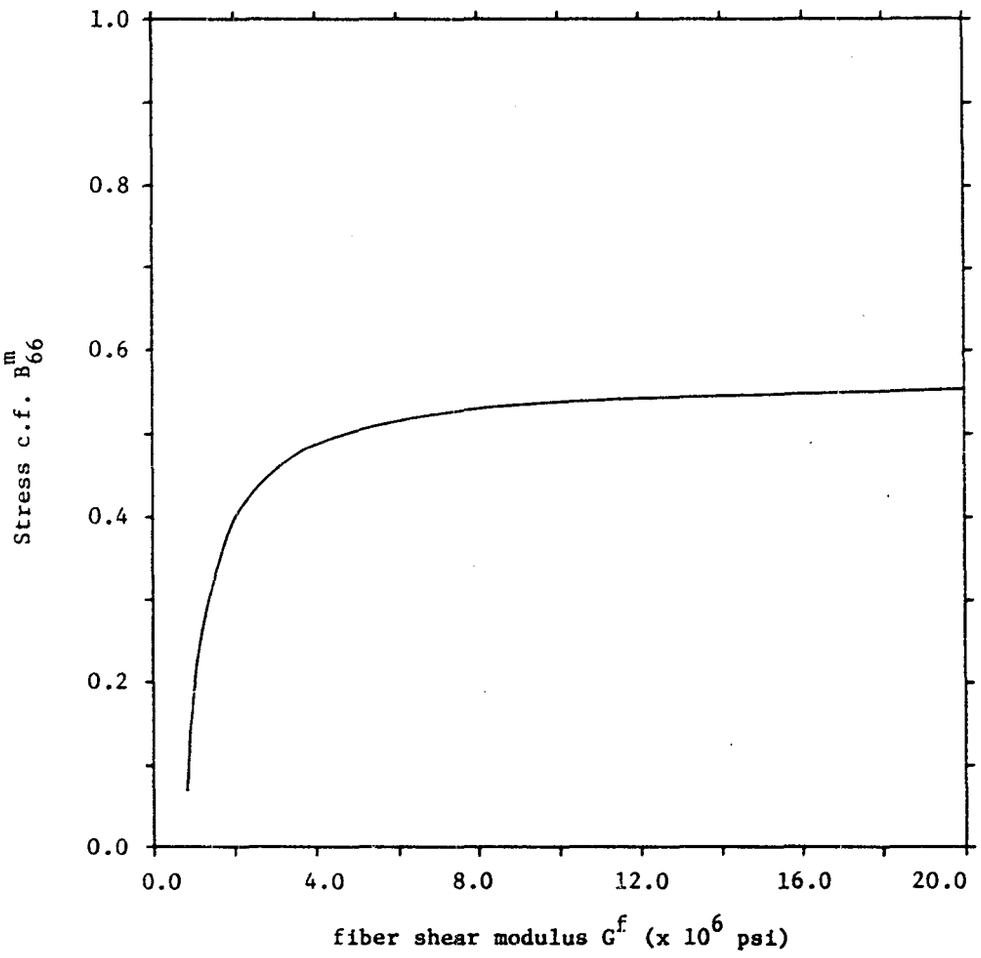

Fig. D.6 Matrix stress concentration factor B_{66}^m as a function of the fiber shear modulus G^f

DISTRIBUTION LIST

Prof. Donald F. Adams
Dept. Of Mechanical Engineering
University Of Wyoming
Larmie, WY 82070

Dan Adams
Dept. of Engineering Science
and Mechanics
Virginia Tech
Blacksburg, VA 24061-4899,

Dr. M. B. Adsit
General Dynamics Convair
P.O. Box 80837
San Diego, CA. 92138

Winfield H. Arata, Jr.
4414 Countrywood Drive
Santa Maria, CA 93455

Dr. Clifford J. Astill
Solid Mechanics Program
National Science Foundation
1800 G St. N.W.
Washington, D.C.

AVCO, Systems Division
Subsystems & Meth. Structures
201 Lowell Street
Wilmington, MA. 01887

Dr. J. A. Bailie
D81-12 Bldg. 154
Lockheed Missiles & Space Co,Inc
1111 Lockheed Way
Sunnyvale, CA. 94088

Dr. Charles W. Bert, Director
School Of Aerospace, Mechanical
& Nuclear Engineering
The University Of Oklahoma
Norman, Oklahoma 73069

Dr. C. M. Blackmon
NSWC, Code K21
Dahlgren, VA 22448

Mr. Richard Boitnott
Mail Stop 190
Nasa-Langley Research Center
Hampton, VA. 23665

Mr. David Bowles
Mail Stop 188B
NASA-Langley Research Center
Hampton, Va. 23665

Dr. H. F. Brinson
ESM Dept.
Virginia Tech
Blacksburg, VA. 24061

Mr. Ernie Brooks
Code 1844
DTNSRDC
Bethesda, MD 20084

Matthew B. Buczek
Dept. of Engineering Science
and Mechanics
Virginia Tech
Blacksburg, VA 24061-4899

Dr. Michael P. Card
Mail Stop 190
NASA-Langley Research Center
Hampton, VA 23665

Doug Carper
Dept. of Engineering Science
and Mechanics
Virginia Tech
Blacksburg, VA 24061-4899

Dr. C. Chamis
NASA-Lewis Research Center
2100 Brook Park Rd.
Cleveland, Ohio 44135

Dr. Paul A. Cooper
Mail Stop 190
NASA-Langley Research Center
Hampton, Va. 23665

Dr. Frank Crossman
Lockheed Research Lab
Org. 52-41, Bldg. 204
3251 Hanover Street
Palo Alto, CA. 94304

Dr. L. M. Daniel, Manager
IIT Research Institute
10 West 35 Street
Chicago, IL. 60616

Dr. John R. Davidson
Mail Code 188E
MD-Structural Integrity Branch
Langley Research Center
Hampton, VA. 23665

Dr. John G. Davis, Jr.
Mail Stop 188A
Langley Research Center
Hampton, VA. 23665

Mr. Jerry M. Deaton
Mail Stop 188A
NASA-Langley Research Center
Hampton, VA. 23665

Mr. H. Benson Dexter
Mail Stop 188A
NASA-Langley Research Center
Hampton, VA. 23665

Mr. O. Earl Dhonau
Section 2-53400
Vought Corp.
P.O. Box 5907
Dallas, TX. 75222

Dr. M. P. Duggan
52-33/205/2
Lockheed Palo Alto Lab.
3251 Hanover St.
Palo Alto, Ca. 94304

Prof. John C. Duke, Jr.
ESM Dept.
Virginia Tech
Blacksburg, VA. 24061

Prof. George J. Dvorak
Civil Engineering
University of Utah
Salt Lake City, UT. 84112

Dr. Wolf Elber
Mail Stop 188E
NASA-Langley Research Center
Hampton, VA. 23665

Mr. Dave Erb
Freightline Corp.
Mail Code 700-383
P.O. Box 3849
Portland, Oregon 97208

Mr. Gary L. Farley
Mail Stop 188A
NASA-Langley Research Center
Hampton, VA. 23665

Mr. Larry Fogg
Lockheed-California
Dept. 7572, Bldg. 63, Plant A1
P.O. Box 551
Burbank, CA. 91520

Dr. R. L. Foye
USAMRDL
SAUDLAS (207-5)
Moffet Field, CA. 94035

Dr. D. Frederick
ESM Dept.
Virginia Tech
Blacksburg, VA. 24061

Mr. Samuel P. Garbo
McDonnell Aircraft Co.
Bldg. 34, Post 350
St. Louis, MO. 63166

Mr. Ramon Garica
FAA Technical Center
ACT-330
Atlantic City, NJ 08405

Prof. Jim Goree
Dept. of Mechanical Engr.
Clemson University
Clemson, S.C. 29631

Dr. Login B. Greszczuk
McDonnell Douglas Astr. Co.
5301 Bolas Avenue
Huntington Beach, CA. 92647

Dr. O. Hayden Griffin, Jr.
Bendix Advanced Technology Ctr.
9140 Old Annapolis Road
Columbia, MD 21045

Mr. Glen C. Grimes
Dept. 3852/82
Northrop Corp., Aircraft Div.
3901 West Broadway
Hawthorne, CA. 90250

Dr. H. T. Hahn
Washington University
St. Louis, MO. 63130

Dr. J. C. Halpin
Flight Dynamics Lab
Wright-Patterson AFB
Ohio 45433

Professor Z. Hashin
School of Engineering
Solid Mech. Materials & Struc.
Tel Aviv University
Tel Aviv, Israel

Dr. R. A. Heller
ESM Dept.
Virginia Tech
Blacksburg, VA. 24061

Dr. E. G. Henneke
ESM Dept.
Virginia Tech
Blacksburg, VA. 24061

Prof. Carl T. Herakovich
Department of Engineering
Science & Mechanics
Virginia Tech
Blacksburg, Virginia 24060

Professor Phil Hodge
107 Aeronautical Engr. Bldg.
University of Minnesota
Minneapolis, MN 55455

Dr. K. E. Hofer
IIT Research Institute
10 West 35 Street
Chicago, Illinois 60616

Mr. Edward A. Humphreys
Materials Science Corporation
Blue Bell Office Campus
Blue Bell, PA. 19422

Dr. Michael W. Hyer
ESM Dept.
Virginia Tech
Blacksburg, VA. 24061

Dr. Eric R. Johnson
Dept. of Aerospace and
Ocean Engineering
Virginia Tech
Blacksburg, VA. 24061

Dr. M. J. Johnson
Mail Stop 226
NASA-Langley Research Center
Hampton, VA. 23665

Dr. Robert M. Jones
Dept. of Engineering Science
and Mechanics
Virginia Tech
Blacksburg, VA 24061-4899

Dr. M. P. Kamat
ESM Dept.
Virginia Tech
Blacksburg, VA. 24061

Dr. Keith T. Kedward
1768 Granite Hills Dr.
El Cajon, CA. 92021

Mr. John M. Kennedy
Mail Stop 188E
NASA-Langley Research Center
Hampton, VA. 23665

Michael S. Kerstetter
Boeing Commercial Airplane Co.
Post Office Box 3707
Mail Stop 6W-13
Seattle, Washington 98124

Mr. Eric Klang
ESM Dept.
Virginia Tech
Blacksburg, VA. 24061

Mr. James F. Knauss
Northrop Corporation
3901 West Broadway
Dept. 3852/82
Hawthorne, CA. 90250

Dr. Ronald D. Kriz
Dept. Com. NBS Bldg. 2
Boulder, CO. 80302

Dr. S. V. Kulkarni
1342 Lawrence Livermore Lab
P. O. Box 808
Livermore, Ca. 94550

Dr. Trent R. Logan
Mgr. Structures, Design, Dev.
Boeing Commercial Airplane Co.
P.O. Box 3707 - M.S. 3H-23
Seattle, WA. 98124

Dr. M. R. Louthan
Materials Engineering
Virginia Tech
Blacksburg, VA. 24061

Mr. Vic Mazzio
General Electric Co.
P.O. Box 8555
Bldg. 100, Rm. M4018
Philadelphia, PA. 19101

Dr. Martin M. Mikulas
Mail Stop 190
NASA-Langley Research Center
Hampton, VA. 23665

Mr. J. Steve Mills
A3-220 13-3 McDonald Douglas
5301 Bolsa Avenue
Huntington Beach, CA 96247

Dr. D. H. Morris
ESM Dept.
Virginia Tech
Blacksburg, VA. 24061

NASA Scientific & Technical
Information Facility
P.O. Box 8757
Baltimore/Washington Inter. Air.
Baltimore, MD. 21240

Mr. Michael Nemeth
Mail Stop 190
NASA-Langley Research Center
Hampton, VA 23665

Newman Library
Virginia Tech

Mr. David A. O'Brien
5902 Kingsford Pl.
Bethesda, MD 20034

Dr. Donald W. Oplinger
Army Materials & Mechanics
Research Center
Department of the Army
Watertown, MA. 02171

Dr. Nicholas J. Pagano
WPAFB/NBM
Wright Patterson AFB
Ohio 45433

Mr. Michael Parin
3M Co., 3M Center
Bldg. 230-1F
St. Paul, MN. 55101

Dr. Nicholas Perrone, Director
Structural Mechanics Program
Department of the Navy
Office of Naval Research
Arlington, VA. 22217

Prof. T. H. H. Pian
Mass. Inst. of Tech.
Dept. of Aero. & Astr.
Cambridge, MA. 02139

Dr. Marek-Jerzy Pindera
Materials Science Corporation
Blue Bell Office Campus
Blue Bell, PA 19422

Dr. R. Byron Pipes
Dept. of Mech. & Aero. Engr.
107 Evans Hall
University of Delaware
Newark, DE. 19711

Prof. Robert Plunkett
Dept. Aero & Eng. Mech.
Aero 107
University of Minnesota
Minneapolis, MN. 55455

Dr. J. N. Reddy
Dept. of Engineering Science
and Mechanics
Virginia Tech
Blacksburg, VA 24061-4899

Dr. K. L. Reifsnider
ESM Dept.
Virginia Tech
Blacksburg, VA. 24061

Dr. Gary D. Renieri
McDonnell Douglas Astro. Co-East
P.O. Box 516
Bldg. 106, Level 4, Post C-5
St. Louis, MO. 63166

Dr. Michael W. Renieri
McDonnell Aircraft Co.
Bldg. 34, Post 350
St. Louis, MO. 63166

Dr. Larry Roderick
Mail Stop 188E
NASA-Langley Research Center
Hampton, VA. 23665

Dr. B. W. Rosen
Materials Science Corporation
Blue Bell Office Campus
Blue Bell, PA. 19422

Dr. R. E. Rowlands
Dept. of Engineering Mechanics
University of Wisconsin
Madison, WI. 53706

Dr. Edmund B. Rybicki
Mechanical Engineering Dept.
The Univ. of Tulsa
Tulsa, OK. 74104

Mr. Harminder Saluja
Boeing Vertol Company
Structural Technology
P.O. Box 16858
Philadelphia, PA. 19142

Dr. J. Wayne Sawyer
Mail Stop 190
NASA-Langley Research Center
Hampton, VA. 23665

Dr. George P. Sendeckyj
Structures Division
Air Force Flight Dynamics Lab.
Wright-Patterson AFB
Ohio 45433

Mr. John S. Short, Jr.
Mail Stop 188B
MD-Materials Research Branch
Langley Research Center
Hampton, VA 23665

Mr. Mark J. Shuart
Mail Stop 188
NASA-Langley Research Center
Hampton, VA. 23665

Prof. George Springer
Dept. Mechanical Engineering
and Applied Mechanics
University of Michigan
Ann Arbor, Michigan 48109

Dr. J. R. Stafford
B.F. Goodrich
500 S. Main St.
D/6145, B/10-E
Akron, Ohio 44318

Dr. James H. Starnes, Jr.
Mail Stop 190
NASA-Langley Research Center
Hampton, VA. 23665

Prof. Yehuda Stavsky
Gerard Swope Prof. of Mech.
Technion-Israel Inst. of Tech.
Technion City, Haifa, Israel

Dr. W. W. Stinchcomb
ESM Dept.
Virginia Tech
Blacksburg, VA. 24061

Dr. W. Jefferson Stroud
M.S 190
NASA Langley Research Center
Hampton, VA 23665

Dr. Darrel R. Tenney
Mail Code 188B
MD-Materials Research Branch
Langley Research Center
Hampton, VA. 23665

Steve Tompkins
M.S. 188B
NASA Langley Research Center
Hampton, VA 23665

Dr. S. W. Tsai
Nonmetallic Materials Division
Air Force Materials Laboratory
Wright-Patterson AFB
Ohio 45433

Dr. J. B. Vinson
Dept. of Mech. & Aero. Engr.
107 Evans Hall
University of Delaware
Newark, DE. 19711

Mr. M. Z. Waddoups
General Dynamic Corp.
Fort Worth, TX 76101

Dr. W. J. Walker
Boeing Aerospace Co.
Post Office Box 3999
Seattle, WA 98124

Prof. A. S. Wang
Mechanical Engineering
Drexel University
Philadelphia, PA. 19104

Prof. S. S. Wang
Dept. Theoretical & Applied
Mechanics
University of Illinois
Urbana, IL. 61801

Dr. T. A. Weissbaar
School of Aero. & Astro.
331 Grisson Hall
Purdue Univ.
West Lafayette, IN. 47907

Dr. J. M. Whitney
Nonmetallic Materials Division
Air Force Materials Laboratory
Wright-Patterson AFB
Ohio 45433

Dr. Ernest G. Wolff
The Aerospace Corp.
P.O. Box 92957
Los Angeles, CA. 90009

Judy Wood
ESM, 225 Norris Hall
Virginia Tech
Blacksburg, VA 24061

Dr. Edward Wu
Lawrence Livermore Lab.
University of California
Box 808, L-338
Livermore, CA. 94550

Mr. Thomas A. Zeiler
School of Aero. & Astro.
Grissom Hall
Purdue Univ.
West Lafayette, IN. 47907

Dr. Carl H. Zweben
General Electric Co.
Space Division
P.O. Box 8555
Philadelphia, PA. 19101

End of Document